CFD STUDIES ON STRATUM VENTILATION INSTALLED WITH A VRF/VRV SYSTEM FOR TROPIC BUILDINGS

UMAIR AHMED

FACULTY OF ENGINEERING
UNIVERSITY OF MALAYA
KUALA LUMPUR

2022

CFD STUDIES ON STRATUM VENTILATION INSTALLED WITH A VRF/VRV SYSTEM FOR TROPIC BUILDINGS

UMAIR AHMED

THESIS SUBMITTED IN FULFILMENT OF THE REQUIREMENTS FOR THE DEGREE OF DOCTOR OF PHILOSOPHY

FACULTY OF ENGINEERING
UNIVERSITY OF MALAYA
KUALA LUMPUR

2022

UNIVERSITY OF MALAYA

ORIGINAL LITERARY WORK DECLARATION

Name of Candidate: **UMAIR AHMED**

Matric No: **KVA180054 (OLD) 17198679/1 (NEW)**

Name of Degree: **DOCTOR OF PHILOSOPHY**

Title of Thesis: **CFD STUDIES ON STRATUM VENTILATION INSTALLED WITH A VRF/VRV SYSTEM FOR TROPIC BUILDINGS**

Field of Study: **HEAT TRANSFER (ELECTRICITY AND ENERGY)**

I do solemnly and sincerely declare that:

(1) I am the sole author/writer of this Work;
(2) This Work is original;
(3) Any use of any work in which copyright exists was done by way of fair dealing and for permitted purposes and any excerpt or extract from, or reference to or reproduction of any copyright work has been disclosed expressly and sufficiently and the title of the Work and its authorship have been acknowledged in this Work;
(4) I do not have any actual knowledge nor do I ought reasonably to know that the making of this work constitutes an infringement of any copyright work;
(5) I hereby assign all and every rights in the copyright to this Work to the University of Malaya ("UM"), who henceforth shall be owner of the copyright in this Work and that any reproduction or use in any form or by any means whatsoever is prohibited without the written consent of UM having been first had and obtained;
(6) I am fully aware that if in the course of making this Work I have infringed any copyright whether intentionally or otherwise, I may be subject to legal action or any other action as may be determined by UM.

Candidate's Signature Date: 04/11/2022

Subscribed and solemnly declared before,

Witness's Signature Date: 05/11/2022

Name:

Designation:

[CFD STUDIES ON STRATUM VENTILATION INSTALLED WITH A VRF/VRV SYSTEM FOR TROPIC BUILDINGS]

ABSTRACT

In buildings, air conditioning and mechanical ventilation (ACMV) systems are the major shareholders of overall energy consumption. Energy-efficient designs of the ACMV systems for building applications are therefore needed. While designing an efficient ACMV system, consideration must be given to the growing concerns of enhanced thermal comfort and improved indoor air quality (IAQ). The variable refrigerant flow (VRF) system is a widely adopted alternative to the existing building cooling systems due to the higher energy efficiency and individualized temperature control feature. However, it suffers from shortcomings such as no outdoor air induction for ventilation and higher initial cost. Therefore, this work was intended to design the variable refrigerant flow (VRF) integrated stratum ventilation/air distribution systems for tropical buildings. Performance evaluation of different configurations of the integrated design is carried out in this study. To obtain an efficient air distribution terminal device for large tropical applications, different devices were experimentally and numerically investigated and compared. This study also presents the development and validation of a simplified nodal model that predicts the vertical temperature profile of the integrated design for large domain. The energy simulation models of the VRF-SV hybrid system using TRNSYS software were also developed in this study to compare the annual energy consumption of the fully integrated and decoupled designs of the VRF-SV system with multi-split AC systems and standalone VRF system. Lastly, the air distribution performance of the architecturally designed high-capacity linear diffuser in a large tropical atrium building is also evaluated in this work as a case study. Following a suitable design approach, the combined system provides better thermal

comfort with enhanced indoor air quality and improved energy savings to relatively large space building. This system has also shown an excellent potential to be installed in any building regardless of the size and heat load. With a fully integrated design approach, a horizontal air jet at head level, a slight and reverse thermal gradient between the head and foot levels ($\Delta T_{1.5\text{-}0.1}$ = -2.85ºC), and a low percentage of thermally dissatisfied people (<25%) are noticed under this investigation. The configuration 5 (wall exhaust configuration) showed overall good results in terms of thermal comfort indices. The doubled deflection grille was found most efficient air terminal type for providing throw to a larger distance. A good match is also observed in the simulated and modified nodal model's calculations. Therefore, this model can be used for energy calculation and in practical engineering design. The TRNSYS simulation results of the energy use analyses of the ACMV system in the tropical building revealed that the decoupled design of the VRF-SV hybrid system could save a significant amount of energy compared to the other investigated systems. Results obtained from the case study revealed a relatively longer airflow jet at 0º blade angle through the high-capacity diffuser. Based on the above outcomes, the VRF-SV hybrid system was found as an energy efficient substitute of the conventional ACMV systems for tropical buildings.

Keywords: VRF integrated stratum ventilation system, computational fluid dynamics, tropical buildings, thermal comfort, energy analyses

[KAJIAN CFD MENGENAI PENGUDARAAN STRATUM YANG DIPASANG DENGAN SISTEM VRF/VRV UNTUK BANGUNAN TROPIK]

ABSTRAK

Sistem penghawa dingin dan pengudaraan mekanikal (ACMV) merupakan faktor utama dalam penggunaan tenaga keseluruhan dalam sesebuah bangunan. Oleh itu, pelan sistem ACMV yang menyediakan penggunaan cekap tenaga dalam bangunan amat diperlukan. Apabila mereka bentuk sistem ACMV yang cekap, pertimbangan harus diberikan kepada keselesaan terma dan peningkatan kualiti udara dalaman (IAQ) yang semakin diberi keutamaan. Disebabkan kecekapan tenaga yang lebih tinggi dan ciri kawalan suhu individu, penyejukan aliran berubah (VRF) dalam sistem penyaman udara adalah alternatif yang kerap digunakan dalam membina sistem penyejukan. Tetapi, ia juga mempunyai kelemahan seperti kekurangan induksi udara luar untuk pengudaraan dan kos permulaan yang lebih tinggi. Oleh itu, kajian ini mereka bentuk sistem pengudaraan stratum / pengagihan udara bersepadu dengan penggunaan penyejukan aliran berubah (VRF) dalam sasaran bangunan tropika yang besar. Penilaian prestasi pelbagai konfigurasi reka bentuk bersepadu telah dijalankan. Untuk mendapatkan peranti terminal pengedaran udara yang cekap untuk aplikasi tropika yang besar, peranti yang berbeza telah disiasat dan dibandingkan secara eksperimen dan berangka. Kajian literatur menunjukkan bahawa suhu udara bekalan, kelajuan aliran udara dan corak aliran adalah parameter paling utama untuk dioptimumkan dalam pelan sistem pengedaran udara kerana ia sangat mempengaruhi penggunaan tenaga keseluruhan sistem. Oleh itu, untuk mendapatkan peranti resapan udara yang cekap dalam aplikasi tropika yang besar, peranti bekalan udara yang berbeza disiasat secara eksperimen dan dibandingkan. Kajian ini juga menunjukkan pembangunan dan pengesahan model nod dipermudah yang meramalkan profil suhu menegak reka bentuk bersepadu untuk domain besar. Dengan pertimbangan penuh mekanisme pengudaraan stratum dan kesan

penghantaran haba sampul surat, profil suhu menegak dalam sistem VRF-SV di kemudahan runcit besar diramalkan. Melalui pelan yang sesuai, sistem gabungan memberikan keselesaan terma yang lebih baik kerana ia menyediakan kualiti udara dalaman dan penjimatan tenaga yang lebih tinggi kepada ruang yang agak besar. Sistem ini juga menunjukkan potensi yang sangat baik untuk dipasang di mana-mana bangunan tanpa mengira saiz dan beban terma. Dengan pendekatan reka bentuk bersepadu, pancutan udara mendatar pada paras kepala, kecerunan terma rendah dan penyongsangan antara paras kepala dan kaki ($\Delta T_{1.5–0.1}$ = 2.85ºC), didapati hanya peratusan yang rendah dalam kalangan mereka yang tidak berpuas hati dengan terma (< 25 %) Dalam kajian ini. Konfigurasi 5 (konfigurasi ekzos dinding) menunjukkan hasil keseluruhan yang baik dari segi indeks keselesaan terma. Jeriji pesongan berkembar didapati jenis terminal udara yang paling cekap kerana ia memberikan lontaran pada jarak yang lebih jauh. Padanan yang baik juga diperhatikan dalam pengiraan model nod simulasi dan pengubahsuaian. Oleh itu, model ini boleh digunakan untuk pengiraan tenaga dan reka bentuk kejuruteraan praktikal. Keputusan analisis simulasi TRNSYS penggunaan tenaga sistem ACMV di bangunan tropika mendedahkan bahawa reka bentuk decoupled sistem hibrid VRF-SV boleh menjimatkan sejumlah besar tenaga berbanding sistem lain yang disiasat. Keputusan yang diperolehi daripada kajian kes menunjukkan pancutan aliran udara yang agak panjang pada sudut bilah 0o melalui peresap berkapasiti tinggi. Berdasarkan keputusan di atas, sistem hibrid VRF-SV didapati sebagai pengganti cekap tenaga untuk sistem ACMV konvensional untuk bangunan tropika.

Kata Kunci: Sistem pengudaraan stratum bersepadu VRF, pengiraan dinamik bendalir, bangunan tropika, keselesaan terma, analisis tenaga

ACKNOWLEDGEMENTS

Thanks to ALLAH Almighty who has showered his blessings upon me and enabled me to accomplish such an uphill task.

It is the matter of great pleasure to acknowledge my deepest thanks and gratitude to my supervisor, Professor Ir. Dr. Yau Yat Huang for suggesting the topic of this research, for providing invaluable advice, and supportive encouragement throughout this research work. It is really a great honor for me to work under him.

Besides my supervisor, I would like to acknowledge the Higher Education Commission, Pakistan, who provided me the opportunity and financial assistance for conducting my PhD research work at the Department of Mechanical Engineering, University of Malaya. Thanks, are also extended to the University of Malaya, Malaysia, for providing resources and facilities necessary to accomplish my research work. In addition, special thanks are extended to PrudentAire Engineering Sdn Bhd and Daikin R&D Sdn Bhd for their contributions in conducting the experimental work in this project.

My sincere thanks and appreciation also goes to Dr. Wai Meng Chin of DAIKIN Malaysia, Mr. Kai Sin Poh of Hisense HVAC, Mr. Veer Munirathinam of Prudent Aire Engineering for their technical support throughout this research work. My special thanks are extended to Mr. Le Viet Vu, design engineer at Prudent Aire, Mr. Amir Roslan, Postgraduate research student for their continuous assistance during the research work.

Last but not the least, I am also deeply thankful to my family: my dear parents, my beloved wife, my sweetest sons and rest of the family members and friends for their cheerful encouragement and spiritual support while carrying out this research work.

TABLE OF CONTENTS

LIST OF FIGURES

LIST OF TABLES

LIST OF SYMBOLS AND ABBREVIATIONS

ABBREVIATIONS

AC	:	Air-conditioning
ACMV	:	Air conditioning and mechanical ventilation
ADPI	:	Air distribution performance index
AHU	:	Air handling unit
ASHRAE	:	American Society of Heating, Refrigerating and Air-Conditioning Engineers
ASTDs	:	Air supply terminal devices
BC	:	Boundary conditions
BG	:	Bar grille
BMI	:	Body mass index
BSA	:	Body surface area (m^2)
CAV	:	Constant air volume
CFD	:	Computational fluid dynamics
CFM	:	Cubic feet per minute (ft^3/min)
CMH	:	Cubic meter per hour (m^3/h)
COP	:	Coefficient of performance
DBT	:	Dry bulb temperature (^oC)
DDG	:	Double deflection grille
DLD	:	Drum louver diffuser
DOAS	:	Dedicated outdoor air system
DPT	:	Dew point temperature (^oC)
DV	:	Displacement ventilation
DX	:	Direct expansion
EA	:	Exhaust air

EDT	:	Effective draft temperature
EUC	:	Energy utilization coefficient
EW	:	Enthalpy wheel
FAP	:	Fresh air processor
FCU	:	Fan coil unit
HCLSD	:	High capacity linear slot diffuser
HVAC	:	Heating, ventilation, and air conditioning
IAQ	:	Indoor air quality
IU	:	Indoor unit
JSD	:	Jet slot diffuser
MV	:	Mixing ventilation
OU	:	Outdoor unit
PPD	:	Percentage of people dissatisfied
PMV	:	Predicted mean vote
PPM	:	Parts per million
RA	:	Return air
Re A	:	Recirculated air
RH	:	Relative humidity
RN	:	Re-Normalization group
HP	:	Horse power
HR	:	Humidity Ratio
RNG	:	Re-Normalization Group
SA	:	Supply air
SV	:	Stratum ventilation
SW	:	Sensible wheel
TC	:	Thermal comfort

TCV	:	Thermal comfort vote
TMY	:	Typical mean year
TSV	:	Thermal sensation vote
UDF	:	User defined function
URF	:	Under relaxation factor
VAV	:	Variable air volume
VRF	:	Variable refrigerant flow
VSD	:	Variable speed drives
WBT	:	Wet bulb temperature

UNITS / SYMBOLS

cc	:	Cooling coil
C_p	:	Specific heat at constant pressure
E	:	Total energy
F	:	Body forces
h	:	Specific enthalpy
k	:	Turbulent kinetic energy
l/s	:	Liter per second
m	:	Meter
mm	:	Millimeter
m/s	:	Meter per second
Pa	:	Pascal
Q	:	Heat load
σ	:	Normal stress
τ	:	Shear stress
ε	:	Dissipation of turbulent kinetic energy
η	:	Ventilation effectiveness

W	:	Humidity ratio
ω	:	Dissipation of turbulent kinetic energy into internal thermal energy
V_0	:	Outdoor air for ventilation
φ	:	Energy dissipation
ʎ	:	Bulk viscosity coefficient
ρ	:	Density
t	:	Time
u	:	Velocity in X-direction
v	:	Velocity in Y-direction
w	:	Velocity in Z-direction
x	:	Coordinate and distance
y	:	Coordinate and distance
z	:	Coordinate and distance

LIST OF APPENDICES

CHAPTER 1: INTRODUCTION

1.1 Research Background

1.1.1 World Energy Situation

According to a comprehensive report published by the World Energy Council (WEC, 2013), the worldwide energy generation would increase between 123% to 150% by 2050, if the current trends continue. Therefore, improving energy efficiency and lowering energy demand are commonly regarded as the most cheapest, promising and fastest ways to combat with the climate change implications (Sorrell, 2015).

Malaysia, being one of the signatory countries of the Kyoto Protocol, pledged to adopt regulations to reduce excessive carbon emissions. As a result, Malaysia is strictly implementing the energy policies to reduce energy use and minimize the environmental impacts. Furthermore, the country's energy policies have emphasized on energy efficient system designs and renewable energy powered applications.

1.1.2 Energy in Building Sector

The substantial development in building sector has resulted in an increase in worldwide energy demand. Buildings account for over 40% of the total global annual energy use, and the total energy demand in buildings is expected to rise by 45% in 2025 (Bakker, 2013).

Buildings are responsible for over 30% of the total primary energy supply in the Southeast Asian region. This is due to the dominating use of the air conditioning systems to provide space cooling for the building's occupants in the hot and humid environment of the tropics. The energy breakdown of the typical buildings in the tropics and the ACMV systems used in such buildings are presented in Figure 1.1 and Figure 1.2, respectively.

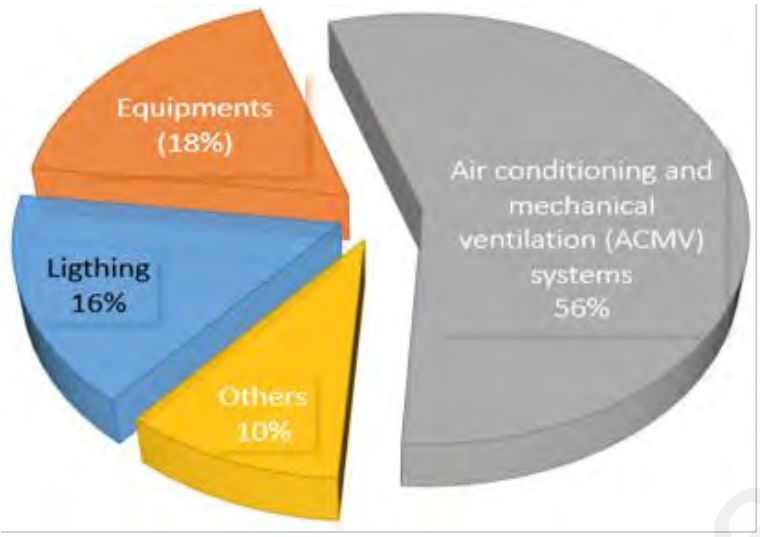

Figure 1.1: Energy breakdown in typical buildings in the tropics (Katili et al., 2015)

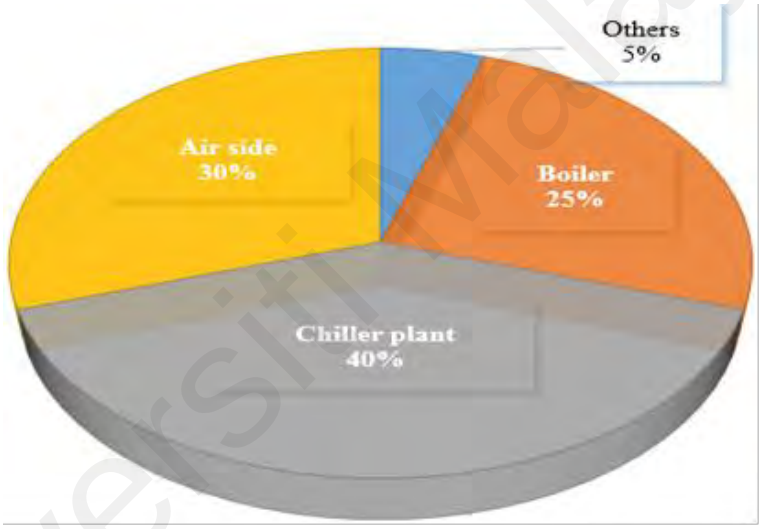

Figure 1.2: Energy breakdown of the ACMV systems in typical buildings (Katili et al., 2015)

Energy-intensive chiller based vapour compression ACMV systems account for more than 50% of the energy consumed in buildings, rising to 80% at peak times (Ahmadzadehtalatapeh, 2011; Saber, Tham, & Leibundgut, 2016). These are considered as the most common and largely used air conditioning technology installed in buildings. This technology is popular because it has good performance stability, a long functional life, and is simple to regulate. It does, however, consume a lot of electricity as well as require a large space for the system installation (Katili, Boukhanouf, & Wilson, 2015). The component wise energy use of the entire chiller plant is shown in Figure 1.3.

Furthermore, in hot and humid tropical climate, ACMV systems need to handle the indoor air humidity by lowering the air temperature below the dew point temperature, resulting in temperatures that are much lower than required, thus wasting energy even more.

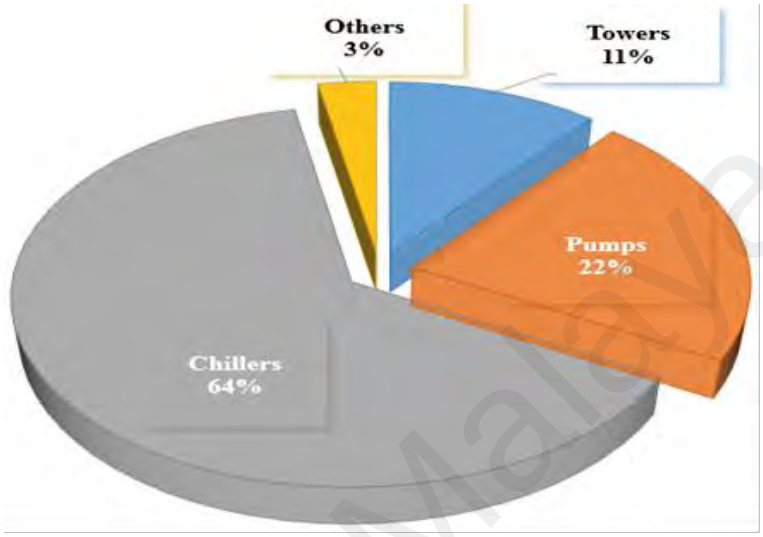

Figure 1.3: Component wise energy use of the entire chiller plant (Katili et al., 2015)

The general distribution of energy use in building sector in Malaysia is shown in Table 1.1. In commercial building such as offices and shopping malls, more than 90% of the energy is consumed by only ACMV systems and lighting applications (Ahmadzadehtalatapeh, 2011). Therefore, it is obvious to take energy efficiency measures by implementation of energy recovery technologies for high demand applications.

Table 1.1: Energy consumption distribution in the Malaysian buildings (%)

	Lighting	Air-Conditioning	Total
Residential Buildings	25.3	8.3	33.6
Hotels	18	38.5	56.5
Shopping Malls	51.9	44.9	96.8
Office Buildings	42.5	51.8	94.3

This data indicates that there is a huge need and opportunity for energy-saving measures in Malaysian buildings. A substantial amount of energy can be saved by implementing energy-efficient solutions. Moreover, the operating energy cost of the ACMV systems accounts for more than half of the entire energy bill. Therefore, a considerable amount of energy can be saved with the dvelopment in efficient ACMV system designs.

1.1.3 Air Conditioning in Large Tropical Buildings

The current economic stability and developing modern urbanization in several tropical countries like Malaysia, Brunei and Singapore have pushed the population to live and work in modern style, tightly packed high rise buildings. Due to uncomfortable outside thermal conditions, the air conditioning and mechanical ventilation (ACMV) systems have become the crucial part of such buildings.

On the other hand, the exigency towards more energy conservation and improved indoor air quality is also being critically considered in Air conditioning and mechanical ventilation (ACMV) systems' designing, specifically for large buildings. Mechanical ventilation and air distribution methods are important in buildings for indoor thermal environments and air quality. Effective distribution of airflow for indoor built environments with the aim of simultaneously offsetting thermal and ventilation loads in an energy efficient manner has been the research focus in the past several decades (Yang et al., 2019). The ACMV system typically combines an air conditioning system that removes the excess heat from the air in the room and the ventilation system replaces the contaminated air with fresh air to provide better indoor air quality (IAQ) (T. Yao & Z. Lin, 2014a). The two systems account for more than 60% of the overall energy utilization in buildings (Department of Energy, 2015). Many countries have adopted several techniques to cope with the energy needs of these systems (Zheng et al.,

2018). The traditional ACMV systems commonly used in tropical buildings are the central all-air systems, which uses a central chiller plant to supply chilled water to air handling units, that serve multiple thermal zones. Variable or constant air volume (VAV/CAV) systems regulated by user-controlled thermostat control the flowrate of the supply air which maintains the desire temperature in each thermal zone (Saber et al., 2016). The main drawback of these chiller based ACMV systems is that, they consumes enormous amount of energy. Therefore, a lot of development in the design and control strategies of energy efficient ACMV systems for tropical buildings have been made in recent years (Azad et al., 2018; Chiang, Wang, & Huang, 2012; Saber et al., 2016; Hua Yin et al., 2020).

In order to fulfill the individual thermal comfort requirments, a VRF system was introduced in more than thirty-five years ago as a viable substitute of the traditional central air conditioning systems. Since its introduction into the global HVAC arcade, the VRF system is being used in almost 1/2 of the medium-size and around 1/3 of the large commercial buildings (Goetzler, 2017; Park, Yun, & Kim, 2017; Yonghua Zhu, Xinqiao Jin, Zhimin Du, Xing Fang, & Fan, 2014; R. Zhang, Sun, Hong, Yura, & Hinokuma, 2018). The detailed hierarchy of the central HVAC systems is presented in Figure 1.4.

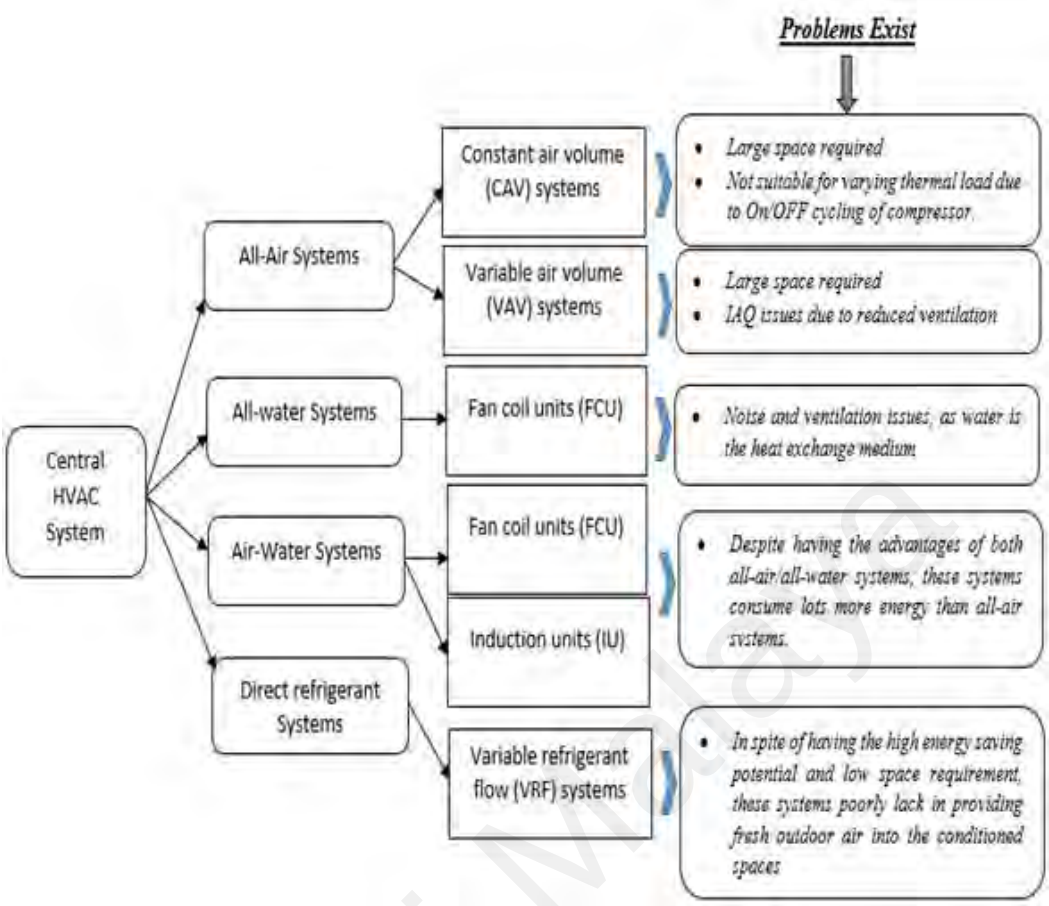

Figure 1.4: Hierarchy of the central HVAC systems

1.1.4 Ventilation Air Distribution in Large Tropical Buildings

Ventilation air distribution is an important factor need to be considered for energy efficient buildings. Uniform air distribution contributes to improve indoor air quality, which significantly affects the well-being of the occupants and improve the living quality and work productivity (Giama, 2022). Various ways of room air distribution have been developed and adopted in different types of buildings, such as shopping malls, atriums, railway stations and offices (Hua Yin et al., 2020). Some of the conventional methods are still used in buildings, such as mixing ventilation (MV) and under floor air distribution (UFAD) (Yau, K. S. Poh, & A. Badarudin, 2018). However, new air distribution strategies are currently being implemented for evaluation in wider applications, such as the impinging jets (IJ) and the confluent jets (CJ) air distribution systems (Awbi, 2015). Despite recent breakthroughs in building ventilation, complaints

about poor indoor air quality have significantly increased in recent years. In order to satisfy building occupants and meet new building energy requirements, it is necessary to examine existing building ventilation methods and design ventilation systems capable of providing high IAQ in energy efficient manner. For this purpose, the unconventional room air distribution methods must be encouraged in buildings to deal with the IAQ and thermal comfort issues (Awbi, 2015).

1.2 Formulation of Problem

To address the ventilation deficiency, the VRF systems have been integrated with different mechanical ventilation systems for complete ACMV solutions for buildings (Aynur, Hwang, & Radermacher, 2010b; Laughman, Bortoff, & Qiao, 2018; Wan, Cao, Hwang, & Oh, 2020). Most of the studies adopted decouple design integration for independent control of temperature and humidity, particularly under hot and humid climates (Yonghua Zhu et al., 2014; Zhao, Jianbo, Haizhao, & Lingchuang, 2017). Some designs incorporated outdoor air processing systems (W. Kim, Jeon, & Kim, 2016), whilst the systems designed for moderate or cold climates used energy recovery ventilators for fresh air ventilation (Aynur, Hwang, & Radermacher, 2008a).

However, several issues in adopting these systems still exist, such as higher initial cost, complex integrated control, and the lack of fresh air provision for ventilation (Goetzler, 2017; Park et al., 2017; K. Yu, Cao, & Liu, 2017). To provide an adequately dehumidified fresh air for ventilation, Aynur et al. (Aynur, Hwang, & Radermacher, 2010a) integrated an innovative vapour compression heat pump (HP) desiccant system with the VRF system. The integration proofed to provide significant energy savings, enhanced IAQ and improved thermal comfort. Yonghua Zhu et al. (2014) accommodated the VRF system with the variable air volume (VAV) controlled outdoor air processing (OAP) unit. The results showed a substantial reduction in the combined

system's energy consumption without sacrificing thermal comfort and IAQ. Having observed significant leverage over all other ACMV systems, the HVAC industry, yet inconvenient with the integration and the obscured control configuration of the ventilation integrated VRF system due to higher capital cost, benightedness with the advance technology and most importantly by the safety issues associated with indoor refrigerant leakage. Therefore, research in the integration of the VRF system with a separate mechanical ventilation system is required to be carried out to provide a suitable ACMV system for large buildings in the tropics.

1.3 Research Aims and Objectives

The first aim of this study is to design the stratum ventilation integrated variable refrigerant flow (VRF) system for large tropical buildings considering multiple design choices. The second aim is to investigate the performance of different configurations of the designed system in terms of thermal comfort and indoor airflow pattern. It is anticipated that analyzing the different design configurations will further improve the realization of getting suitable ACMV system for tropical buildings.

The third aim is to explore the most efficient air supply terminals which can throw and diffuse the air to a large distance, since the integrated design uses stratum ventilation system for room air distribution. The fourth aim is to carry out the annual energy use analyses of the hybrid system when installed in a large tropical building. Hence, the design could be made fully adoptable for practical use if all the targets set in this research are achieved.

The following scopes were set to accomplish the desired goal of this study:

1. To integrate the stratum ventilation (SV) air distribution with the variable refrigerant flow (VRF) system and to

2. investigate the performance of different design configurations of the combined system using CFD simulations and experimentations.
3. To optimize the performance of VRF-SV hybrid system using different types of air supply terminal devices.
4. To develop and validate a simplified nodal model for prediction of vertical temperature profile in a large application installed with VRF-SV hybrid system and to evaluate the energy use analyses of the hybrid system using TRNSYS.
5. To evaluate the ventilation air distribution performance of the HCLSD in a large tropical atrium (case study).

1.4 Significance of the Study

The findings and conclusions of this research work will contribute to the following:

- The VRF system was successfully integrated with the stratum ventilation system using two-wheels configured DOAS system for a large tropical building (i.e., retail shop). The hybrid system could be used in tropical buildings as an energy efficient alternative of the conventional all air system.
- A detailed design guidelines of the VRF-SV hybrid system with coupled, decoupled, and fully integrated design approaches were successfully developed. The guidelines will help the design engineers to construct the integrated system which combines the VRF system with different mechanical ventilation systems.
- The air distribution and thermal comfort performance of the VRF-SV hybrid system under different design configurations were numerically evaluated. The findings revealed a good potential of the fully integrated design of this hybrid system in large tropical buildings.
- The performance of the hybrid system was optimized by investigating five air supply terminal devices (ASTDs), including bar grille, double deflection grille, jet

slot, perforated and drum louver diffusers. The findings of this study will help the building services engineers to select the most suitable ASTD for ACMV systems.

- The energy audit was performed for the VRF-SV hybrid system (decoupled and fully-integrated designs) and their annual energy consumption in the retail shop building was compared with the VRF only and multi-split type AC system. The results suggest that the VRF-SV hybrid system can saves more energy when compared with the VRF or split type air conditioning systems.
- The performance of the architecturally designed, vertically-oriented high capacity linear slot diffuser (HCLSD) in a large atrium was also studied as a part of this thesis using numerical simulations and physical experimentation. More than 33% increase in the air velocity due to the 0^{o} deflector angle of the HCLSD is noticed. Which indicates that an optimization of the diffuser design is a must for improvement in air distribution system.

1.5 Outline of the Dissertation

This thesis consists of ten chapters. The main contents of each chapter are briefly summarized as follows:

Chapter 1 is about the introduction of the research carried out. It includes the research question, aim and objectives and research significance.

Chapter 2 is the literature review of the current topic being studied. General overview of the VRF system and commonly used mechanical ventilation/air distribution methods are presented there in. It also encompasses the detailed insight of the studies involving VRF and mechanical ventilation design integration and their performances in the built environment.

Chapter 3 introduces the methodologies applied in this research which include the establishment of guidelines for designing the VRF-SV hybrid system. To enhance the broad application of the integrated design, different design approaches were presented

in this chapter. The parametric analyses were also presented to investigate the effect of varying indoor design conditions on the combined system capacity.

Chapter 4 discusses the performance evaluation of the novel system which combines the VRF system with the stratum ventilation system in six different configurations for a large retail facility. This chapter presents the series of numerical simulations conducted by employing a validated computational fluid dynamics (CFD) model to investigate the performance of the combined system in terms of temperature field distribution and airflow patterns for all the designed configurations. The experimental work performed in a scaled environmental chamber for further validation of the numerical method was also elaborated in this chapter.

Detailed thermal comfort performance of the designed system was then evaluated using standard indices. The results obtained through thermal comfort study are presented and described in Chapter 5.

Chapter 6 discusses the experimental investigations of the effects of different types of ASTDs on the performance of a novel VRF-SV hybrid system. The investigations performed in two steps. The first step was to study the impacts of top, side and bottom orientations of plenum collars on jet outflows from the ASTD. In the second step, the effects of five different types of ASTDs on the thermal comfort and air distribution performances of the VRF-SV hybrid system were investigated.

Chapter 7 is composed with the numerically investigations of the effects of different types of ASTDs on thermal comfort, indoor air quality (IAQ) and air distribution performance when installed with the novel VRF-SV hybrid system.

Chapter 8 summarizes the two studies, the first was to develop the simplified nodal model of the VRF-SV hybrid system when installed in a large retail shop in the tropics. The second was to develop the TRNSYS simulation model of the VRF-SV hybrid system and to compare the annual energy consumption of the fully integrated and

decoupled design configuration of the hybrid system with multi-split AC systems and standalone VRF systems.

In the last part of this research and as a case study, the evaluation of the performance of architecturally designed, vertical oriented, high capacity linear slot diffuser (HCLSD) under a low-level wall mounted air distribution system in the atrium building is presented. To avoid the computational complexities in using the actual atrium model, a simplified model of the atrium building was initially developed and the verification and validation of the commonly used turbulence models were performed against experimental data. The results of this study is discussed in Chapter 9.

Chapter 10 concludes the findings obtained from all the studies and their significance, as well as discussion on some recommendations for future research.

CHAPTER 2: LITERATURE REVIEW

2.1 Introduction

Statistics indicated that 30% of the global generated power is consumed by the building sector only, while ACMV systems being the biggest contributor in buildings energy consumption which take half of that share. The increasing demand for energy to operate ACMV systems in buildings has made the engineers realized the improvement in the design of the energy-efficient HVAC systems without compromising the IAQ and thermal comfort. In response to that, many strategies have been developed and investigated for the built environment.

A variable refrigerant flow (VRF) system was introduced more than thirty-five years ago as an energy-efficient substitute for conventional air conditioning systems. Studies reported the VRF system as more energy-efficient among all ACMV systems due to the part-load performance and individualized temperature control features (Zhou, Wu, Wang, & Shiochi, 2007). As the indoor units in VRF system are directly connected to the outdoor unit by refrigerant lines, it lacks in providing fresh outdoor air for ventilation into the conditioned environment (Aynur et al., 2010b). Significant work has been carried out on VRF systems in the last 20 years, covering almost every aspect of the system from system configuration to its development in terms of components, performance, technology and applications.

In order to address the ventilation deficiency, the VRF systems have been integrated with different mechanical ventilation systems for complete ACMV solutions for buildings (Aynur et al., 2010b; Laughman et al., 2018; Wan et al., 2020). Most of the studies adopted decouple design integration for independent control of temperature and humidity, particularly under hot and humid climates (Yonghua Zhu et al., 2014; Zhao et al., 2017). Some designs incorporated outdoor air processing systems (Electric, 2018;

W. Kim et al., 2016), whilst the systems designed for moderate or cold climates used energy recovery ventilators for fresh air ventilation (Aynur, Hwang, & Radermacher, 2008b; Shaik Gulam Abul Hasan, Syeda Saniya Fatima, & Kumar, 2015). Thus, a comprehensive review of all those studies involving integration of the VRF system with different ventilation systems can explore the opportunities for further improvement in the design and performance of the combined system.

No review study is known to have combined and compared the design integration of VRF and ventilation systems. Therefore, this review chapter is written to bridge this knowledge gap. This chapter is broadly structured into five sections. The introduction is given in Section 1. Section 2 highlights the thermal comfort standards and criteria for buildings under different climates. Section 3 provides a brief overview of the VRF system, its applications, prospects and challenges. Mechanical ventilation systems and air distribution design are contrastively discussed in section 4. In section 5, the past ten years studies on the design integration, performance evaluation and energy utilization of the VRF and ventilation combined systems are critically reviewed. Concluding remarks are also presented at the end.

2.2 Thermal Comfort

Realizing thermal comfort is not only imperative in designing buildings, but also plays a decisive role in formulating the complete air conditioning and ventilation solutions for buildings' occupants. Thermal comfort is such a condition of mind, which indicates pleasure of indulgence with the thermal settings (Raish). Due to its adaptability, thermal comfort criteria vary with persons, places, and climates (Nicol & Roaf, 2017).

Macpherson (Macpherson, 1973) has characterized six variables, which influence thermal sensation. These variables are ambient temperature, mean radiant temperature,

relative humidity, air motion, clothing insulation and metabolic rate. The understanding of these variables is foremost in making a decision when planning, selecting or designing an air conditioning and ventilation system for indoor environment (Raish). In ASHRAE standard 55-2020 (ASHRAE, 2020), the thermal comfort requirements for large commercial buildings are mentioned as in Table 2.1.

Table 2.1: Factors to be considered for buildings' thermal comfort

Temperature	Humidity	Clothing Insulation	Air Velocity	Metabolic Rate
The allowable temperature gradient between head and ankle ≤ 5.4F	Dew point temperature < 62.2	Depends upon operative temperature	<50FPM (cooling) <30FPM (heating)	1.0 (sedentary) to 1.3 (casual movement).

Thermal comfort analyses have been carried out in different types of environments (e.g. indoor, outdoor or semi-outdoor) (Hirashima, Katzschner, Ferreira, Assis, & Katzschner, 2018; Shang, Huang, Zhang, & Chen, 2019; Sookchaiya, Monyakul, & Thepa, 2010). If we look only at the indoor thermal comfort, the modern researches focus on two main approaches. The first approach is based on the model of heat balance in the air-conditioned spaces developed by Fanger in 1970s (Fanger, 1970). Fanger's approach predicts the percentage of dissatisfaction with the thermal settings and the mean vote of a group of people, asserted by the Predicted Mean Vote-Predicted Percentage Dissatisfied (PMV-PPD) index (Fanger, 1970). This approach is also adopted by the international standards in thermal comfort design guidelines for prescribing the ideal thermal comfort for buildings (55-2004, 2004; CR-1752, 1999; EN-15251, 2006; "International Standard Organization (ISO-7730) -Ergonomics of the thermal environment," 2005).

The second approach is the adaptive model, developed after De dear and Brager (Brager & de Dear, 1998) challenged the universal applicability of previously formulated standards (based on Fanger's model). The adaptive approach states that, people react differently to restore their comfort when there are variations occur that cause discomfort (Fergus Nicol, Michael Humphreys, & Susan Roaf, 2012; RJ & GS, 2002). These variations in indoor thermal comfort exist due to change in seasons, culture and climates (Nicol & Roaf, 2017). According to Nicole et al. (1999), 90% of Japanese feel comfortable in an indoor environment with a temperature range of 18ºC to 28ºC, whereas for office workers in Pakistan is 21-30ºC. The literature reveals that, different acceptable temperature ranges in different regions heavily rely upon the individual's liberty to alter the condition such as the provision to change clothing or activity. However, in commercial buildings, it is not possible for office workers to change the activity level or clothing type according to their local thermal environment. The thermal neutral sensation for different countries represents different climatic zones is presented in Figure 2.1.

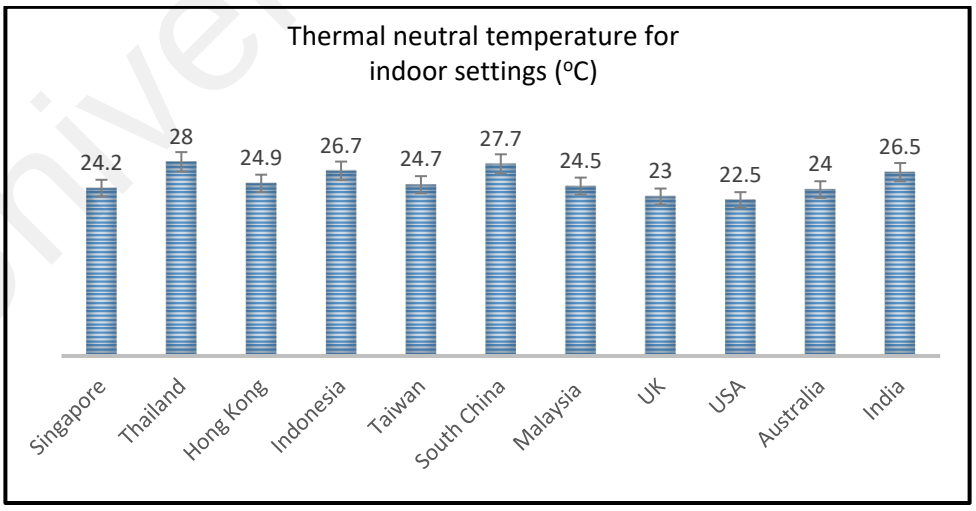

Figure 2.1: Thermal neutral temperature for countries under different climates

2.2.1 Thermal Comfort Studies in Different Climates

Different parts of the world have different climatic conditions (Felix & Elsamahy, 2017). These climates have very strong influence on the human thermal comfort

(Hirashima et al., 2018). The simple classification divides the whole world into six climate zones, which includes, Equatorial (tropical), Arid (desert/subtropical), Mediterranean (hot/dry summer & cool winter), Snow (hard winter), Polar (coldest), and Temperate (moderate climate) (Köppen, 2012).

The tropical climatic regions are distinguished as extreme rainfall, ample sunshine, and highly humid. These features of tropical climate have an adverse impact on the building's thermal environment (Jamaludin, Mohammed, Khamidi, & Wahab, 2015). Many studies have been conducted on thermal comfort assessment using mechanical/natural control of indoor environments under different climatic conditions (Daghigh, 2015; Mallick, 1996; Rupp, Vásquez, & Lamberts, 2015). Humphreys and Hancock (2007) reviewed 36 studies under a variety of climates and found a statistical dependency of thermal neutrality on mean indoor temperature. These studies support the hypothesis that the people in a naturally controlled environment are less sensitive to indoor temperature change than those in air conditioning (Dennis, 2017). Another field investigation by Dear et al., (1991) in a multi-story building in Singapore highlighted that the indoor climates of naturally ventilated spaces do not satisfy the ISO standards and caused thermal discomfort to the occupants. A field study in Thailand suggested the room temperature of 26ºC, RH at 50-60% and the air movement of 0.2 m/s with clothing 0.5 clo are the conditions of thermal comfort standard for air conditioned spaces (Yamtraipat, Khedari, & Hirunlabh, 2005). A study of office environment in Hong Kong on Chinese sedentary subjects found the neutral temperature around 25.4ºC with clothing insulation 0.55 clo, air speed 0.2 m/s and metabolic rate of 1 met (Chow, Fong, Givoni, Lin, & Chan, 2010). The distinct values of thermal comfort parameters for air conditioned environments under a variety of climatic conditions are presented in Table A.1 in Appendix A.

Ricciardi and Buratti (2012) conducted a comparison test for actual (sensational) and predicted (Fanger's model) thermal comfort in a controlled office environment in Italy. They found a weak relation between both and concluded that, it is due to the lack of adaptive thermal control, low air movement and thermal dissatisfaction due to high thermal gradient between head and foot levels. In a similar study performed in Singapore found overcooling as the main reason for weak correlation. The occupants preferred elevated operative temperatures (A. Chen & Chang, 2012). In another study, conducted under ASHRAE comfort range (ASHRAE, 2010) in 20 office buildings in the US (Choi, Loftness, & Aziz, 2012), the authors recommended a 2^{o}C raise in summer indoor temperatures for improved thermal satisfaction by the occupants.

2.3 Overview of the Variable Refrigerant Flow (VRF) System

VRF systems are large capacity variants of ductless multi-split AC systems. They consist of an outdoor unit containing one or more variable speed inverter/stepped compressors, condenser, accumulator, receiver, expansion device and controls, connected to a variety of indoor units containing a fan, evaporator, expansion device and controls (Olanrewaju et al., 2019). At least two indoor units (at most 64 (Goetzler, 2017)) and one outdoor unit and a remote or central controller are included with each VRF system (Olanrewaju et al., 2019). The outdoor unit and multiple indoor units are connected directly through refrigerant lines (Goetzler, 2017; Zhai & Rivas, 2018), as illustrated in Figure 2.2. Due to demand-controlled capacity and flexibility in adjusting the refrigerant volume, VRF system has become a hot choice in many European countries. It has also been widely adopted by several Asian countries (D. Kim, Cox, Cho, & Im, 2018), but still new in Southeast Asian countries (Suhafizudin Bin Zainal Anuar, Mohamad Suhaimi Bin Yahaya, Jusnan Bin Hasim, Suhilah Binti Mohd Ali, & Shamsuddin, 2016). Since its emergence in japan in 1982 by the trademark name VRV, this system is being used in almost 50% of the medium-size and around 30% of the

large-size commercial buildings (Goetzler, 2017). In the open literature the VRF/VRV is also called multi-split VRF (Z. Li et al., 2017), multi-evaporator AC system (Elliott & Rasmussen, 2013). The VRF systems are broadly sorted by their capability of attending a heat recovery function among IUs, and with this primary difference, they are named as the heat pump type VRF (i.e. HP VRF, two pipe system) and the heat recovery type VRF (i.e. HRVRF, three pipe system) (X. Lin, Lee, Hwang, & Radermacher, 2015). The VRF system utilizes the second most efficient refrigerant after ammonia, R410A (Saab, Al Quabeh, & Hassan Ali, 2018). A recent study (Devecioğlu & Oruç, 2020) conducted using R466A refrigerant in the VRF system recommended its use over R410A, as it provides higher COP. The ability of supplying the refrigerant at varying rate according to heating and/or cooling load not only enables the system to use different capacities of indoor units in combination with single outdoor unit, but also addresses the issue of having separate control of the thermal environment to each zone, concurrent heating and cooling in different zones of the same building (N.Aynur, 2010).

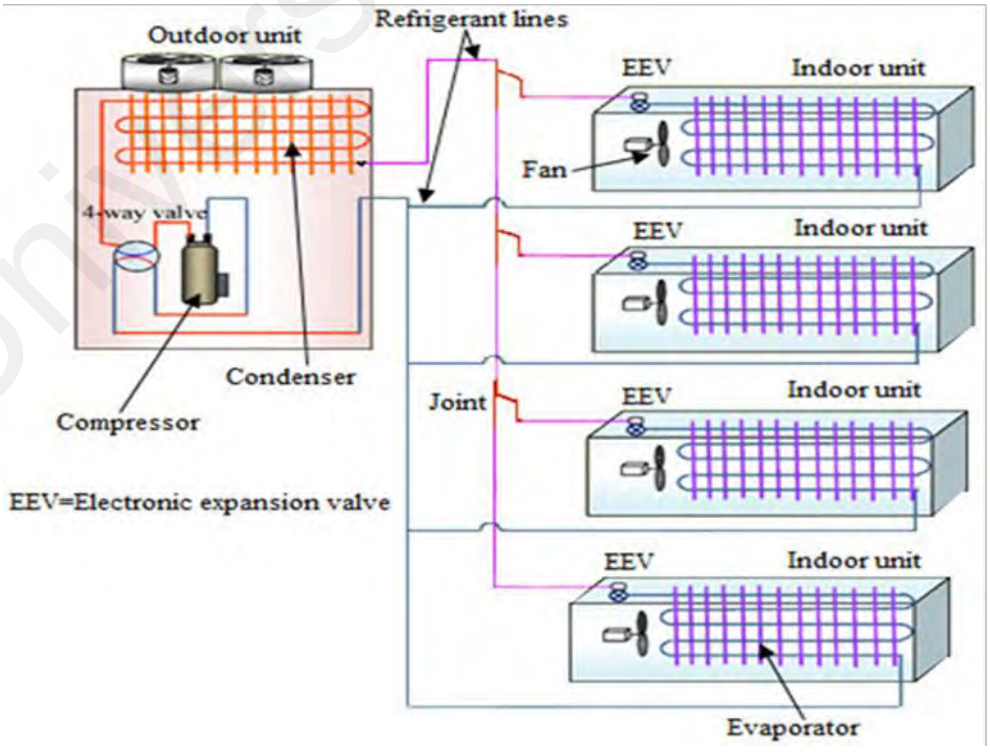

Figure 2.2: Design schematic of a typical VRF system (Modified based on reference (Devecioğlu & Oruç, 2020))

2.3.1 Application of the VRF System

The VRF system is undoubtedly an efficient and time demanding alternative to the centralized HVAC systems globally due to many reasons, such as less space required for installation, best under part load operation and zone-wise temperature control. In a recent study conducted by Alahmer and Alsaqoor (2018) in a hotel in Amman, Jordan, found that the VRF could be the best option, especially in small rooms due to its part-load energy efficiency. The VRF system is a good substitute of conventional central AC systems in areas where scarcity of water and/or space is dreadfully high. Since its inception into the world's HVAC market, the engineers are looking for its wide application in high performance buildings (Goetzler, 2017; Saab et al., 2018; Zhu, Jin, Du, Fang, & Fan, 2014). As no ductwork is required, the VRF systems can also be installed in the existing buildings by minor retrofitting (III, 2017).

2.3.2 Prospects and Challenges of the VRF System

Due to the part-load attainment, the VRF system has potential to save a huge amount of energy (about 30% or higher compared to the other HVAC systems (Suhafizudin Bin Zainal Anuar et al., 2016), thus, reduces the carbon emission (Afify, 2008). This promising feature may lead the employer to become a hot candidate for LEED certification (Lojuntin, 2017). An important aspect of the VRF system is its simultaneous accomplishment of the heating and cooling loads by heat recovery via 3-pipe design (Zhai & Rivas, 2018). The noise level of the VRF system is also very low, which makes it suitable to operate in the night or in a quiet office environment (Suhafizudin Bin Zainal Anuar et al., 2016). Unlike through ducts in the conventional central AC systems, the VRF system provides sensible cooling or heating to each zone through refrigerant lines, which makes it ideal to be installed in structures where the ductwork is arduous and costly (Zhai & Rivas, 2018). Note that the maintenance, operation and commissioning costs for the VRF systems are lower than that of the

standard chilled water systems. Besides these key advantages, a heavy transportation is also not needed in shifting the components of the VRF system from one place to another, in contrast, it is must require in the case of a chiller or other conventional central air-conditioning systems (Suhafizudin Bin Zainal Anuar et al., 2016).

Apart from the benefits presented above, the VRF system comes with many shortcomings. The main barrier in installing this system with every demanding application is its higher initial cost (X. Lin et al., 2015). The long refrigerant lines with a large number of joints could result in the refrigerant leakage, which is not only difficult to diagnose, but also causes safety and repairing issues (Ammi Amarnath & Morton Blatt, 2008). The refrigerant pipe length can be a restricting factor in designing VRF systems, especially for the high-rise buildings (III, 2017). As the VRF system does not provide fresh outdoor air in conditioned spaces, a separate ventilation system is required to meet the latent load and better IAQ in the occupied zone. Hence, it certainly adds up the initial cost of the entire system.

2.4 Stratum Ventilation System

Recent high-speed growth in modern developments in the building sector accentuated the pairing of mechanical ventilation with all types of air conditioning systems to satisfy the standard thermal comfort requirements as well as the reduction in the total energy utilization of these systems. Researchers (A. Melikov, Ivanova, & Stefanova, 2012; Seppänen, 2008), pointed out that the grievances related to IAQ have increased and the indoor environmental issues associated with the tightly packed modern style buildings have become so critical in recent years.

Lin et al., (2009) in 2009, proposed stratum ventilation (SV) to cope with the elevated indoor temperature requirements implemented by Southeast Asian countries (Kam, 2006; National Development and Reform Commission (NDRC)). The fresh air in

SV is supplied directly into the occupied zone from the head level supply terminals (T. Yao & Z. Lin, 2014a, 2014b). As air is provided directly into the breathing zone, SV creates a relatively younger air layer than other ventilation methods. The logic behind the development of this novel strategy was to save the energy that consumes in maintaining the thermal comfort and IAQ beyond the breathing zone. A lot of research is being continuously carried out using the stratum ventilation in HVAC systems. Comparative studies on the SV with other ventilation strategies have also been conducted by many researchers to understand its airflow behavior under different climates and variety of spaces (Ameen, Choonya, & Cehlin, 2019; Z. LIN, 2014; Navid & Maerefat, 2015).

2.4.1 Comparison Studies with other Mechanical Ventilation Systems

Selecting an appropriate ventilation strategy with the HVAC system can improve the IAQ while reducing energy consumption. For last many years, scientists and researchers have been involved in determining the best possible ventilation solution for modern buildings. Figure 2.3 shows the schematic layout of the most common mechanical ventilation systems.

Zhou et al., (2018) performed a comparative study to investigate the performance of mixing and displacement ventilation in terms of air temperature, relative humidity, contaminant concentration and energy consumption, subjected two adjacent classrooms of a university in Australia. The results unexpectedly shown more energy consumption by the DV than the MV since the DV exhibited a better efficiency in the control of humidity and contaminant concentration.

Zhang et al., (2011) have compared the annual energy performance of the three most efficient ventilation systems using TRNSYS software in an office, a retail shop and a classroom in the sub-tropical Hong Kong. They concluded that in comparison with the

MV and DV, the stratum ventilation (SV) offered great energy saving potentials. By reducing the ventilation and transmission loads and increasing the chiller COP, the stratum ventilation can save up to 44% and 25% annual energy than mixing and displacement ventilation respectively.

Fong et al., (2015) experimentally investigated the acceptable thermal conditions and the energy use of mixing, displacement and four different configurations of stratum ventilation systems. Tests were performed in a specially designed in a medium size classroom on forty-eight college-aged human subjects. It was concluded that the stratum ventilation with inlets and outlets located at a similar height on opposite walls can satisfy human thermal comfort needs with the least value of power consumption. Table A.2 in appendix A presents the comparison of some important studies performed using aforementioned mechanical ventilation systems.

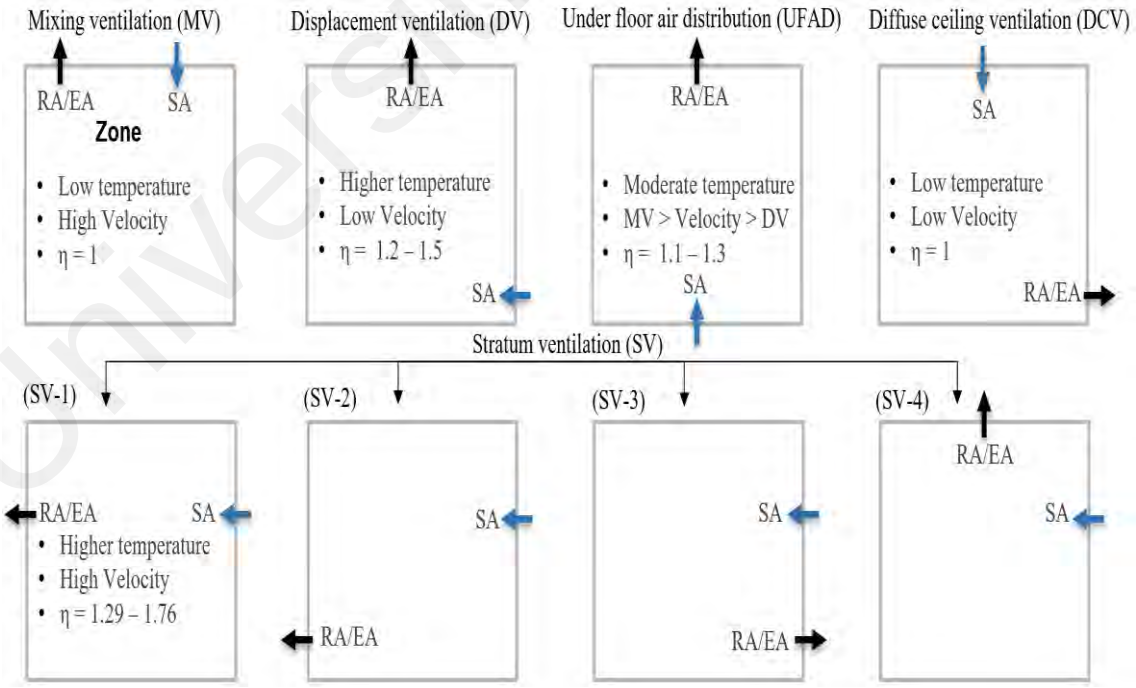

Figure 2.3: Design layout of the different mechanical ventilation systems (SA= Supply air; RA/EA= Return air/Exhaust air)

2.5 Ventilation Integrated VRF System (Combined System)

The VRF integrated mechanical ventilation systems have many advantages over existing central air conditioning systems. Several studies have been conducted on the design, control optimization and performance assessment of VRF and ventilation combined systems. The combined system with temperature and humidity independent control (THIC) is preferred in large applications in hot and humid regions, whereas the chilled ceiling or radiant cooling based on the VRF systems are mostly adopted in small-to-medium residential or commercial buildings (Zhao et al., 2017). The combination of packaged terminal air conditioner (PTAC) and VRF systems is another very popular integration solution seen today in the hospitality industry. In these solutions, PTAC units support the individual spaces, while VRF systems manage the living areas, the lobby and small offices. Integrating a VRF system with many other heating, ventilation and air-conditioning (HVAC) systems is now much simpler with the large variety of manufacturer's products and kits (Technologies, 2014). Most of the studies reviewed focused on the improvement in control methods of the combined systems due to their complex design structure and components settings.

2.5.1 Design Strategies of the Combined System

According to the ASHRAE design guide for dedicated outdoor air system (DOAS), there are broadly three methods to deliver outside air for ventilation into the conditioned environment, coupled (integrated), decoupled and direct (ASHRAE, 2015), as illustrated in Figure 2.3. Depending upon their application in different climatic conditions each of these methods come with some pros and cons.

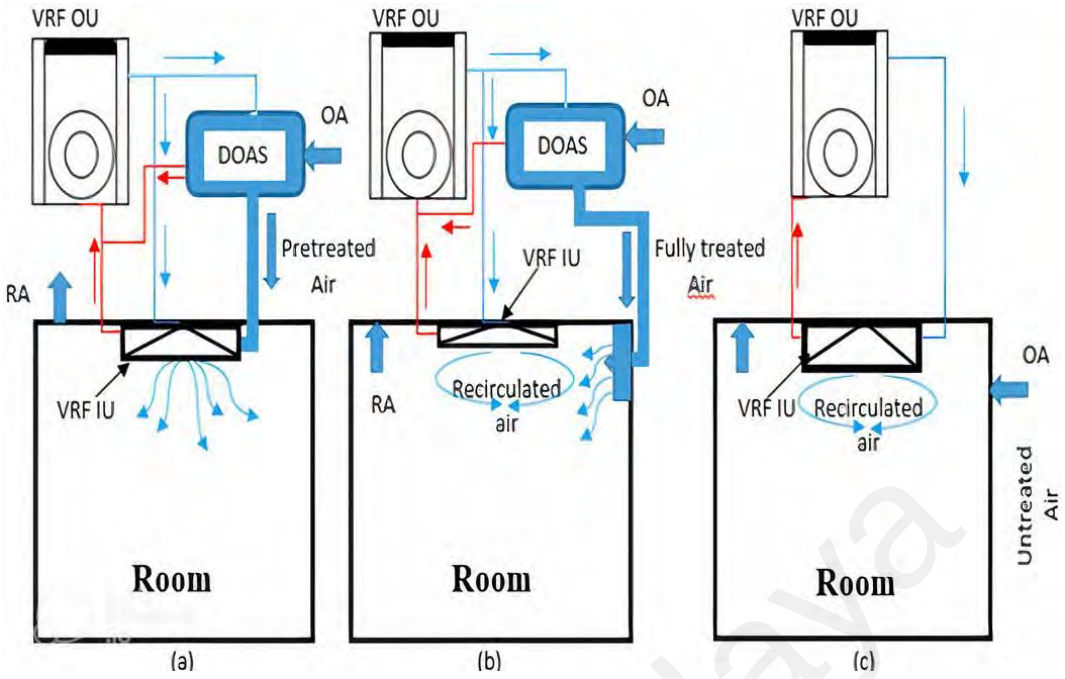

Figure 2.4: Schematic diagram of the VRF ventilation design (a) Integrated design (b) Decoupled design and (c) Direct design (RA=Return air; OA=Outdoor air) (Technologies, 2014)

2.5.1.1 Coupled/Integrated Design

In this design, the outdoor air is preconditioned through DOAS or ERV system before delivering to the occupied space. Preconditioning is done to remove both the sensible and latent load from OA. In this method, after pretreatment the air can be delivered directly to the space or into the return duct of air handler/fan coil units (Technologies, 2014). Unfortunately, not all the VRF fan coil units are structured to integrate with the direct air connection (Electric, 2018).

2.5.1.2 Decoupled Design

To supply fully treated outdoor air, this method utilizes a DOAS or air processing equipment. The conditioned outdoor air is supplied to the space through grill or diffusers. During cooling operation, the air processing unit conditions the outdoor air to the dew point temperature (saturation) lower than the desired space humidity ratio (SHR). In results, the dry and cold air if supplied to the space can partly offset the space

sensible load, which in turn reduce the terminal capacity of the indoor system (Electric, 2018). This method is recommended to be considered in design for hot and humid environment where the fresh air requirement is high.

2.5.1.3 Direct Design

This design is considered as the cheapest option available for the ventilation integration with the VRF system, as it does not require a separate air processing equipment. The untreated outdoor air directly supplies to the space through a dedicated duct. The terminal system capacity must therefore be capable enough to bear the space as well as outdoor air heating/cooling loads (ASHRAE, 2015). One negative of the direct design method is that, unconditioned outdoor air is supplied to the space, which may create thermal discomfort until the room thermostat activate the terminal heating/cooling coil (Electric, 2018). By using this method, it is also important to consider the filtration of outdoor air before supplying to the indoor space. In tropical environment this design is not recommended for ventilation integration due to humid outdoor air.

2.5.2 Combined System Design Studies

2.5.2.1 VAV Integrated VRF System

It is the integration of two most energy efficient air conditioning systems, namely VAV and VRF. Targeting the benefits of both, the combined system was investigated by many researchers (Karunakaran, Iniyan, & Goic, 2010; Yonghua Zhu et al., 2014; Zhu, Jin, Fang, & Du, 2014). The design schematic covering all the control features of the VRF-VAV combined system is shown in Figure 2.4. The VAV system, consisting outdoor air processing (OAP) unit and VAV box is basically designed to deliver better IAQ and good thermal comfort performance at reduced energy consumption and less maintenance requirements (Zhu, Jin, Du, Fan, & Fang, 2014). It cools and dehumidifies

the outdoor air through the cooling coil and the enthalpy wheel of the OAP unit (Yonghua Zhu et al., 2014). The treated air is then supplied to the indoor spaces, where the flow in each zone is controlled by VAV box. Whereas, the VRF system modulates the refrigerant flow according to the sensible load requirements of the indoor spaces/zones (Technologies, 2014). Karunakaran et al. (Karunakaran et al., 2010) proposed a VRF-VAV combined AC system to analyze the enhanced energy efficiency performance over constant air volume (CAV) AC system. The proposed design when compared with conventional AC system exhibited enthralled benefits, which makes it suitable to be installed in modern HVAC applications.

A simulation study on the combined design model is performed by Zhu et al. (2014). The results showed that the VAV system operates more dynamic than a VRF system in combined system and offers the best OA supply temperature set point to optimize the energy consumption of the combined system. Foregoing studies (Yonghua Zhu et al., 2014; Zhu, Jin, Du, Fan, et al., 2014; Zhu, Jin, Du, Fan, & Fu, 2013; Zhu, Jin, Du, Fang, et al., 2014; Zhu, Jin, Fang, et al., 2014) revealed that the integrated system could maintain the multi zone environment efficiently regardless of the variation in thermal load in each zone. It can greatly solve the ventilation shortcoming of VRF system. Moreover, this design is found suitable for both heating (Yonghua Zhu et al., 2014) and cooling (X. Yu, Yan, Sun, Hong, & Zhu, 2016) seasons. In these studies, each IU of the VRF system controlled the zonal temperatures of the multi zones, while the zones' IAQ and humidity were monitored by the treated air using the VAV system. This strategy causes over ventilation in some whilst under ventilation in other zones during attaining the significant changes in the cooling/heating loads of the conditioned spaces.

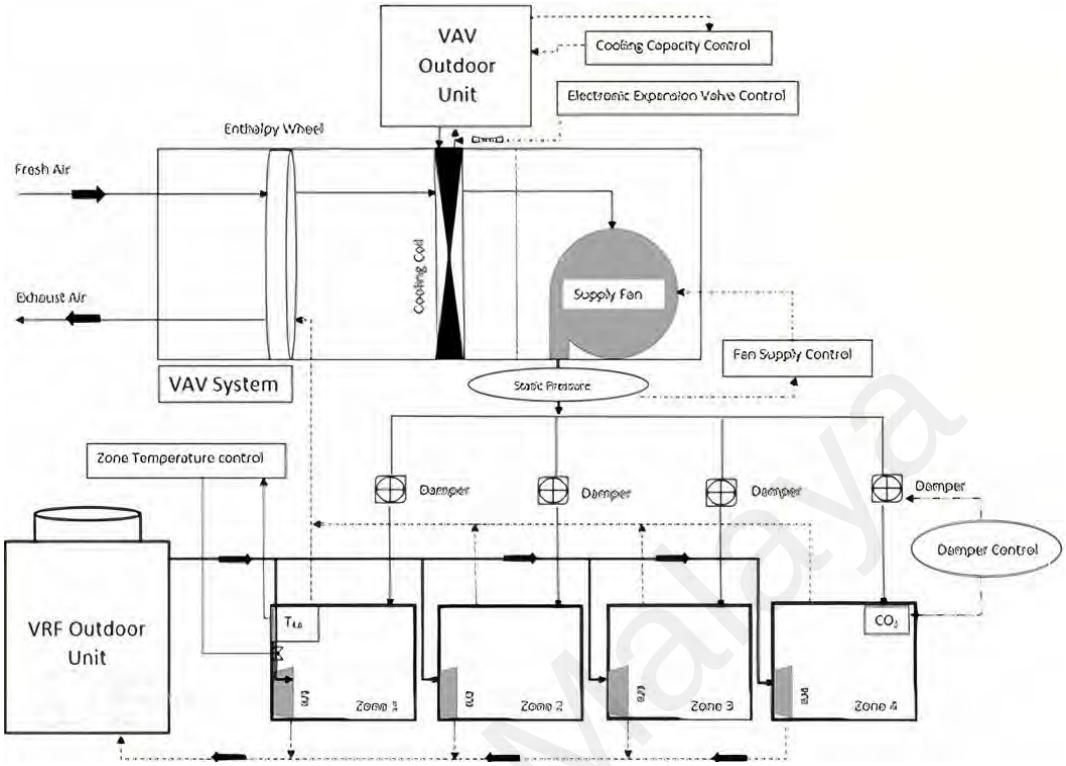

Figure 2.5: Decoupled design of VRF-VAV AC system (Modified based on references (Zhu et al., 2013; Zhu, Jin, Du, & Fang, 2015; Zhu, Jin, Fang, et al., 2014))

2.5.2.2 DOAS Integrated VRF System

The dedicated outdoor air system (DOAS) integrated VRF system was introduced to handle the sensible and latent loads separately. OA is treated standalone and makes no share with the air conditioning system in the combined strategy. It further improves the IAQ due to the more and more provision of the fresh air while limiting the energy consumption of the combined system (W. Kim et al., 2016). A simple schematic design of the VRF-DOAS combine system is shown in Figure 2.5. Unlike VRF-VAV system, DOAS in this design is used to handle the full latent load and even some portion of the sensible load of the indoor spaces by cooling and dew point dehumidification of the outdoor air. The rest of the load (sensible) is efficiently managed by the VRF indoor units (Feit, 2019; Milind Vishwanath Rane, Deepa M Vedartham, & Niranjan Bastakoti, 2016).

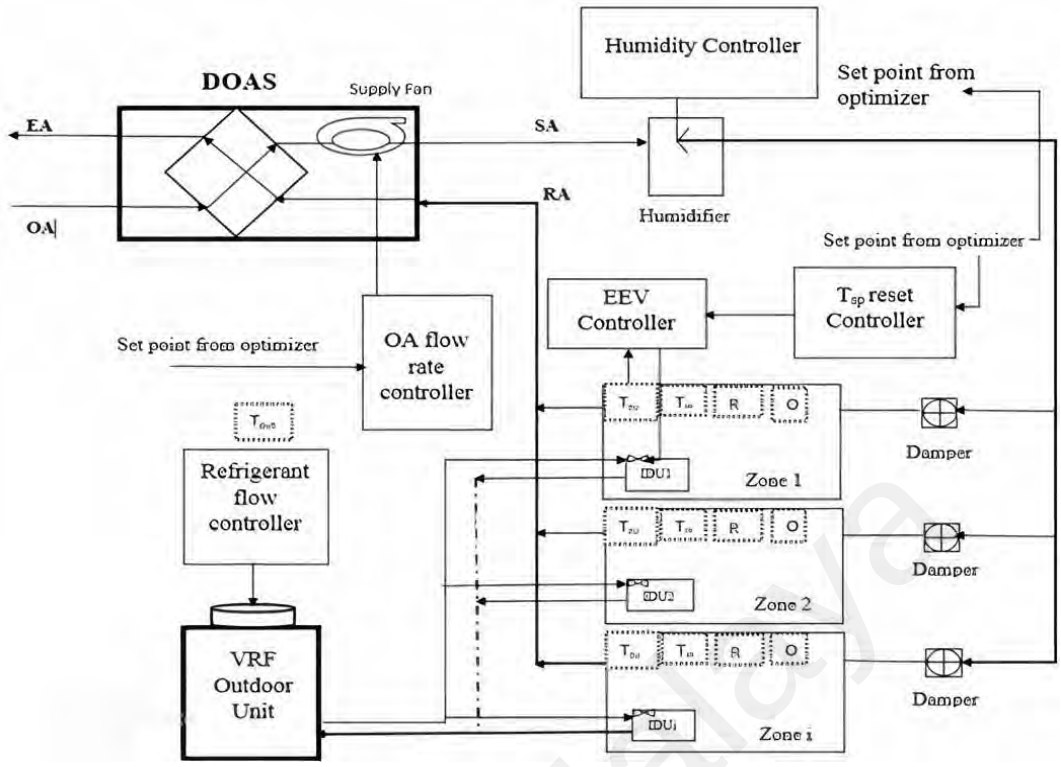

Figure 2.6: Decoupled design of VRF-DOAS AC system (Modified based on (W. Kim et al., 2016))

Kim et al., (2016) proposed an integrated design of VRF system and a DOAS system to cut down the energy cost associated with the HVAC system without sacrificing the IAQ. The system yielded a significant reduction in energy consumption with a substantial increase in the IAQ and thermal comfort. Rigorous design strategies and control methods have also been investigated to achieve the optimum performance and maximum benefits of these assorted system combinations (Laughman et al., 2018; Zhu et al., 2013; Zhu et al., 2015; Zhu, Jin, Fang, et al., 2014).

2.5.2.3 OAD Integrated VRF Radian Cooling System

The above presented combined systems are designed keeping in mind the wide application of the VRF systems for large scale high performance buildings (Electric, 2018). On the other hand, small-to-medium scale residential or office buildings are still common place for conventional chilling dehumidification systems (Han, Zhang, Wang, & Niu, 2013). To explore the combined system performance, Zhao et al., (2017) developed a novel house-hold VRF based independent temperature/humidity control

AC system for small-to-medium scale residential or office buildings. The sensible cooling in this hybrid design is provided by the radiant cooling terminal whereas, the latent load is attained by the outdoor air humidifier (OAD). Both the radian cooling system and OAD are connected to the VRF system with separate refrigerant loops. The plate type heat exchanger is adopted in this study to exchange the heat between refrigerant circuit and cooling water circuit. For better understanding, the schematic of the system is shown in Figure 2.6. This combined system provides much simpler configuration to cope with the higher latent loads in hot and humid regions, as well as enhanced IAQ and thermal comfort. The results of this study suggested promising performance of the system in applications where independent control of humidity and temperature is needed.

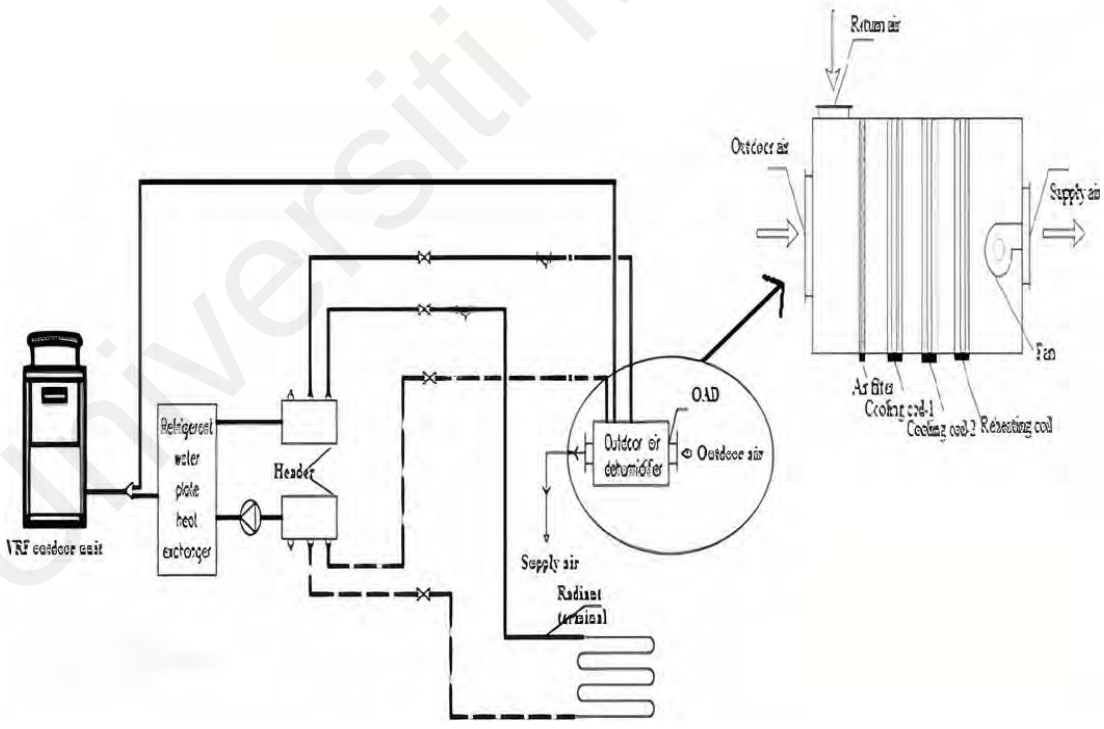

Figure 2.7: Decoupled design of OAD-VRF radiant cooling system (Modified based on reference(Zhao et al., 2017)

2.5.2.4 FAP Integrated VRF System

Fresh air processor integrated variable refrigerant flow system was initially developed by Tu et al., (2011). As a new air handling unit, the Fresh Air Processor (FAP) integrated VRF system utilized coupled design strategy for the provision of clean air, elimination of indoor air contaminants and improvement in IAQ. The characteristic of this hybrid system is that the static pressure variable can be realized by controlling the damper in the pipe. The air flow rate can therefore be adjusted to fulfill the fresh air needs of various spaces of varying sizes and distances. The simple diagram of the combine system is shown in Figure 2.7.

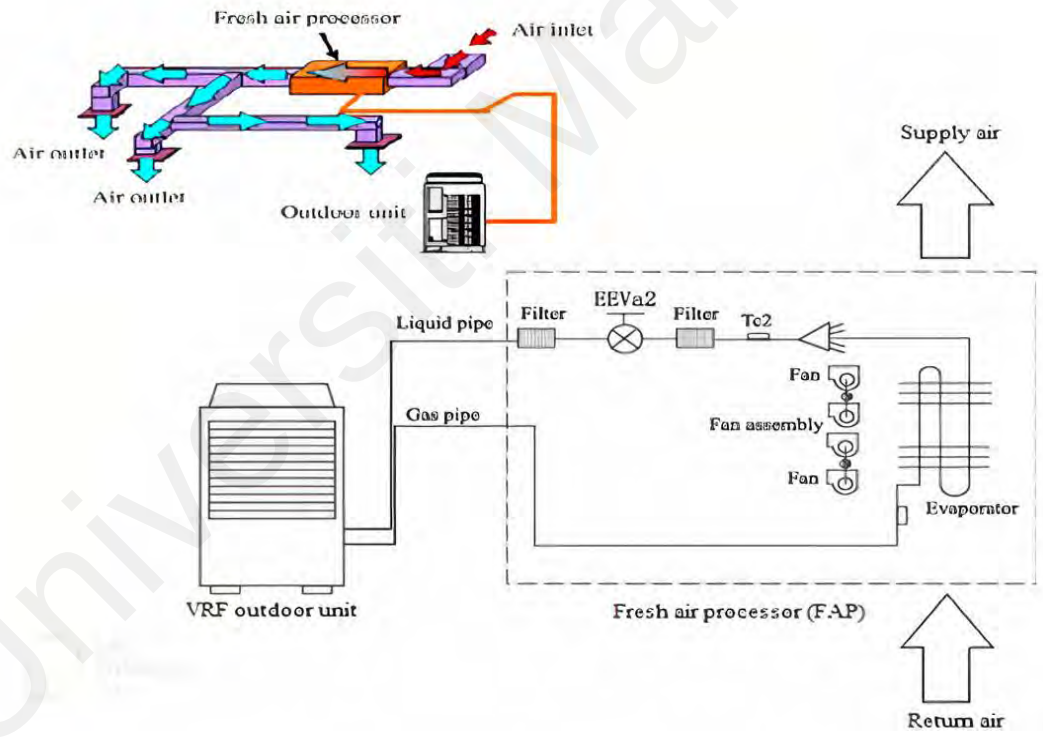

Figure 2.8: Coupled design of VRF-FAP system (Redrawn and modified based on reference (Tu et al., 2011))

2.5.3 Performance Evaluation of the Combined System

The core objective of all the studies performed with the combined system was to be benefitted with the VRF system without sacrificing the IAQ and human thermal comfort. The effect of combining the ventilation system with the VRF system was

initially studied by Aynur et al., (2008a). They performed an experimental study using a heat recovery ventilator (HRV) as the ventilation system and stated that the ventilation does not affect considerably the indoor thermal environment, and thus the efficiency of the VRF system. Instead overloads the system by increasing the indoor humidity ratio. The results were then verified through simulation work (Aynur et al., 2008b). For a schematic drawing of the VRV-HRV combined system please refer (Jiang, Ge, & Wang, 2013), the HRV system provides fresh outdoor air into the conditioned space, and thus it is not suitable to be introduced in the humid environment. To provide a dehumidified outdoor air as supply air, a novel vapour compression heat pump desiccant (HPD) system was integrated with the VRF system (Aynur et al., 2008b). This integration showed a better result in terms of energy conservation of the combined system with the acceptable level IAQ and thermal comfort. The structural diagram of the system can be found in reference (Aynur et al., 2010a). The energy consumption of this integrated system increases with the increase in outdoor air temperature and humidity, because of the more dehumidification operation. So, less considerable in relatively hot and humid regions.

To continue the research in this direction and to thoroughly solve the ventilation shortcoming, Zhu et al., (2014) evaluated the performance of VAV ventilated VRF system, hereinafter called VRF-VAV combined system. The outdoor air processing (OAP) unit with VAV box was used in this system to treat outdoor air to meet the IAQ requirement. The results were positive with the significant reduction in energy consumption of the combined system without sacrificing the thermal comfort and IAQ. After the introduction of the strict policy regarding maintaining proper IAQ based on ASHRAE standard 62.1 (ASHRAE, 2013), the VAV system was viewed as inappropriate in the changed scenario. Rane et al. (Milind Vishwanath Rane et al., 2016) introduced the VRF-DOAS combined system for the attainment of sensible and latent

loads of the conditioned spaces separately. DOAS system treated the OA and made the combined system enable to supply that air in increased quantity to meet the IAQ standard.

Park et al., (2017) investigated the performance of a VRF system with three different configurations, namely VRF without ventilation, with ERV and with DOAS. The experimental and simulation results were very similar with a mean difference in the value of the monthly energy consumption under summer and winter design conditions was 3.3% and 3.6% respectively. The indoor thermal comfort data provided by the VRF without ventilation system was not well falling within the ASHRAE comfort zone under both seasons. Contrarily, 93.9% and 83.8% of the indoor air condition data achieved by VRF-DOAS combined system fulfilled the standard comfort requirement in the winter and summer seasons respectively. Although these values for VRF-ERV system were 76.8% in winter and 65.7% in the summer, this reduction in percentage is due to the high humidity control of the VRF-DOAS system than VRF-ERV system. In terms of energy consumption, the VRF-ERV system consumed 16.8% and VRF-DOAS system consumed 26% less energy than VRF without ventilation system. However, the saving in energy can never be compromised with the IAQ and thermal comfort requirements, and thus VRF-DOAS was recommended as a best combination among others. The more relevant data in-line with the energy saving and performance studies are briefly summarized in Table 2.2.

Despite that the ventilation integrated VRF systems have lots of benefits over all other ACMV systems, the HVAC industry still feels unease in the application, integration and the complex control configuration of the VRF and ventilation combined systems. The reason is the higher initial cost, lack of familiarity with the advanced technology and most importantly, the safety issues with the refrigerant leakage

associated with VRF systems. To come up with the solutions of these highlighted issues can be a new inside in this emerging AC system.

Table 2.2: Summary of the energy saving studies on the combined system

Author (Year)	HVAC System	Season	Control Strategy	Energy conservation/ Simulation accuracy
(Karunakaran et al., 2010)	VRV-VAV combined system	Summer /Winter	Intelligent fuzzy logic controller (FLC)	37% (summer/FV) 44% (summer/DCV) 63% (winter/DCV)
(Qiu et al., 2011)	VRF-FAP integrated system	Winter	Ordinary control method	Improved the reliability of energy savings
(Zhu et al., 2014)	VRF-VAV Combined system	Winter	Load allocation optimization technique	5.17%
(Zhu et al., 2014)	VRF-VAV combined system	Summer /Winter	Load ratio based optimization control	2.47% (winter) 32.17% (summer)
(Zhu et al., 2014)	VRF-OAP unit system	Winter	DCV & Economizer cycle technique	12.45%
(Zhu et al., 2015)	VRF-VAV combined system	Summer	Model based online control strategy	6.27%
(Kim et al., 2016)	VRF-DOAS combined system	Winter	Model-based multi objective optimal control using GA & RSM	20.4%
(Lee et al., 2017)	VRF-DOAS combined system	------	Experimental based control strategy	15-17%
(Laughman et al., 2018)	VRF combined with DOAS/FCU/ERV	Summer	Modelica language	27%

2.5.4 Energy and Economic Audit of the Combined System

Ventilation integrated VRF systems have the potential to be an effective solution to improve the IAQ and human thermal comfort requirements. However, the ventilation system itself is a major contributor of energy consumption, especially in densely populated spaces. Studies have been conducted to investigate the overall energy consumption and construction cost of the integrated systems. Abe et al., (2006) highlighted that the ERV with VRF systems found in most of the application, but this integration could consume extra energy due to the constant rather than demanded supply of OA into the conditioned zones. In the VAV integrated VRF system, developed by Karunakaran et al., (2010) the OA flow can be adjusted, but it does not fully utilize the energy efficient features of the VRF system. However, due to its demand controlled ventilation with the aid of VAV dampers and efficient control optimization, the significant energy can be conserved (Zhu, Jin, Fang, et al., 2014). By optimizing the supply air temperature in a VRF-OAP system developed by Im et al., (2016), Lee et al., (2017) found the energy reduction of 15–17% at 100% load, and 4–20% at a 75% load.

Furthermore, due to the integration of two systems i.e. ventilation system (ERV/DOAS/VAV) and air-conditioning system (VRF), the combined system initially costs significantly higher in construction and installation. However, it could be paid off by minimized the running cost through efficient use of the ventilation system.

2.6 Summary

The studies cited above clarify that there is an opportunity to improve thermal comfort in office buildings by appropriately control the indoor air temperature and velocity, this strategy could also reduce the energy consumption by AC systems. Most of the studies based on field experiments in the tropics/sub-tropics not complying with Fanger's model suggested a value for the neutral temperature to be above 24.5ºC for air-

conditioned offices and non-commercial buildings, as recommended by ASHRAE standard 55.

The appealing energy efficiency and promising features have made the VRF system popular among contemporary HVAC systems. Due to having a modular capacity enhancement, VRF units are widely adopted in high-rise buildings. Different mechanical ventilation and air distribution methods have been discussed in this chapter. Their performances were investigated using experimental and numerical approaches. Most of the studies highlighted better performance of new ventilation techniques over existing traditional methods. Stratum ventilation showed good potential under elevated indoor temperature settings. Different layouts for SV have been designed to meet with the variety of space requirements. Therefore, scientist and researchers are encouraged to explore the new hybrid air distribution designs with improved energy conservation and enhanced thermal comfort targeting small-to-large size buildings.

In this chapter, different ventilation integration solutions with VRF system are also discussed, their performances are compared and their schematics are presented. Various design approaches provided significant improvement in IAQ and thermal comfort by the combined systems. Performances of the combined systems were also evaluated based on thermal comfort and energy consumption. To the best of the authors' understanding, it is evident that a suitable VRF and ventilation design could not only address the outdoor air deficiency of the VRF system but also improves the energy efficiency of the combined system. In other words, inadequate ventilation integration either results in more energy consumption and degraded thermal comfort with poor IAQ. It is misfortune that most of the research pursued in past 10 years on VRF and ventilation designs aimed at using different air processing devices and control optimization techniques, no data is available with different air distribution techniques.

CHAPTER 3: DESIGN AND DEVELOPMENT OF THE VARIABLE REFRIGERANT FLOW INTEGRATED STRATUM VENTILATION SYSTEM: VRF-SV HYBRID SYSTEM

3.1 Introduction

The VRF system is gaining popularity in most Asian countries as a new HVAC technology compared to traditional ones (Enteria, Cuartero-Enteria, & Sawachi, 2020). However, several issues in adopting these systems in the region still exist, such as higher initial cost, complex integrated control, and lack of fresh air provision for ventilation (Aynur et al., 2008a; Goetzler, 2017; Park et al., 2017; K. Yu et al., 2017). To overcome the ventilation issue, the VRF systems are being integrated and installed with different mechanical ventilation systems in buildings (Technologies, 2014). The reviewed literature reveals that the research in this direction is being carried out to explore the new hybrid air conditioning systems in terms of higher energy savings and improved thermal comfort performance (Khan et al., 2021; Z. Lin, Lee, et al., 2011; Park et al., 2017).

Therefore, this study was aimed to design the most energy-efficient ACMV solution for tropical buildings. A novel attempt was made in this study by integrating the VRF system with the stratum ventilation system. The conceptual diagram of the integrated system is illustrated in Figure 3.1. To enhance the broad application of the integrated system, different design approaches were adopted in this study. The proposed system is designed as a case study for a large retail facility located in the tropics to understand the design guidelines. The parametric analyses were also carried out to investigate the effect of varying indoor design conditions on the combined system capacity.

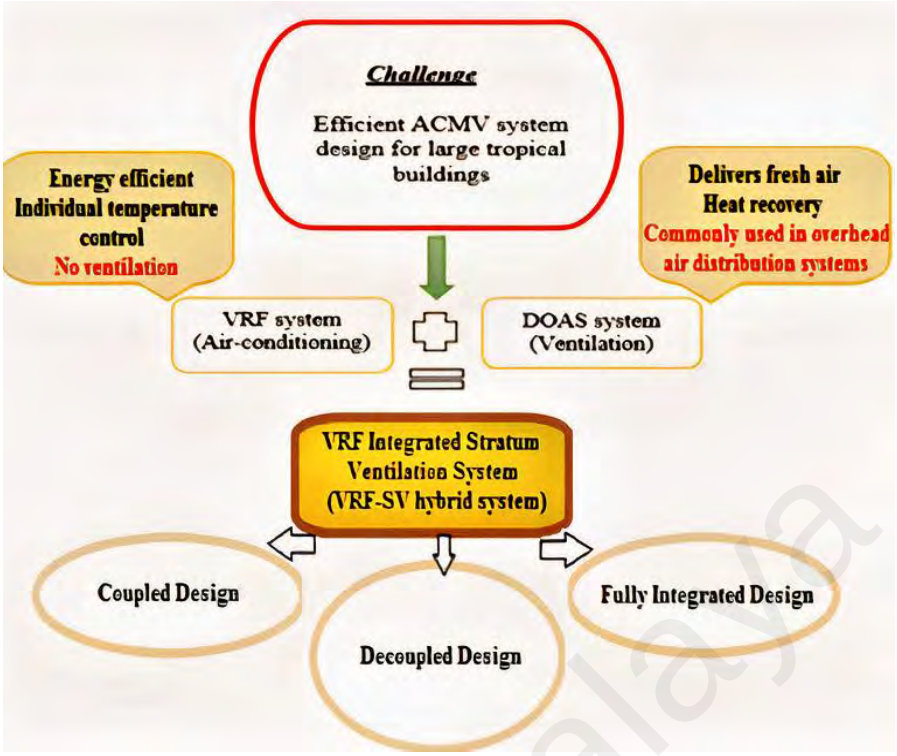

Figure 3.1: Concept of the novel VRF-SV system

3.2 VRF-SV Hybrid System Design

3.2.1 Decoupled Design

In this design method, the two systems are combined in a way to achieve their tasks separately, as seen in Figure 3.2. The VRF indoor terminal unit caters to the sensible load, whereas the OAP unit treats the OA. The fully conditioned air is then supplied into the space through grilles or diffusers for attaining the latent load. During cooling operation, the air processing unit conditions the OA to the dew point temperature (saturation) lower than the desired space humidity ratio (SHR). However, if the dry and cold air is supplied to the space, it could partly offset the space sensible load, which in turn reduces the terminal unit capacity of the VRF system (Electric, 2018). This method is recommended to be considered in the tropical environment where the fresh air requirement for ventilation is high.

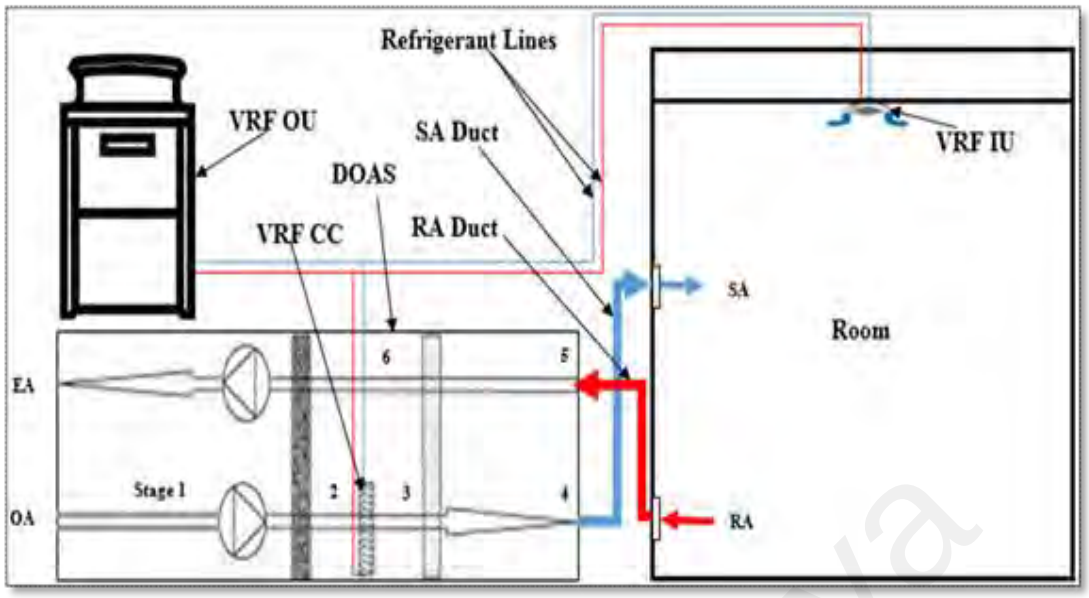

Figure 3.2: VRF-SV system design using decoupled method. (Stage 1: outdoor air; 2: air after enthalpy wheel; 3: air after cooling coil at DP saturation; 4: supply air; 5: return air; 6: air after sensible wheel)

3.2.2 Coupled/Integrated Design

In this approach, the OA is pretreated through DOAS before delivering to the targeted space. Preconditioning removes both the sensible and latent loads from the OA. The pretreated air from the DOAS is then delivered into the return air duct of the VRF terminal units (DAIKIN, 2019), as shown in Figure 3.3. Improved IAQ, enhanced thermal comfort, increased energy efficiency and low-cost system installation are some of the benefits provided by this method. One major drawback of this method is that if the failure occurs in the air handling equipment, the terminal system must be capable enough to bear the extra load of the OA to avoid any loss in the controlled thermal environment (Electric, 2018).

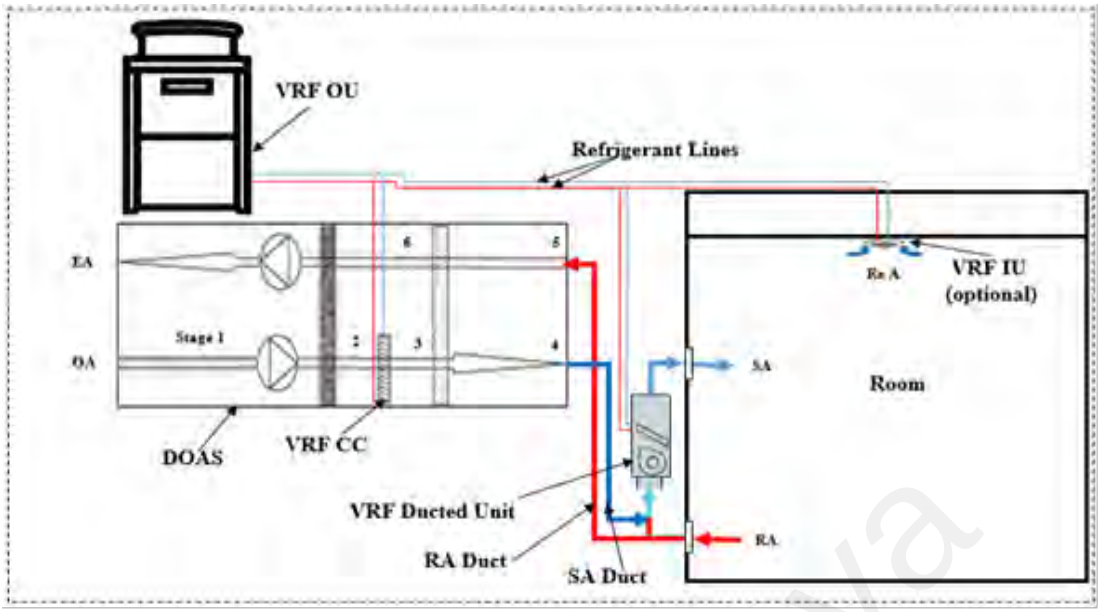

Figure 3.3: Typical VRF-SV system design using coupled method. (Stage 1: outdoor air; 2: air after enthalpy wheel; 3: air after cooling coil at DP saturation; 4: partially conditioned air; 5: return air; 6: air after sensible wheel)

3.2.3 Fully Integrated Design

Figure 3.4 shows the new method of integrating the VRF system with the DOAS system to supply fully conditioned air directly into the space through stratum ventilation air distribution strategy. The conditioned air at elevated temperature is provided to cater to the complete load of the space. No separate VRF indoor terminal is required in this design method. This design approach reduces the overall system capacity and overcomes the large installation space requirement by the ACMV systems in tropical countries like Malaysia and Singapore.

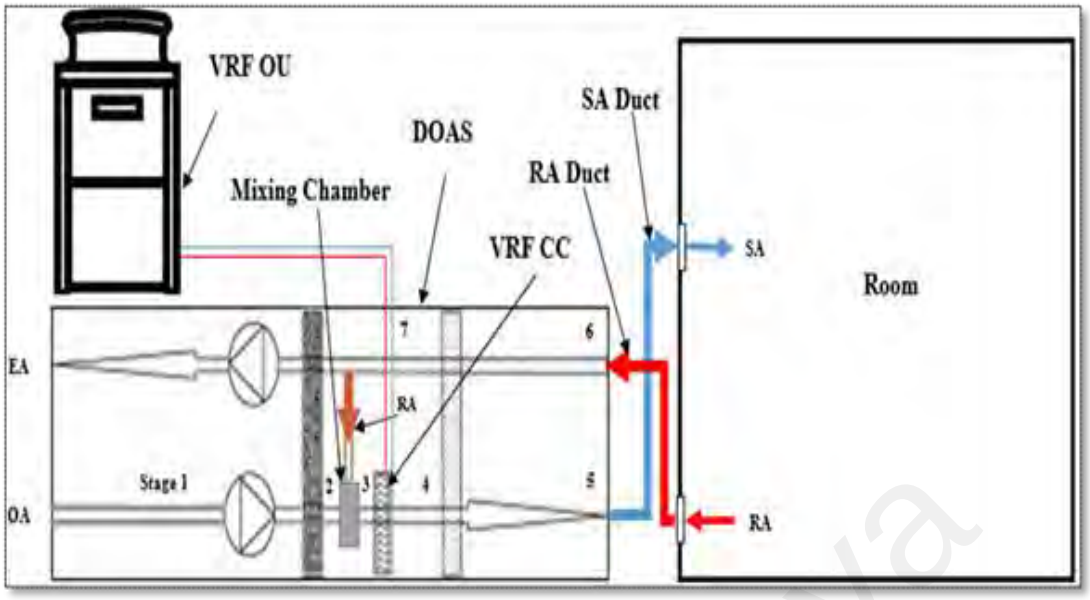

Figure 3.4: Typical VRF-SV system design using the fully integrated method. (Stage 1: outdoor air; 2: air after enthalpy wheel; 3: air after mixing with return air in mixing chamber; 4: air after cooling coil at DP saturation; 5: supply air; 6: return air; 7: air after sensible wheel)

3.3 Overview of the Case Study Building

This study employs the aforementioned design methods to integrate the DOAS with the VRF system for stratum ventilation air distribution to be installed in a large retail shop located at the ground floor of a building in Kuala Lumpur, Malaysia (see A.3 in Appendix A). Table 3.1 presents the detailed description of the retail shop facility.

For a proper selection of the design conditions, ASHRAE stipulates three OA design data sets:

1. Peak WB with mean coincident DB temperature.
2. Peak DB with mean coincident WB temperature.
3. Peak DP with mean coincident DB temperature.

These data sets are used to determine the peak total cooling load, peak sensible cooling load and peak latent cooling load, respectively. The second data set was selected in this design, considering the removal of the excess heat and moisture contained in the OA stream by the DOAS enthalpy wheel, as seen in Table 3.2.

Table 3.1: Basic design details for the retail shop

Region	Asia/Pacific (Kuala Lumpur, Malaysia)
ACMV system	VRF+SV system
Retail Shop Area Ceiling Height	346 m^2 (3724 ft^2) 2.7 m (9ft)
Occupancy	6.2 m^2 per person
Activity	Sales
Occupant load	Sensible: 73.2 W per person Latent: 58.6 W per person
Roof U-value	No sunlit roof (Ground floor)
Lighting load	33.7 W/m^2
Equipment Load	9 W/m^2
Minimum ventilation Requirement	7.5 cfm per person (3.5×10^{-3} m^3s^{-1} per person) 0.12 cfm. ft^{-2} (6.1×10^{-4} m^3s^{-1} per m^2 floor area)
Assumptions	• No infiltration, • No latent heat generation source except people • Adiabatic condition • No sunlit wall

Table 3.2: The data of the outdoor design conditions

Data set	Design Condition	Enthalpy
Kuala Lumpur, Malaysia (annual percentile 0.4)		
Peak WB, MCDBT	27.3 ºC WBT 31.5 ºC DBT	104.06 kJ/kg
Peak DB, MCWBT	35.0 ºC DBT 27.8 ºC WBT	106.06 kJ/kg (selected)
Peak DP, MCDBT	26.2 ºC DPT 29.2 ºC DBT	102.43 kJ/kg

3.3.1 Heat Load Calculation

Based on the basic design data provided in Table 3.1 and the outdoor/indoor design conditions, the sensible and latent loads for the retail shop are calculated. The minimum ventilation required for the space is estimated by following ANSI/ASHRAE standard 62.1-2019 (ANSI/ASHRAE-62.1, 2019). Table 3.3 shows the cooling load components and the minimum ventilation rate required for the case study building.

Table 3.3: Heat load components and minimum ventilation requirement for the space

Sensible Load	Latent Load	No. of Occupants	Min. OA for ventilation (By components)	Total OA for ventilation (V_0)	Total outdoor SA quantity $\dot{V}_{sa,total} = \frac{V_0}{\eta}$
21.16 kW	3.28 kW	56	420 cfm (0.19m^3/s) (Person) 447 cfm (0.21m^3/s) (Floor area)	867 cfm (0.41 m^3/s)	619 cfm (0.29 m^3/s)

3.4 Design Guidelines of the VRF-SV System (case study)

There is no existing guideline for designing this novel hybrid system. This section provides the details to assist the HVAC engineers with the complete road map of developing the VRF-SV system using different approaches. Figure 3.5 highlights the key steps involved in the design, while the description of each step is given in the subsequent sections.

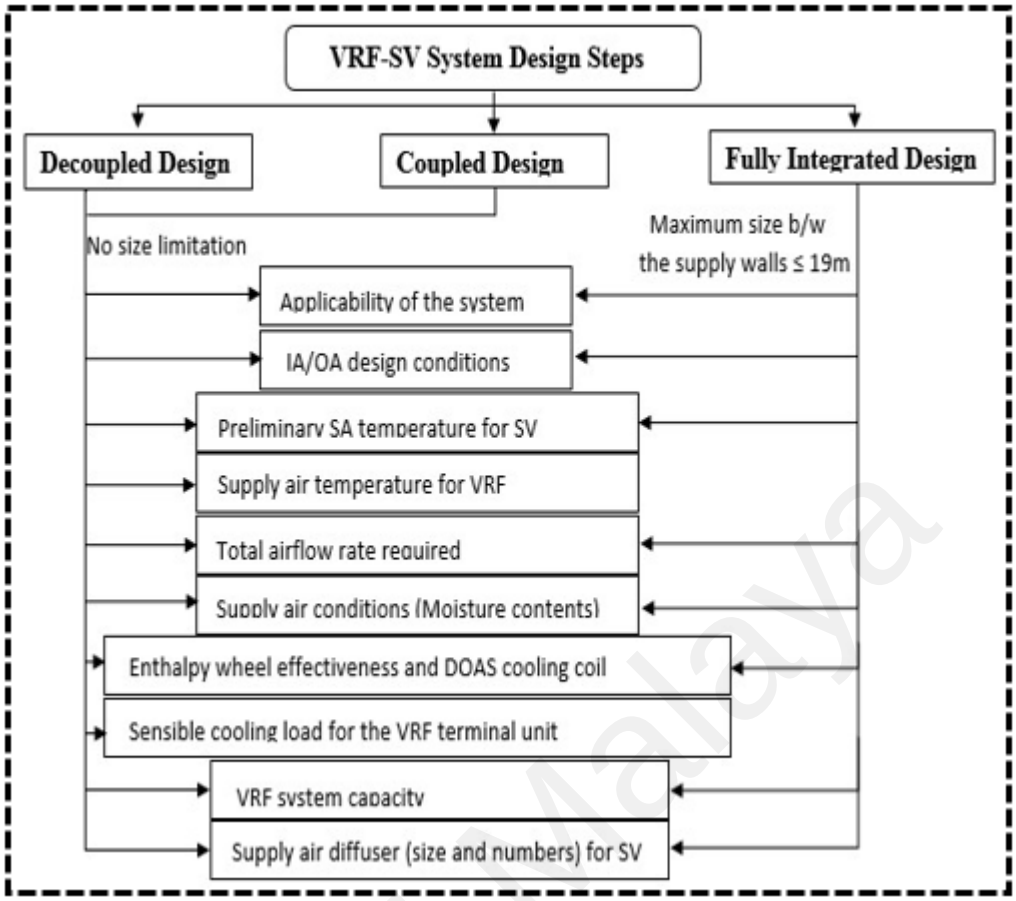

Figure 3.5: Flow chart of the complete design process of the VRF-SV system

Step (1): Check the applicability of the system

As mentioned in the SV design guidelines (Z. Lin, Yao, Chow, Fong, & Chan, 2011), the airflow path should not exceed 9 m, restricting its application to only small and medium-size spaces. In comparison, the VRF-SV design provides HVAC engineers with a relief to supply the air to even large spaces. The coupled and decoupled designs of the VRF-SV system can be installed to any size of the large buildings as they come with separate indoor terminal units for sensible cooling. However, there is a limitation in the applicability of a fully integrated design. In this design type, the total heat load of the space is catered by the conditioned air supplied through wall-mounted diffusers from two opposite walls.

Step (2): Determine IA/OA design conditions

The DOAS in this design reduces the enthalpy of the OA by the enthalpy wheel. Therefore, the OA design condition is determined among the data sets with the highest OA enthalpy value. Thus, the peak dry-bulb (35ºC DBT) and the mean coincident WBT (27.8ºC WBT) data set was considered under this study.

The Malaysian standard (MS1525) recommended minimum DBT is 23ºC, and RH is 50% -70% for air-conditioned spaces. Therefore, 24ºC DBT and 55% RH are selected as the space conditions for the current hybrid system design for buildings in the tropics.

Step (3): Determine the preliminary SA temperature for SV

Due to the head level air supply directly into the breathing zone, the suggested comfort temperature for stratum ventilation is between 20-23ºC (Z. Lin, Yao, et al., 2011). In a study conducted on SV integrated hydronic radiant cooling system in a residential application, the recommended supply air temperature was 19ºC (66.2 ºF) (Navid & Maerefat, 2015). Thus, considering a similar design approach and to cater to the maximum sensible load of the space, 19ºC temperature was selected as a preliminary value for the SV air supply.

Step (4): Determine the SA temperature for VRF (Coupled/Decoupled design)

Considering the limitations with airflow rate capacity in different VRF indoor terminals, the VRF unit supply temperature was determined based on the target sensible cooling load. The load is calculated by deducting the sensible load attained by the SV from the total sensible load of the space (using Equations 3.1 and 3.2). For this design, the chosen temperature was 15ºC (59 ºF), which also fulfils the condition that the coil surface temperature must be higher than the room DP temperature in the hybrid HVAC system design (Jae-Weon Jeong & Stan Mumma, 2006).

$$Q_{sen,SV} = \rho C_p \dot{V}_{sa}(T_{sp-} T_{sa}) = 1.2\ \dot{V}_{sa}(T_{sp-} T_{sa}) \quad (3.1)$$

$$Q_{sen,VRF} = Q_s - Q_{sen,SV} \quad (3.2)$$

where

$Q_{(sen, SV)}$ = SV supply air cooling load, kW

$Q_{(sen, VRF)}$ = VRF system cooling load, kW

Qs = Space sensible cooling load, kW

$\dot{V}_{sa}$ = Supply air flow rate, m^3/s

T_{sp} = Space DB temperature, ^oC

T_{sa} = Supply air DB temperature, ^oC

ρ = Density of air (1.202 kg/m^3)

C_p = Specific heat of air (1.00g kJ/kg.^oC)

Step (5): Calculate total airflow rate required

Flow rate of ventilation

The required ventilation rate for the studied space is approximated using ASHRAE standard 62.1-2019 guidelines. According to that, a retail shop (sales) requires $3.5x10^{-3}$ m^3/s per person and 6.1×10^{-4} m^3s^{-1} per m^2 floor area (as seen in Table 3.3). The calculated value was felt inadequate for the uniform supply of ventilation air through SV air distribution. Thus, the following strategy was adopted to add extra ventilation load for each of the designed method.

Decoupled Design

The sufficient amount of air to be supplied through SV air distribution is initially approximated in the decoupled design. The approximation is made by calculating the total airflow rate required to be supplied through diffusers for the uniform distribution

of air into the domain. In this case, 5 bar grille diffusers were selected, each requiring 297.2 cfm (0.14 m^3/s) of air to supply at a distance of 9.5 m with 2.5 m/s face velocity and 0.25 m/s terminal velocity. The total amount of supply air required was 1,486 cfm (0.70 m^3/s). To fulfil this requirement, an extra amount of 867cfm (0.41m^3/s) of OA was added into the minimum required ventilation load.

Coupled/Integrated Design

In the coupled design method, the extra amount of air needed to be supplied uniformly through the SV air distribution system was achieved by the return air from the VRF ducted unit. The estimated minimum ventilation air (as per ASHRAE 62.1) after preconditioning through the DOAS was supplied to the return air duct of the VRF ducted unit.

Due to the limitations in using a certain percentage of the ducted type VRF unit out of the total VRF indoor unit, the rest of the space sensible cooling load is attained by the separate non-ducted VRF units (DAIKIN, 2019).

Fully-Integrated Design

In this novel approach, the VRF and DOAS systems are integrated in way so that no separate VRF indoor units are required for sensible cooling. Unlike the coupled method where the separate VRF ducted units are used to achieve the adequate ventilation air supply, this method utilized the VRF cooling coil installed inside the DOAS system to fully treat the required amount of supply air (OA+RA).

The required supply air quantity for the studied space is estimated first by considering the supply air temperature and total sensible cooling load. The initially calculated minimum OA for ventilation (0.29m^3/s) is supplied into the mixing chamber

in the DOAS system after passing through the enthalpy wheel. To fulfil the supply air requirement, the remaining amount of air obtained from the return air duct is also directed to the mixing chamber. The mixture of both air streams is then cooled (at saturation point) by the VRF cooling coil and reheated by the sensible wheel before supplying through the SV diffusers.

Step (6): Check SA conditions

In the VRF-SV system, the supply air from the DOAS must be dehumidified enough to meet the target space requirement. For the studied space, the supply air dryness is determined using equation (3.3) (Jae-Weon Jeong & Stan Mumma, 2006).

$$W_{sa} = W_{sp} - \frac{Q_L}{1.202 \times Q_{vap} \times \dot{V}_{sa}} \quad (3.3)$$

where,

W_{sa} = Supply air humidity ratio, kg water/kg dry air

W_{sp} = Space humidity ratio, kg water/kg dry air

Q_L = Space latent load, kW

$\dot{V}_{sa}$ = SA flowrate, m^3/s

Q_{vap} = Latent heat vaporization (2,454 kJ/kg)

Step (7): Calculate enthalpy wheel effectiveness and DOAS cooling coil load

The designed DOAS cooling coil capacity can be determined once the enthalpy of the OA leaving the wheel is known. To estimate the enthalpy value at stage 2, the enthalpy wheel leaving supply air DBT and HR need to be calculated using equations 3.4 and 3.5 (ASHRAE, 2015). The prerequisite for this calculation is the DBTs and HRs of the OA and EA streams at the wheel entrance and the latent and sensible effectiveness of the enthalpy wheel.

$$T_2 = T_1 - \varepsilon_s \frac{(\dot{m}C_p)_{min}}{(\dot{m}C_p)_1} \tag{3.4}$$

$$W_2 = W_1 - \varepsilon_L \frac{\dot{m}_{min}}{\dot{m}_1}(W_1 - W_6) \tag{3.5}$$

where,

$T_1, T_2,$ and T_6 = DB temperatures at stage 1, 2, and 6, °C

$W_1, W_2,$ and W_6 = Humidity ratios at corresponding stages, kg/kg

$(\dot{m}C_p)_{min}$ = Min. capacitance flow rate between SA and EA, W/°C

m_{min} = Min. flow rate between SA and EA, kg/s

ε_s and ε_L = Sensible and latent effectiveness of the enthalpy wheel, respectively.

The EW effectiveness values can be obtained from the manufacturers' data or through online software with the help of some known parameters, wheel material, entering air conditions, entering velocity, airflow ratio (ratio of the SA to EA) (Jae-Weon Jeong & Stan Mumma, 2006).

However, in this study, the empirical enthalpy wheel effectiveness correlations described by Jeong and Mumma (2005) are adopted. These correlations approximate the required effectiveness values for the silica gel or molecular sieve coated enthalpy wheel using six known parameters, including wheel entering SA and EA DBTs and RHs, entering velocity and airflow ratios.

The OA and EA flows are assumed to be the same at the wheel entrance; thus, the airflow ratio equals 1. The design entering velocity of the air is taken as 2.5 m/s. The other four parameters have already been calculated in the previous steps. A MATLAB program was developed to carefully calculate the respective values of sensible and latent effectiveness for both of the wheel types in all design conditions (MATLAB,

2005). The silica gel enthalpy wheel provided greater sensible and latent effectiveness values in all the designed cases, thus selected in the design approaches.

Once all the psychrometric properties of the SA before and after the cooling coil are known, the DOAS cooling coil capacity is calculated using equation (3.6). The average density (ρ) of the SA before and after the cooling coil is approximated to 1.202 kg/m^3 for all designed cases (ASHRAE, 2015; Jae-Weon Jeong & Stan Mumma, 2006).

$$Q_{cc} = \rho \times \dot{V}_{sa,t} (h_2 - h_3) \quad (3.6)$$

where

Q_{cc} = cooling coil capacity, kW

ρ = SA density, kg/m^3

$\dot{V}_{sa,t}$ = SA flowrate (total), m^3/s

h_2 & h_3 = SA enthalpy at stages 2 and 3, kJ/kg

Step (8): Calculate sensible cooling load for the VRF terminal unit

In the decoupled and coupled design approaches, the separate VRF terminal units installed in the room must accommodate the rest of the sensible load not met by the supply air through the SV method. The difference between the total sensible load and the sensible cooling capacity of the SV supply determines the load required to be achieved by the VRF terminal units.

Step (9): Determine VRF system capacity

The VRF system capacity for attaining the rest of the sensible cooling load in the coupled and decoupled design methods is determined from the manufacturer's catalogue or using a system selection software.

Step (10) Select supply air diffuser (size and numbers) for SV

In summer design conditions at all design airflow rates, the ratio of the diffuser's throw to the length of the supply path is used in the selection process to achieve an acceptable air distribution performance index (ADPI). A higher ADPI value is desirable as it relates to higher thermal comfort. Based on the ADPI, the following procedure is adopted to select diffusers for the SV air distribution.

1. In the SV system, the diffuser(s) are positioned on the wall(s) at 1.3 m or 1.9 m height from the floor depending on the occupants' activities, i.e., sedentary or standing. The walls for installing diffusers are selected, which are more likely to be faced by the occupants under normal situations.
2. The air supply path, usually called characteristic length (L), is the distance from the diffuser to the wall or the mid-plane between diffusers (Hout, 1998).
3. Select the prescribed $T_{0.25/L}$ ratio as shown in Table 3 ("ASHRAE Handbook-Fundamentals," 2017).
4. The throw value can be determined by multiplying the ratio $T_{0.25/L}$ by L.

Once the size of the diffuser is determined, the required number of diffusers for the space can be estimated by dividing the airflow rate required for each diffuser by the total airflow rate.

3.5 Different Design Configurations of the VRF-SV Hybrid System

Keeping in mind the four different air terminal layouts recommended for stratum ventilation (Yao & Lin, 2014a), and the large size of the retail facility together, only two air terminal layouts were considered in this study. The selected air terminal layouts are (1) return at the low level of the same wall and (2) return at the ceiling. Based on these two layouts and coupled/decoupled design strategies, a total of six configurations for the combined system were designed, numerically modeled and simulated. The schematic design for these configurations is shown in Figure 3.6. The prior four configurations are

designed with separate VRF indoor units for sensible cooling along with the SV air distribution system. The configurations 1 and 2 are designed with the four-way cassette type VRF indoor units, whereas configurations 3 and 4 include with the floor standing console type VRF indoor units. In these configurations, the temperature of 19ºC was set for the SV supply (Morovat & Maerefat, 2013) and 13.5ºC for the VRF terminals. The supply air velocity was also calculated separately for both the systems. To comply with the minimum ventilation requirement based on ASHRAE 62.1 (ASHRAE, 2019) and to target the smooth air delivery to the entire domain, an optimized number of customized bar grilles were used. The 2.5 m/s inlet velocity was calculated considering the grille's neck area and the supply airflow rate. The VRF supply velocity was calculated by dividing the airflow volume by the slot area of the terminals, which is 1.7 m/s. The last two configurations employed an integrated or coupled approach, in which the VRF cooling coil was installed inside the air processing unit and the space is conditioned by the SV system only. The customized bar grille type diffuser is used in all the configurations to supply conditioned air into the space due to its long airflow throw with desired face velocity. The bar grilles are installed on the opposite walls at 1.9m above the floor because of the standing occupancy in the retail shop (Z. Lin, Yao, et al., 2011). The return/exhaust terminals are positioned at 0.33m above the floor in configurations 1, 3 and 5, whereas for the configurations 2, 4 and 6, the terminals are installed on the ceiling. The explanation and specifications of the individual components used in different configurations are also provided in Table 3.4.

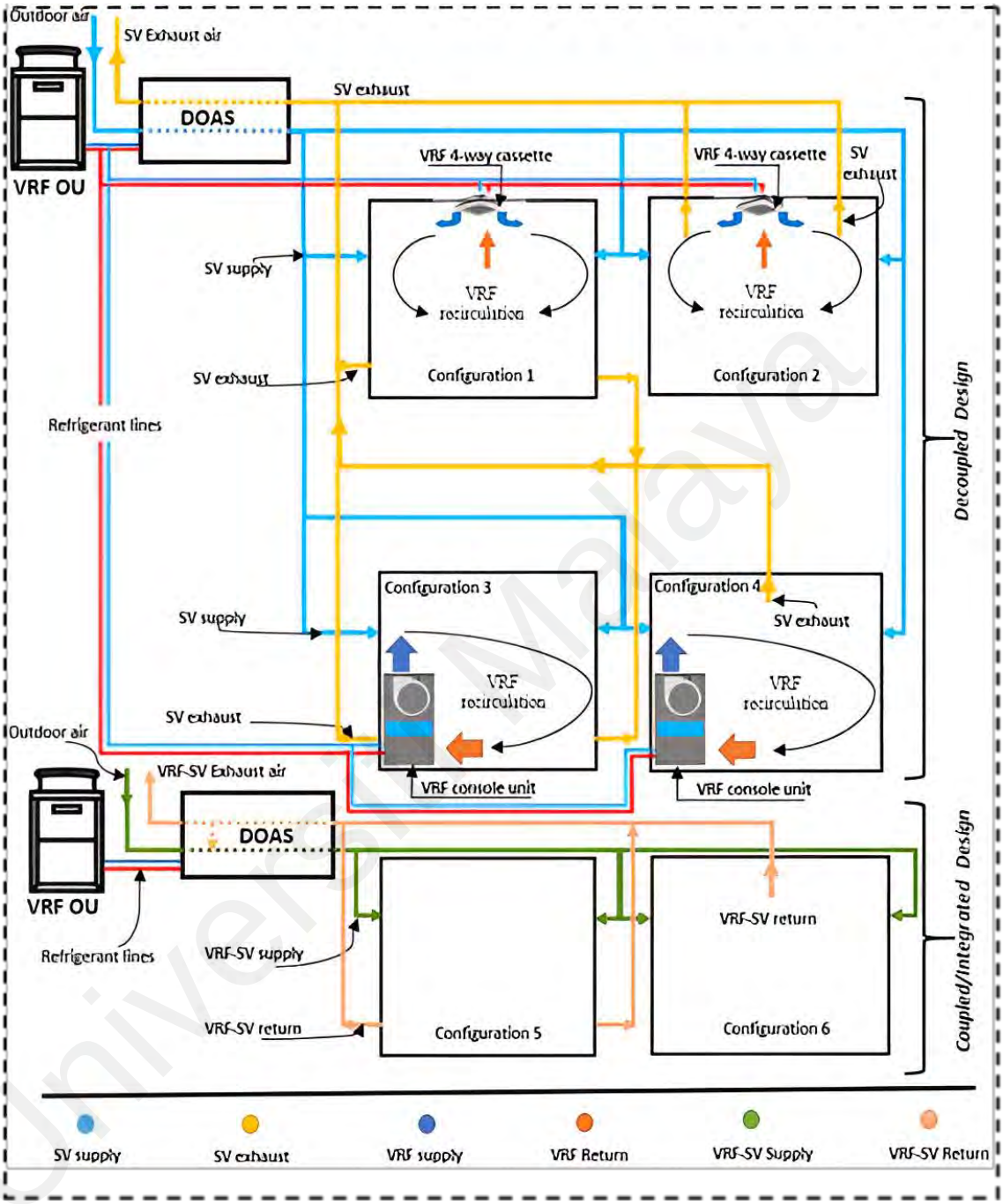

Figure 3.6: Schematic design of all six (6) configurations

Table 3.4: Details of the individual components used in different configurations

Conf.	Design	Return/ Exhaust position (SV)	Supply diffuser Type (Flowrate) Size(mm) Nos.	Return/Exhaust terminal Size(mm) Nos.	VRF FCU Type (Flowrate) Nos.
1	Decoupled	330 mm (same walls)	Bar grille (0.14m^3/s) 210×500 5	210×500 5	4-way cassette (0.25m^3/s) 6
2		Ceiling	Bar grille (0.14m^3/s) 210×500 5	750×350 2	4-way cassette (0.25m^3/s) 6
3		330 mm (same walls)	Bar grille (0.14m^3/s) 210×500 5	210×500 5	Floor standing console (0.25m^3/s) 5
4		Ceiling	Bar grille (0.14m^3/s) 210×500 5	500×500 (1) 370×370 (2)	Floor standing console (0.25m^3/s) 5
5	Coupled/ Fully integrated	330 mm (same walls)	Bar grille (0.22m^3/s) 300×500 17	300×500 17	___
6		Ceiling	Bar grille (0.22m^3/s) 300×500 17	650×650 6	___

3.6 Parametric Analyses of the VRF-SV Hybrid System

The parametric analyses were carried out to investigate the overall capacity of the combined system with different design methods under various indoor design conditions. Table 3.5 presents the details of the different scenarios considered in these analyses. The outdoor design conditions such as 35ºC DBT and 27.8ºC WBT were assumed unchanged for all the case scenarios.

Table 3.5: Parametric details of the 27 cases of the VRF-SV combined system

Cases	Design Method(s)			Indoor design condition	Supply T (ºC)
1	Decoupled Design	Coupled/Integrated Design	Fully Integrated	24ºC DBT/ 55% RH	19
2				24ºC DBT/ 55% RH	20
3				24ºC DBT/ 55% RH	21
4				25ºC DBT/ 55% RH	19
5				25ºC DBT/ 55% RH	20
6				25ºC DBT/ 55% RH	21
7				26ºC DBT/ 55% RH	19
8				26ºC DBT/ 55% RH	20
9				26ºC DBT/ 55% RH	21

3.6.1 Effect of SA Temperature on Combined System Capacity

The impact of the supply air temperature on the overall system capacity is analyzed at 24ºC/55% RH indoor design conditions for the studied space. It was observed that the coupled design method for designing the VRF-SV system was found not suitable because of the higher capacity demands due to the induction of separate ducted unit.

It can be seen in Figure 3.7 that the supply air temperature of SV has a greater impact on the overall system capacity. The increase in the supply temperature in a decoupled

strategy decreases the DOAS cooling coil size and thus reduces the overall system capacity. On the other hand, a negative impact was seen with the coupled design approach.

As no separate VRF indoor terminal is required in the fully integrated approach, the DOAS cooling coil size defines the overall system capacity, which increases slightly due to the increase in the supply air temperature. However, the least overall system capacity was achieved with this design method. Thus, recommended to be installed in large applications in the tropics.

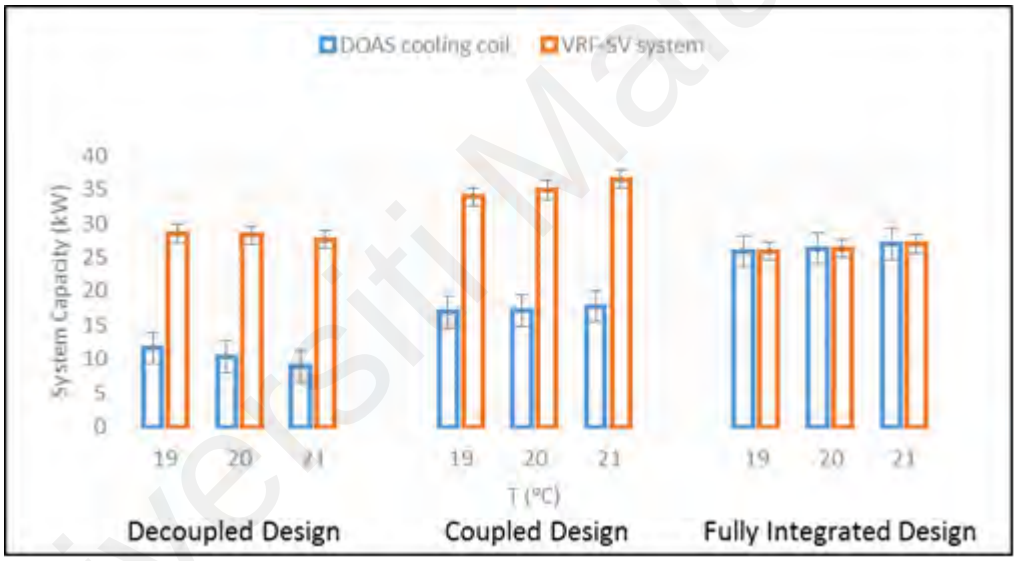

Figure 3.7: Effect of the SA temperature on the total system capacity @ 24ºC DBT/55% RH of the targeted space conditions

A similar trend was observed in the system capacity size when varying the targeted space conditions, as seen in Figures 3.8 and 3.9. The highest system capacity was calculated for the coupled design method at 21ºC supply air temperature under 25ºC DBT/55% RH targeted space conditions. The lowest total capacity was found with the fully integrated design at 19ºC supply temperature in 24ºC DBT/55% RH indoor design conditions.

This parametric study concluded that there is no significant impact of the supply air temperatures on the total system capacity of the VRF-SV system when designed with a decoupled or fully integrated approach. In contrast, the coupled design method showed a considerably higher impact on the system capacity with the variation in the indoor design conditions.

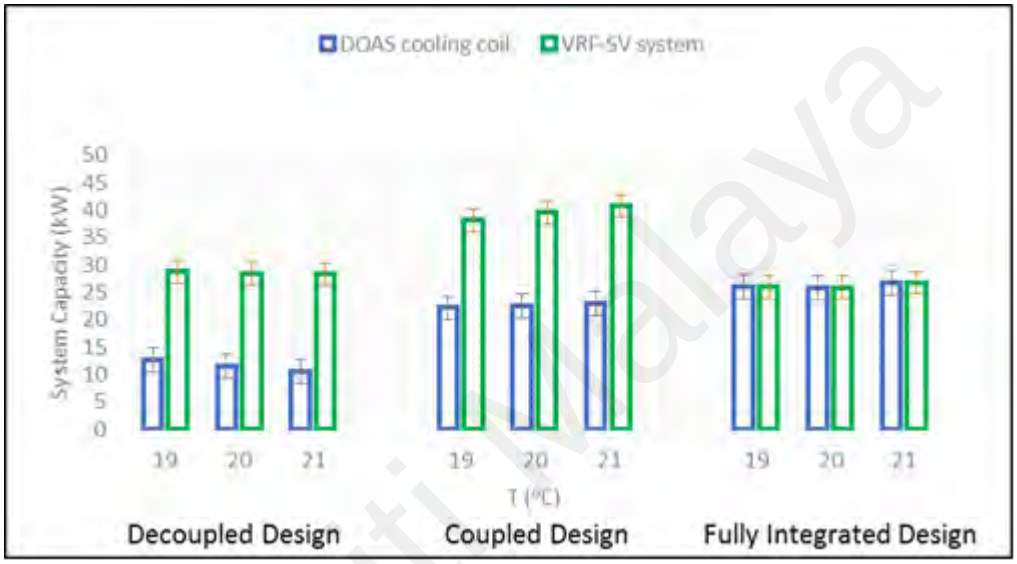

Figure 3.8: Effect of the SA temperature on the total system capacity @ 25°C DBT/55% RH targeted space conditions

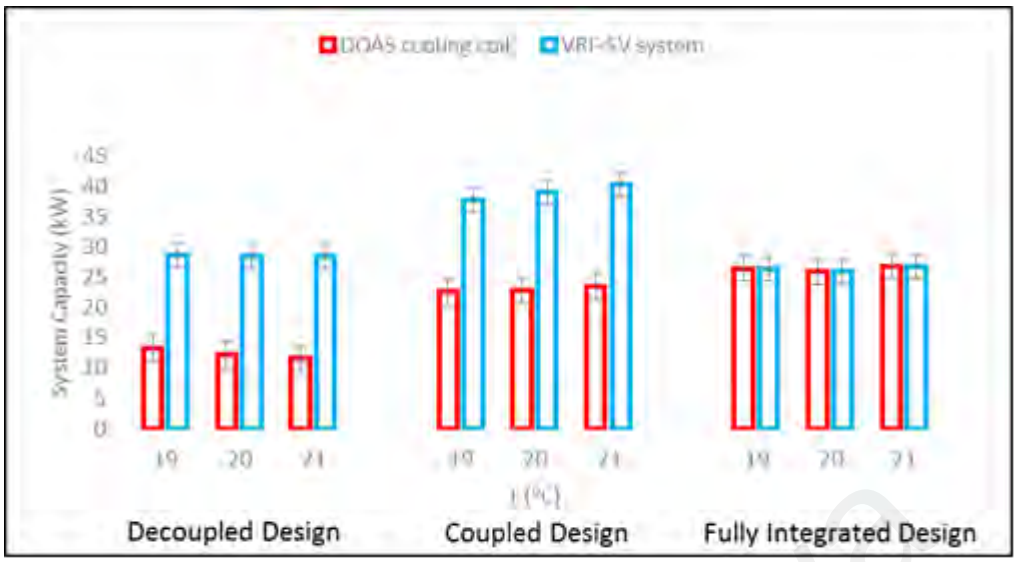

Figure 3.9: Effect of the SA temperature on the total system capacity @ 26ºC DBT/55% RH of the targeted space conditions

3.7 Summary

This chapter was aimed to present an integrated design of the variable refrigerant flow integrated stratum ventilation (VRF-SV) system for tropical buildings using coupled, decoupled, and a newly proposed fully integrated approach. The VRF-SV hybrid system was designed for a fictitious retail shop building located in the tropics. A detailed design guidelines of the VRF-SV hybrid system with coupled, decoupled, and fully integrated approaches were successfully developed in this study. The designing procedure was figured out with the help of computed data and numerical investigations of the sample case studies. The parametric analyses were also carried out to investigate the effect of varying indoor design conditions on the combined system capacity.

CHAPTER 4: NUMERICAL SIMULATIONS OF THE VRF-SV SYSTEM PERFORMANCE IN A CASE STUDY BUILDINGS IN THE TROPICS

4.1 Introduction

The ACMV system typically combines an air conditioning system that removes the excess heat from the room air and the ventilation system replaces the contaminated room air with fresh air to provide better indoor air quality (IAQ) (Yao & Lin, 2014b). The two systems account for more than 60% of the overall energy utilization in buildings (Department of Energy of US, 2015). Many countries have adopted several techniques to cope up with the energy needs of these systems (Zheng et al., 2018). Some tropical/subtropical countries proposed that an increment in indoor air temperature can significantly reduce the energy needs of the building sector (Z. Lin, Tian, Yao, Wang, & Chow, 2011).

A few studies have also been reported studying the integration of the VRF system with the ventilation system in different climatic conditions. Taking the advantages of both, the combined system performance was found outstanding in terms of improved thermal comfort (TC), more energy saving, and better indoor air quality (IAQ) (Aynur et al., 2010b; Yonghua Zhu et al., 2014). Novel combined systems have been proposed for the South Korean buildings under heating conditions that use demand control ventilation (DCV) and dedicated outdoor air system (DOAS) together with the VRF system to reduce the building energy consumption while improving the IAQ with minimum OA. Furthermore, the DOAS allows the flexibility in controlling the IAQ by separating the latent load from sensible load (W. Kim et al., 2016).

Literature revealed that the investigations of the ventilation integrated VRF systems have been largely focused on the design integration (Milind Vishwanath Rane et al., 2016), control optimization (Chung, Yang, Lee, Lee, & Moon, 2017; W. Kim et al.,

2016; Laughman et al., 2018; Yonghua Zhu et al., 2014), actual energy use and energy saving potential (Karunakaran et al., 2010; J. Kim et al., 2020) of the combined system. To the best of authors knowledge, a very few studies have been conducted on the combined system performance evaluation in the tropical climatic conditions and the studies that have been reported actually investigated the combined systems that were installed with the overhead air distribution system for fresh air ventilation. In view of this, the current study was designed to integrate the VRF system with a DOAS installed with a novel air distribution system; stratum ventilation, to provide an efficient ACMV solution for large buildings in the tropics.

This novel study combines the VRF system with the stratum ventilation system in six different configurations for a large retail facility (refer Figure 3.6). A series of numerical simulations are conducted by employing a validated computational fluid dynamics (CFD) model (Coussirat et al., 2008; Gebremedhin & Wu, 2003; Rohdin & Moshfegh, 2007; Stavrakakis, Koukou, Vrachopoulos, & Markatos, 2008) to investigate the performance of the combined system in terms of temperature field distribution and airflow patterns for all the designed configurations. The experiments in a scaled environmental chamber were performed for further validation of the numerical method. The comprehensive details on the system configurations, design and simulation setup will be elaborated in the subsequent sections.

4.2 CFD Models of the Designed Configurations

In order to come up with the efficient solution for the VRF-SV hybrid system in large tropical applications, the aforementioned configurations of the combined system were designed using coupled and decoupled strategies for a large retail facility located in the tropics. Figure 4.1 shows the detailed physical illustration of configuration 1 and 2 in the large retail facility.

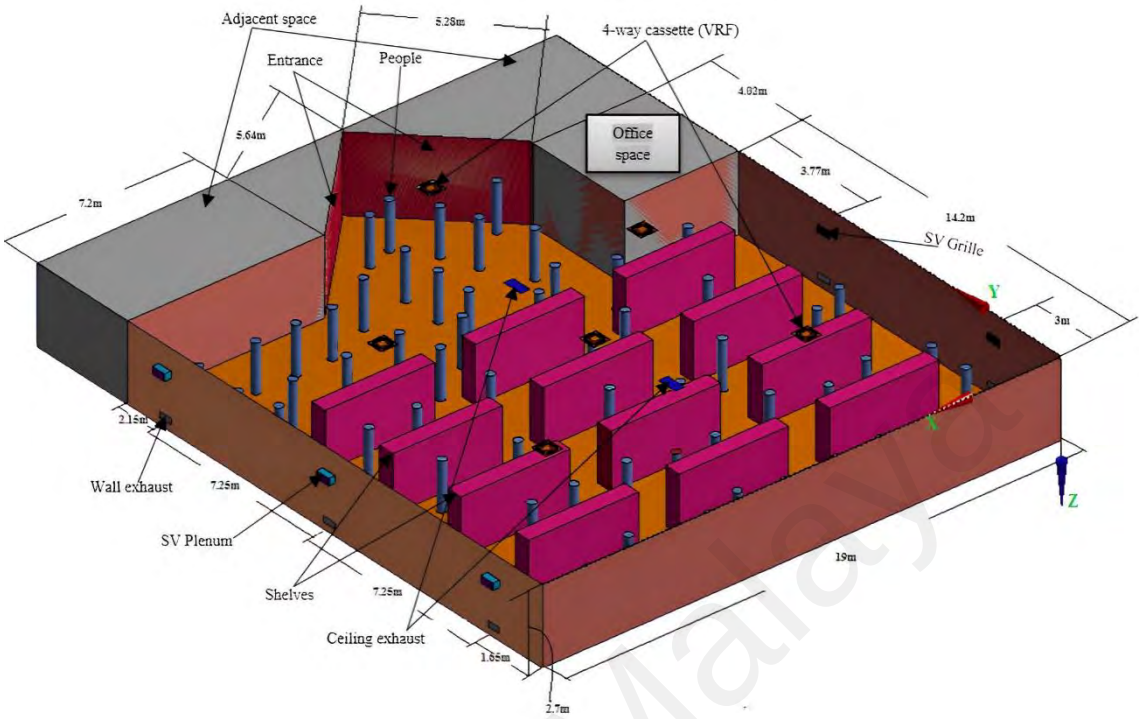

Figure 4.1: Illustration of configurations 1 & 2 for large retail facility

4.3 Experimental Work

The experiments were carried out in the air terminal testing laboratory at Prudentaire Engineering Private Ltd. The laboratory was located at the core of a building under controlled ambient conditions. A small scale simplified model was set up in the laboratory to resemble a portion of the retail shop with dimensions 6 m (L) x 5.4 m (W) x 2.74 m (H). The similar layout of the entities was setup in the laboratory as arranged in the selected portion of the actual retail shop model. Due to the lack of technical resources, only the VRF-SV fully-integrated design (configurations 5 and 6) was selected for validation of the numerical study. The schematic diagram of the experimental arrangement is illustrated in Figure 4.2. The experimental setup was established by installing three bar grille diffusers on the side wall of the laboratory at height of 1.9 m from the floor, while the return grilles were installed on the ceiling or at low level (0.33m from floor) of the supply wall. To verify the numerical model used and to validate the simulation results obtained, the smoke test was also performed along

with the measurement of velocity and temperature at measuring locations. The bar grille diffusers of dimensions 300 mm x 500 mm were used in the experimental setup. The insulated flexible ducts of diameter 200 mm were connected to the oval-shaped neck of the plenum boxes attached to each bar grille. The plenum boxes were sized according to the size of the bar grilles. A ceiling concealed VRF ducted unit was employed to supply the conditioned air through the stratum ventilation air distribution system. To adjust the airflow for uniform supply through all the terminals, the VAV dampers with actuators were installed in each supply duct in the experimental setup. The supply air temperature was monitored by adjusting the off-coil temperature settings. The room temperature was controlled by the wall mounted wired thermostat. The smoke was supplied into the flexible duct connecting the bar grille after controlling the flowrate through the VAV damper.

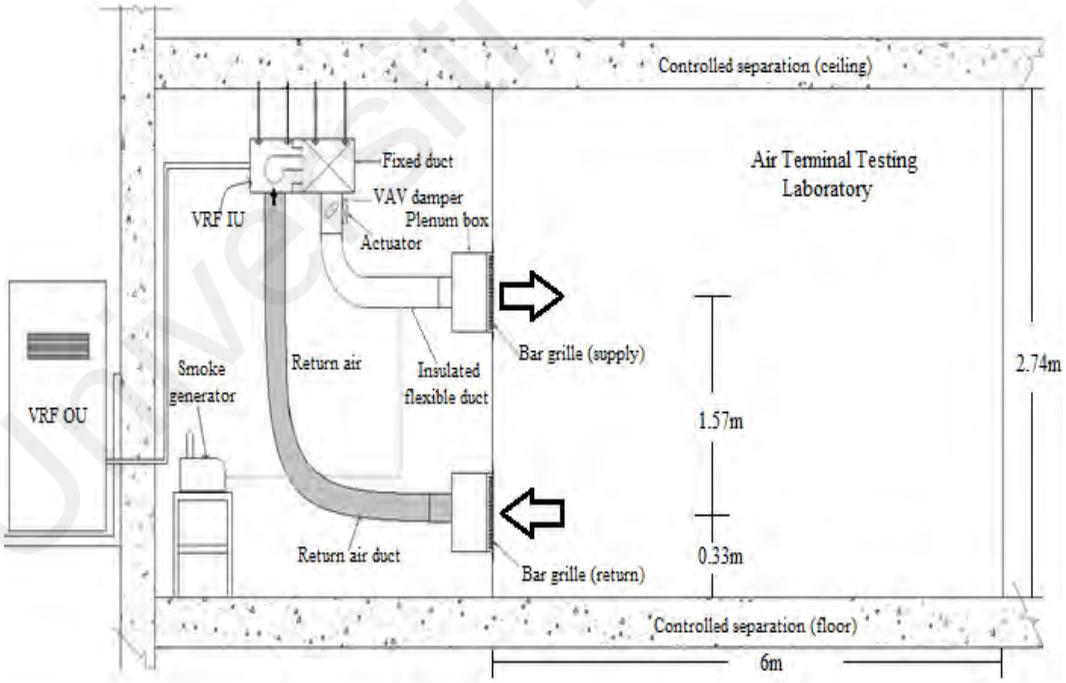

Figure 4.2: Schematic diagram of the experimental chamber

4.3.1 Measurement Methods and Equipment

The detailed environmental conditions of the laboratory were measured before the testing started. The temperature of all the internal surfaces was checked by using the

HI147 HANNA temperature adjustment tool. The ZTH-VAV Belimo tool was used to adjust the airflow rate required. The small scale simplified model [indicated in Figure 4.3(a)] is used to verify the numerical model in the present work and the Alnor 440-A hot wire hand-held anemometer [shown in Figure 4.3(b)] was employed to measure the indoor air temperature and velocity distributions. The accuracy of temperature, velocity and relative humidity for the measuring equipment is ±0.3ºC, 0.05 m/s and ± 3% respectively. The actual measurements were recorded after ensuring the steady state conditions in the laboratory environment.

There was no possibility for the installation of the return grille in the laboratory chamber as it is positioned in configuration 6 in the actual retail shop model. Hence, the assumption was made by positioning the return grilles on the ceiling at the farthest distance from the supply during the experiments by considering the insignificant effect on the flow pattern with the said arrangement (Sun & Smith, 2005). The indoor air temperature and velocity are measured along 11 sampling lines (i.e., L1 - L11) at thirteen different heights above the floor as shown in Figure 4.3(c). For each height along the vertical lines, five testing samples were taken and the average values of the variables were recorded for comparison with the simulation results.

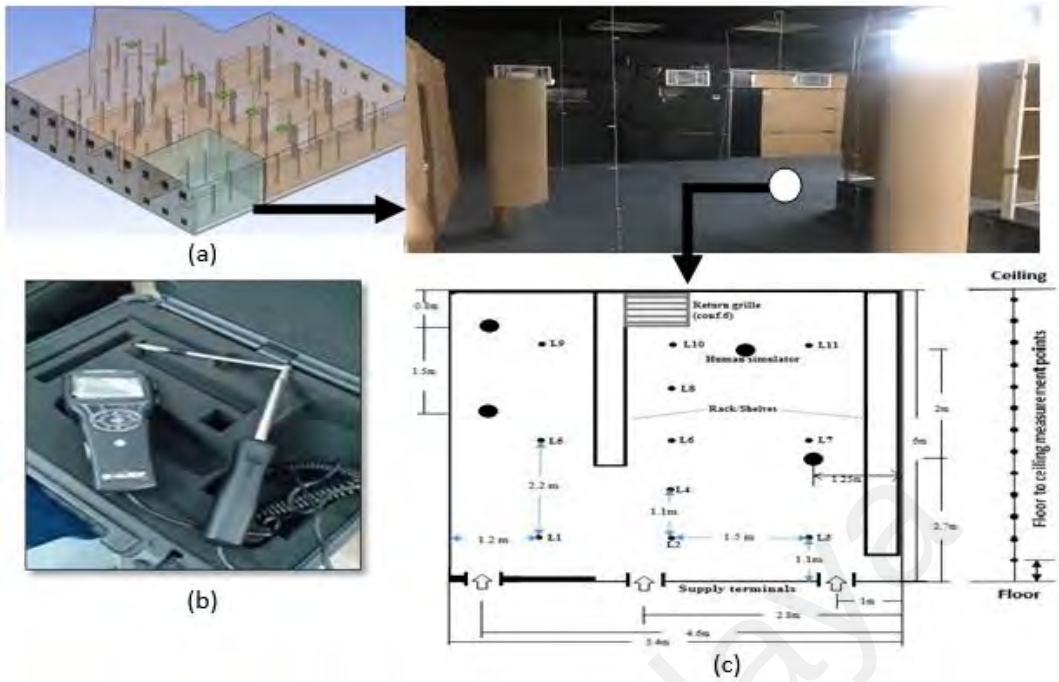

Figure 4.3: (a) Retail shop model (configuration 5&6) with selected corner and experimental setup (b) hot wire anemometer (c) Measurement locations

4.4 Computational Fluid Dynamics (CFD) Simulation

4.4.1 Background Theory

The temperature field distribution and airflow motion in the studied domain are completely governed by the laws of conservation of mass, momentum, and energy. The mathematical models for these three laws are solved in this study using a commercially available CFD program, ANSYS fluent. The models are as follows:

Conservation of mass:

$$\partial\rho/\partial t + \partial(\rho u)/\partial x + \partial(\rho v)/\partial y + \partial(\rho w)/\partial z = 0 \quad (4.1)$$

Conservation of momentum:

x-momentum,

$$\rho\frac{Du}{Dt} = \partial\sigma_{xx}/\partial x + \partial\tau_{xy}/\partial y + \partial\tau_{zx}/\partial z + \sum F_x(\text{body forces}) \quad (4.2)$$

y-momentum,

$$\rho\frac{Du}{Dt} = \partial\tau xy/\partial x + \partial\sigma yy/\partial y + \partial\tau zy/\partial z + \sum F_y(\text{bodyforces}) \quad (4.3)$$

z-momentum,

$$\rho\frac{Du}{Dt} = \partial\tau xz/\partial x + \partial\sigma yz/\partial y + \partial\tau zz/\partial z + \sum F_z(\text{bodyforces}) \quad (4.4)$$

where, σ_{xx}, σ_{yy} and σ_{zz} are the stresses due to normal viscous components acting perpendicular to the dimensions.

Conservation of energy:

$$\rho\frac{DE}{Dt} = \partial/\partial x\left[\lambda\frac{DE}{Dt}\right] + \partial/\partial\left[\lambda\frac{DE}{Dt}\right] + \partial/\partial z\left[\lambda\frac{DE}{Dt}\right] - \partial(up)/\partial x - \partial(vp)/\partial y - \partial(wp)/\partial z + \varphi \quad (4.5)$$

where, φ is the function that shows energy dissipation work done on the fluid, later converted into thermal energy.

4.4.2 CFD Model and Boundary Conditions

In this work, the RNG k-ε (2-equation) model was applied to accurately predict the indoor airflow distribution. This model has been widely validated for internal airflow and heat transfer simulations (Hussain & Oosthuizen, 2012a; Yao & Lin, 2014b; Yau et al., 2018). The governing equations mentioned above, have been discretized with the SIMPLE algorithm using a second-order upwind scheme. To obtain the flow properties near-wall region, a standard wall function was employed in the present study. The Boussinesq model was used in studying the buoyancy effect. The solution was considered to be converged when the residual values reach 10^{-3} except for the energy residual which was set at 10^{-6}. The under relaxation factors (URF) for density, pressure,

energy, momentum, turbulent viscosity, turbulence dissipation rate, and kinetic energy (respectively) were set to arrive at the converged solution. Simulations were carried out using two Workstations, each equipped with Intel Xeon(R) CPU E3-1240 v5 3.5GHz processor, 32GB RAM, Windows 7 Professional 64-bit operating system that required roughly 48 h to 96 h to reach at the solution completion for the generated grids. To produce meaningful results and to set up the fluent program, a proper set of boundary conditions was finalized, which can be found in Table 4.1.

Table 4.1: Boundary conditions setup of the CFD simulation

Boundary	Simulation setup
Stratum ventilation	**(ventilation)**
SV air inlet	2.5m/s, 19 ºC
SV air outlet	0 pa gauge pressure, 24 ºC
VRF air-conditioning	**(air-conditioning)**
VRF air inlet	1.7m/s, 13.5 ºC
VRF air return	0 Pa gauge pressure, 24 ºC
VRF-SV hybrid	**(ventilation + air-conditioning)**
Supply air inlet	2.5m/s, 19 ºC
Exhaust/Return air outlet	0 pa, gauge pressure
Ceiling/Floor/Walls	Adiabatic walls
SV diffuser grille	19 ºC (Adiabatic)
VRF terminal panel	13.5 ºC (Adiabatic)
Plenum box	19 ºC (Adiabatic)

4.4.3 Mesh Sensitivity Analysis

Due to the geometrical similarities between configurations 1 & 2, 3 & 4, and 5 & 6, except their return/exhaust positions, the mesh independence tests were performed only for configurations 1, 3, and 5 to discover the grids independent of mesh size for the present study. The global mesh control using size function was used to generate the mesh with greater control (Control., 2020). A very small element size was selected for the SV/VRF supply and exhaust air terminals, due to their complex and delicate design features. The rest of the fluid domain and boundary surfaces were then discretized with

unstructured tetrahedral mesh elements of different qualities (coarse to fine) by varying the elements and wall/surface sizes. As shown in Figure 4.4, the meshes generated are highly unevenly characterized by higher cell density near walls and the locations, such as in between the floor and ceiling, where more temperature and velocity gradients are expected due to the thermal stratification. It is also based on the reason that the supply airflow rate has a strong connection with the supply air momentum flux, which significantly affects the vertical temperature gradient of the indoor environment from floor to ceiling (Lin & Tsai, 2014).

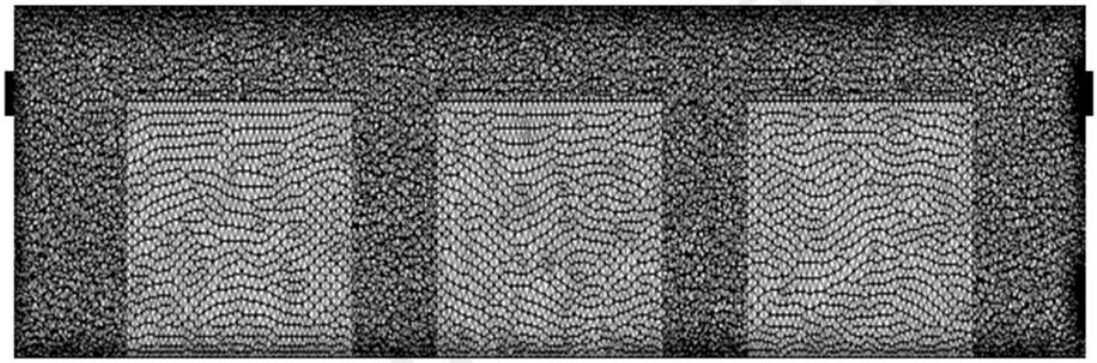

Figure 4.4: A mid plane sectional view of the studied domain with uneven grid

The details of the grids used in domain discretization of configuration 5 are shown in Table 4.2. Principally, in the grid independence studies, the mesh incremental step of 1.5 from the coarser mesh is usually considered for refining the mesh globally (Bhatia; Control., 2020). However, this incremental step may not be feasible in cases where the total number of grids are higher than 3 x 10^6 elements (Yau et al., 2018). It is because the higher number of elements require greater computational time and power. Therefore, to run the simulation uninterruptedly under computational limitations, a low incremental step up to 1.07 is used in the current study to generate the refined mesh. The mesh refining was continued until the volumetric average indoor temperature for consecutive mesh sizes dropped below 0.01°C. The higher incremental step of 1.47 was also used to super refine the Mesh- IV (Table 4.2) in order to assess the results accuracy

and independency at very large number of grids. The consistency in the volumetric mean of the space temperature values for successive mesh sizes led the authors to consider the mesh independence at coarser mesh (Mesh- III), as seen in Figure 4.5. Further analyses were performed using the selected mesh settings.

Mesh	Mesh Details and size		Mesh element	Mesh nodes	Increment step
I	Global element size	1.5m	29,546,967	5,620,305	1.07
	Surface size (Wall)	0.5m			
II	Global element size	0.5m	31,799,046	6,047,202	
	Surface size (Wall)	0.1m			1.14
III	Global element size	0.1m	36,513,027	6,850,217	
	Surface size (Wall)	0.1m			1.03
IV	Global element size	0.05m	37,655,173	7,065,997	
	Surface size (Wall)	0.1m			
V	Global element size	0.01m	55,462,143	10,388,112	1.47
	Surface size (Wall)	0.1m			

Table 4.2: The mesh details on grid independence study (configuration 5)

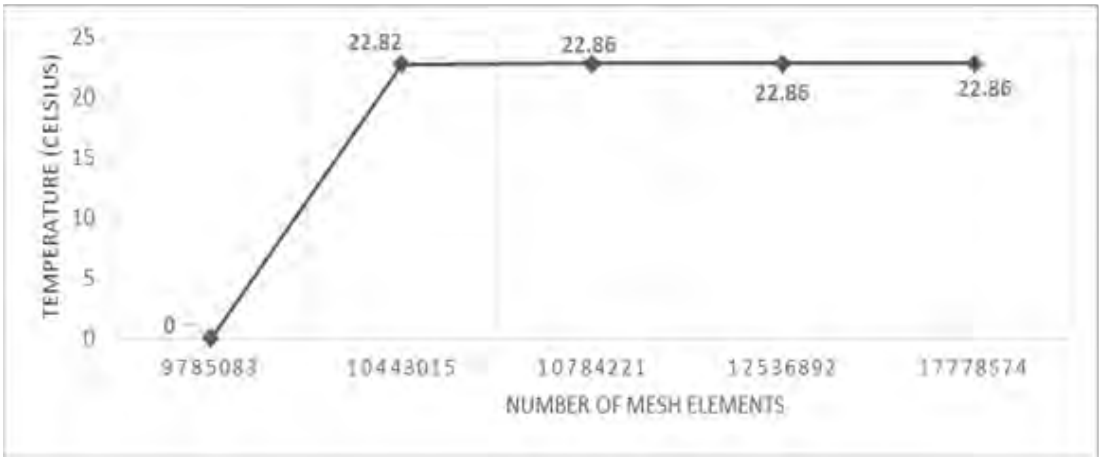

(a)

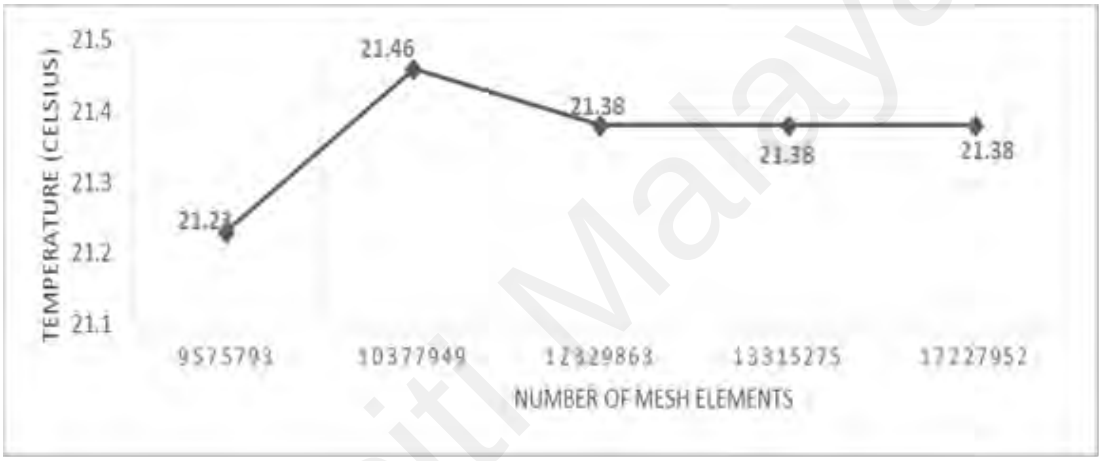

(b)

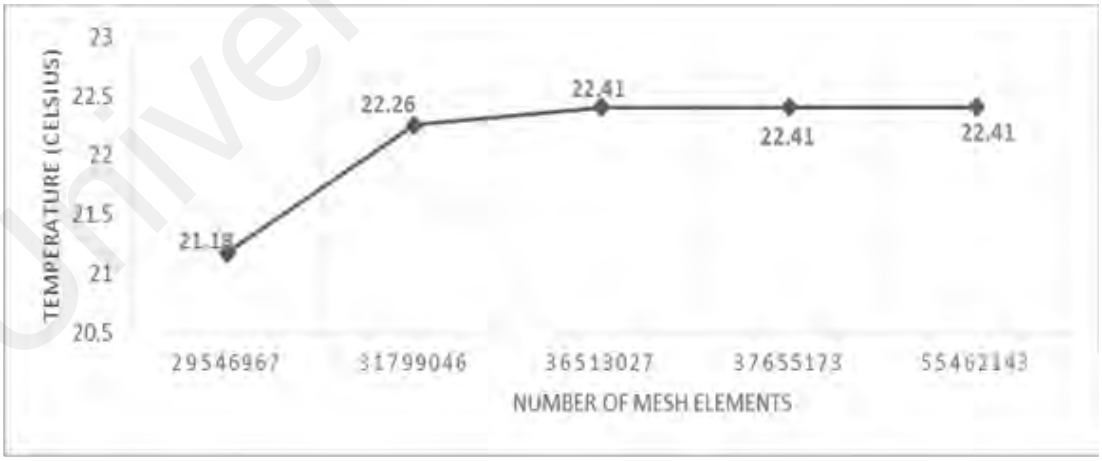

(c)

Figure 4.5: Volumetric mean temperature at different grid sizes (a) configuration 1 (b) configuration 3 (c) configuration 5

4.5 Performance Evaluation Criteria

The only purpose of installing the ACMV system in space is to produce an environment with acceptable thermal comfort and better IAQ. Thus, this study investigates the performance of the different configurations of the combined system using the following indicators:

1. Temperature field distribution
2. Airflow pattern
3. Energy utilization coefficient (EUC)
4. Quantitative assessment of the temperature and velocity

EUC is an energy performance coefficient used to evaluate the energy utilization efficiency of air distribution systems (W. Liu, Lian, & Yao, 2008). It represents the usefulness of energy utilization in air distribution to the occupied zone in order to achieve an acceptable level of indoor thermal comfort (Ga, 1995). The zone from the floor to 1.8m height and 0.15m distance from the side walls is considered as the occupied zone (W. Liu et al., 2008). According to the definitions available in the literature (Ga, 1995), the EUC is not only influenced by the condition of the air supplied and extracted from the occupied zone, but also affected by the occupancy pattern and the air distribution system configurations. Therefore, given the provided conditions for designed configurations of the VRF-SV system, this index can be used to evaluate their air distribution performances quantitatively. A high value of EUC indicates the efficient use of energy by the air distribution system with an acceptable indoor environment. It can mathematically be expressed as follows:

$$\mathrm{EUC} = \frac{T_{uz} - T_s}{T_{oz} - T_s} \tag{4.6}$$

where, T_{uz}, T_{oz}, and T_s are the temperatures at unoccupied zone, occupied zone and supply inlet respectively.

This equation could only be applied to the cooling mode. The T_{oz} and T_{uz} values are calculated by taking the volumetric mean temperature for the occupied and unoccupied zones, respectively. The separate arbitrary volumes were created using volume by surface method in the ANSYS post processing module. The rest of the volume of the CFD domain was considered as the volume of the unoccupied zone.

For stratum ventilation, the thermal comfort is considered acceptable, when the airflow velocity in the occupied zone is not more than 0.8m/s (Yao & Lin, 2014b). As this study integrates the two advanced systems (i.e., SV and VRF), the need for the performance judgment is crucial. The aforementioned three indicators can finely evaluate the system performance in the designed configurations.

4.6 Results and Discussion

For the measurement of air temperature and velocity distribution, the evaluation strategy put forward by Zheng et al., (2018) is adopted. Both the air temperature and velocity are directly extracted on the contour planes. On the bases of these two parameters the thermal comfort analyses are carried out for designed configurations.

4.6.1 CFD Model Validation

To validate the employed model, a small-scale experimental setup was established in the current study as detailed in the previous section. Following the similar settings as that in the simulations, the CFD predicted air velocities and temperatures are compared with the experimental measurements. In general, the simulated air temperatures and velocities have shown almost the similar profile variation as those of the experimentally measured values (Figure 4.6). Nevertheless, some discrepancies were observed with

temperature distribution at certain locations (as can be seen in Figure 4.6 (a) and (b)). This may be due to some assumptions made in mimicking the retail shop in the laboratory chamber, as already discussed in section 4.3.1.

The differences can also be attributed to the errors in measurement methods, which includes the difficulties in maintaining the experimental boundaries in steady state and the low accuracy of the measurement using a handheld anemometer device due to low air velocities at certain locations (A. K. Melikov, Popiolek, Silva, Care, & Sefker, 2007). Similar findings have also been reported in other studies (Z. Lin, Tian, et al., 2011; S. Zhang et al., 2019; Zheng et al., 2018). Those results are comparable with the presented data with no consideration to specific geometry type. In this study, the mean absolute deviations (MADs) of the air temperature and velocity values between the simulated and the experimental measurements for configuration 5 are 0.2ºC and 0.05 m/s, respectively. For configuration 6, the MADs are 0.02ºC and 0.01 m/s. The highest value of velocity and the lowest air temperature are observed at the height of 2 m from the floor in both the CFD predictions and experiments. It is because of the good throw performance obtained by the bar grille diffusers installed at 1.9 m height from the floor. The large differences in velocity and temperature values are noticed at almost all the locations (L - L11) near the floor and ceiling heights (y/H), which may be caused by the reasons just discussed above. Overall, a satisfactory agreement between the predictions and experimental results' profile has been observed. Thus, the model adopted is considered valid for further studies.

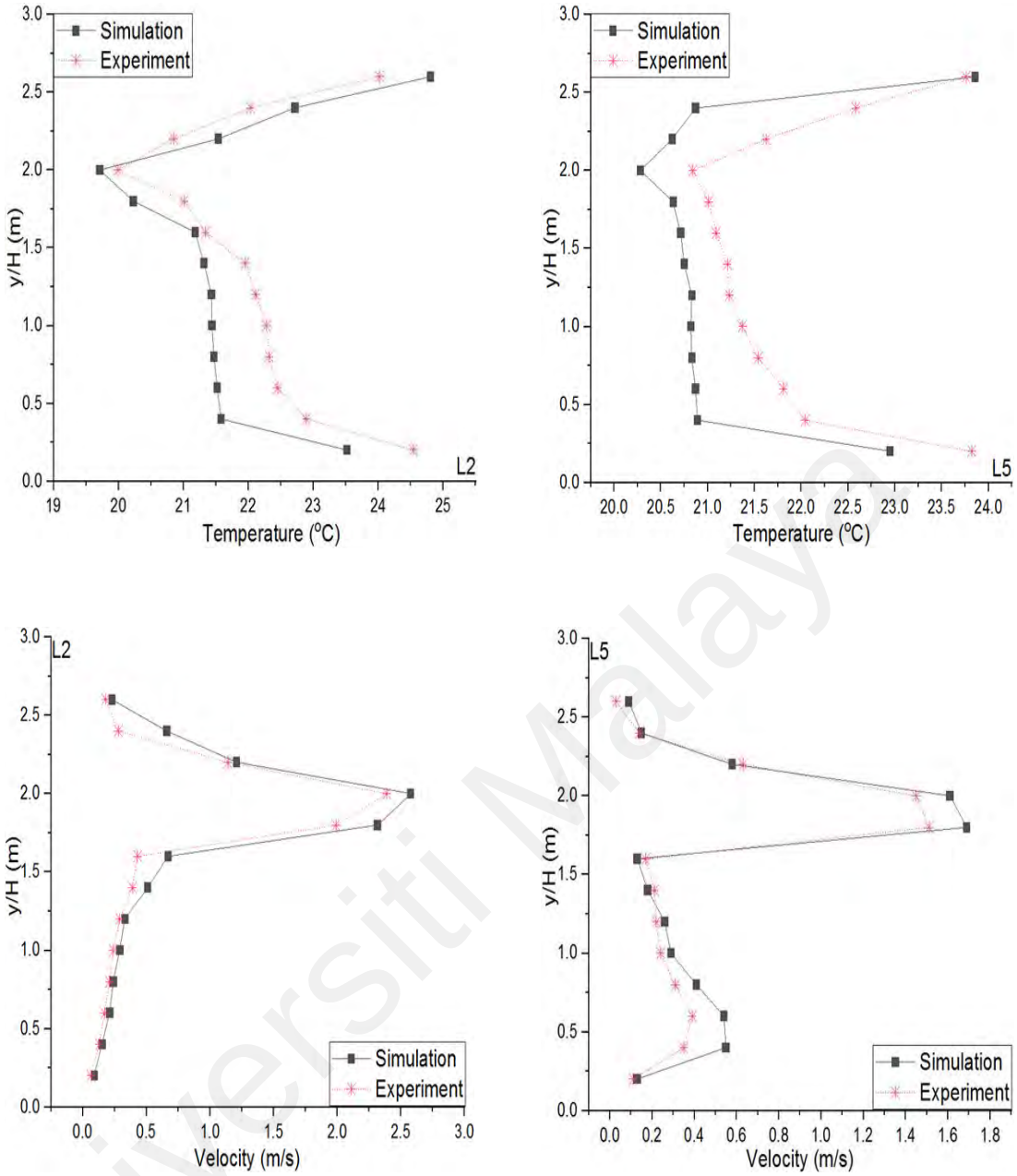

(a)

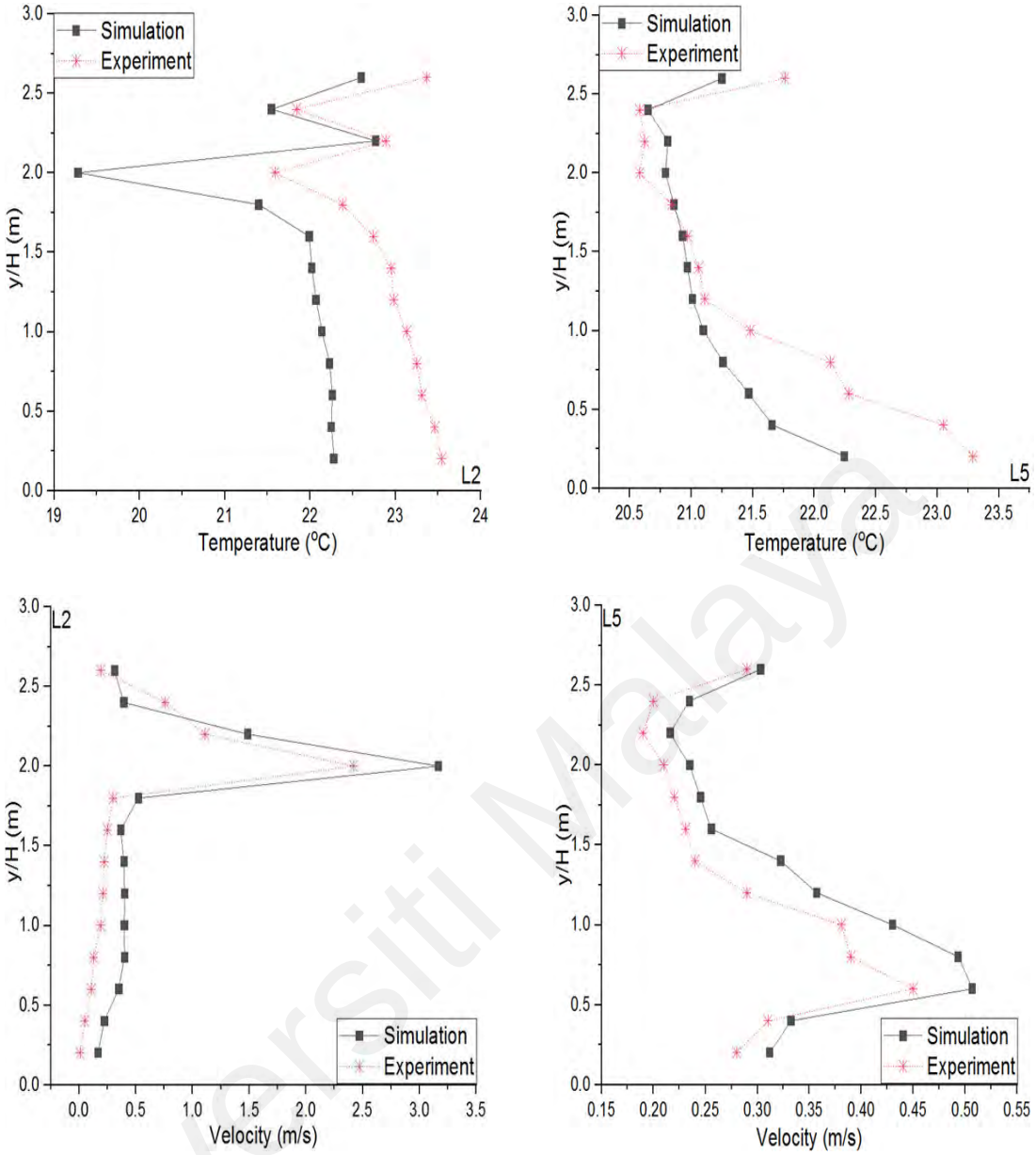

(b)

Figure 4.6: Comparison of experimental and simulated results for two configurations (a) Configuration 5 (b) Configuration 6 (Note: L2 / L5 are two sampling lines) [y/H= Height from floor to ceiling]

4.6.2 Temperature Field Distribution

The thermal distribution within the studied domain is presented and compared between configurations 1 and 2, configurations 3 and 4 and configurations 5 and 6. These configurations are paired based on their similar design layouts, except for the return air terminal position. The air temperature diffusion on the selected sectional planes (X= 9.8 m, Y= 16.8m, Z= 0.9 m) is numerically illustrated in Figures 4.7, 4.8

and 4.9. The supply air temperature for SV in all configurations is set to 19ºC, as recommended by (Morovat & Maerefat, 2013) and the refrigerant evaporating temperature for the VRF cooling coil in configurations 1-4 is set to 13.5ºC.

As shown in the Plane XZ in Figure 4.7(a), the temperature dips down more deeply as compared to Figure 4.7(b), it is due to the low pressure at the ceiling exhaust terminal in configuration 2. There is no significant change seen in the temperature stratification for both of the configurations at plane XZ, except the colder air reaches a little far in configuration 2 than in configuration 1. An obvious uniformity in temperature distribution for configuration 1 can be seen on Plane XY. The temperature was slightly lower at the bottom under the configuration 1. A poor thermal distribution performance on all the planes in configurations 3 and 4 can be observed in Figures 4.8(a) and (b), respectively. Both of these configurations employed floor-mounted console units. An added plane at Y= 5 m is also created to illustrate the thermal field performance of these units.

Figures 4.9 (a) and (b) captured the better thermal distribution performance rendered by configurations 5 and 6, respectively. Both these designs supply the conditioned air through the wall-mounted inlets, whereas, no separate VRF indoor terminal units were employed. While comparing the performance, configuration 5 was found most efficient amongst all in terms of uniform thermal distribution within the breathing zone of the domain. To verify the thermal uniformity of the VRF-SV coupled design, the results of this study can be compared with the studies under stratum ventilation in a variety of environment (Z. Lin, Yao, et al., 2011; Yao & Lin, 2014b, 2014c).

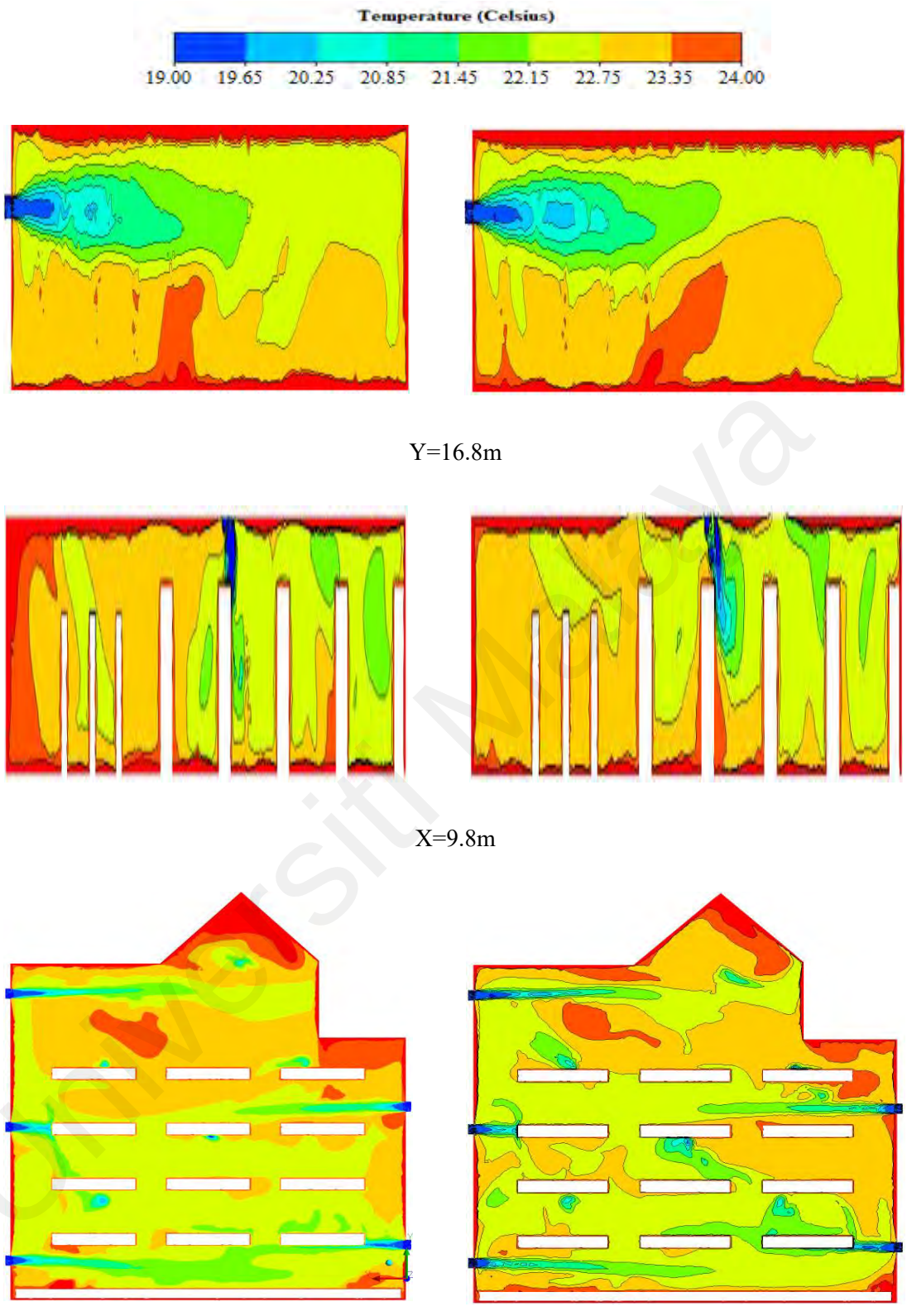

Figure 4.7: The temperature distribution in the retail shop (a) configuration 1 (b) configuration 2

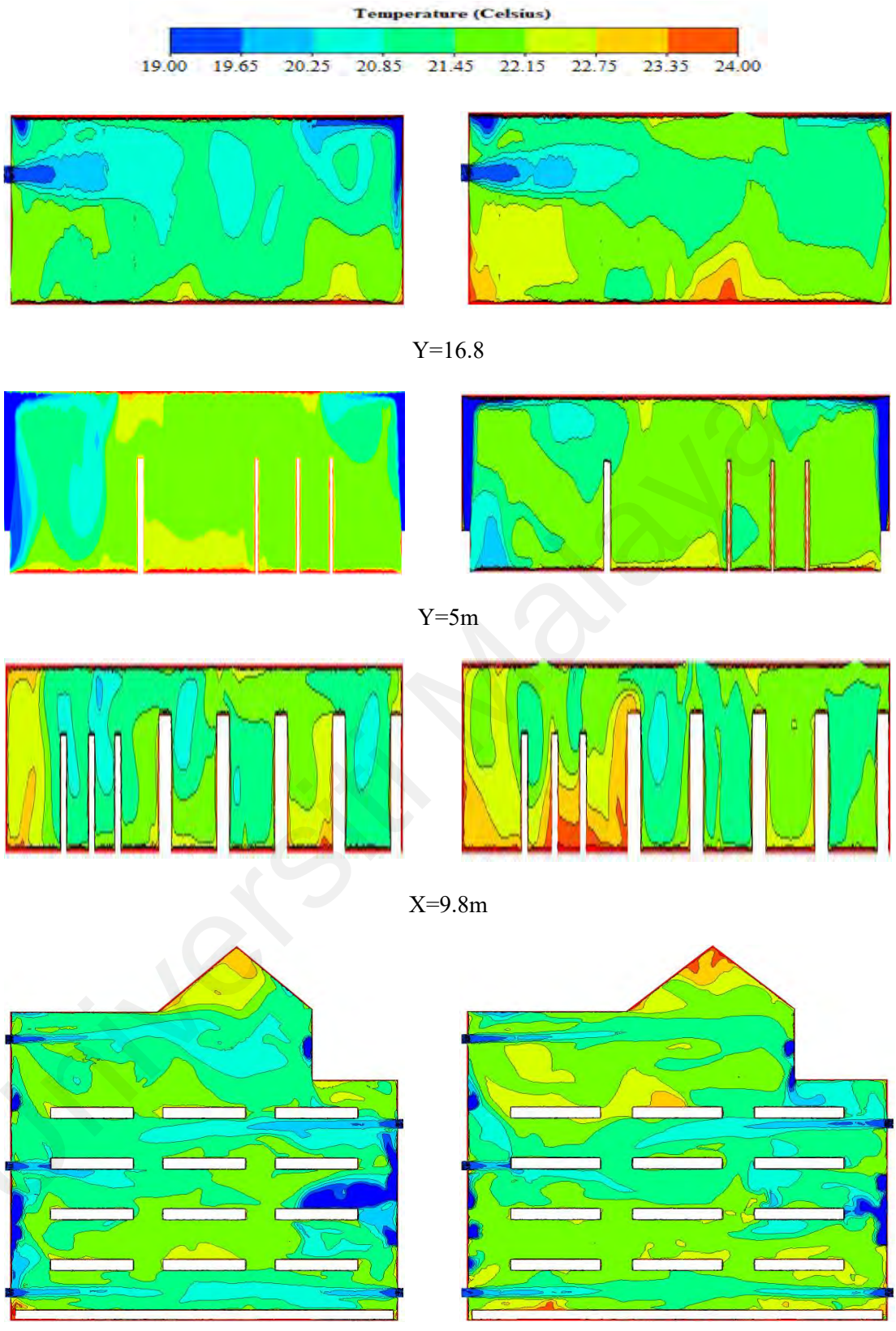

Figure 4.8: The temperature distribution in the retail shop (a) configuration 3 and (b) configuration 4

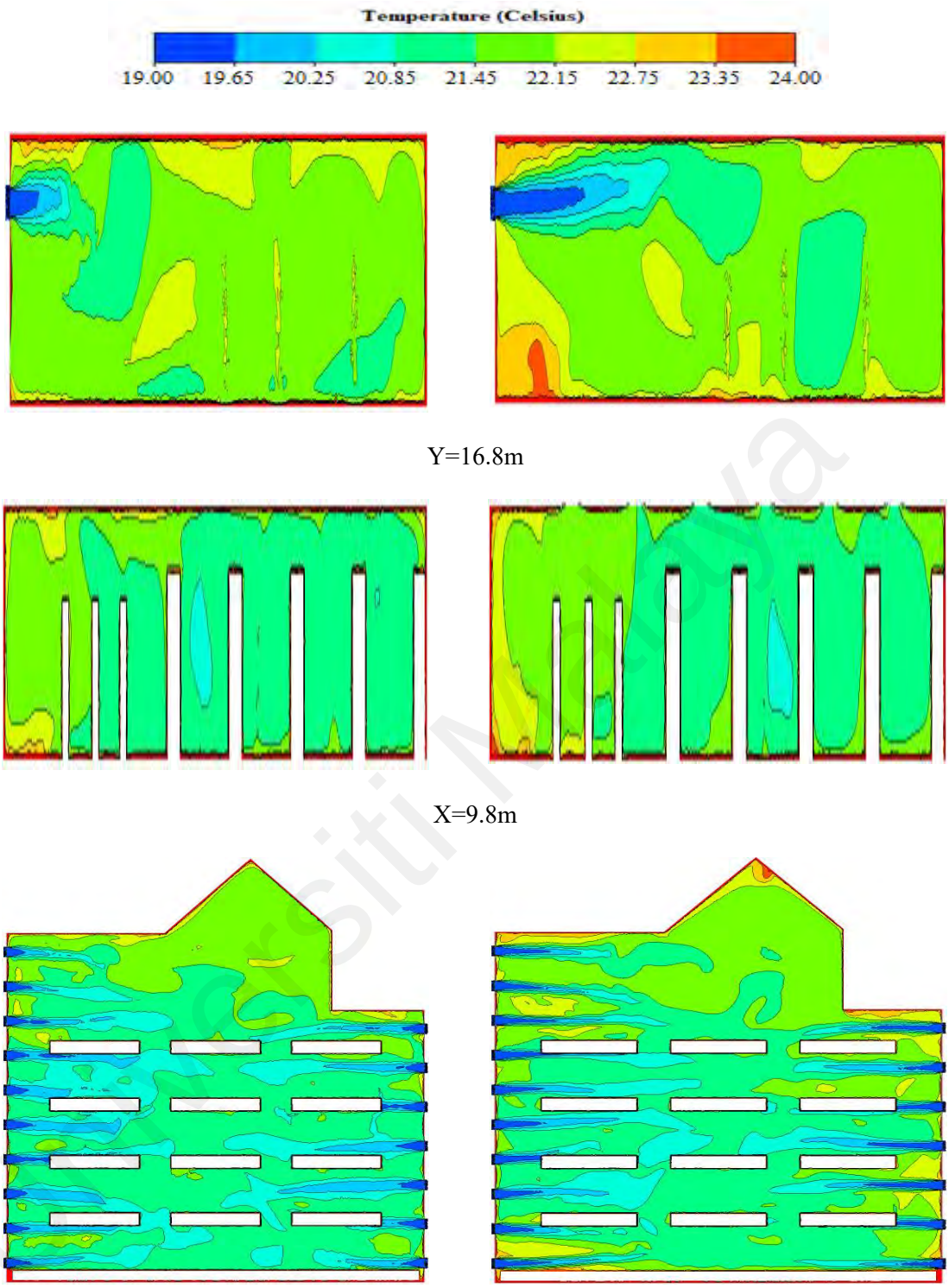

Figure 4.9: The temperature distribution in the retail shop (a) configuration 5 and (b) configuration 6

4.6.3 Airflow Pattern

The airflow pattern created by different ventilation strategies has great impact on the indoor thermal comfort (Tian, Lin, & Wang, 2011), therefore the indoor airflow under designed configurations were extracted and shown in Figures 4.10, 4.11, and 4.12. The sectional planes drawn in the previous section were used to study the airflow distribution inside the retail shop. A similar fashion with respect to airflow pattern was observed when compared to the configurations 1 & 2 and configurations 3 & 4, except some eddies that are generated near the VRF indoor unit supply due to reversed airflow towards return outlets.

As seen in Figures 4.10 and 4.11 (Plane XY), a strong airflow throw came into view for both of the configurations. This was because of the good throw performance of the bar grill diffuser with the desired face and terminal velocities. The Plane XZ in Figure 110 (b) showed the airflow direction moving upward after exiting the SV air supply. This is due to the fact that exhausts were positioned on the ceiling in that configuration. This air short-circuiting is avoided in configuration 5, using low-level wall mounted exhaust terminals. The cooled air after exiting the SV supply air terminal went straight towards the center and it then fell down due to gravity. This is why the airflow field in the breathing zone was more stable and uniform within the specified range of wind speed (Z. Lin, Yao, et al., 2011). Because of the shelves and occupants, several eddies are formed in all the configurations. Overall, the mixing of the cooled supply air and indoor air in the lower zone in configuration 5 was higher, that makes the occupied zone more thermally comfortable (Zheng et al., 2018).

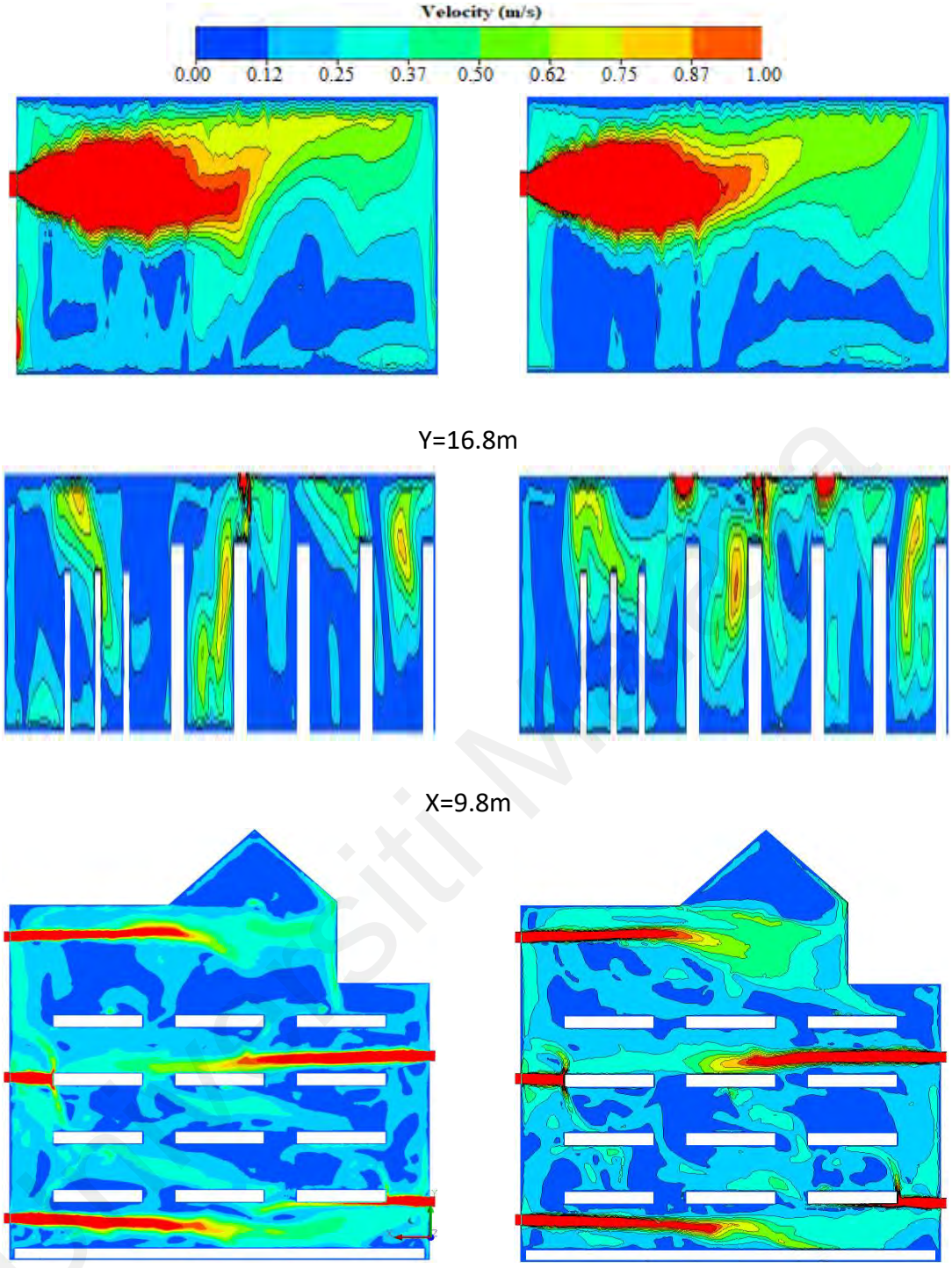

Figure 4.10: The airflow distribution in the retail shop (a) configuration 1 (b) configuration 2

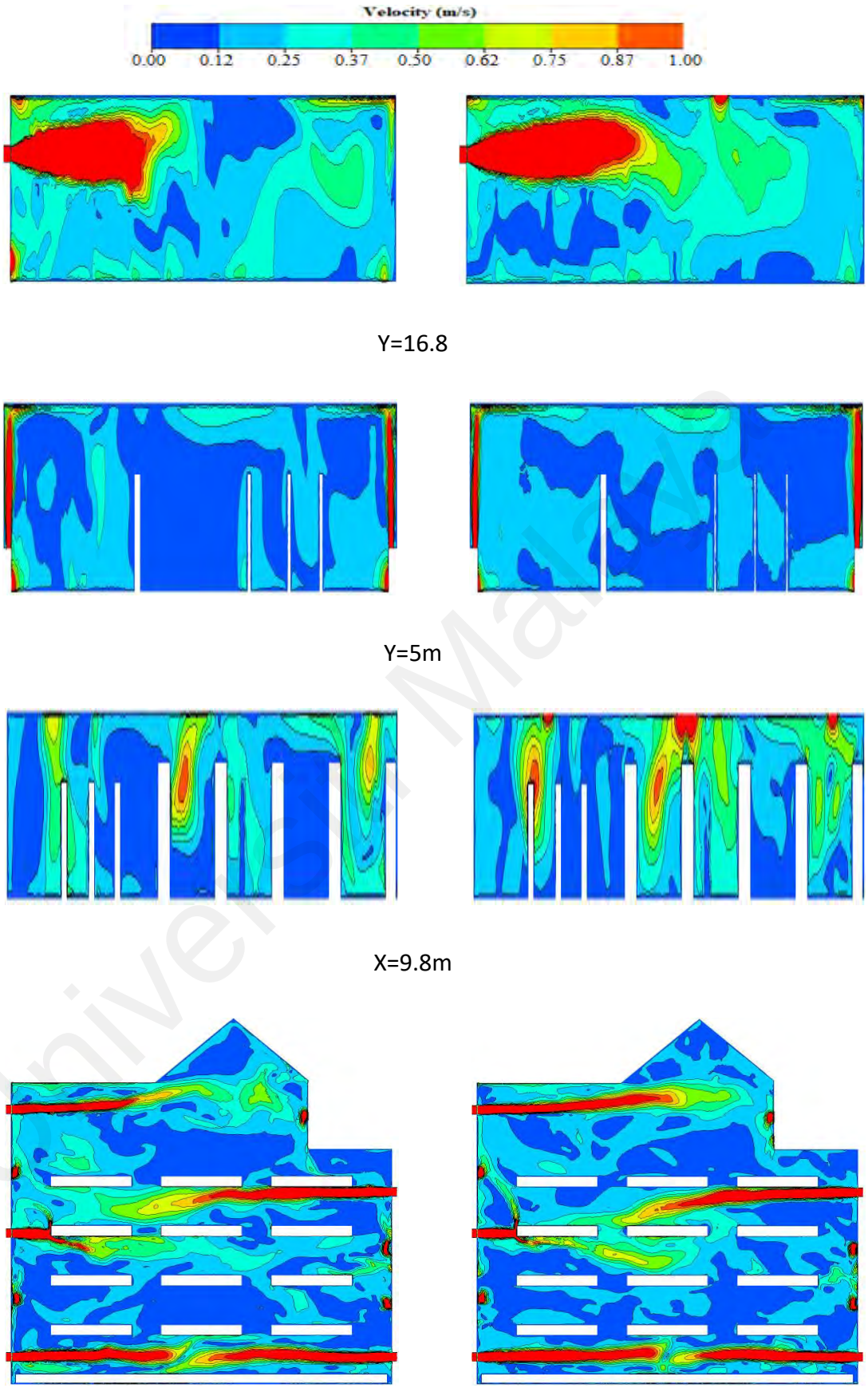

Figure 4.11: The airflow distribution in the retail shop (a) configuration 3 (b) configuration 4

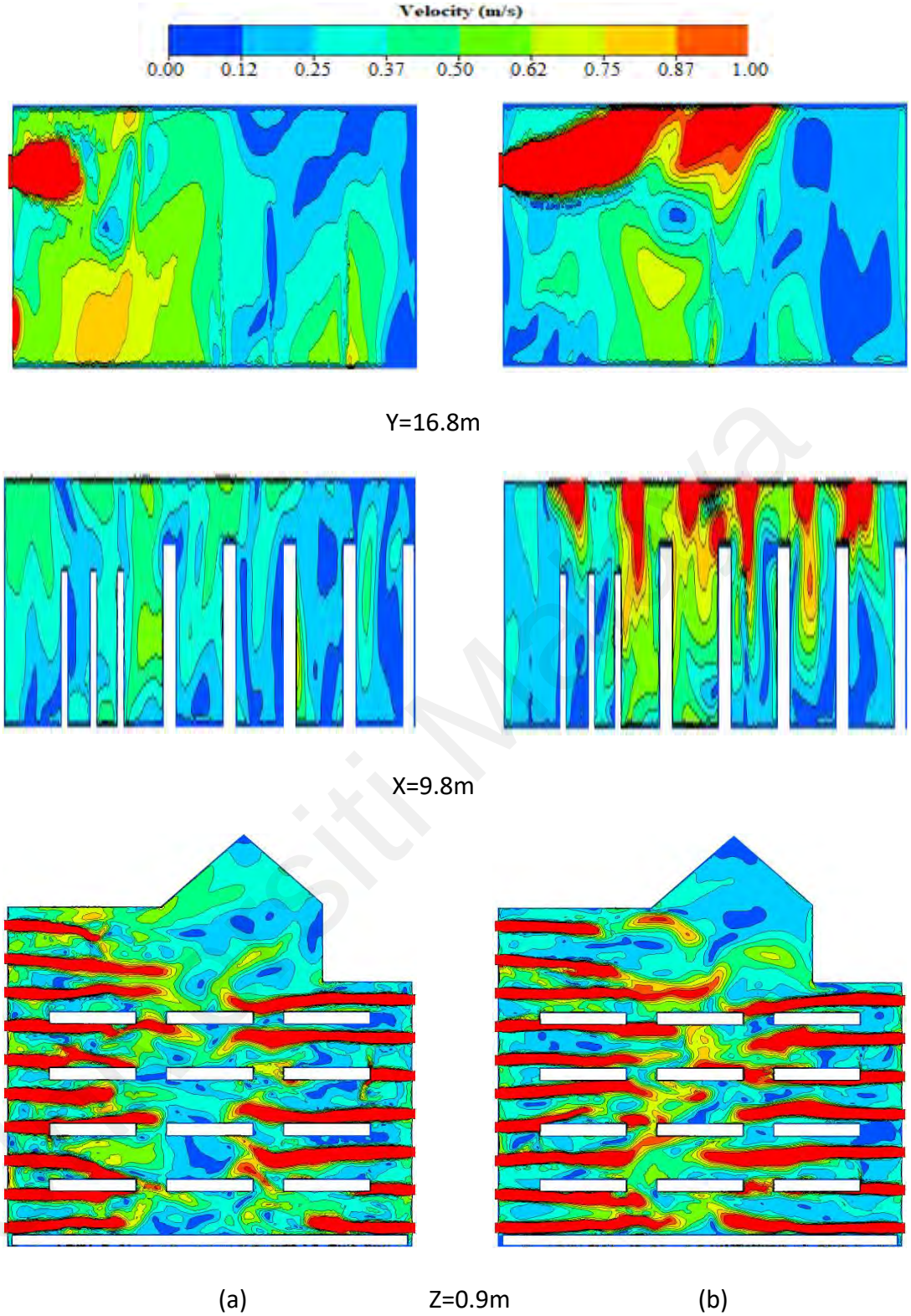

Figure 4.12: The airflow distribution in the retail shop (a) configuration 5 (b) configuration 6

4.6.4 Energy Utilization Coefficient (EUC)

The comparison of the EUC values for the studied configurations is given in Table 4.3. The supply temperature for configuration 1 to 4 is determined by taking the

weighted average of the SV and VRF supply temperatures based on the volume of the air supplied. Owing to its greater mixability, the heat exchange between the supplied air and the air in the occupied zone found better in configuration 5. Though, configuration 1 gives a slightly higher value of EUC than configuration 5, but it does not provide a uniform distribution of temperature and velocity in the entire breathing zone (as seen in figures 4.7 and 4.10).

Table 4.3: The EUC values for studied configurations of the VRF-SV hybrid system

S. No.	T_s, ºC	T_{uz}, ºC	T_{oz}, ºC	EUC
Configuration 1	15.47	22.95	22.87	1.01
Configuration 2	15.47	22.80	22.92	0.98
Configuration 3	15.47	21.24	21.52	0.95
Configuration 4	15.47	21.55	21.76	0.96
Configuration 5	19.00	21.34	21.36	0.99
Configuration 6	19.00	21.66	21.72	0.98

4.6.5 Quantitative Assessment

Considering the better outcome obtained with configuration 5, a detailed investigation was also carried out to further examine its design suitability for large tropical applications. For detailed analyses, the temperature and velocity distributions are measured at 7 different locations (A-G) as shown in Figure 4.13. These locations are marked randomly to obtain the results at every part of the studied domain. Few locations were chosen near to the supply diffusers, whereas location C was selected at the geometric center of the domain. Along the vertical lines drawn at these locations, 10 measuring heights at a distance of 0.27m each from the floor to the ceiling were points to record the temperature values.

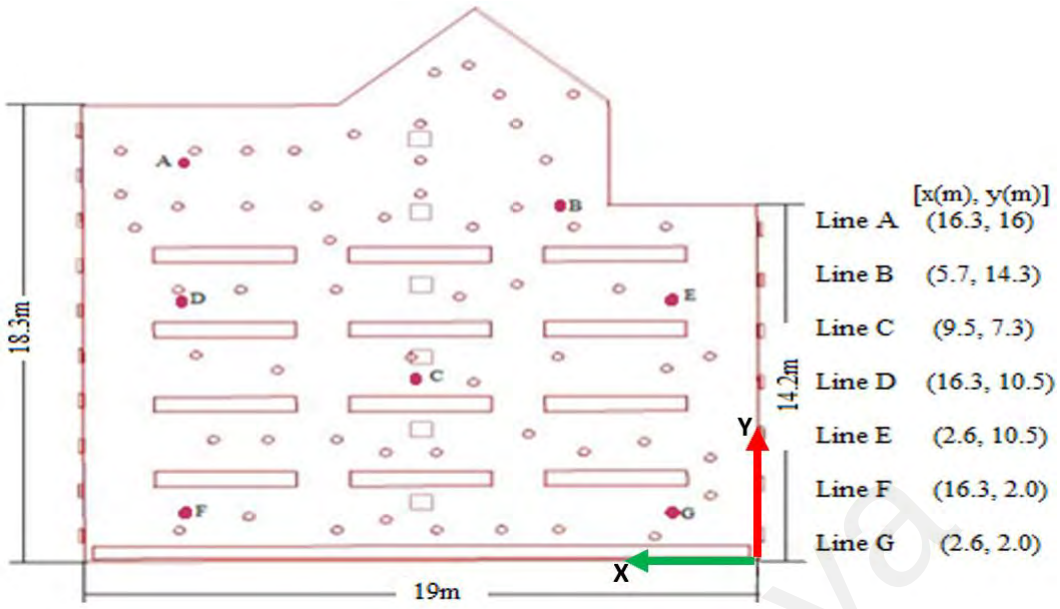

Figure 4.13: Selected measuring locations (A-G) and their coordinates

Figure 4.14, delineated the indoor temperature distribution at described locations. A positive thermal gradient between the head and foot level, a good temperature stratification and a uniform temperature distribution of about 20.5ºC - 21.7ºC in the occupied zone were observed. The temperature values in the entire zone found within the ASHRAE comfort range.

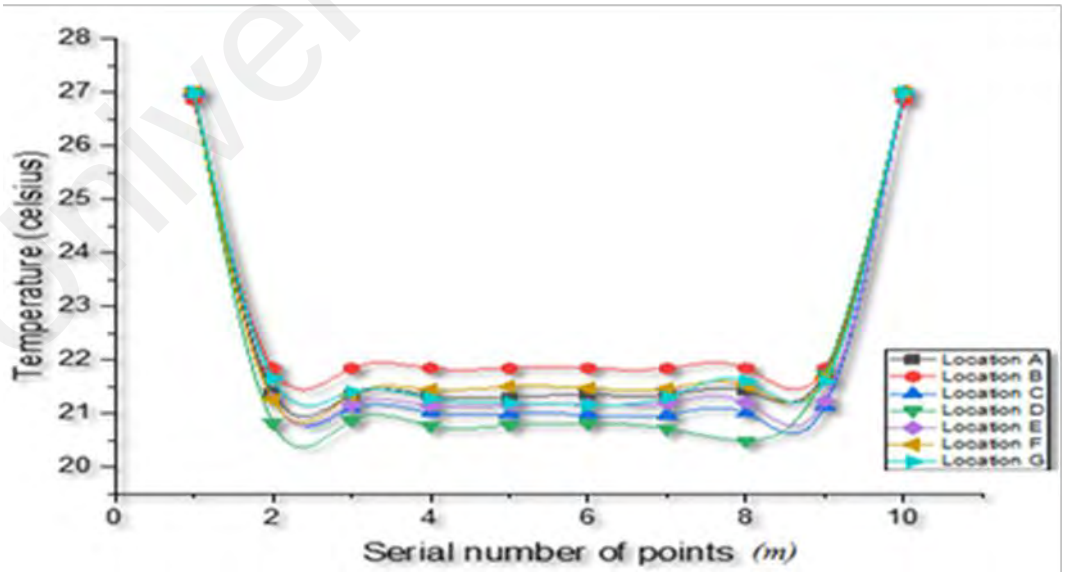

Figure 4.14: Temperature distribution along vertical lines at selected locations

The airflow movement was also recorded at these locations to evaluate the high draft risk issue in the occupied zone. For configuration 5, the indoor air velocity values at given locations within the breathing zone were also found under acceptable range as per ASHRAE standards 55 (ASHRAE, 2020) (see Figure 4.15). The higher velocity values of about 0.60 - 0.75 m/s were noticed at location G for the entire breathing height. The airflow velocity within the occupied zone has not exceeded the value 0.8 m/s. This ensures the high percentage of thermally satisfied people in the space due to the air draft.

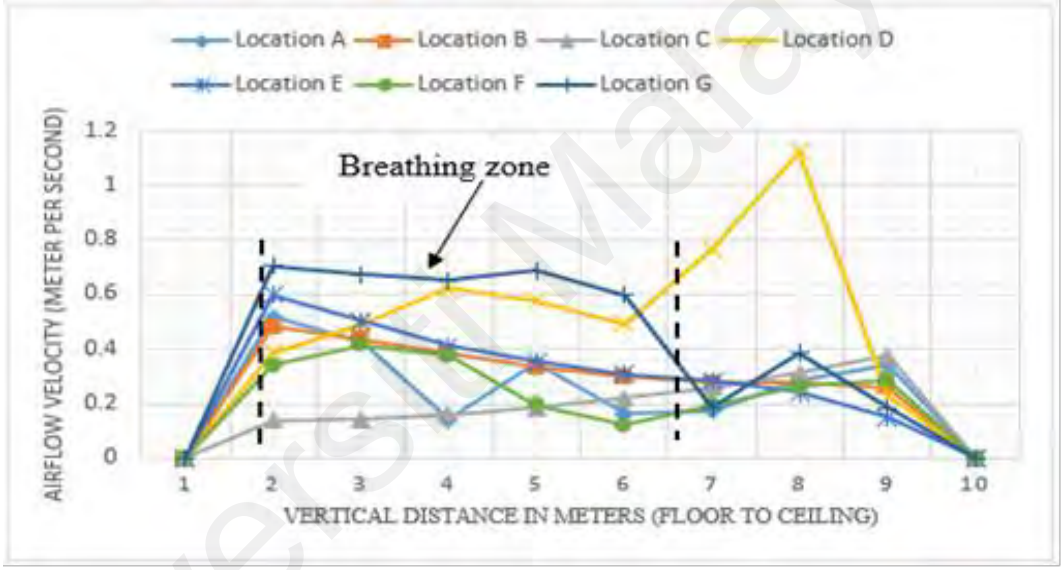

Figure 4.15: Airflow distribution along vertical lines at selected locations

4.7 Summary

The airflow performance of the VRF-SV hybrid system under different design configurations was numerically studied for a large retail facility. Two ventilation integration design strategies (i.e. coupled and decoupled) were adopted for an in-depth understanding of the combined system performance. The decoupled design with configurations 1 to 4 has provided a non-uniform temperature and velocity distribution in the occupied zone, whereas the last two configurations served by the VRF-SV coupled design shown that the thermal comfort can be uniformly realized in the entire occupied zone. The results revealed from configurations 5 and 6 confirmed a good

potential of the VRF-SV integrated design to be employed in large ACMV applications in the tropics. Nonetheless, the excessive supply airflow should be avoided because it may create a draught risk problem to the occupants near the supply locations.

The indoor air velocity was modest in the work zone of the retail facility and has not exceeded 0.8 m/s throughout the zone, and thus, it complies with the standard ASHRAE 55-2020 (ASHRAE, 2020). The thermal gradient was found positive and under an acceptable range between the head and foot level for standing occupants. Both the simulation results and experimental assessment suggest that the thermal environment created in the occupied zone by the VRF-SV integrated design can be treated as uniform with energy saving potentials.

CHAPTER 5: THERMAL COMFORT ASSESSMENT OF THE VRF-SV HYBRID SYSTEM: CFD SIMULATIONS

5.1 Introduction

The variable refrigerant flow (VRF) air-conditioning system is a widely adopted alternative to the existing building cooling systems due to the higher energy efficiency and individualized temperature control feature. In the VRF system, the refrigerant is modulated based on the capacity requirement, and thus, energy saving is achieved.

In previous chapter, the air distribution performance of the VRF-SV hybrid system under different design configurations was numerically studied for a large retail facility. The results revealed from configurations 5 and 6 confirmed a good potential of the VRF-SV integrated design to be employed in large ACMV applications in the tropics.

To extend the research in this direction and thoroughly evaluate the performance of the VRF-SV hybrid system the study in this chapter was aimed to numerically investigate the thermal comfort performance of the selected configurations (Configuration 5 and 6). Based on standard thermal comfort indices, the extended performance of the selected configurations was evaluated. The parametric analyses were also carried out to investigate the effect of varying indoor design conditions on the combined system capacity.

5.2 Thermal Comfort Assessment: CFD Simulations

5.2.1 Physical Models of the Studied Domain

The present study investigated different design configurations of the VRF-SV hybrid system for a large retail shop in the tropics. Figure 5.1 illustrates the typical design configurations with coupled, decoupled and fully integrated methods. A series of numerical simulations were conducted using all the designed configurations to obtain sufficient information for evaluation of thermal comfort standards.

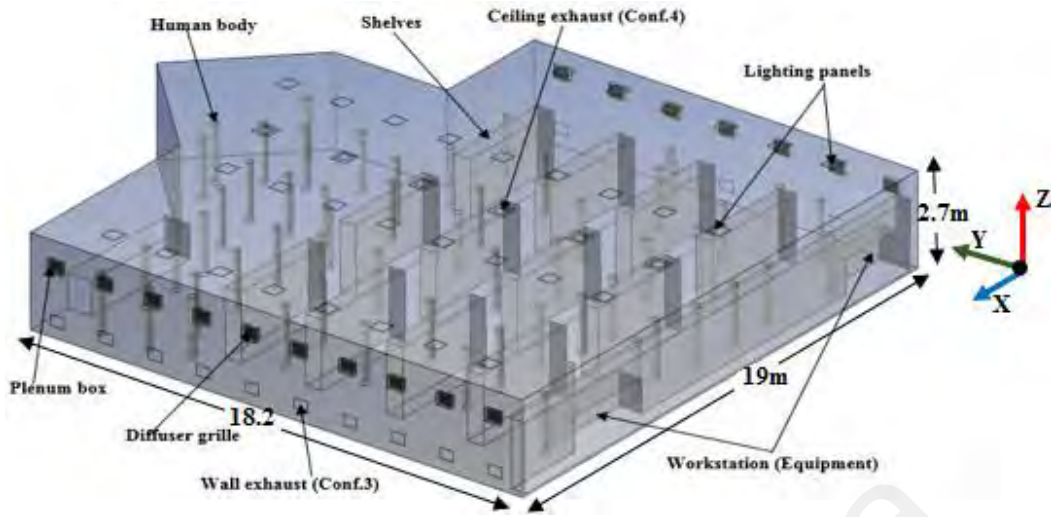

(a)

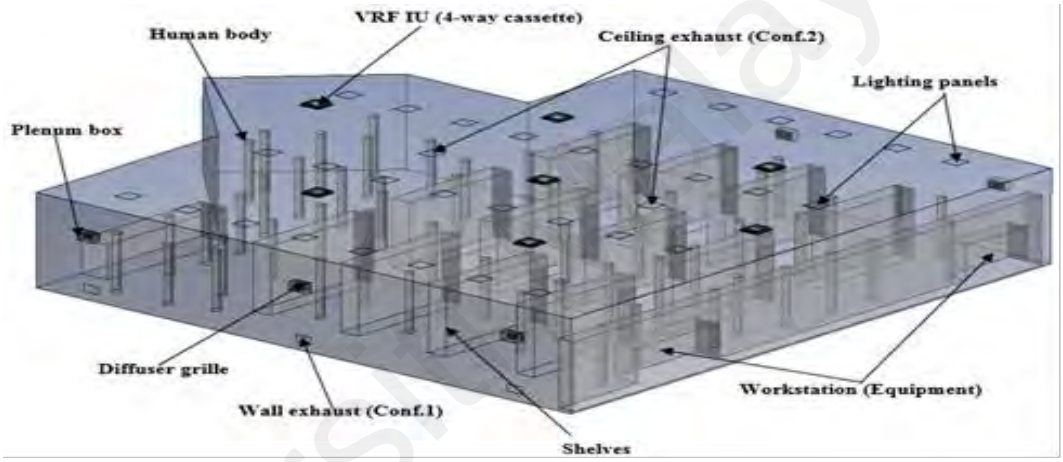

(b)

Figure 5.1: CFD model of the VRF-SV system (a) fully integrated approach (b) decoupled or coupled approach

5.2.2 Governing Equations

The temperature and airflow field distributions in the studied domains are governed by the conservation laws of mass, momentum and energy. The momentum equation is solved by inducing the buoyancy effect, whereas the air density is treated as incompressible, obeying the ideal gas law. The mathematical models for these three laws (as expressed in section 4.4.1) are solved in this study using a commercially available CFD program, ANSYS fluent.

5.2.2.1 Mathematical Model

The RNG k-ϵ model is employed in the numerical simulations in this study. This model is a variant of the standard k-ϵ model and is derived using the renormalization group (RNG) theory. This model has an additional term in the ϵ equation, which further refines the accuracy of the solution. The effect of swirling in the turbulent flow is also included in this model (Kubicek et al., 2009). The transport equations for the RNG k-ϵ model can be defined as,

$$\frac{\partial}{\partial t}(\rho k) + \frac{\partial}{\partial x_i}(\rho k \mu_i) = \frac{\partial}{\partial x_j}\left(\alpha_k \mu_{eff} \frac{\partial k}{\partial x_j}\right) + G_k + G_b - \rho\epsilon - Y_M + S_k \quad (5.1)$$

$$\frac{\partial}{\partial t}(\rho\epsilon) + \frac{\partial}{\partial x_i}(\rho\epsilon\mu_i) = \frac{\partial}{\partial x_j}\left(\alpha_\epsilon \mu_{eff} \frac{\partial \epsilon}{\partial x_j}\right) + C_{1\epsilon}\frac{\epsilon}{k}(G_k + C_{3\epsilon}G_b) - C_{2\epsilon}\rho\frac{\epsilon^2}{k} - R_\epsilon + S\varepsilon \quad (5.2)$$

The values for constant terms used in the RNG k-ϵ model are given as follows:

$$C_{1\epsilon} = 1.42, C_{2\epsilon} = 1.68, C_\mu = 0.0845, \sigma_k = \sigma_\epsilon = 1.39, \sigma_t = 0.85$$

5.2.3 Numerical Scheme and Boundary Conditions Setup

In this research, the turbulence k-ε (2-equation) model was applied to predict indoor airflow distribution. The governing equations have been discretized using a second-order upwind scheme with the SIMPLE algorithm. A standard wall function was employed in the present study to obtain the flow properties near-wall region. The Boussinesq model was used in studying the buoyancy effect. The solution was considered converged when the residual values reached 10^{-3} except for the energy residual, which was set at 10^{-6}. Simulations were carried out using two workstations. Each specifies with Intel Xeon(R) CPU E3-1240 v5 3.5 GHz processor, 32GB RAM,

Windows 7 Professional 64-bit operating system that required roughly 48 h to 96 h to reach the solution completion for the generated grids. To evaluate the thermal comfort indices, a user defined function (UDF) code was written and compiled with the commercial CFD program, Ansys Fluent (Ansys, 2015). The UDF code written for this study is presented in appendix G of this thesis.

To produce meaningful results and to set up the fluent program, a proper set of boundary conditions was finalized, which can be found in Table 5.1. Further details of the CFD simulations are same as presented in Chapter 4.

Table 5.1: Boundary conditions setup for the CFD simulation

Boundary	Simulation setup
SV supply air inlet	2.5m/s, 19 ºC (fully-integrated)
VRF terminal inlet	2.7m/s, 16 ºC (coupled/decoupled)
Exhaust air outlet	0 pa, gauge pressure, 24ºC
Equipment load	64.54 W/m^2
Lighting load	1514.8 W/m^2
Nostrils	0.00672 Kg/s, 34ºC
Shelves	25.0 ºC, surface temp
Human body	Constant energy source
Ceiling/Floor/Walls	Adiabatic walls
SV diffuser grille	19 ºC (Adiabatic)
Plenum box	19 ºC (Adiabatic)

5.2.4 Experimental Setup for Validation Study

The experiments were carried out in the air terminal testing laboratory located at the core of a building in Prudentaire engineering, Kuala Lumpur, Malaysia. A small scale

simplified model was set up in the laboratory to resemble a portion of the CFD model of the retail shop with dimensions 6 m (L) x 5.4 m (W) x 2.74 m (H). Similar experimental methods was adopted in this study for the validation of simulation results as presented in details in the previous chapter.

5.2.5 Evaluation Criteria

The functional performance of an HVAC system can be judged through the provided thermal comfort, IAQ and power consumption. Thermal comfort is evaluated by the thermal field distribution and effective draft temperature (EDT). The EDT for stratum ventilation was already developed by Zhang Lin (2011), which is calculated using Equation 5.3. For IAQ, the most effective evaluating parameter is the mean age of air in the conditioned environment. The system's power consumption is directly related to the ventilation rate required and the room temperature distribution. Thus, to thoroughly investigate the thermal comfort performance of the combined system, the following parameters are evaluated by incorporating user-defined functions (UDF) into the CFD program, Ansys Fluent.

- Thermal field distribution
- Airflow pattern
- EDT
- Predicted mean vote (PMV)
- Percentage dissatisfied due to draft (PD)
- Mean age of air
- Carbon dioxide (CO_2 concentration)

The EDT equation developed for stratum ventilation is mentioned here as (Z. Lin, 2011),

$$\theta_{edt} = (T_x - T_r) - (\vartheta_x - 1{,}1);\ -1.2K \leq \theta_{eds} \leq 1.2K \quad (5.3)$$

where,

θ_{edt} = effective draft temperature for SV, K

T_x = local air DBT, ^oC

T_r = Room air average DBT, ^oC

ϑ_x = Local air centerline velocity, m/s

5.3 Results and Discussion

5.3.1 Validation of the Numerical Model

This study utilized the RNG k-ε turbulence model for numerical simulations of the studied cases. This model has been extensively verified and validated for stratum ventilation in a variety of environments (Z. Lin, 2011; Z. Lin, Tian, et al., 2011; T. Liu, Liu, Li, & Zuo, 2015; T. Yao & Z. Lin, 2014a). In this study, it is further validated for the studied cases. Limited by length, only few results obtained through experiments and simulation in a fully integrated design are compared. Figure 5.2 demonstrates the validity of the numerical model by comparing the results in terms of velocity and temperature at the selected locations. The slight disagreement between the experimental and simulated values at different line locations is maybe due to the measurements performed using a handheld anemometer device. However, the overall trend between both of these approaches seems uniform; thus, the model was considered to be used for detailed simulations studies.

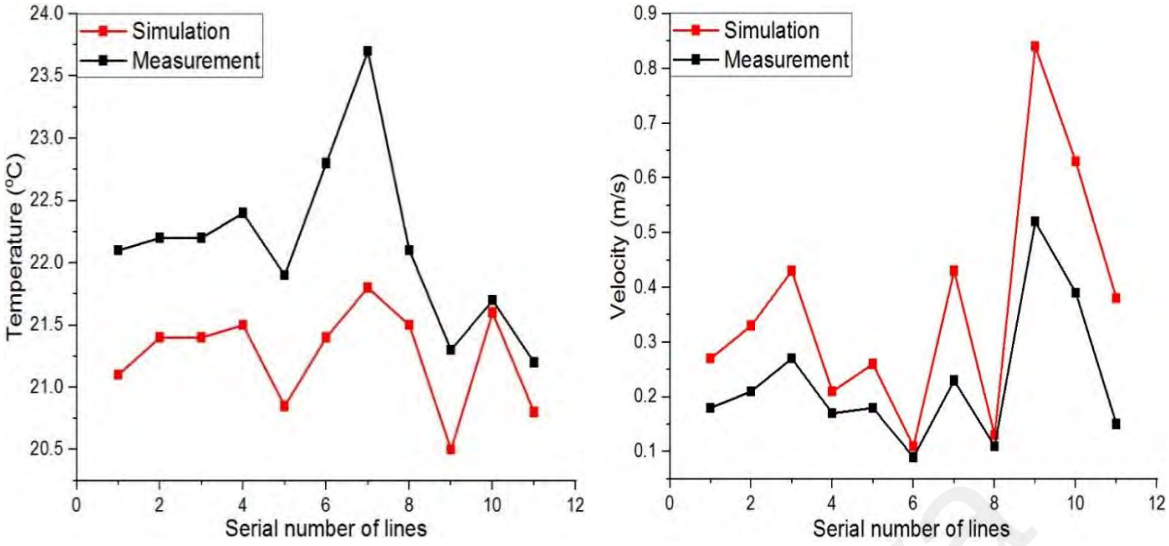

Figure 5.2: Experimental validation of the CFD results at measuring line locations (at 1.1m height) (a) Temperature comparison (b) Velocity comparison

5.3.2 Temperature Field Distribution

Figure 5.3 shows the temperature field distribution on the sectional planes of A, B and C at Z=2m, Y=1.02, and X=9.65m, respectively. The temperature in the lower or occupied zone is significantly lower than the unoccupied zone of the case study building. A reverse thermal gradient is also noticed within the occupied zone. The lower temperature is seen at the head level and a bit higher at the foot level, which prevents the occupants from thermal discomfort (Tian et al., 2011). The temperature contour at plane C shows that the supply air reaches the central part of the space, thus reduces the zone temperature to 22.15ºC, which also justifies the suitability of the VRF-SV system for large applications.

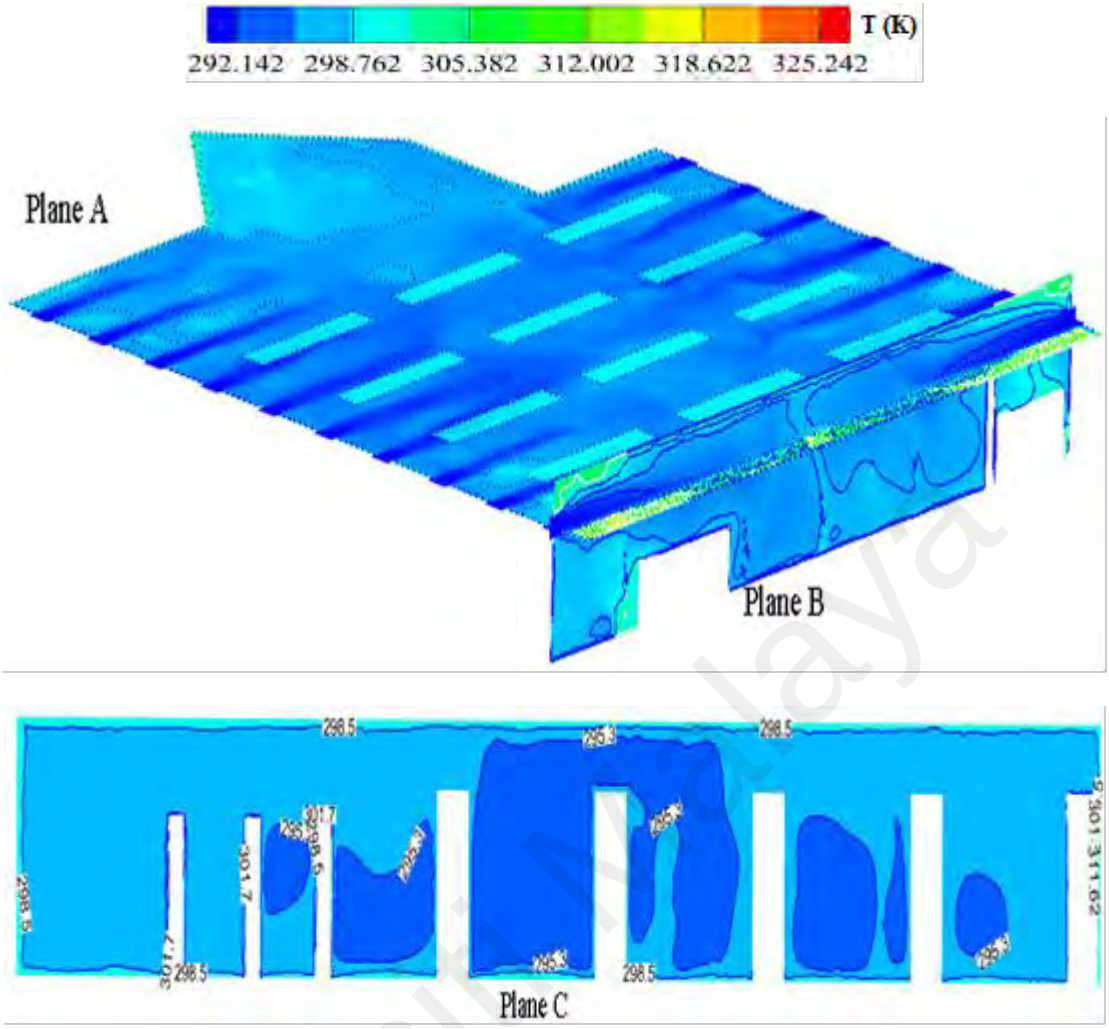

Figure 5.3: Temperature distribution in the retail shop (K)

5.3.3 Airflow Pattern

The air velocity could be a key factor for human thermal comfort assessment in indoor spaces. For good thermal comfort, the mean value of the air speed should not be greater than 0.15m/s in the entire breathing zone. Due to the elevated supply temperature in SV, this limit is further relaxed to 0.8m/s (Z. Lin, Yao, et al., 2011). Therefore, the airflow field distribution on the above mentioned three planes in the retail shop is presented in Figure 5.4. After exiting the VRF-SV supply air terminal, the cooled air went straight towards the centre of the domain then dipped down due to gravity. This is why the airflow field in the breathing zone was more stable and uniform within the acceptable range of wind speed. Overall, the mixing of the cooled supply air and indoor air at the lower zone was higher.

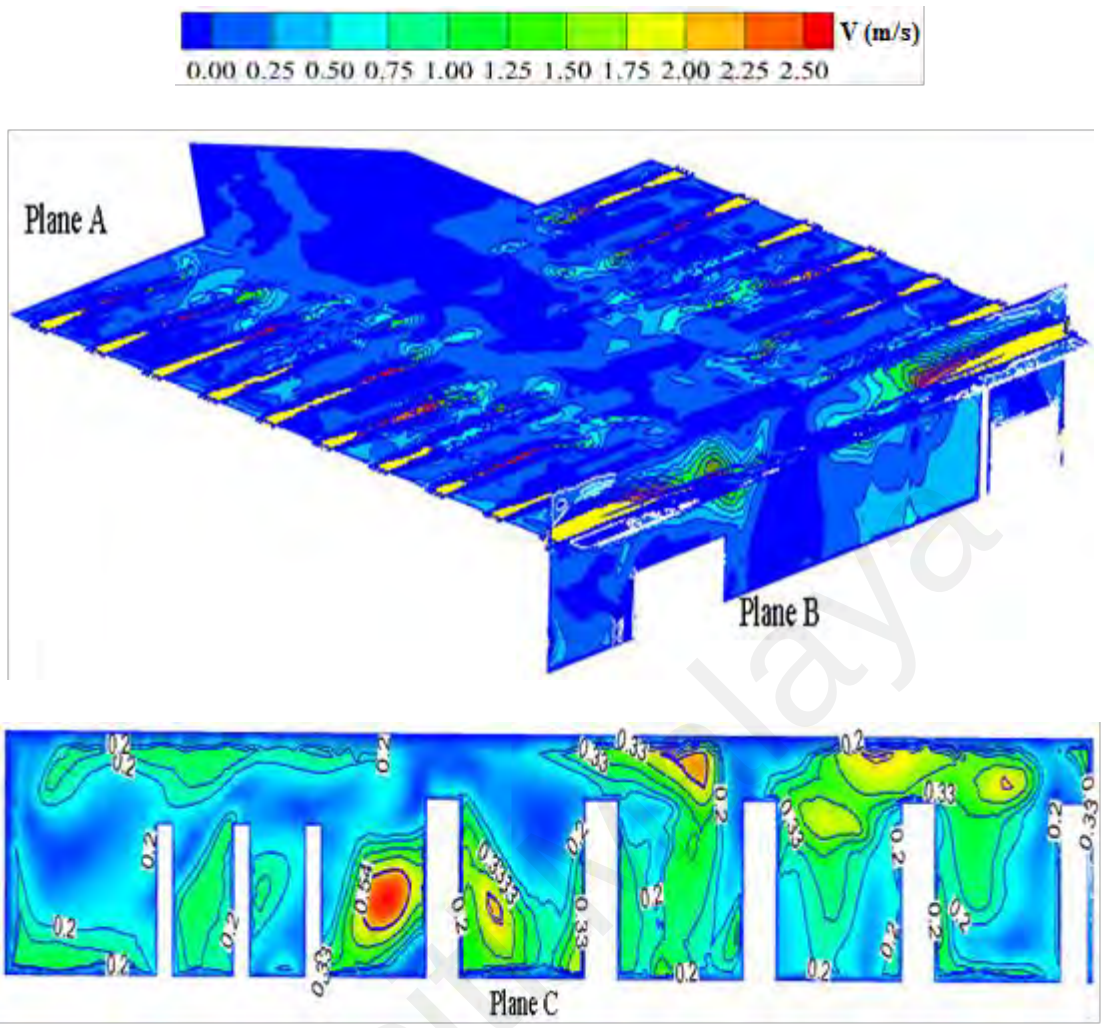

Figure 5.4: Airflow distribution in the retail shop (m/s)

5.3.4 Effective Draft Temperature for SV

The effective draft temperature (EDT) distribution in this chapter is determined using the formula developed by Zhang et al., (2011). The good thermal stratification with the VRF-SV system created a lower EDT in the occupied region than that of the upper zone, as seen in Figure 5.5. The largest values of the EDT occur near the supply jets due to the elevated face velocity in the VRF-SV system. Therefore, the selection and positioning of the supply terminals should be planned carefully.

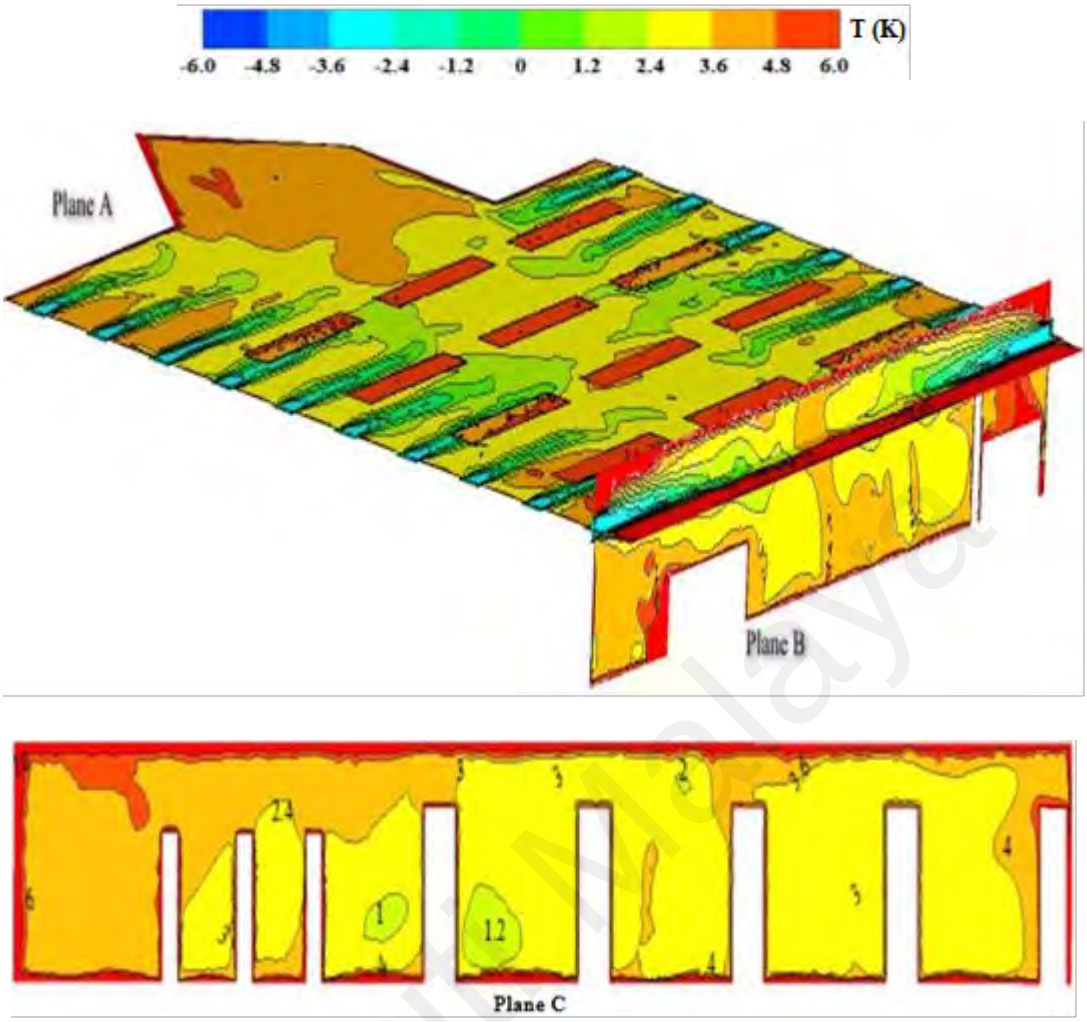

Figure 5.5: EDT distribution in the retail shop (K)

5.3.5 Predicted Mean Vote (PMV)

The PMV value represents the mean value of the votes of a group of people (0.6 clothing insulation) in the thermal environment on seven scale points between 3(Hot) and -3(Cold). While the midst 0 represents the thermal neutral condition. Except for the zones near the supply jets, as shown in plane A (Figure 5.6), the overall occupied zone comes between -0.5 to 0.5 scale. Thus, good occupant satisfaction was observed in the occupied region with the VRF-SV system.

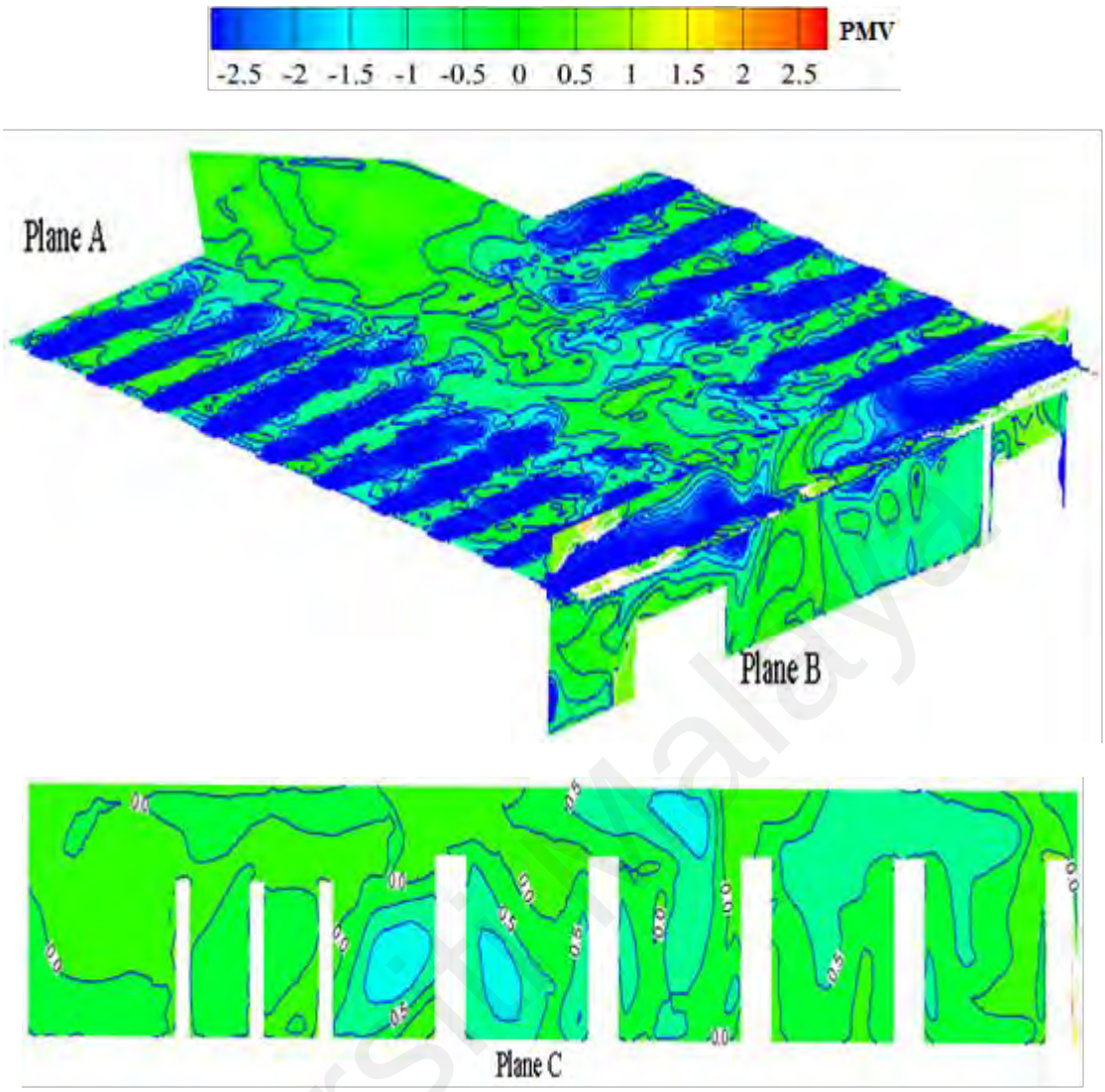

Figure 5.6: PMV distribution in the retail shop (standard scale)

5.3.6 Percentage of Dissatisfied People Due To Draft (PPD)

According to the CR-1752 1998, the PPD for a class C indoor thermal environment must not be greater than 25% (Z. Lin, 2011). Figure 5.7 shows the values at different planes, and all come under the acceptable range except for some locations near the supply diffusers. The PPD forms a direct relationship with the supply air velocity: the lower the velocity value, the more insignificant the percentage of the PPD. Even on plane A (supply plane), the PPD values are less than 25% in most regions, thus satisfying the performance of the VRF-SV system in the large domain.

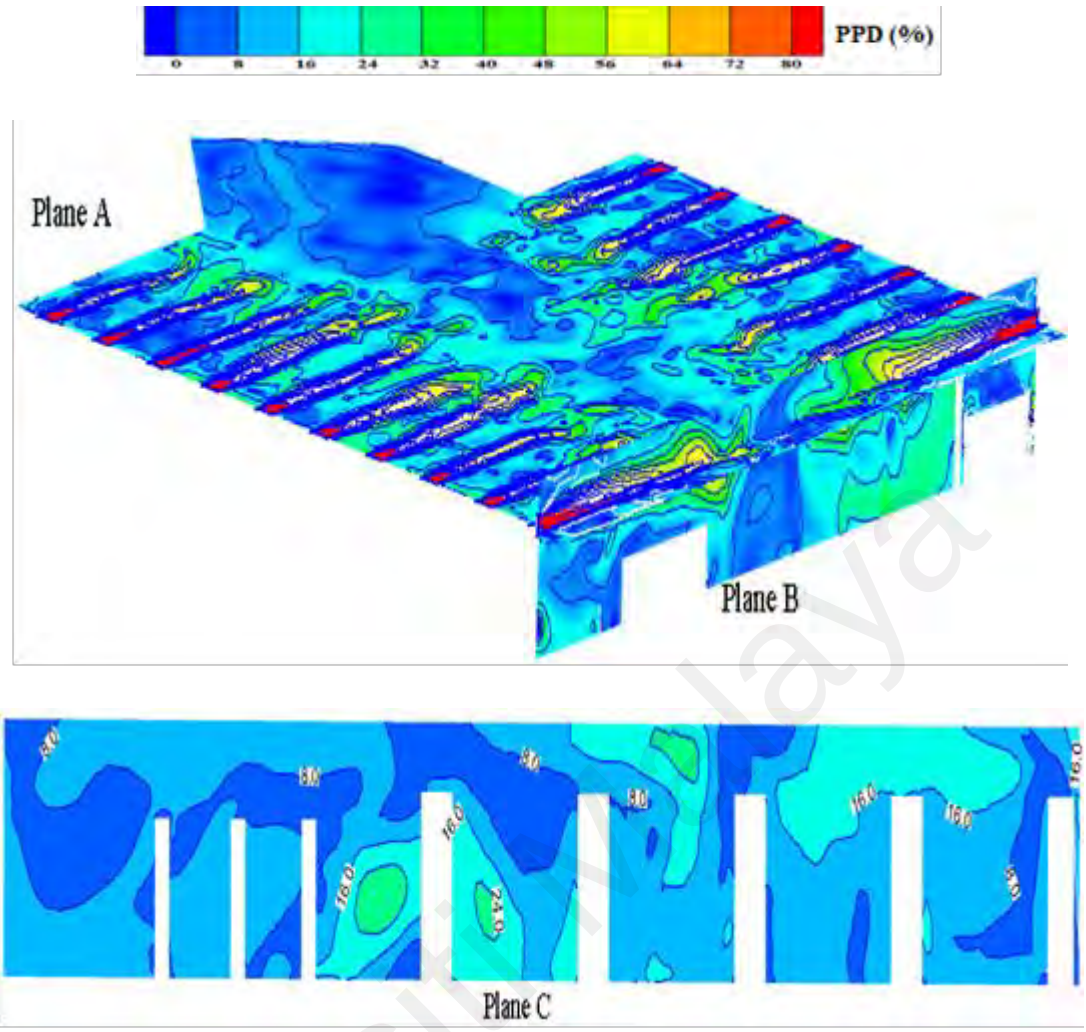

Figure 5.7: PPD distribution in the retail shop (%)

5.3.7 Local Mean Age of Air

The local mean age values for the indoor air is illustrated in Figure 5.8. The supply air is younger near the inlet and older at the center of the domain. The mean age of air is around 165 seconds at the retail entrance where supply air is not reaching properly. Between 90 to 150 seconds, the local mean age is observed within the entire occupied space, which also validates the IAQ performance of the VRF-SV system in large domains.

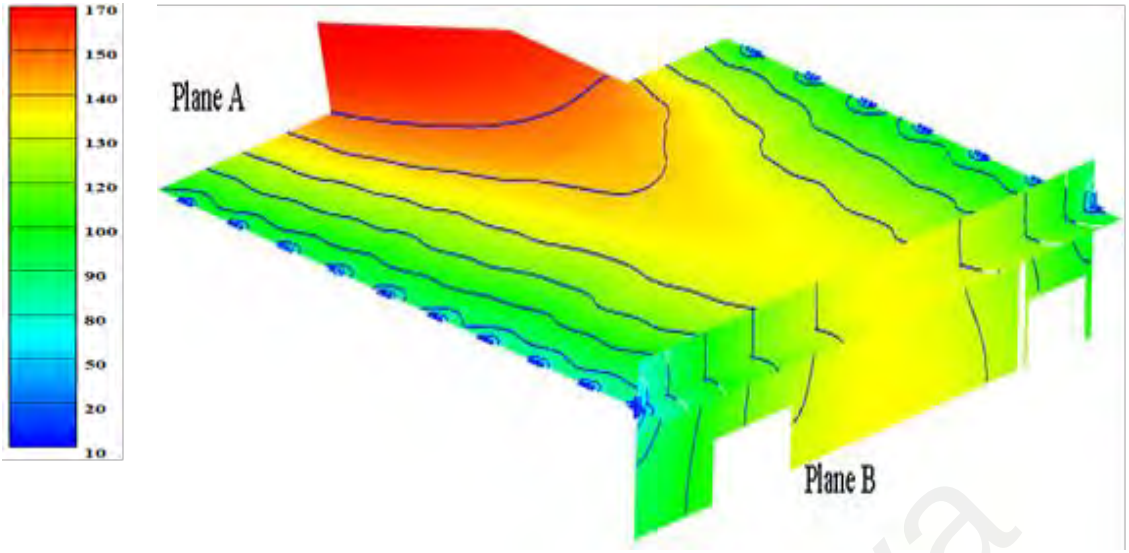

Figure 5.8: Mean age of air distribution in the retail shop (second)

5.3.8 Carbon Dioxide (CO_2) Concentration

The CO_2 concentration in the retail shop is shown in Figure 5.9. The initial CO_2 concentration in the retail shop was 385ppm, and the concentration in the supply air was 382ppm. The CO_2 breath out by each occupant within the domain was 36000ppm. The lower value of CO_2 concentration is seen in the breathing zone while on the plane near the head level of the occupants and near the supply air jet, the CO_2 was higher.

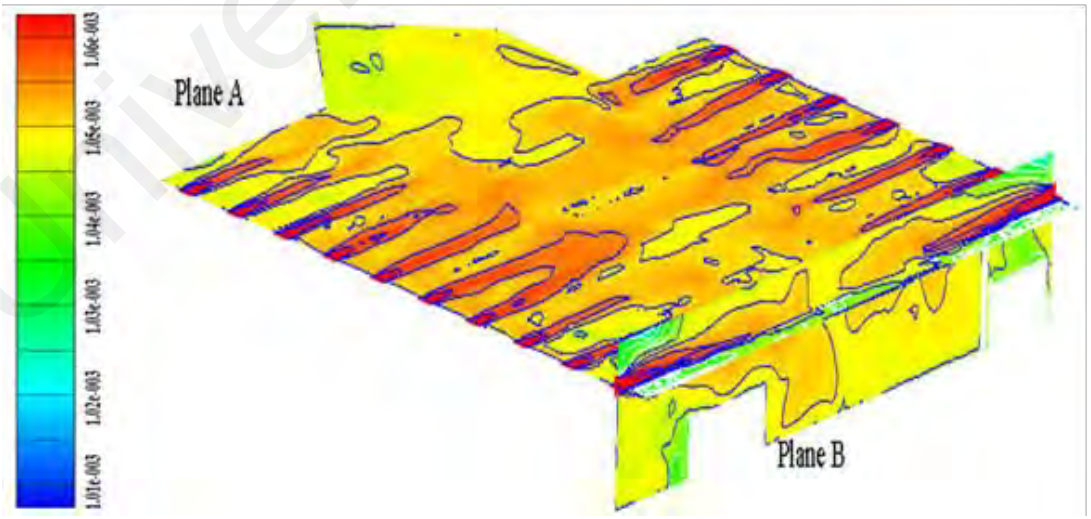

Figure 5.9: CO_2 concentration in the retail shop (Mass fraction)

5.4 Validity of the CFD Results

To validate the CFD results presented, this study was compared with a relevant study (Z. Lin, Yao, et al., 2011). Limited by length, the comparisons were made only for airflow pattern and temperature distributions. Figure 5.10 (a) and (b) show the airflow pattern generated under this study and the reference study, respectively. The contours of these two parameters were generated on a vertical sectional plane (normal to the supply diffuser) for both studies. The velocity distribution on both of the contours was similar. However, higher velocity values were seen at some locations in the VRF-SV system, as seen in Figure 5.10(a). This is because of the higher airflow rate at the supply inlet. The similar results were also seen for the temperature distribution contours in this study and the reference study, as shown in Figures 5.11 (a) and (b), respectively. Due to the low supply air temperature, i.e. 19ºC (292.15 K) in this study, the temperature values at most locations are lower than the values found in the reference study.

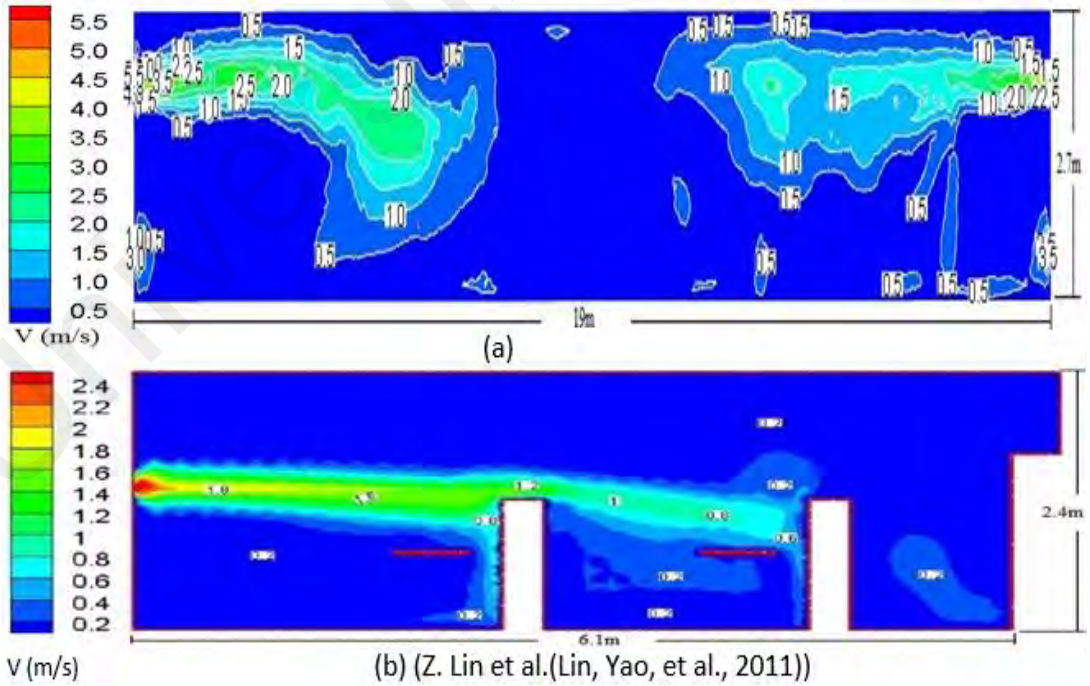

Figure 5.10: Comparative analyses of the airflow distribution on the vertical plane (a) VRF-SV system in retail shop (b) SV system in classroom

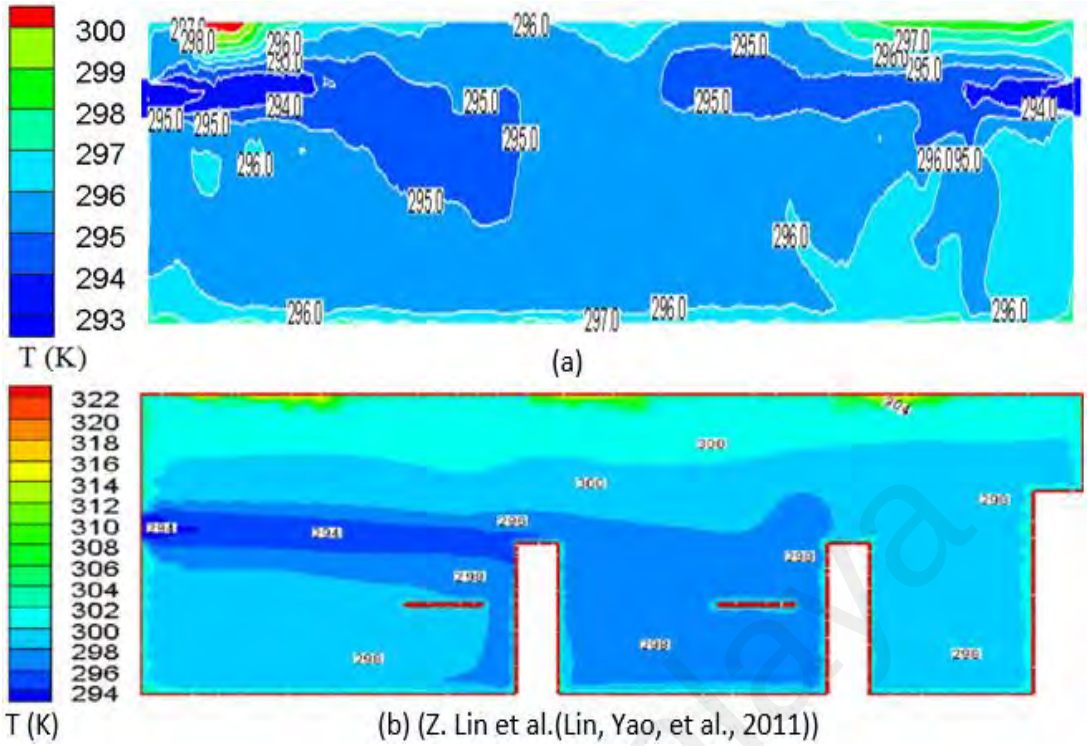

Figure 5.11: Comparative analyses of temperature distribution on the vertical plane (a) VRF-SV system in retail shop (b) SV system in classroom

5.5 Summary

Compared with the so-called stratum ventilation (SV), the opposite walls supply and low-level exhaust return configuration of the VRF-SV system in large retail shops provided better performance in terms of all thermal comfort indicators. The acceptable range of the air velocity (less than 0.8m/s) was seen in the occupied space. Further investigations revealed that, with a fully integrated design approach, a horizontal air jet at the head level, a slight and reverse thermal gradient between the head and foot levels ($\Delta T_{1.5\text{-}0.1}$ = -2.85ºC), and a low percentage of thermally dissatisfied people (<25%) were noticed. Compared with the limitations of the stratum ventilation system designed for small-to-medium spaces only, the VRF-SV hybrid system was found suitable for even large tropical applications. Considering the energy-efficient design, increased IAQ and enhanced thermal comfort performance, the VRF-SV hybrid system has a great potential to be employed in large tropical buildings.

CHAPTER 6: EFFECTS OF AIR SUPPLY TERMINAL DEVICES ON THE PERFORMANCE OF VARIABLE REFRIGERANT FLOW INTEGRATED STRATUM VENTILATION SYSTEM: AN EXPERIMENTAL STUDY

6.1 Introduction

Increasing concerns about high indoor air quality (IAQ) and excessive energy use in built environments (Baglivo, 2021; Ejaz, Jamil, & Ali, 2022) demand continuous development of efficient air conditioning and mechanical ventilation (ACMV) systems. ACMV systems in buildings are utilized to remove excess heat from indoor spaces and to replace polluted indoor air with fresh outdoor air. As the major shareholder of a building's energy consumption, an ACMV system is comprised of two different systems: the air conditioning system and the mechanical ventilation system (H. Chen, 2014).

The literature study revealed that airflow patterns generated by ACMV systems have a huge impact on room IAQ and occupant TC (Nada, El-Batsh, Elattar, & Ali, 2016; Y.H. Yau, K.S. Poh, & Badarudin, 2018). Furthermore, the airflow pattern in a room is driven by many factors, such as the ASTD type and number, position layout, building envelope, flowrate and temperature of the supply air (Z. Lin, Chow, Tsang, Fong, & Chan, 2005; Said et al., 2021; Sui & Zhang, 2012a). A great deal of research work has been carried out to investigate the impact of the geometry of the air terminal devices on the airflow pattern (Szczepanik-Scislo & Schnotale, 2020). Nielsen (Nielsen, 2000) worked on the airflow distribution in a room to ensure the occupants' thermal comfort. The findings concluded that the room airflow pattern, originated through an air terminal device, influenced thermal comfort significantly. A similar study was performed by Kalmar (2015) under personalized ventilation using different types of ASTDs. The results suggested that the adaptation of different geometries for ASTDs improved the thermal conditions of the ventilated zone. Hu (Hu, 2003) investigated the airflow

characteristics of the vortex diffuser using experimental and numerical methods. The study revealed that the flow pattern near the diffuser was 3-dimensional and highly turbulent. It also showed that a vortex diffuser had a higher room entrainment ratio than a circular type multi-cone diffuser. Entrainment ratio is a jet characteristic, commonly used to evaluate the airflow throw from the diffuser face (Zhivov et al., 2001). In another study, Nastase et al., (2011), using the mixing ventilation method, compared a lobed grille with a standard grille. They found that the lobed grille provided better airflow distribution, and thus improved indoor thermal comfort. Other studies reported the impacts of lip and blade angles of different types of diffusers on the room airflow pattern (Sajadi, Saidi, & Mohebbian, 2011; Sun & Smith, 2005).

The studies reviewed above highlighted the importance of the ASTD type on the air distribution performance of the ACMV systems. Furthermore, ASTDs are usually selected based on jet throw data provided by the diffuser manufacturers. The manufacturers collect the data by treating the uniform jet outflow from the diffuser. However, the air jet flows from the diffuser are affected by many factors. In most cases, the diffusers are connected to the ventilation duct by plenum boxes (Villafruela, Sierra-Pallares, Castro, Álvaro, & Santiago-Casado, 2018) installed above the suspended ceilings or outside of the side walls, depending on type of the diffuser applied. Plenum boxes are designed with top, bottom or side collars for air supply inflow (Smoljan, Balen, & Hr, 2010). For ceiling-mounted diffusers, the air outflow from the diffuser created better room entrainment when the collar was attached at the top surface of the plenum box compared to when the collar was at the side surfaces. This was due to the creation of large numbers of air vortices in the plenum box with side collar orientation; they provided a uniform jet throw. However, the selection of the plenum and the collar orientation is usually performed by looking at the installation space, which may affect the uniformity of the jet outflow (Smoljan et al., 2010).

To the best of authors' knowledge, only very limited studies on the effects of ASTD types, geometry and layouts exist in the open literature for SV air distribution system (Ting Yao & Lin, 2014; T. Yao & Z. Lin, 2014a; Yong CHENG, Zhang LIN, Weiqin WU, & YAO, 2014; H. Zhao, Liu, & Zuo, 2015). No study found conducted research on the effects of ASTD on air distribution performance when SV was combined with a VRF system. This research was therefore designed with an aim to investigate the effects of different types of ASTDs on the performance of a novel VRF-SV hybrid system. This research had two main objectives. The first objective was to study the impacts of top, side and bottom orientations of plenum collars on jet outflows from the ASTD. In the second objective, the effects of five different types of ASTDs on the thermal comfort and air distribution performances of the VRF-SV hybrid system were investigated. Additionally, quantitative analyses of the hybrid system's effective draft temperature (EDT) and air distribution performance indices (ADPI) of the five ASTDs were formulated. For the visualization of flow pattern driven by the selected ASTDs, smoke tests were carried out. Thermal sensation votes and comfort surveys were also conducted with different types of ASTDs installed in a meeting room environment.

6.2 Selection of Air Supply Terminal Devices (ASTDs)

In total, five types of commonly used air supply terminal devices were studied. These are all shown in Figure 6.1. Different cases with these air terminal devices were studied under constant airflow rate. Considering the fact that exhaust terminal type had an insignificant impact on the airflow pattern (T. Yao & Z. Lin, 2014a), the bar grille diffuser was used as an exhaust terminal in all studied cases. The supply air terminals were installed on the side wall at 1.9 m height and the return/exhaust terminal at 0.33 m height from floor. These heights were selected based on the design guidelines devised for the stratum ventilation system (Z. Lin, Yao, et al., 2011). The indoor design temperature and the walls' internal temperatures were all set to 26 °C, which were

strictly monitored and adjusted by the locally installed thermal sensor (room thermostat). The detailed experimental parameters and the diffusers' dimensions are shown in Table 6.1.

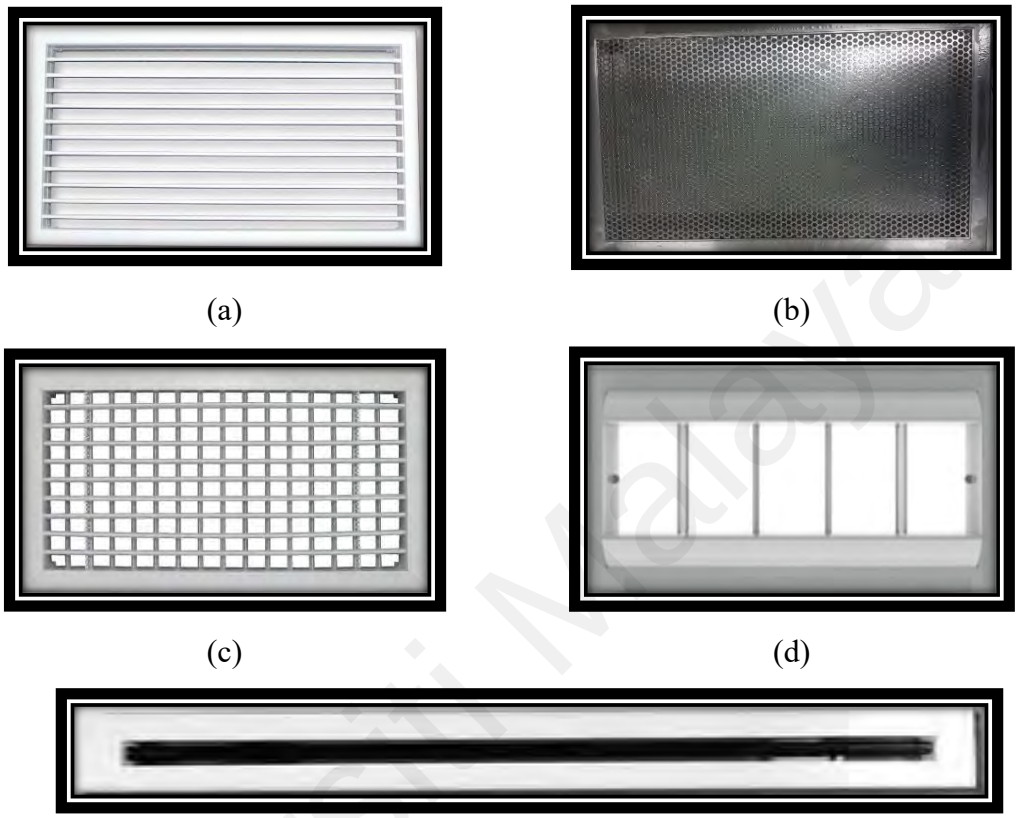

Figure 6.1: Types of supply air terminals: (a) bar grille (b) perforated diffuser (c) double deflection grille (d) drum louver and (e) jet slot diffuser

Table 6.1: Details of the initial/boundary parameters

Case	Diffuser Type	Diffuser Size (mm)	Airflow Rate	Supply Temperature (°C)	Room Temperature (°C)
1	Bar grille diffuser	500 × 300	0.25m^3/s	18.7 ± 0.3	26.0 ± 0.1
2	Perforated diffuser	500 × 300	0.25m^3/s	18.5 ± 0.2	26.0 ± 0.2
3	Double deflection grille	500 × 300	0.25m^3/s	18.5 ± 0.1	26.0 ± 0.1
4	Drum louver diffuser	500 × 300	0.25m^3/s	18.8 ± 0.3	26.0 ± 0.1
5	Jet slot diffuser	1000 × 135	0.25m^3/s	19.0 ± 0.1	26.0 ± 0.1

6.3 Experimentations

To investigate the effects of ASTDs installed with the novel VRF-SV hybrid system, the experiments were carried out in an air diffuser testing laboratory at Prudentaire Engineering Private Ltd. (Malaysia). The laboratory was located at the core of a building with no boundary wall exposed to solar radiation. Thus, the walls' internal surface temperatures were controlled by adjusting the surrounding ambient temperature to the same value, i.e., 26 °C (room design temperature), so that the adiabatic condition was achieved with no heat flow in and out of the testing chamber. The laboratory was 6.0 m in length, 5.4 m in width and 2.74 m in height. The plenum box collar orientations, experimental chamber and air conditioning system setup are shown in Figure 6.2. Prior to starting experimentation, the heat load of the laboratory was measured; the calculated details are shown in Table 6.2.

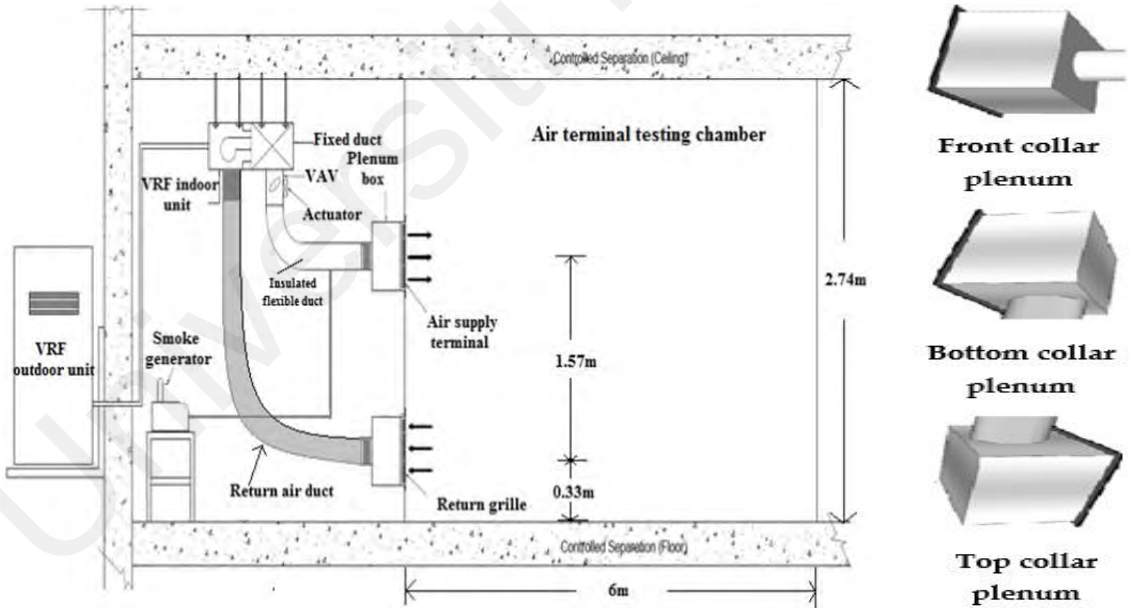

Figure 6.2: Experimental chamber setup and plenum boxes with front, bottom and top collar orientation

Table 6.2: Calculated thermal Load

Entity		People	Other Heat Sources		
			Computer	Equipment	Lighting
Heat Load	Testing chamber (for ASTD testing)	70 W =2 × 70 = 140W	2 × 90 = 180 W	500 W	100 W
	Meeting Room (for comfort survey)	70 W = 10 × 70 = 700			

In the air distribution side of the VRF-SV system, an insulated flexible duct of diameter 200 mm was attached to the oval-shaped collar of the plenum box. The plenum box was sized as per the geometry of the ASTD type. A smoke generator was also employed to visualize the airflow pattern. The smoke was supplied into the flexible duct after controlling the flowrate through the VAV damper. To comply with the principle of comparison, all the cases were investigated under similar settings.

6.3.1 Measurement Methods and Equipment

Detailed environmental conditions of the laboratory were measured before the actual testing started. The temperatures of all the internal surfaces were checked using the HANNA HI 147-00 surface temperature measuring tool. The airflow rate at room level, at the face of the ASTD was measured and monitored by ZTH-VAV belimo device. The Alnor 440-A hot wire anemometer (seen in Figure 6.3) was used to measure the indoor temperature at different locations for the determination of the room average. The accuracy of the anemometer was ±0.3 °C for temperature, 0.015 m/s for velocity and ±3% for relative humidity (RH). The actual measurements were taken every 1 h after the VRF began delivering air at full fan capacity with a fluctuation of less than 5%. At the 4th hour of fan operation, the room achieved steady-state condition, when the mean air temperatures at the supply inlet, return outlet, and at the center of the room did not exceed more than 1 °C variation. The difference in the room's internal surface

temperatures was also recorded below 0.1 °C during that period. This was all done to make the environment behave as nearly isothermally as possible. The experimental setup in the testing chamber and the measuring line locations are shown in Figure 6.4.

(a) (b) (c)

Figure 6.3: (a) Alnor 440-A hot wire anemometer (b) HANNA HI 147-00 surface temperature measuring tool (c) ZTH-VAV belimo pressure adjustment device

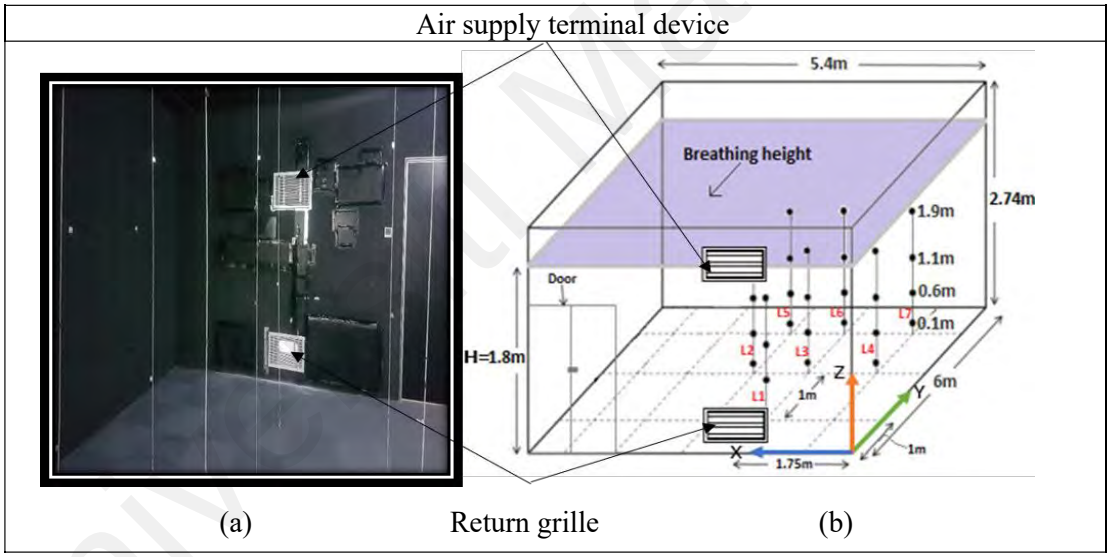

(a) (b)

Figure 6.4: (a) Experimentation in the testing chamber (b) The layout and measurement locations.

6.4 Evaluation Criteria

This study investigated the performance of different air distribution terminals (ASTDs) using the following indices:

- Temperature field distribution
- Velocity distribution
- Airflow throw
- Effective draft temperature (EDT) and air distribution performance index (ADPI)

- Airflow pattern
- Thermal sensation and comfort feedback

Koestel and Tuve investigated the effects of airflow velocity and temperature on human thermal comfort. They also defined the air draft (Effective Draft) as any localized feeling of coldness or warmth on any part of the body caused by the combined effect of air velocity and temperature, while the humidity and radiation remained constant. To determine the effective draft temperature (EDT, θ_{edt}) for stratum ventilation, Lin et al. (Z. Lin, 2011) developed an equation, shown as Equation (6.1).

$$\theta_{edt} = (T_x - T_c) - (V_x - 1.1) \quad (6.1)$$

where,

θ_{edt} = Effective draft temperature, K

T_x = Local air DB temperature, °C

T_c = Mean DB temperature of the room, °C

V_x = Local air stream speed, m/s

For stratum ventilation air distribution, the ranges defined for good and satisfactory thermal comfort conditions at velocity <0.8 m/s were −0.6 k < θ_{edt} < 0.6 K and −1.2 K< θ_{edt} < 1.2 K, respectively. The ADPI was defined in percentages, in which the measurements taken in an occupied space where the effective draft temperature found within the range mentioned above to the measurements taken in total. The most desirable condition for an efficient air distribution system occurs if the ADPI approaches 100%, whereas the ADPI must not be less than 80% in a good air distribution system (S. Liu & Novoselac, 2015). The expression for ADPI is given below,

$$\text{ADPI}(\%) = \frac{(N_\theta \times 100)}{N} \quad (6.2)$$

where,

θ_{edt} = Effective draft temperature, K,

N_θ = Points measured in the occupied space that falls within $-1.2\ K < \theta_{edt} < 1.2\ K$,

N = Total points measured in the occupied space.

The laboratory chamber was converted into the meeting room to conduct the thermal sensation and comfort survey, as shown in Figure 6.5. The thermal load calculated for the meeting room was presented earlier (Table 6.2). A total of 10 subjects (4 female and 6 male) were formally hired for the survey-based tests in order to investigate the effects of ASTDs on human thermal sensation and comfort. All those subjects were from the office staff and were young and healthy. They were all active in the discussion during the meeting and did not do any tiring activity before the experiments started. The tests were conducted during their break hours and took around 2 weeks for complete data collection. The subjects all wore short or long-sleeved thin cotton shirts and trousers, with a clothing value limited to 0.5 clo (0.078 m^2 K/W). Considering the meeting room environment with discussion process going on, the activity level chosen was 1.2 met. The complete anthropometric description of the subjects is presented in Table 6.3. On average, 30 minutes after establishing the steady state conditions in the meeting room, the experiments were conducted for selected ASTDs. The survey was completed by adopting a questionnaire (Appendix A) containing two questions based on the ASHRAE's 7-point scale thermal sensation vote (TSV) and thermal comfort vote (TCV), as mentioned in Table 6.4.

Figure 6.5: Meeting room environment

Table 6.3: Details of the experimental parameters

Index	Female (n = 4)		Male (n = 6)		Total (n = 10)	
	Mean ± SD	Range	Mean ± SD	Range	Mean ± SD	Range
Age (years)	26.5 ± 2.0	25–30	28.8 ± 2.8	25–33	27.9 ±2.8	25–33
Height (m)	1.55±0.04	1.5-1.62	1.67±0.08	1.62–1.81	1.62 ±0.08	1.5-1.8
Body mass (kg)	57 ± 1.4	55–58	66.2 ± 9.0	51–78	62.5 ± 8.3	51–78
BMI * (kg/m^2)	23.55±1.5	21.5-25.8	23.7 ± 2.9	18.7–27.1	23.63 ±2.4	18.7-27.1
BSA ** (m^2)	1.57±0.02	1.55–1.6	1.75 ± 0.1	1.53–1.94	1.68 ± 0.1	1.53–1.94

* Body mass index (BMI) = $(W/H^2) \times 104$.
** Body surface area (BSA) = $(W0.425 \times H0.725) \times 0.007184$

Table 6.4: Details of the experimental parameters

TSV scale	Meaning	TCV Scale	Meaning
−3	Cold	0	Comfortable
−2	Cool	+1	Slightly uncomfortable
−1	Slightly cool	+2	Uncomfortable
0	Neutral	+3	Very uncomfortable
+1	Slightly warm		
+2	Warm		
+3	Hot		

6.5 Bias Uncertainty Analysis

Bias uncertainty analysis, sometimes known as error analysis, is a statistical technique used to evaluate the amount of uncertainty present in any experimental data. The bias uncertainty (Δx) is the deviation of the measured value from the true value and calculated using Equation (6.3) (Y. H. Yau, K. S. Poh, & A. Badarudin, 2018a).

$$\Delta x = \frac{R}{2} \tag{6.3}$$

where R is the range and can be determined by taking difference between maximum and minimum values of the experimental data (x).

$$R = x_{max} - x_{min} \tag{6.4}$$

The uncertainty between measured and true value can then be converted into percentage uncertainty using Equation (6.5).

$$\text{Percentage uncertainty (\%)} = \left(\frac{\Delta x}{\bar{x}} \times 100\right) \tag{6.5}$$

where $\bar{x}$ is the mean of the measured values for single experimental reading.

The bias uncertainty analyses performed for the current study are presented in Table B.1 (Appendix B). Restricted by the table length and width, the analysis was carried out for two height locations (0.6 m and 1.1 m from the ground). The errors found in the velocity and temperature measurements indicated that the uncertainty was there in the collected data. However, the primary aim of this study was to evaluate the effects of ASTDs on the VRF-SV system performance, so high precision in the collected data was not the authors' objective. Moreover, the data were collected at multiple locations in the room and at different heights using a handheld measurement device. Therefore, bias uncertainty analysis was essential to check the acceptability of the error present in the collected data. The percentage uncertainty in the mean airflow velocity (as seen in Table B.1) was in the range of 8.47% to 108.33% in the case with a bar grille, 9.61% to 95.45% in the case with double deflection grille, 11.53% to 150% with the perforated diffuser case, 10.29% to 150% with the drum louver diffuser and 0% to 150% for the jet slot diffuser case. The higher percentage of error in the collected data may be due to the low airflow rate at the measuring locations, as Hashemian et al. (H. M. Hashemian, M. Hashemian, & Riggsbee, 1995) determined that the low air velocity (<0.5 m/s) significantly reduced the sensitivity.

The bias uncertainties calculated for temperature distributions at the measuring locations were in the range of 0–0.85%, 0–7.51%, 0–7.44%, 0–1.39% and 0–1.29% for the cases with bar grille, double deflection grille, perforated, drum louver and jet slot diffusers, respectively. As seen in Table B.1, the bias uncertainty for all the diffuser types was relatively insignificant. This may have been due to the more uniform temperature distribution compared to the velocity distribution within the breathing zone. However, these results suggested that low to high numbers of uncertainties were present during field work measurements for all types of ASTDs.

6.6 Results and Discussion

6.6.1 Effect of the Plenum Collar Orientation on Jet Outflow

As seen in Figure 6.6, the temperature and velocity distributions showed similar patterns with front, top and bottom collar orientations at heights 0.1 m and 1.9 m from the floor. This indicated that different types of collar orientation did not greatly influence the regions near the floor and at the diffusers' mid-level heights. Moreover, the highest deviation in velocity values was noted with a front orientation at location 4, which was around 33.3% and 50.0% higher than the top and bottom orientations, respectively. Similarly, a maximum of 1 °C temperature difference was observed throughout the measurement locations. However, at height y/H = 0.6 m and 1.1 m, a non-uniform distribution of temperature and velocities was seen. The lowest temperature of about 21.8 °C was recorded at location L4 (at 0.6 m height) with the bottom orientation of the plenum collar. In terms of velocity distribution, the highest deviation recorded for the case with the front collar was at location L7, which is about 0.12–0.45 m/s higher than the top collar and 0.16–0.5 m/s higher than the bottom collar orientations. Similar results can also be found in reference (Halibart, Zwolińska, Borowski, & Jaszczur, 2021) for the top and side entries of the plenum box. Therefore, based on the obtained results, front collar orientation was considered in this study to investigate the effects of ASTDs on the performance of the VRF-SV hybrid system.

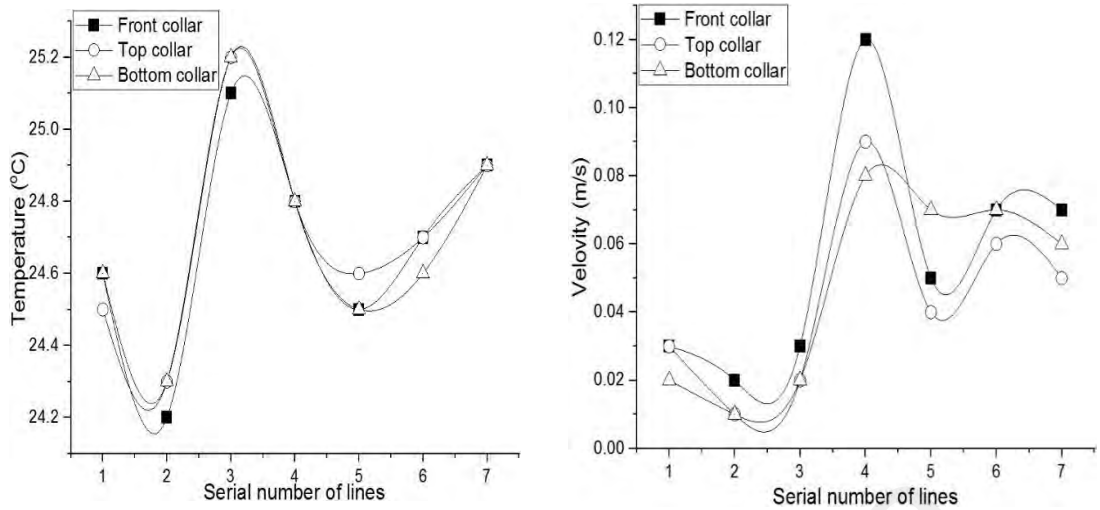

y/H = 0.1m

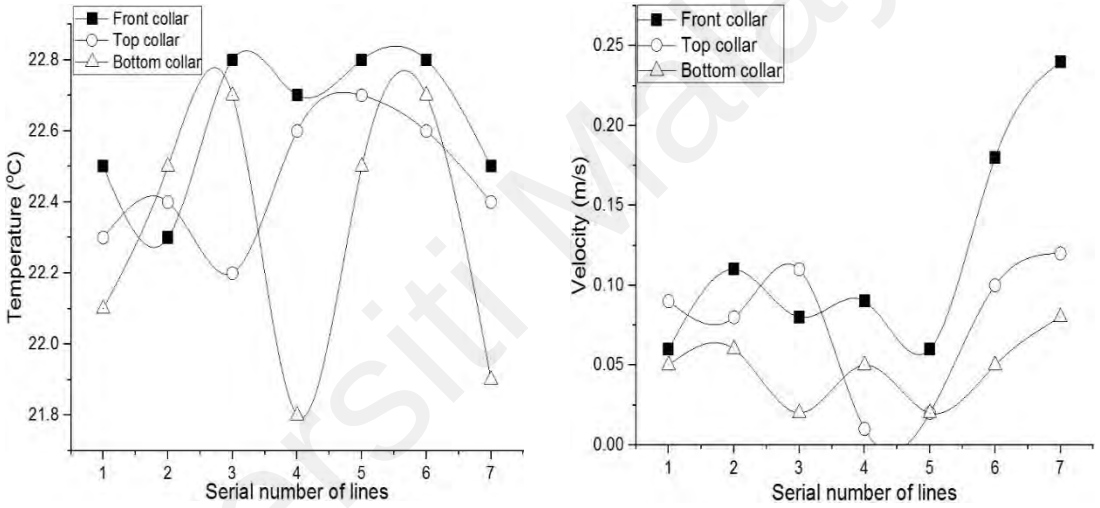

y/H = 0.6m

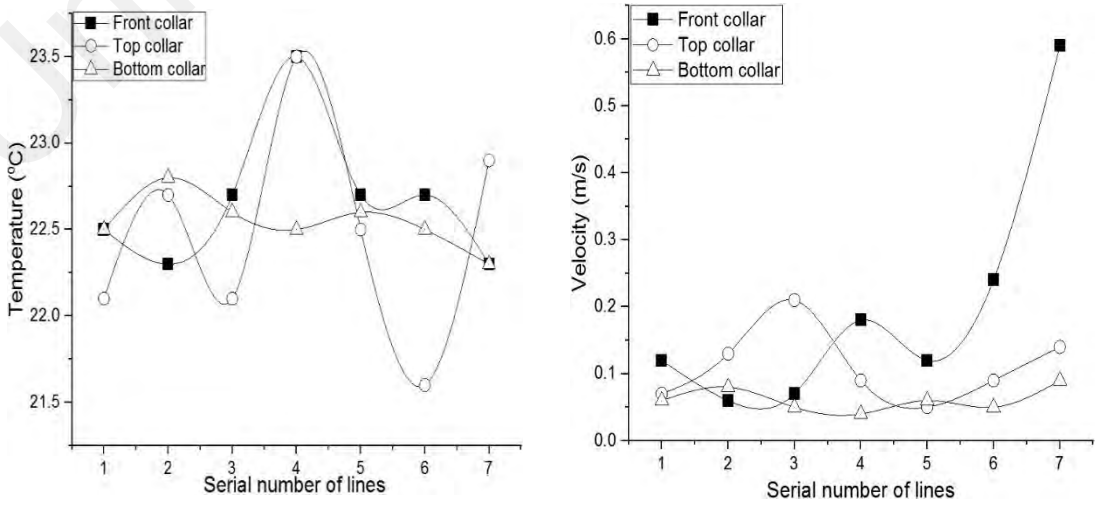

y/H = 1.1m

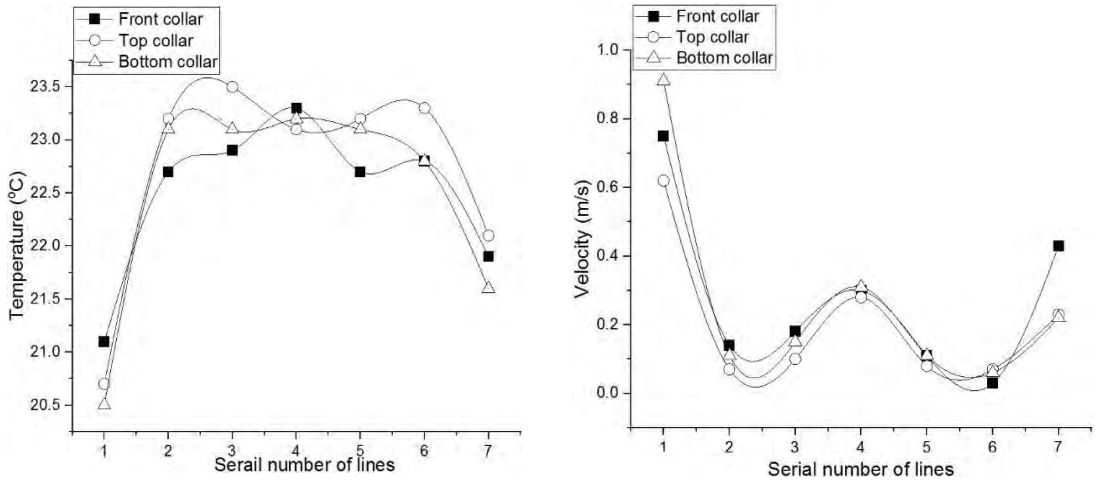

y/H = 1.9m

Figure 6.6: Comparison of temperature and velocity values for different orientations of the flexible duct collar along measured locations at heights 0.1, 0.6, 1.1 and 1.9 m from the floor

6.6.2 Effect of ASTDs on Air Distribution Performance

6.6.2.1 Effect on Temperature Field Distribution

Figure 6.7 (a) and (b) shows the temperature field distribution at different positions (L1 to L7) at heights of 0.6 and 1.1 m, respectively. The higher temperature values of 22.8 °C to 24.8 °C were recorded at all the locations for the jet slot diffuser, demonstrating the unsuitability of these types of diffusers in VRF integrated stratum ventilation systems. Its poor performance may have been due to the horizontal installation on the sidewall. The lowest temperature by these ASTDs was observed with the perforated type diffuser at location L1 at the measured heights. After exiting the supply inlet in the perforated diffuser, the air dipped down deeply into the room with very low entrainment and momentum. It could be a reason for the lowest temperature values of about 21.5 °C and 21.28 °C observed at the measuring heights at location L1. However, at all other locations and on both the measuring heights, temperature ranges of about 21.5–23.4 °C, 21.2–23.3 °C and 22.3–23.5 °C were noted for the drum louver diffuser, double deflection grille and bar grille diffuser, respectively. Moreover, the bar grille diffuser showed uniform temperature distribution at all locations. The value

fluctuated at about 22.5 °C, except location L4 at height 1.1 m, where the maximum deviation was 1 °C from the mean.

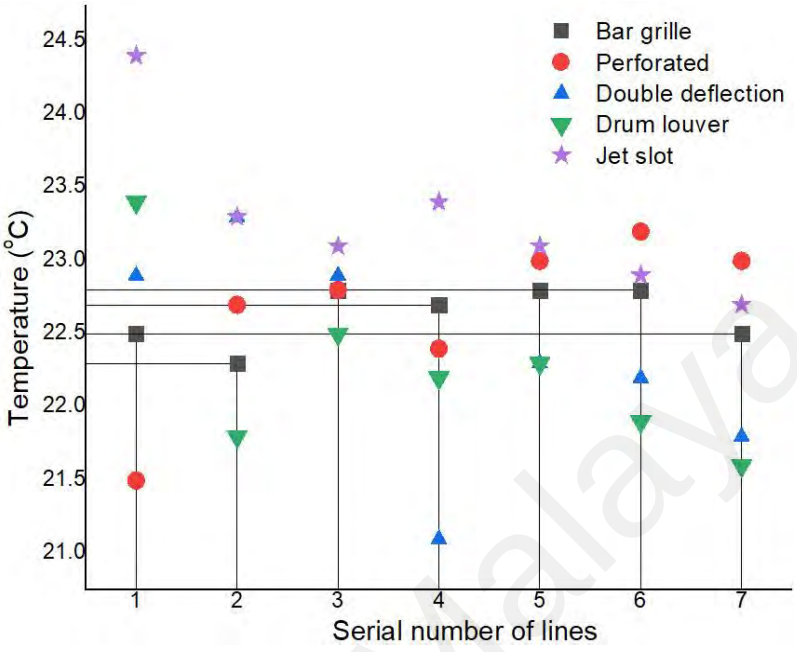

(a)

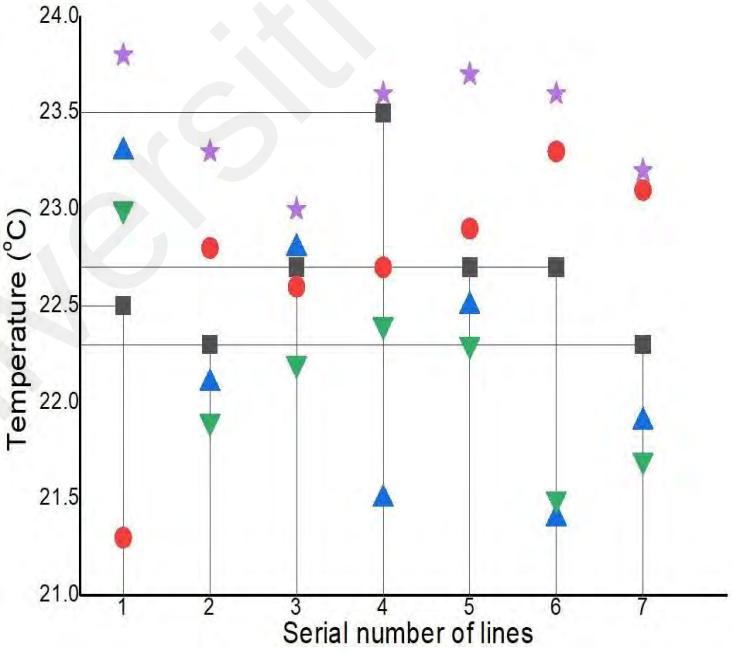

(b)

Figure 6.7: Temperature distribution at Positions L1 to L7 at the height of (a) 0.6 m and (b) 1.1 m from the floor

6.6.2.2 Effect on Velocity Distribution

The higher velocity value of >0.1 m/s was seen with a double deflection grille at 0.6 m and 1.1 m heights at location L1, as shown in Figure 6.8. All other ASTDs showed lower values at this location, especially in the case with the drum louver diffuser, where the velocity at height 1.1m at location L6 was measured highest, about 0.7 m/s. Due to the low velocity values at all the locations and poor airflow distributions by the perforated and jet slot diffusers, both were found unsuitable for VRF-SV hybrid system applications. However, for other terminals, the effects of ASTDs on the VRF-SV system performance in terms of velocity distribution was found to be less influential. It was similar for all measuring locations except L6 and L7, where the deviations recorded were 0.03–0.5 m/s and 0.01–0.46 m/s, respectively. Therefore, any of the remaining three diffuser types can be installed with the VRF-SV hybrid system to obtain more uniform airflow distribution.

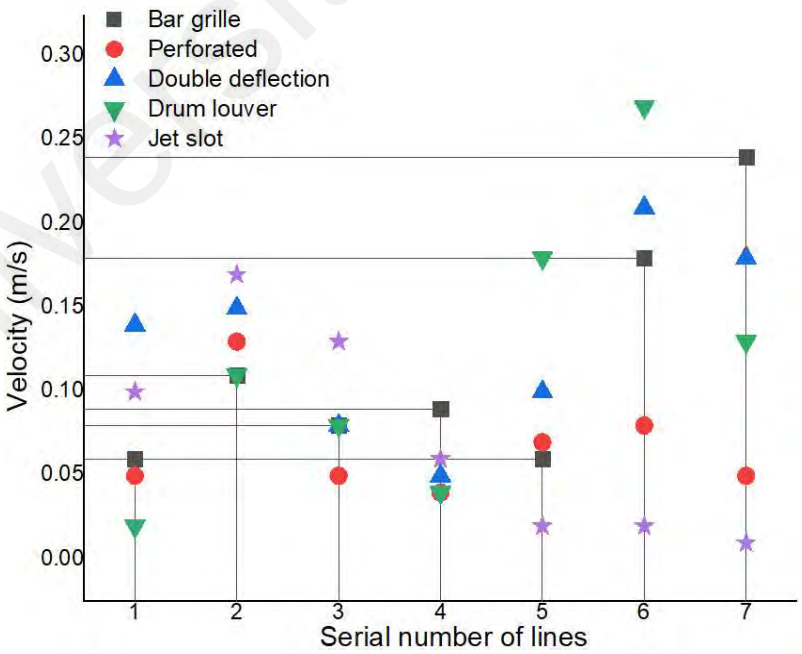

(a)

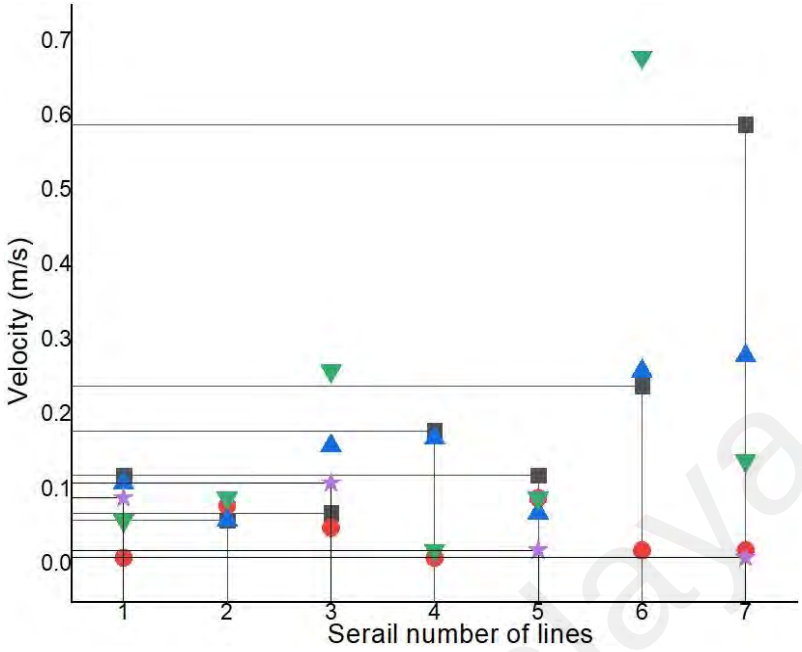

(**b**)

Figure 6.8: Velocity distribution at Positions L1 to L7 at the height of (a) 0.6 m and (b) 1.1 m from the floor

6.6.2.3 Effect on Airflow Throw

To further explore the effects of ASTDs, Figure 6.9 presents the airflow throw analyses for all the studied terminals. The measuring height selected for diffusers' throw analysis was 1.9 m from the floor. It was at the mid-height of the ASTD. The airflow through different diffusers was measured at five different locations. These locations were in front of the supply terminals in the throw direction. The skewedness in the case with the jet slot diffuser at a 2 m distance from the diffuser face was due to the uneven airflow from the jet slot diffuser. Air velocity at the diffuser center was low (<0.1 m/s) and it was higher at both ends (>0.1 m/s). For double deflection grille, bar grille and drum louvre diffuser, the jet of air decayed proportionally to the distance from the diffuser. Among them, the airflow velocity of the double deflection grille case decayed most rapidly at a distance of about 3 m from the grille face. In case of bar grille diffuser, the jet of air almost vanished after 3m distance from the diffuser face. However, with double deflection grille the jet of air lasted for 5 m distance from the diffuser face.

Furthermore, the air jet through the drum louver diffuser also reached the same distance achieved by the double deflection grille with even low face velocity than the former. Therefore, these diffusers, i.e., bar grille, perforated diffuser, double deflection grille and drum louver diffuser, were further investigated for smoke test analyses.

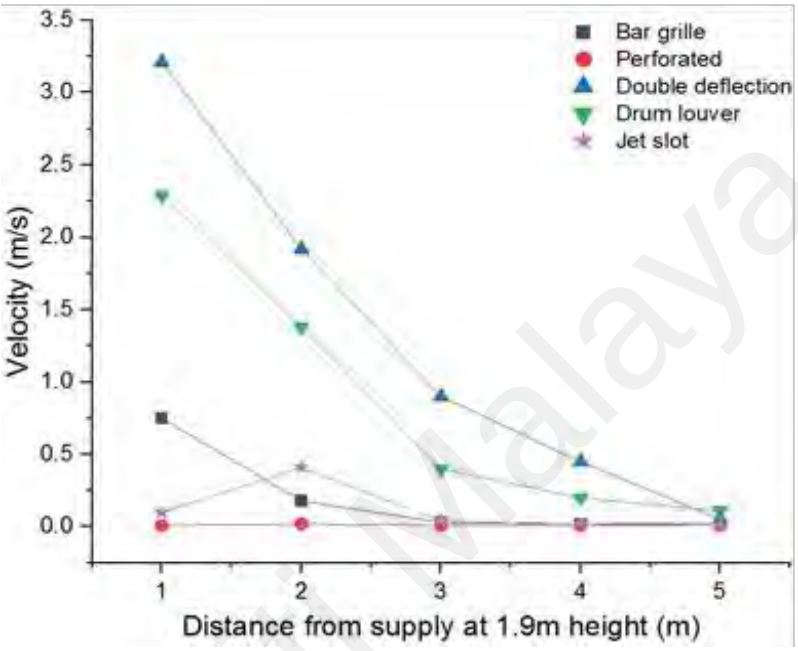

Figure 6.9: Comparison of airflow throw from different diffusers

6.6.2.4 Effect on EDT and ADPI

Equation (6.1) determined the EDT for VRF-SV hybrid system using selected ASTDs, at different heights of 0.1, 0.6, 1.1 and 1.9 m from the floor. Limited by length, only the values at 0.6 and 1.1m heights were presented, as seen in Figure 6.10. All the EDT values of the bar grille case were found within the acceptable range of $-1.2\ k < \theta_{edt} < 1.2\ K$, except one value (1.3 K) at line location 4 and height 1.1m found out of the acceptable range. Most of the EDT values for the four diffusers (bar grille, perforated, double deflection and drum louver) were found within the acceptable limits defined in ASHRAE standards. However, the EDT values of the jet slot diffuser case were all found to be out of the specified limits. This may have been due to improper distribution of temperature and velocity by this type of diffuser. Based on the calculated values, the

ADPI for all the ASTDs were determined, as presented in Table 6.5. In order to properly distribute the temperature and airflow velocity and to comply with the ASHRAE thermal comfort standards, the ADPI value must not be lower than 80% in summer conditions ("ASHRAE Handbook-Fundamentals," 2017). The ADPI value obtained for the case with bar grille diffuser satisfied this standard. Thus, this type of diffuser can be recommended to be installed with VRF-SV hybrid systems in buildings.

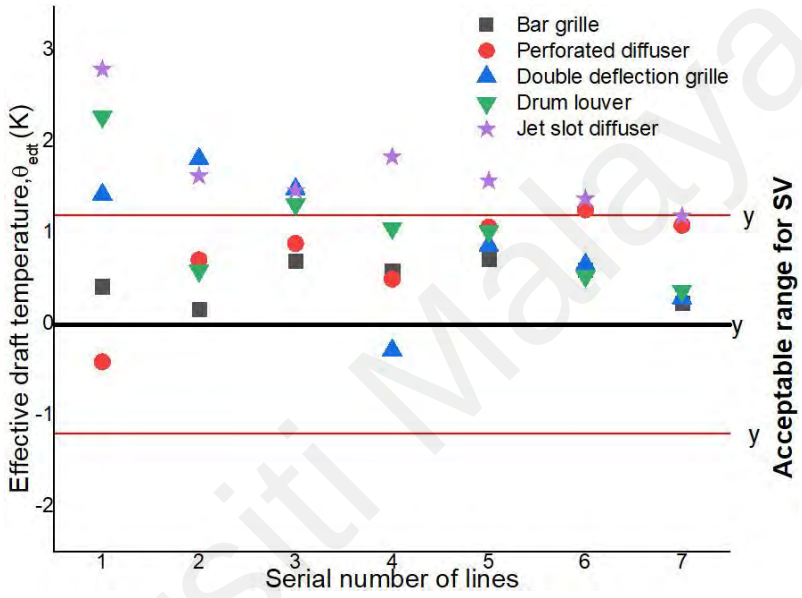

(a)

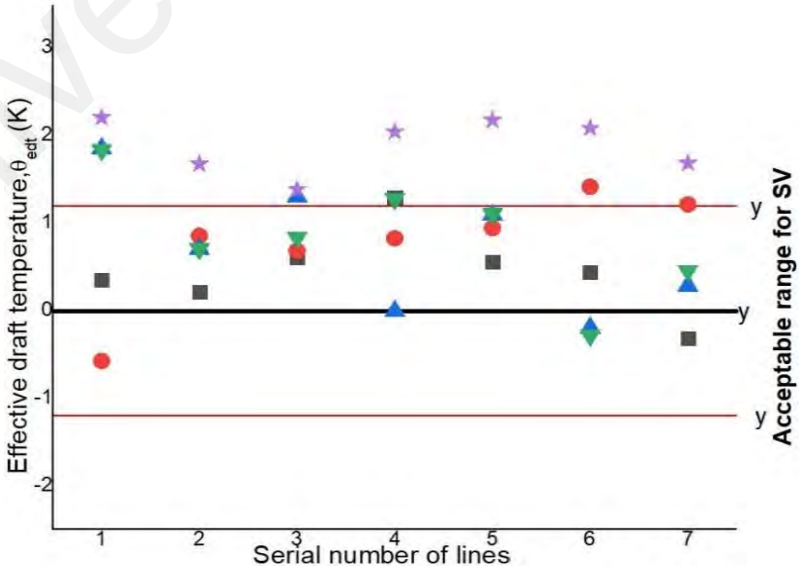

(b)

Figure 6.10: Effective draft temperature, θ_{edt} at the height (a) 0.6 m & (b) 1.1 m

Table 6.5: ADPI value for studied ASTDs

ASTD	Bar Grille	Perforated Diffuser	Double Deflection Grille	Drum Louver Diffuser	Jet Slot Diffuser
ADPI	92.8%	78.6%	64.3%	71.4%	28.5%

6.6.2.5 Effect on Airflow Pattern (Smoke Test)

Airflow visualization testing is more commonly known as smoke testing. The smoke tests rely on visual smoke generated in the cleanroom or laboratory environment. The smoke tests visualize the supplied air in the room through ASTDs. Figure 6.11 shows the visuals of different flow patterns through bar grille, double deflection grille, perforated and drum louver diffusers. The longer airflow throw could be seen in the case with double deflection grille, while flow in the perforated diffuser case was short and highly diffusive. Weak entrainment was also observed with this type of diffuser. A medium but strong air entrainment and momentum was observed with the bar grille diffuser case.

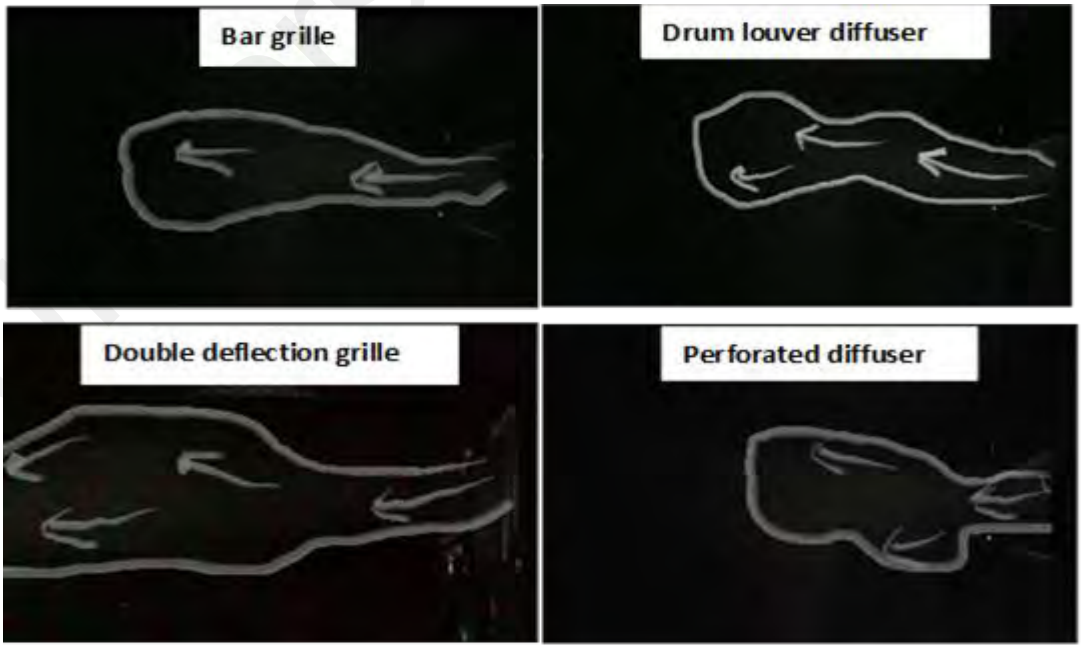

Figure 6.11: Airflow pattern at 0° blade angle through different ASTDs (smoke visualization)

6.6.2.6 Effect on Thermal Comfort (Subjective Test)

Figure 6.12 shows the responses of the subjects surveyed under the meeting room environment to investigate the effects of ASTDs on human thermal sensation and comfort. It was noted that all the ASTDs provided different levels of thermal comfort to the occupants, which showed a significant effect of ASTDs on human thermal comfort. The cases with bar grille and double deflection grille performed better than perforated and drum louver diffusers. For the bar grille case, 70% of the subjects graded the thermal sensation as slightly cool, whereas 60% rated the thermal comfort as comfortable. In the case with a perforated diffuser, 20% of the subjects rated the thermal sensation and comfort as slightly warm and uncomfortable. The low throw by this diffuser prevented the subjects sitting far from the supply from feeling the cooling effects.

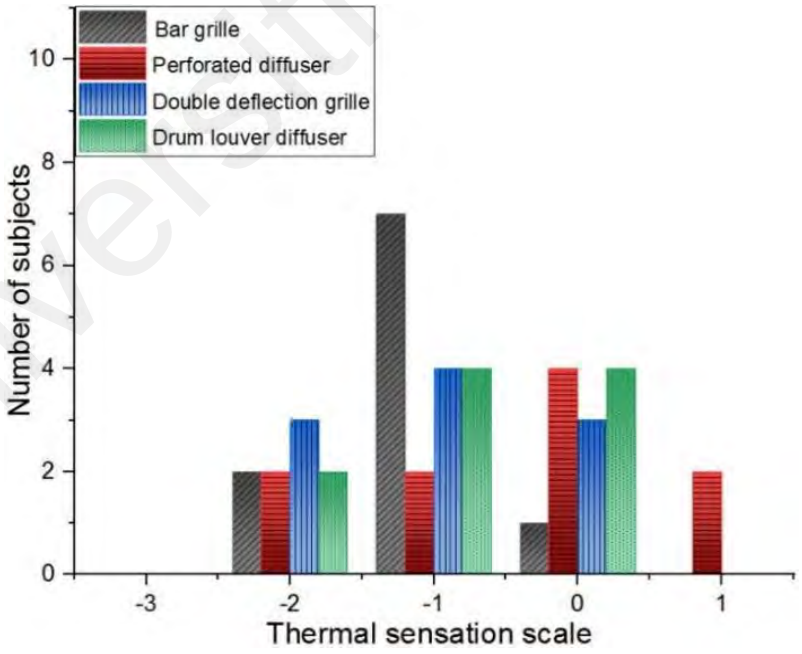

(**a**)

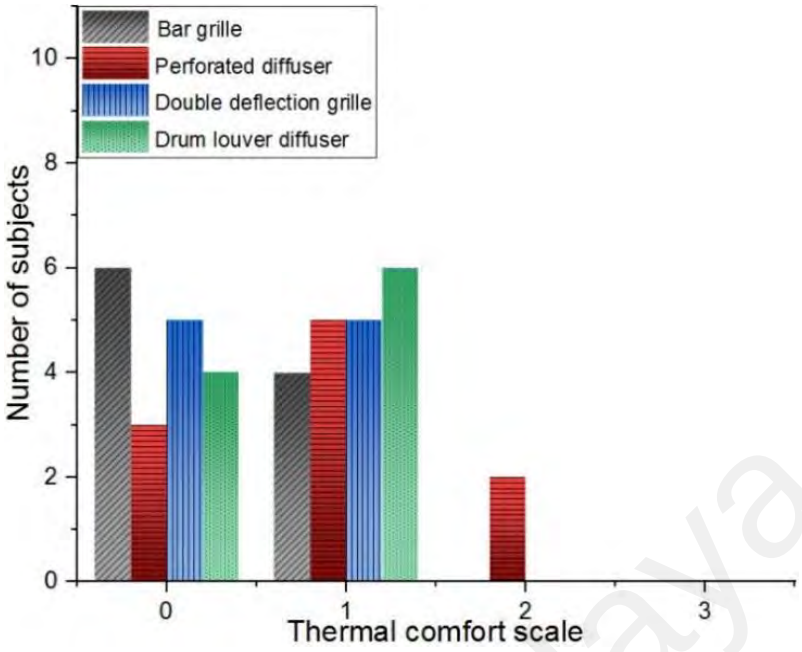

(**b**)

Figure 6.12: Thermal sensation and comfort survey (Human subjects test) (a) TSV and (b) TCV

6.7 Summary

In this study, the air distribution and thermal comfort performance of a VRF-SV hybrid system with five types of ASTD were successfully investigated through laboratory experiments. Under the air distribution aspect, airflow distribution, airflow pattern, EDT and ADPI were evaluated. The thermal comfort performance delivered by each ASTD was measured quantitatively by subjective assessments. Before the actual experimental measurements, the uniformity of the axial airflow jet (that is, discharge from different ASTDs and the effects of top, side and bottom collar orientations on it) were briefly investigated. It was concluded that the plenum collar orientation had a more significant impact on airflow velocity distribution than the temperature distribution. The higher outflow was observed when the supply air entry was in line with the flow direction with collar attachment on the front face of the plenum box (Front collar orientation).

Based on the detailed experimental results, we concluded that:

- Uniform temperature distribution at all locations was created with bar grille diffuser, while the temperature value fluctuated at about 22.5 °C.

- Influential or distinct performance in terms of velocity distribution was not observed with any of the studied diffuser types.

- The ADPI for the bar grille was calculated as 92.8%. The ADPI values for all other ASTD types fell below the minimum required range.

- The thermal sensation and comfort survey suggested that the bar grille provided a better thermal environment than all other diffuser types. For the bar grille case, 70% of the subjects graded the thermal sensation as slightly cool, whereas 60% rated the thermal comfort as comfortable.

The airflow visualization using smoke tests showed a longer airflow throw in the case with double deflection grille, while the flow in the perforated diffuser case was shorter and highly diffusive. The jet entrainment with the bar grille case was uniform and moderate.

Above all, the VRF-SV system installed with the bar grille as ASTD provided better thermal comfort, uniform temperature and velocity distribution within the space. Thus, the bar grille can be recommended to be installed with VRF-SV hybrid systems in building applications. The results of this study could also be used as an important guide for optimization of the air distribution performance of the VRF-SV hybrid system in buildings.

CHAPTER 7: A COMPREHENSIVE NUMERICAL STUDY OF THE EFFECTS OF THE AIR DISTRIBUTION TERMINALS ON THE PERFORMANCE OF A NOVEL VRF-SV HYBRID SYSTEM

7.1 Introduction

The room airflow pattern generated in the mechanical ventilation system has a substantial impact on room IAQ and thermal comfort (Nada et al., 2016; Y.H. Yau et al., 2018). There are many factors influence the airflow pattern in the room, including the ASTD type and number, position layout, building envelope, flowrate, and supply air temperature (Z. Lin et al., 2005; Sui & Zhang, 2012b; T. Yao & Z. Lin, 2014a). A number of studies have looked into the impact of different types of ASTDs on the varying performance of mechanical ventilation systems. S.C. Hu (Hu, 2003) investigated the airflow characteristics of the vortex diffuser using experimental and numerical methods. The study revealed that the flow pattern near the diffuser was 3-dimensional and highly turbulent. It was also shown that the vortex diffuser has a better room entrainment ratio than the circular type multi-cone diffuser. The entrainment ratio is a jet characteristic commonly used to evaluate the airflow throw distance from the diffuser face (Zhivov et al., 2020). In another study, Nastase et al., (2011) under the mixing ventilation method compared the lobed grille with the standard grille. They found that the lobed grille provided a better airflow distribution and thus, it has improved the indoor thermal comfort. Some other studies reported the impact of lip and blade angles of different type of diffusers on the room airflow pattern (Sajadi et al., 2011; Sun & Smith, 2005). Conceicao et al., (2010) investigated the turbulent and the mean airflow from the exit of the ATD around the occupant under personalized ventilation. Using two different air speeds with upper and lower exit ATDs, different tests were performed. It was concluded that the occupants found thermally comfortable with the test when the airflow velocity at the upper exit of the ATD was higher. For

stratum ventilation, very limited study is found in the open literature, in which, the effects of ASTD types, geometry and layouts are investigated (Ting Yao & Lin, 2014; T. Yao & Z. Lin, 2014a; Yong CHENG et al., 2014; H. Zhao et al., 2015). All these studies were performed using supply air conditioned by the traditional chiller-based AC system. After having a thorough investigation of the suitable layout for ATDs under stratum ventilation, Yao and Lin (2014a) evaluated the performance of four different types of ASTDs in a classroom environment. The results revealed that the types of ASTDs have significant impacts on the performance of the stratum ventilation system and recommended the circular diffuser for a better thermal comfort and IAQ. This study is therefore designed to numerically investigate the effects of different types of ASTDs on thermal comfort, indoor air quality (IAQ) and air distribution performance when installed with the novel VRF integrated stratum ventilation system.

7.2 Brief Overview of the Novel VRF-SV System

Figure 7.1 shows a novel method of combining the VRF system with the DOAS system to deliver fully conditioned air directly into the space using stratum ventilation air distribution strategy. In the fully integrated method, the room is provided with 100% conditioned air at an elevated temperature to not only meets the entire thermal load of the space, but also to reduce the energy consumption of the system. This design solution eliminates the need for a separate VRF fan coil unit. This design approach not only reduces the overall system capacity, but also overcomes the large space requirement for the HVAC system installation.

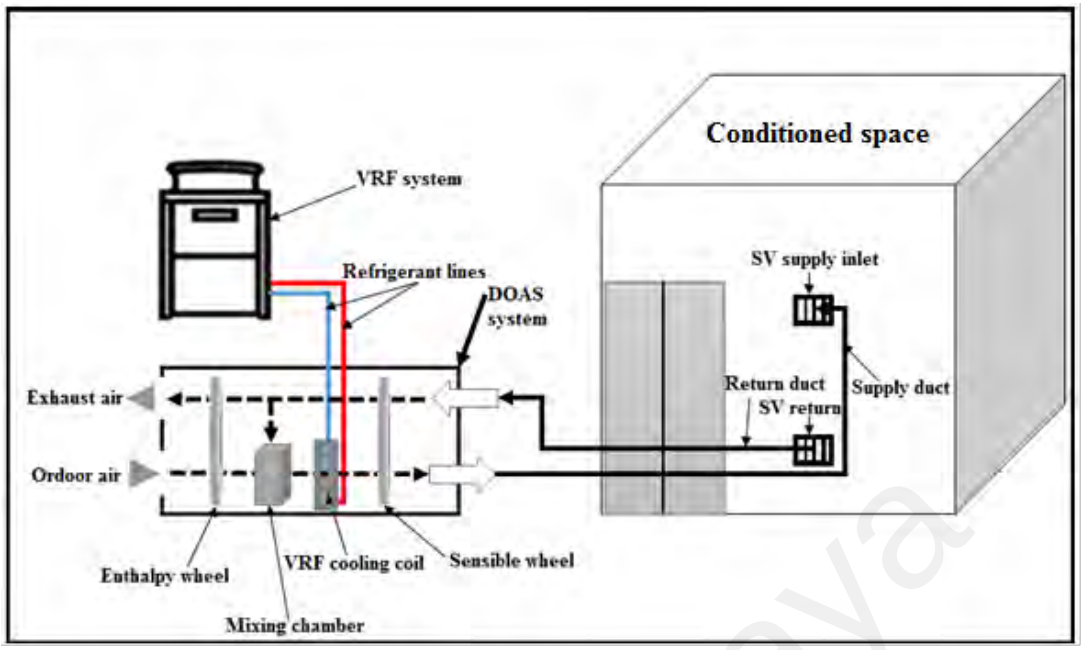

Figure 7.1: VRF installed with the stratum ventilation system (VRF-SV system) using a fully integrated approach

7.2.1 Air Supply Terminal Devices (ASTDs)

A total of four different types of commonly used air supply terminal devices is investigated in the present study. Their models are designed and sketched using solidworks software as shown in Figure 7.2. Note that for a constant supply airflow rate, these ASTDs are evaluated in two different room settings for a better comparison of their performance, i.e., laboratory room and a meeting room. Because of the less significant impact of the type of exhaust terminals on room air distribution pattern, bar grilles were employed as the return terminal for all of the supply terminal types. In all the simulated cases the supply air terminal is positioned at 1.9 m height and the return terminal is installed at the height of 0.33 m from the floor.

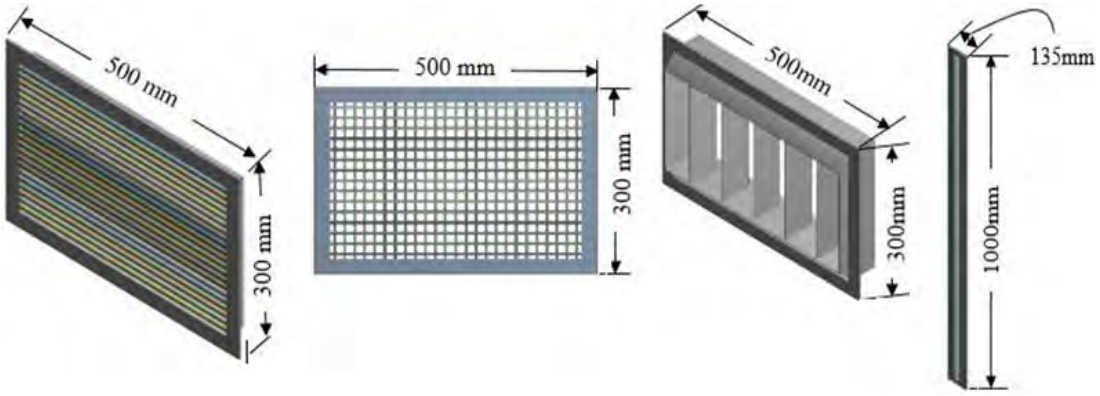

Figure 7.2: ASTDs assembly models using solidworks

7.3 Numerical Method

In this study, a series of simulations were performed to evaluate the air distribution performance of four types of air supply terminal devices in a laboratory and meeting room environments. Different numerical models, i.e., the standard k-ϵ model, renormalization group (RNG) k-ϵ model and realizable k-ϵ models were adopted in the simulation setup of the studied cases. The literature suggested that the RNG k-ϵ model is most suitable in predicting the indoor airflow with air-conditioning system (Gebremedhin & Wu, 2003; Posner, Buchanan, & Dunn-Rankin, 2003; Zheng et al., 2018). However, some other studies have also investigated the airflow behavior in different spaces by employing the standard k-ϵ, realizable k-ϵ or SST k-ω models (Beggs, Kerr, Noakes, Hathway, & Sleigh, 2008; Hussain, Oosthuizen, & Kalendar, 2012; Nada et al., 2016). In order to select one that can give most accurate prediction of the actual physical behavior, all the turbulence models were initially verified and validated through experimental results using the bar grille as the supply air terminal in the meeting room environment. The chosen model was then employed for the simulation of all the other designed cases.

7.3.1 Studied Cases and Geometrical Models

The space under investigation has the dimensions 6m in length, 5.4m in width and 2.74m in height. The humans, personal computers, equipment and lighting lamps were

modeled as internal heat generation sources. The thermal load for each physical model is detailed in Table 7.1. Eight cases were designed for the complete simulation study and the details for each case is presented in Table 7.2. The arrangements and the typical layout of the physical models, i.e. the laboratory and meeting room can be seen in Figure 7.3. The air entered the room through selected diffusers installed at the breathing height and extracted from the bar grille terminal installed at the same wall at a low level (about 0.33m from the floor). The bar grille, double deflection grille and drum louver diffusers have the dimensions [0.5m (L) X0.3m (W)], whereas the dimensions for the jet slot diffuser is [1m (L) X0.135m (W)]. The dimensions for the mannequin in the laboratory environment are 0.3m in diameter and 1.7 m in length. The computers were modeled as cubical boxes with 0.2m dimension. For meeting room case, the mannequins present in the sitting positions are all containing equal surface area as that present in the laboratory room setting. The floor to the center height for all the supply and return terminal type is 1.9m and 0.33m, respectively.

Table 7.1: Details of the cases studied for both types of environments

Entity		People	Other heat sources		
			Computer	Equipment	Lighting
Heat Load	Laboratory room setting	70 W= 2 X70= 140W	2X 90 = 180W	500W	100W
	Meeting Room setting	70 W= 10 X 70= 700			

Table 7.2: Details of the simulated cases

Case	Domain type	Diffuser type	Diffuser Size (mm)	Supply Air velocity	Airflow rate	Supply temperature (°C)	Room temperature (°C)
1	Laboratory/ Meeting room	Bar grille diffuser	0.5m × 0.3m	3.08 m/s	0.25m^3/s	18.7±0.3	26.0 ±0.1
2		Double deflection grille	0.5m × 0.3m	3.08 m/s	0.25m^3/s	18.5±0.1	26.0 ±0.1
3		Drum louver diffuser	0.5m × 0.3m	3.08 m/s	0.25m^3/s	18.8±0.3	26.0 ±0.1
4		Jet slot diffuser	1m × 0.135m	3.08 m/s	0.25m^3/s	19.0±0.1	26.0 ±0.1

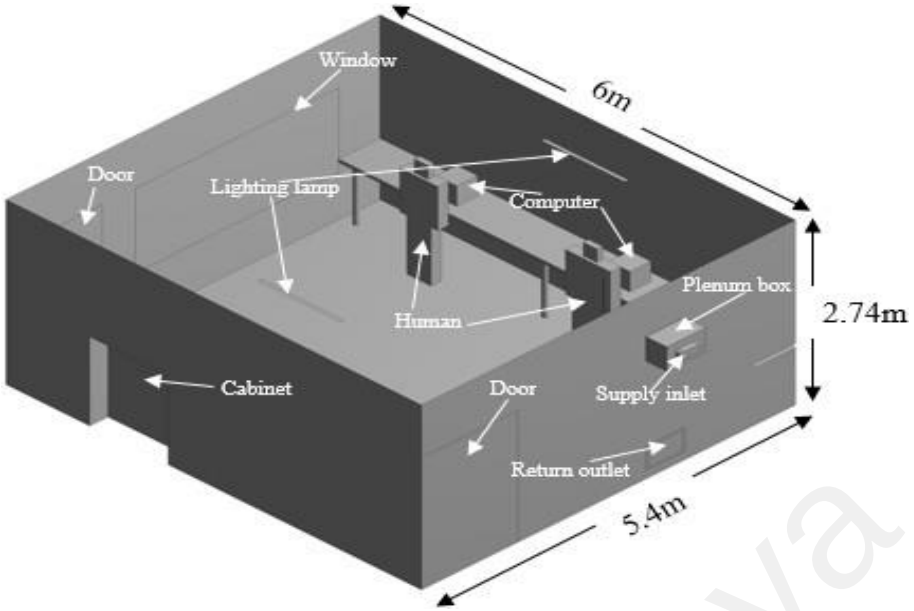

(a)

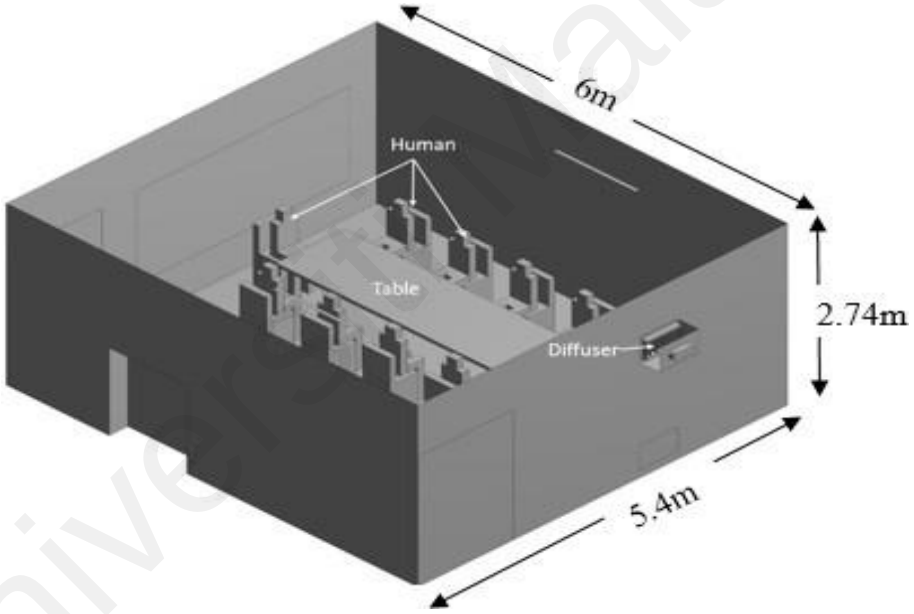

(b)

Figure 7.3: CFD domain of the physical models (a) Laboratory room (b) Meeting room

7.3.2 Governing Equations

Three-dimensional steady state model was selected in order to analyze the flow pattern generated by the selected diffusers, i.e. bar grille, double deflection grille, drum louver diffuser and jet slot diffuser in a laboratory and meeting room environment. The temperature and airflow field distributions in the studied domains are completely

governed by the laws of conservation of mass, momentum and energy. The momentum equation is solved by inducing the buoyancy effect, whereas the density of the air in the domain is treated as incompressible, obeying the ideal gas law. The radiation heat from the internal heat sources and from the building envelope is not taken into consideration in the current study. For a detailed understanding of the physical models, readers can refer to reference (Ansys, 2015). Based on the assumptions made during the simulation studies, the Reynolds-averaged Navier-Stokes (RANS), continuity and energy equations can be modeled as,

$$\frac{\partial U_i}{\partial x_i} = 0 \tag{7.1}$$

$$\frac{\partial(\rho U_j U_i)}{\partial x_j} + \frac{\partial P}{\partial x_i} = \mu \nabla^2 U_i + (\rho - \rho_0) g_i + \frac{\partial}{\partial x_j}\left(-\rho \overline{\acute{u}_i \acute{u}_j}\right) \tag{7.2}$$

$$\frac{\partial(\rho C_P U_i T)}{\partial x_j} - \lambda \nabla^2 T = \frac{\partial}{\partial x_j}\left(-\rho C_P \overline{\acute{u}_i \theta}\right) \tag{7.3}$$

where $\overline{\acute{u}_i \acute{u}_j}$ and $\overline{\acute{u}_i \theta}$ are Reynolds stresses and turbulent heat fluxes. For studying the buoyancy effect using Boussinesq hypothesis, these two terms can be defined as,

$$\rho \overline{\acute{u}_i \acute{u}_j} = \frac{2}{3}\delta_{ij}\rho k - 2\mu_t S_{ij} \tag{7.4}$$

$$\rho C_P \overline{\acute{u}_i \theta} + \frac{\mu_t}{\sigma_t}\frac{\partial T_i}{\partial x_j} = 0 \tag{7.5}$$

where k, μ_t and S_{ij} are the terms representing turbulent kinetic energy, eddy viscosity and strain-rate tensor. The latter can further be expressed as,

$$S_{ij} = 0.5\left(\frac{\partial U_i}{\partial x_j} + \frac{\partial U_j}{\partial x_i}\right) \tag{7.6}$$

7.3.3 Turbulence Modeling (k-ϵ Models)

This section explains the theoretical background of the numerical models adopted in the present research work. Each model utilizes different methods for calculating turbulent viscosity. The following subsections presented the transport equations and methods for calculating the turbulent viscosity for each model. In addition, the model constants are presented separately

7.3.3.1 The Standard k-ϵ Model

The standard k-ϵ model falls under the category of two equations turbulence models. It is based on model transport equations for turbulence kinetic energy (k) and the dissipation rate (ϵ)(Brauer, 1973). In its derivation, the effects of molecular viscosity are considered negligible, and thus it is valid only for fully turbulent flows. The transport equations for turbulence kinetic energy (k) and its dissipation rate (ϵ) can be expressed as follows (Ansys, 2015):

$$\frac{\partial(\rho k)}{\partial t}+\frac{\partial(\rho k\mu_i)}{\partial x_i}=\frac{\partial}{\partial x_j}\left(\left(\mu+\frac{\mu_t}{\sigma_k}\right)\frac{\partial k}{\partial x_j}\right)+G_k+G_b-\rho\epsilon-Y_M+S_k \tag{7.7}$$

and,

$$\frac{\partial(\rho\epsilon)}{\partial t}+\frac{\partial(\rho\epsilon\mu_i)}{\partial x_i}=\frac{\partial}{\partial x_j}\left(\left(\mu+\frac{\mu_t}{\sigma_\epsilon}\right)\frac{\partial\epsilon}{\partial x_j}\right)+C_{1\epsilon}\frac{\epsilon}{k}(G_k+C_{3\epsilon}G_b)-C_{2\epsilon}\rho\frac{\epsilon^2}{k}+S_\epsilon \tag{7.8}$$

where G_k and $G_b$represents the turbulence kinetic energy generation due to the mean velocity gradient and buoyancy, respectively. The term Y_M represents the effect of dilation in compressible turbulence with the overall kinetic dissipation rate. The Prandtl numbers for k and ϵ are represented by σ_k and σ_ϵ, whereas S_k and S_ϵ are the source terms. The $C_{1\epsilon}$, $C_{2\epsilon}$ and $C_{3\epsilon}$ are constants terms having the following default values.

$$C_{1\epsilon}=1.44, C_{2\epsilon}=1.92, C_\mu=0.09, \sigma_k=1, \sigma_\epsilon=1.3$$

For calculating the turbulent viscosityμ_t, k and ϵ are combined as follows:

$$\mu_t = \rho C_\mu \frac{k^2}{\epsilon} \tag{7.9}$$

where C_μ is constant.

7.3.3.2 The RNG k-ϵ Model

The RNG k-ϵ model is termed as a variant of standard k-ϵ model and is derived using a technique called renormalization group (RNG) theory. This model has an additional term in the ϵ equation, which further refines the accuracy of the solution. The effect of swirling in the turbulent flow is also included in this model (Kubicek et al., 2009). The RNG k-ϵ model has a similar form of transport equations as presented for the standard k-ϵ model,

$$\frac{\partial}{\partial t}(\rho k) + \frac{\partial}{\partial x_i}(\rho k \mu_i) = \frac{\partial}{\partial x_j}\left(\alpha_k \mu_{eff} \frac{\partial k}{\partial x_j}\right) + G_k + G_b - \rho\epsilon - Y_M + S_k \tag{7.10}$$

$$\frac{\partial}{\partial t}(\rho\epsilon) + \frac{\partial}{\partial x_i}(\rho\epsilon \mu_i) = \frac{\partial}{\partial x_j}\left(\alpha_\epsilon \mu_{eff} \frac{\partial \epsilon}{\partial x_j}\right) + C_{1\epsilon}\frac{\epsilon}{k}(G_k + C_{3\epsilon}G_b) - C_{2\epsilon}\rho\frac{\epsilon^2}{k} - R_\epsilon + S_\epsilon \tag{7.11}$$

The values for constant terms used in the RNG k-ϵ model are given as follows:

$$C_{1\epsilon} = 1.42, C_{2\epsilon} = 1.68, C_\mu = 0.0845, \sigma_k = \sigma_\epsilon = 1.39, \sigma_t = 0.85$$

7.3.3.3 The Realizable k-ϵ Model

In this model, the term realizable refers to some satisfaction with the mathematical constraints on the Reynolds stresses. Neither of the above presented models are realizable (Ansys, 2015). The realizable k-ϵ model together with the RNG k-ϵ model shown significant improvement in the accuracy of the results when compared with the standard k-ϵ model for flow features include curvature, vortices and rotation. Since the realizable model is still new, it is not strongly evident that in what cases this model clearly outperforms the RNG k-ϵ model (Ansys, 2015).

The transport equations for this turbulence model are given as follows:

$$\frac{\partial}{\partial t}(\rho k) + \frac{\partial}{\partial x_j}(\rho k \mu_j) = \frac{\partial}{\partial x_j}\left(\left(\mu + \frac{\mu_t}{\sigma_k}\right)\frac{\partial k}{\partial x_j}\right) + G_k + G_b - \rho\epsilon - Y_M + S_k \quad (7.12)$$

And

$$\frac{\partial}{\partial t}(\rho \epsilon) + \frac{\partial}{\partial x_j}(\rho \epsilon \mu_j) = \frac{\partial}{\partial x_j}\left(\left(\mu + \frac{\mu_t}{\sigma_\epsilon}\right)\frac{\partial \epsilon}{\partial x_j}\right) + \rho C_1 S_\epsilon - \rho C_2 \frac{\epsilon^2}{k+\sqrt{\nu\epsilon}} + C_{1\epsilon}\frac{\epsilon}{k}C_{3\epsilon}G_b S_\epsilon \quad (7.13)$$

where,

$$C_1 = \max\left[0.43, \frac{\eta}{\eta+5}\right], \eta = S\frac{k}{\epsilon}, S = \sqrt{2S_{ij}S_{ij}}$$

The other terms are the same as described in the previous models. The difference between realizable k-ϵ model and other k-ϵ models is that, the term C_μ is not constant and can be expressed by equation (7.14),

$$C_\mu = \frac{1}{A_0 + A_s\frac{kU^*}{\epsilon}}, \quad (7.14)$$

$$\text{where } U^* \equiv \sqrt{S_{ij}S_{ij} + \tilde{\Omega}_{ij}\tilde{\Omega}_{ij}} \quad (7.15)$$

$$\tilde{\Omega}_{ij} = \Omega_{ij} - 2\epsilon_{ijk}\omega_k \quad (7.16)$$

$$\Omega_{ij} = \overline{\Omega}_{ij} - \epsilon_{ijk}\omega_k \quad (7.17)$$

where, the model constants A_0 and A_s are given by:

$$A_0 = 4.04, \; A_s = \sqrt{6}\cos\phi$$

where,

$$\phi = \frac{1}{3}\cos^{-1}(\sqrt{6}W), W = \frac{S_{ij}S_{jk}S_{ki}}{\tilde{S}^3}, \tilde{S} = \sqrt{S_{ij}S_{ij}}, S_{ij} = \frac{1}{2}\left(\frac{\partial \mu_j}{\partial x_i} + \frac{\partial \mu_i}{\partial x_j}\right)$$

The values for constant terms used in the Realizable k-ϵ model are given as follows:

$$C_{1\epsilon} = 1.44, C_2 = 1.9, \sigma_k = 1.0, \sigma_\epsilon = 1.2$$

7.3.4 Simulation Scheme and Boundary Conditions

In this numerical analysis, the turbulence k-ε (2-equations) models were employed to investigate their accuracy in predicting the indoor air flow distribution. The governing and transport equations mentioned in the earlier sections, have been discretized with the SIMPLE algorithm using a second-order upwind scheme. Simulations were carried out using two workstations; each specifies with Intel Xeon(R) CPU E3-1240 v5 3.5GHz processor, 32GB RAM Windows 7 Professional 64-bit operating system that required roughly 12 h to 24 h to reach at the solution completion for the generated grids. The boundary conditions set up to run the simulations based on this investigation are presented in Table 7.3.

Table 7.3: Boundary conditions setup for the CFD simulation

Boundary	Simulation setup
SV supply air inlet	3.08m/s, 18.7±0.3 °C
Exhaust air outlet	0 pa, gauge pressure, 26°C
Computer/Equipment Load	Constant energy source
Lighting Load	Constant energy source
Nostrils (CO_2 exhalation)	0.89m/s, 0.0067 Kg/s, 34°C
Table	Constant temperature of 26°C
Human Body	Constant energy source
Ceiling	26.3°C (Adiabatic)
Floor	26.3°C (Adiabatic)
Walls	26.3°C (Adiabatic)
SV diffuser/grille blades	18.7°C (Adiabatic)
Plenum box	18.7°C (Adiabatic)

7.3.5 Computational Grids and Sensitivity Analyses

In this study, the mesh module of the Ansys Fluent 20.1 was used to discretize the whole domains into unstructured tetrahedral conformal meshes. A very fine mesh strategy was adopted only for the supply air terminal devices in order to reduce the number of elements of the entire domain. The mesh method for both of the studied domains is the same and based on the varying element sizes (0.3 to 0.05) for the main body. An example of the mesh size for the meeting room case installed with a drum louver diffuser can be seen in Figure 7.4. The mesh size was refined significantly near the wall regions to solve all the boundary layers. During this investigation, the near-wall treatment used the enhanced wall function for all the cases with ASTDs. In most locations of the computational domain, the Y+ of the initial grid was less than 1.0 in all cases. The mesh sizes along with their respective volumetric mean room temperatures in the laboratory environment for each mesh size are reported in Table 7.4.

The in-depth mesh sensitivity analyses were also carried out to obtain the results independent of grid sizes. Figure 7.5 presents the temperature and velocity profiles of the cases simulated using different mesh sizes on a vertical centerline (floor to ceiling), which was drawn at the geometric center of the domain. The profile patterns with mesh sizes, Mesh-III and Mesh-IV found very close with the maximum deviation recorded was about 0.075m/s in velocity and 0.5ºC in temperature. Therefore, to save the computational time, the mesh size (Mesh-III) was selected in this study for further investigations.

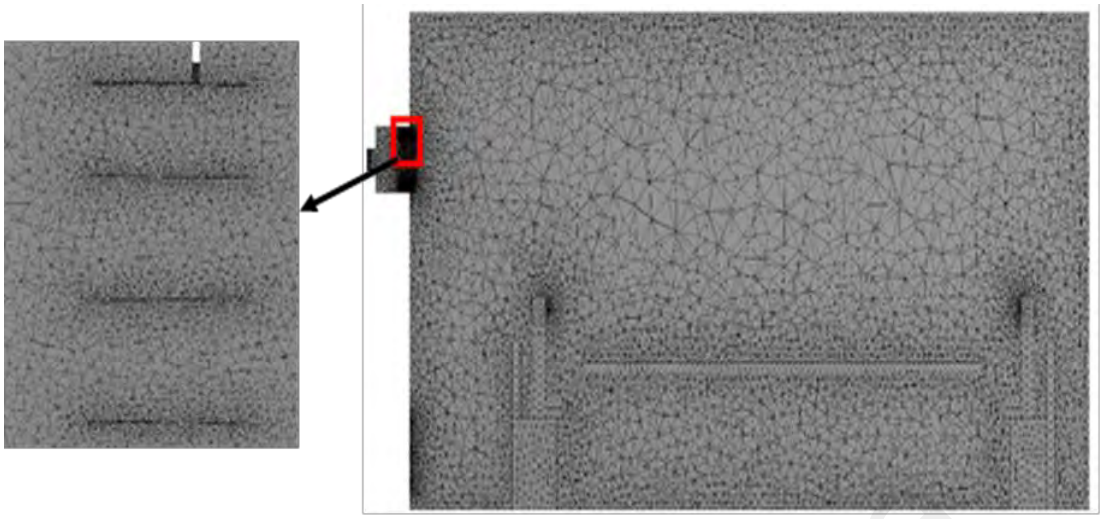

Figure 7.4: Example of the computational grid (Meeting room, drum louver diffuser case)

Table 7.4: Mesh sizes and corresponding volumetric mean temperature (Lab room Case)

Mesh	Body size (m)	No. of Elements (millions)	No. of Nodes (millions)	Mean Room Temperature (°C)	Difference (°C)
Mesh-I	0.3	1.07	0.22	22.98	
Mesh-II	0.2	1.08	0.25	23.67	0.69
Mesh-III	0.1	1.53	0.28	24.14	0.47
Mesh-IV	0.05	6.45	1.11	23.97	0.20

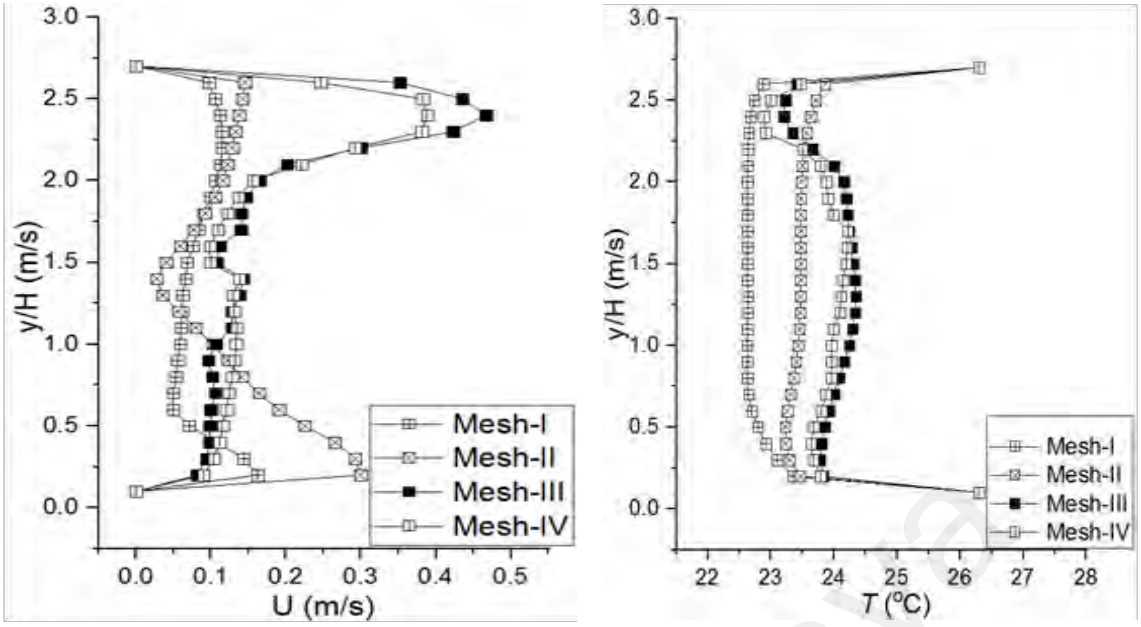

Figure 7.5: Centerline velocity and temperature profiles for studied mesh sizes (Mesh-I: Coarse, Mesh-II: Medium, Mesh-III: Fine, Mesh-IV: Super fine)

7.3.6 Performance Evaluation Criteria

The functional performance of the four air supply terminal devices was evaluated through the provided thermal comfort, IAQ assessment and airflow pattern and distributions. The airflow pattern in both of the studied domains was directly determined through temperature and velocity field distributions using the fluent default parameters. Whereas, thermal comfort is evaluated by the predicted mean vote (PMV) and predicted percentage dissatisfied (PPD). The PMV and PPD were determined based on equations 7.18 and 7.19 defined in ISO7730 ("International Standard Organization (ISO-7730) -Ergonomics of the thermal environment," 2005). For the IAQ assessment, the most effective evaluating parameters are the mean age of air and CO_2 concentration in the conditioned environment. In order to thoroughly investigate the performance of different ASTDs installed with the VRF-SV combined system, the following parameters are examined by incorporating user-defined functions (UDF) code into Ansys FLUENT program. The comfort level and clothing insulation were set at 1.0 met and 0.6 clo, respectively.

- Flow pattern
- Thermal field distribution
- Velocity distribution
- Thermal comfort (PMV, PPD)
- IAQ (Mean age of air, CO_2 concentration)

The mathematical model for the PMV index can be expressed as follows:

$$\begin{aligned}\mathrm{PMV} = {} & (0.303\exp - 0.0336\mathrm{M} + 0.028) \\ & \times \{(\mathrm{M} - \mathrm{W}) - 3.5 \times 10^{-3}\,[5733 - 6.99(\mathrm{M} - \mathrm{W}) - \mathrm{pa}] \\ & - 0.42\,(0\mathrm{M} - 58.15) - 1.7 \times 10^{-5} \times \mathrm{M}(5867 - \mathrm{pa}) \\ & - 0.0014\mathrm{M}\,(34 - \mathrm{ta}) \times 10^{-8}]\end{aligned}$$

Where,

M=metabolic rate, (W/m^2)

W=effective mechanical power, (W/m^2)

Pa= water vapor partial pressure, (Pa)

ta = air temperature, (^oC)

f_{cl} = clothing surface factor

t_{cl} = clothing surface temperature, (^oC)

$\bar{t}_r$ = mean radiant temperature (^oC)

h_c= convective heat transfer coefficient ($W/m^2.K$)

The PPD index defines the quantitative measure of the thermal comfort for indoor air conditioned environment. The mathematical model is expressed as follows:

$$\mathrm{PPD} = 100 - 95\exp(-0.03353.\,\mathrm{PMV}^4 - 0.2179.\,\mathrm{PMV}^2) \qquad (7.19)$$

For the calculation of mean age of air and CO_2 concentration, the UDF coding for the user defined scalar and diffusivity sources were also introduced into the UDF code for compilation into the fluent setup.

7.3.7 Measurement Method and Data Collection

Values for the air temperature and velocity were numerically and experimentally recorded at different positions (L1 to L7) at heights of 0.1, 0.6, 1.1 and 1.9 m in both of the studied domains. The measuring lines positions in the experimental setup are shown in Figure 7.6. The experimental setup was arranged for the laboratory as well as a meeting room by accurately mimicking the numerical settings. For each height along the vertical lines (L1 to L7), five testing samples were taken during experimental measurements and the average values of the measured variables were recorded for comparison with the simulation results. The other evaluating parameters such as the PMV, PPD, mean age of air and CO2 concentration were qualitatively recorded at different planes within the studied domains. A horizontal plane (A) at Y=1.5m and a vertical plane (B) at Z=1.75m, were created for both of the studied domains and the contours for the aforementioned variables were captured on these planes for evaluating the performance of different ASTDs. The qualitative results are compared and analyses are presented in the subsequent result sections.

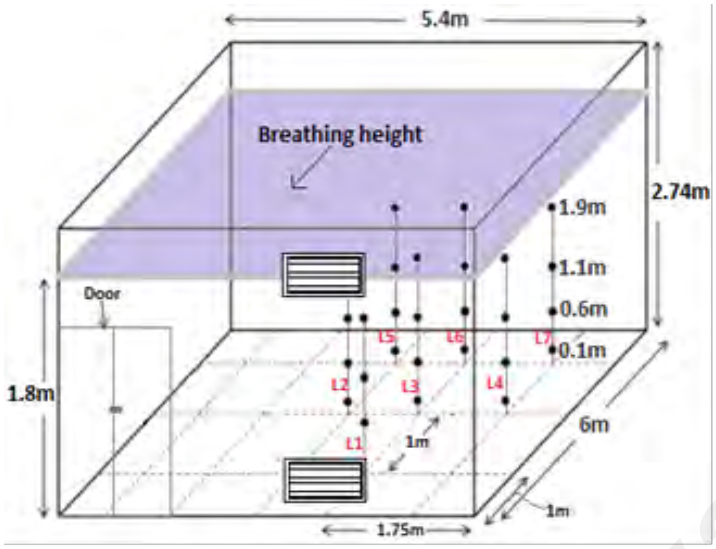

Figure 7.6: Measurement locations and the layout in the testing chamber

7.4 Results and Discussion

7.4.1 Model Verification &Validation

The models adopted in this study have been verified and validated first with the detailed experimental measurements and numerical predictions under the bar grille case. The airflow velocity and temperature profiles were generated for all of the above mentioned positions (see Figure 7.6(b)). As shown in Figures 7.7 and 7.8, the corresponding values of the velocity and temperature at each of the measuring lines (L1 - L7) were compared and presented at four different heights 0.1m, 0.6m, 1.1m, and 1.9m from the ground. Even after performing a series of experimental and numerical work, the accurate match was not found between the measurement and predictions of any of the adopted turbulence models at mentioned positions. The reason may be due to the inconsistency and the transient behavior of the indoor environment in the experimental chamber during experimental measurements. It could also be attributable to measurement inaccuracies up to some extent. However, a relatively good agreement between the measured and numerically predicted profiles was seen with the RNG k-ϵ turbulence model. Quantitatively, the maximum deviations at any location between measured and simulated velocity values are found to be 0.28m/s, 0.5m/s, 0.26m/s for

RNG k- ε, Realizable k- ε and Standard k- ε models, respectively. Similarly, the largest difference of 1.6°C in the temperature magnitude of the measured and simulated results was recorded for standard k- ε model. The above mentioned comparison implied that the RNG k-ε model could be considered accurate enough and the best fit to proceed with the further investigations.

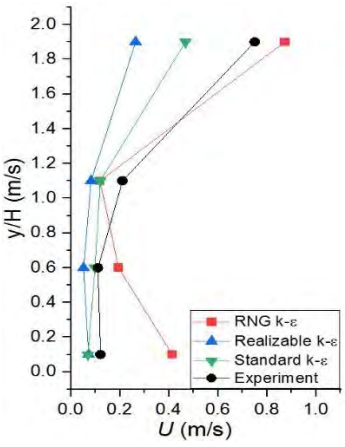

(L1)

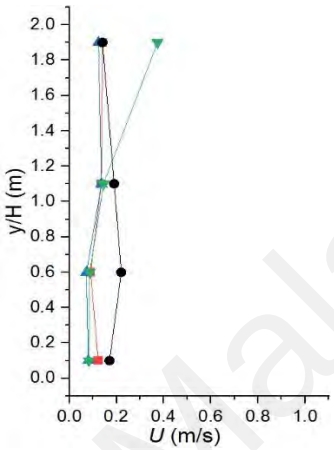

(L2)

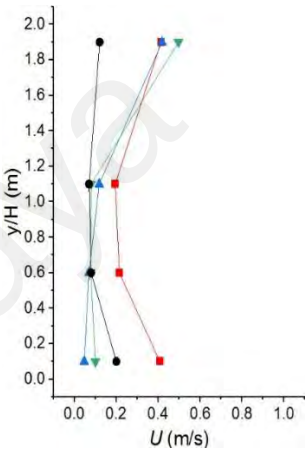

(L3)

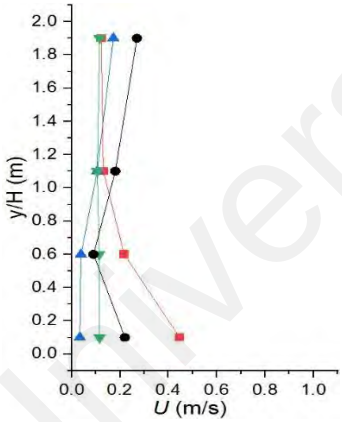

(L4)

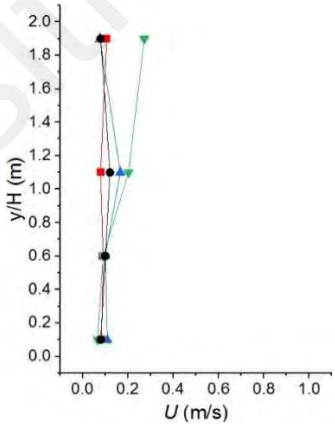

(L5)

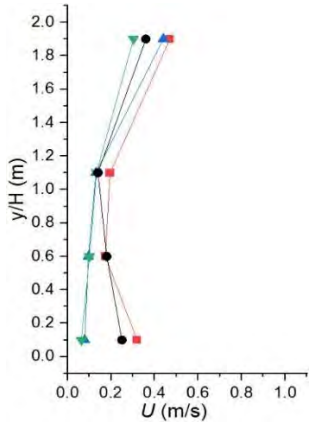

(L6)

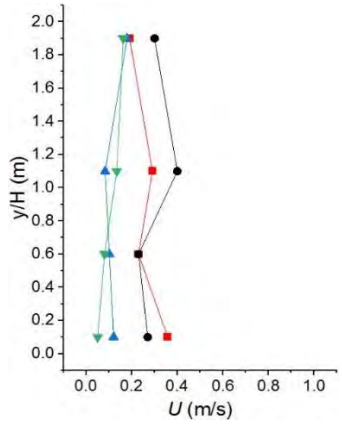

(L7)

Figure 7.7: Measured and predicted velocity profiles at different positions (L1-L7)

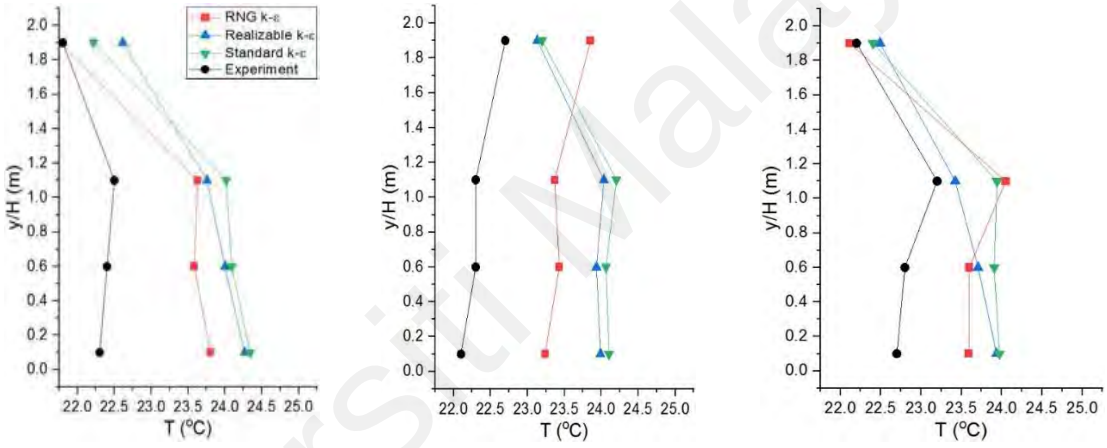

(L1) (L2) (L3)

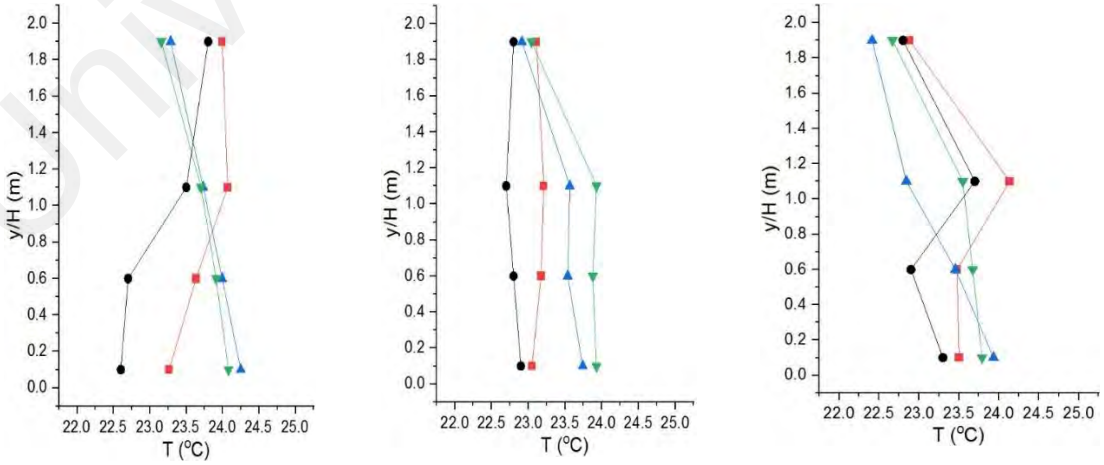

(L4) (L5) (L6)

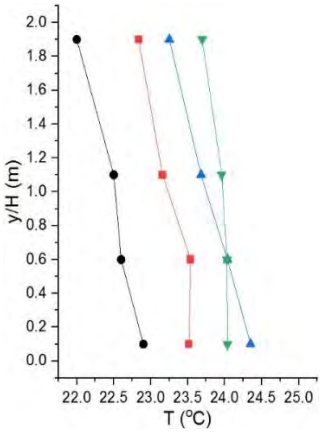

(L7)

Figure 7.8: Measured and predicted temperature profiles at different positions (L1-L7)

7.4.2 CFD Simulation Results

7.4.2.1 Effects of the ASTDs on the Airflow Pattern

The room airflow pattern generated using four air supply terminal devices are presented in Figure 7.9. The flow patterns are represented at the iso-surfaces with the terminal velocity range of 0.8m/s. These figures were drawn based on the meeting room environment settings, where the internal heat sources and four air supply terminal devices were considered. According to Figure 7.9, the drum louver has provided the longest jet throw of about 4m from the supply face, compared to all other terminal types. Furthermore, the larger area with the iso-surface velocity of 0.8m/s was covered in the case with double deflection grille. In the cases with the bar grille and the jet slot diffusers, the flow which the velocities greater than 0.8m/s existed only in a small area near the air supply location. The higher mixing rate and air entrainment are seen with the double deflection grille, since it is designed, considering the combined effect of vertical and horizontal blades, that together can greatly enhance the supply air momentum. Though, the double deflection grille case created more favorable flow pattern, however, it may cause a serious draught risk issue to the occupants due to a strong airflow provoked in the major area of the space (almost 30%). Furthermore, the

flow pattern generated by the bar grille device was found within the acceptable range based on the ASHRAE standard(ANSI/ASHRAE, 2017) where most of the occupied zone found with the air motion limited to or less than 0.8m/s. Another phenomenon observed in the double deflection grille case is that the wall confluent jet is remained attached near the wall surface due to the Coanda effect then moved downward until it reached the floor. In the drum louver diffuser case, the jet was supplied with the strong momentum, but less air mixing is observed the adjacent zones. This type of diffuser may be suitable for large applications that require air to be thrown at larger distances.

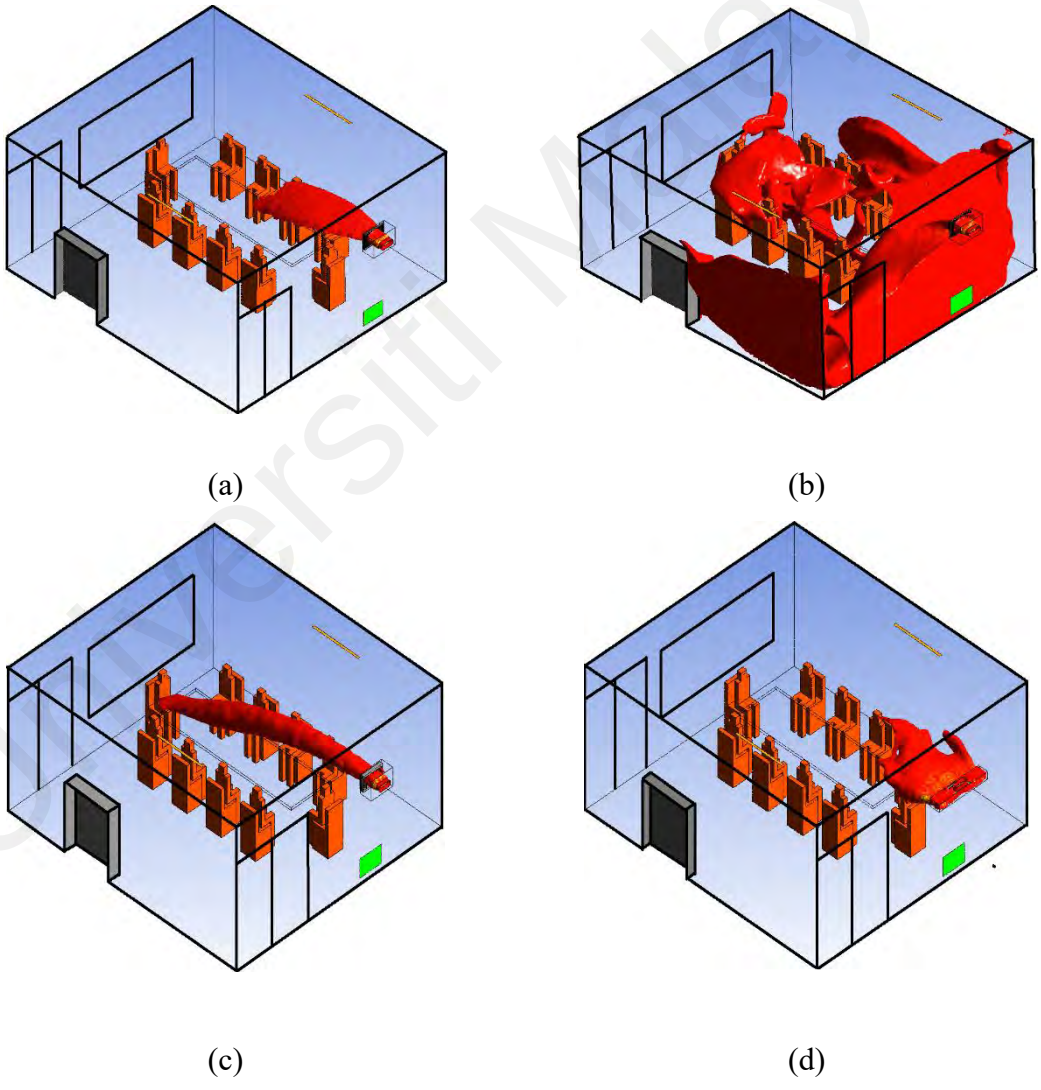

Figure 7.9: Iso-surface of the velocity of 0.8 m/s for meeting room case with (a) Bar grille, (b) Double deflection grille, (c) Drum louver and (d) Jet slot diffuser

7.4.2.2 Temperature and Velocity Distributions

Figure 7.10 shows the temperature and velocity field distributions on the sectional planes A and B at Y=1.5 m, Z=1.75, respectively for the laboratory room environment. The temperature in the zones far from the airflow jet found significantly higher (about 1ºC - 2.5ºC) than the jet regions in all the ASTDs, except the bar grille. Note that some hotspots are detected near the side walls due to the presence of heat sources at those locations. However, the contour of plane A in Figure 7.10(a), the bar grille has provided a uniform temperature distribution with only a 1ºC temperature difference. A reverse thermal gradient (≥ -3ºC) is also noticed within the occupied zone. The lower temperature of about 22ºC is seen at the head level and a bit higher of about 24.8ºC at the foot level, which prevents the occupants from thermal discomfort (Tian et al., 2011).The worst performance is noticed by the jet slot diffuser where the flow jet instead of diffusing on the horizontal plane moves upward, that raises the temperature >25ºC in the entire breathing zone. It may be due to the weak momentum forces and low entrainment induced by this type of diffuser.

For further investigations, the jet throw and temperature decay were also determined along the centerline drawn from the mid of the terminal face in horizontal direction as presented in Figure 7.11 (a) and (b). For the double deflection grille, bar grille and drum lover diffuser, the jet of air decayed gradually along the flow direction. At 4m distance from the supply face, the terminal velocity of 0.72m/s, 0.3m/s and 0.24m/s were recorded in the cases with double deflection, drum louver and bar grille diffusers, respectively. Among all, the airflow velocity of the case with jet slot diffuser decayed most steadily, with only 3 m from the diffuser, the jet of the air was almost vanished.

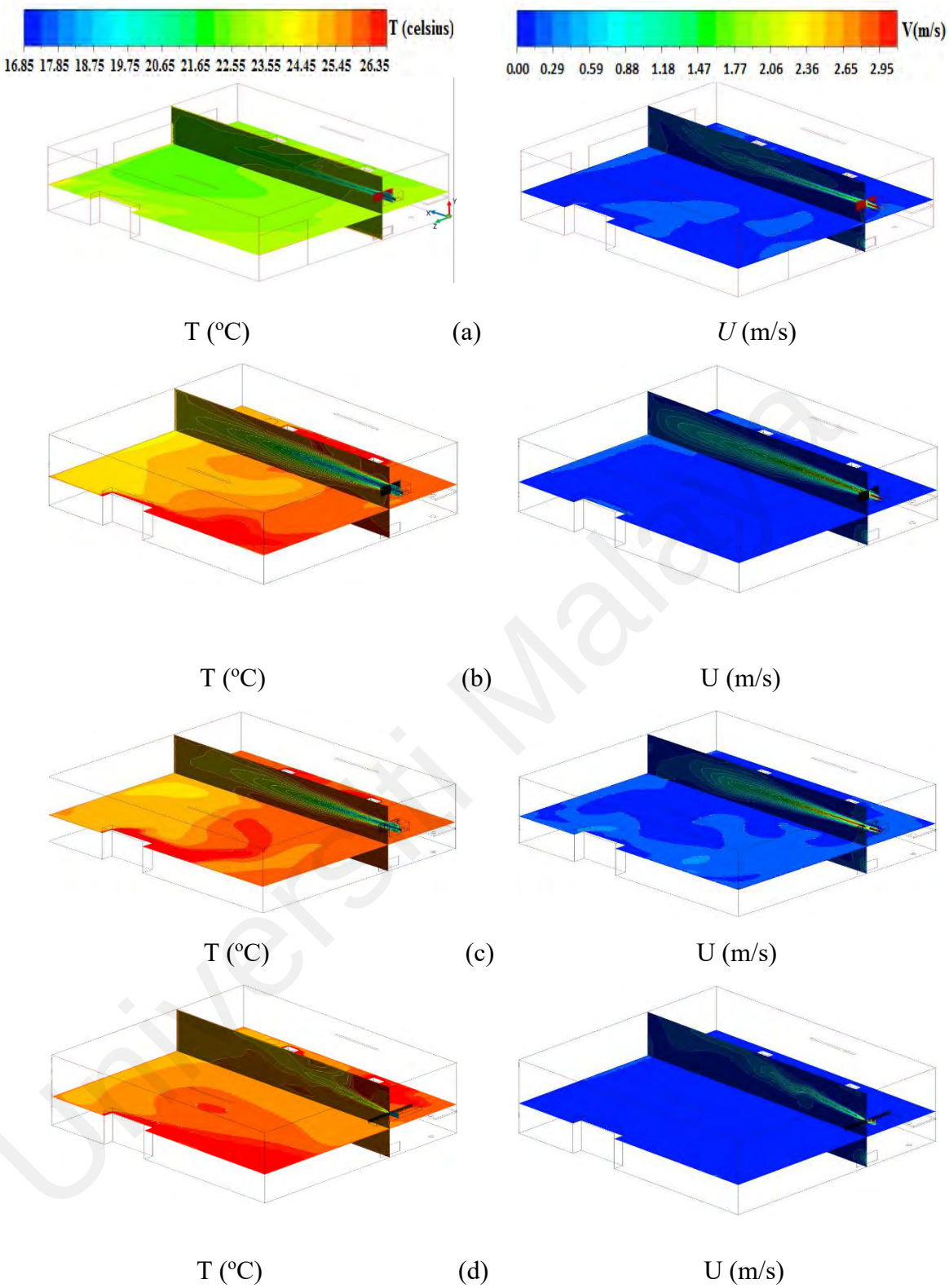

Figure 7.10: Temperature and velocity distributions at Y=1.5m (horizontal plane) and Z=1.75m (vertical plane) for (a) BG(b) DDG, (c) DLD, and (d) JSD

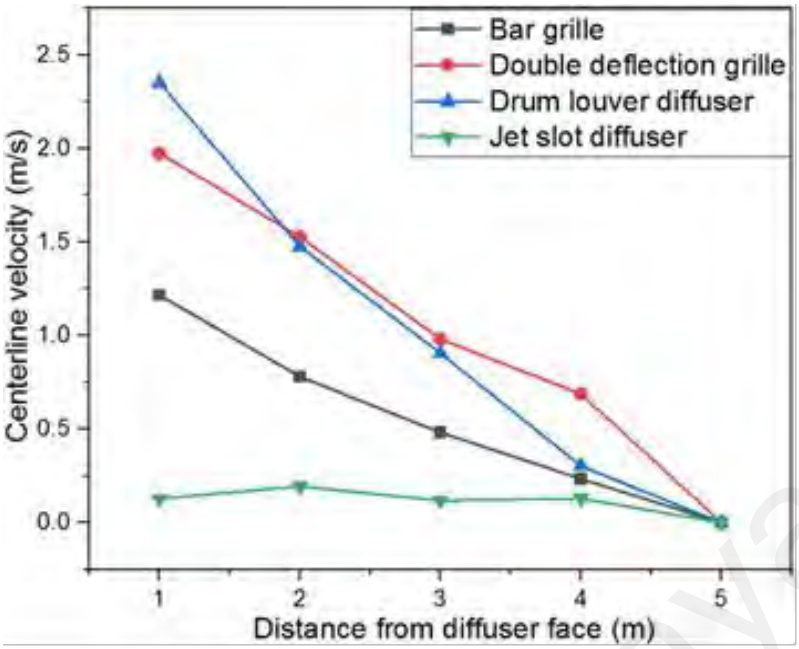

(a)

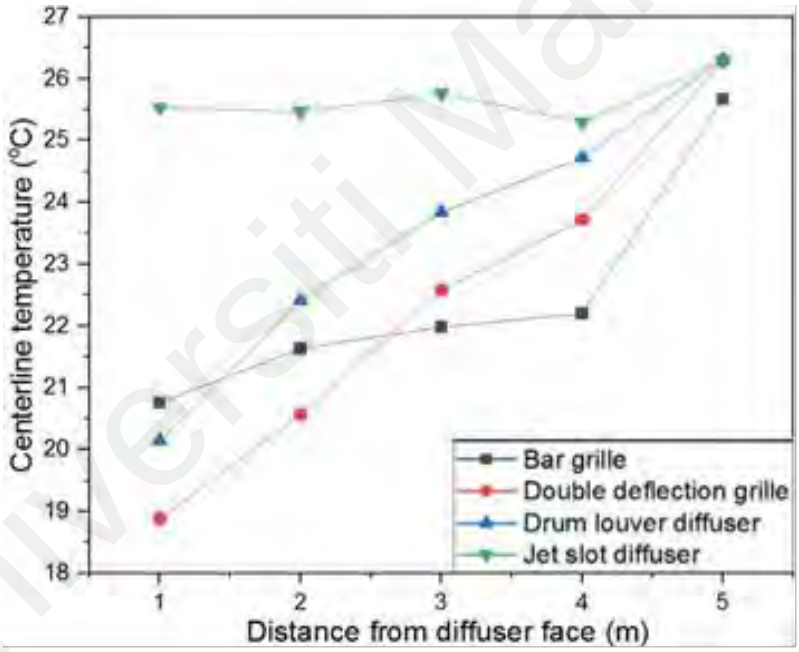

(b)

Figure 7.11: (a) Airflow throw and (b) Temperature decay predicted from different diffusers in the meeting room case

7.4.2.3 Effects of ASTDs on Indoor Thermal Comfort

The indoor thermal comfort evaluations for conditioned spaces are commonly investigated using the PMV and PPD indices. The PMV value represents the mean value of the votes of a bunch of people in the thermal environment on a seven scale points between 3(Hot) and -3(Cold). While the midst 0 represents the thermal neutrality.

Whereas, the PPD index measures the quantitative value of the human thermal sensation with their local environment. Because of the higher occupancy present, the thermal comfort provided by different ASTDs is compared only for the meeting room environment. Except for the case with the bar grille, as shown in Figure 7.12, the overall occupied zone in all other cases observed between -0.6 to 1.2 PMV scale. The bar grille has provided comparatively a better thermal comfort to the occupied zone with the PMV range between -0.6 to 0.6 scale, while most of the region falls under thermal neutrality.

According to the CR 1752 1998, the PPD for class C indoor thermal environment must not be greater than 25% (Fanger, 1970). Figure 7.12 shows the PPD values for all cases at plane B, in the case with bar grille the value was calculated about 23.8%, whereas for the double deflection grille, drum louver and jet slot diffusers the same was recorded at 90%, 33.2% and 30%, respectively. Overall, the human thermal comfort, as measured by the PPD index, is a direct reflection of the occupied zone temperature, i.e., a higher PPD value means the room environment is unsatisfactory, either it is too cool or too warm.

Even on the supply plane (plane B), the PPD values are less than 25% in most of the regions. Thus, it has satisfied the performance of the bar grille type ASTD in the densely occupied environment, i.e., the meeting room. Due to the strong air diffusion and entrainment by the double deflection grille and drum louver diffuser, the PPD index in the regions near the supply terminals found within 30% to 90% range, and thus not recommended for small to medium size applications.

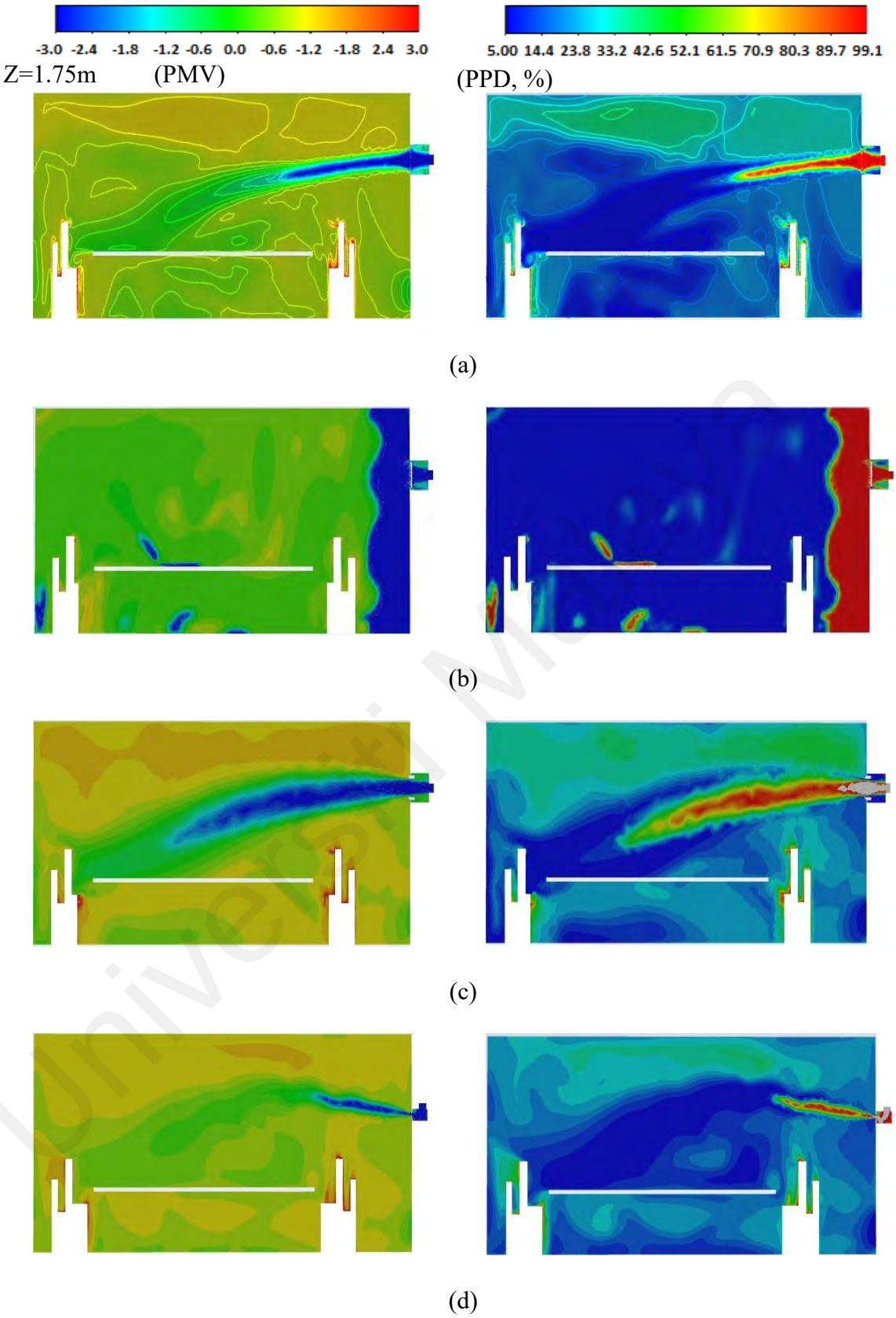

Figure 7.12: Thermal comfort evaluation in meeting room in the cases with (a) Bar grille (b) Double deflection grille (c) Drum louver diffuser and (d) Jet slot diffuser

7.4.2.4 Effects of ASTDs on IAQ

The local mean age of air and the concentration of CO_2 on given plane-A were investigated to evaluate the IAQ provided by different ASTDs (Figures 7.13 and 7.14). From Figure 7.13, the older air age was observed for the drum louver diffuser case, which was between 360s to 480s in the populated region of meeting room environment. This was mainly because of the improper and non-uniform air diffusion in the lower part (occupied region) of the room with this terminal type. The air age in the case with double deflection grille found between 60s and 180s within the entire sitting area, it may be due to the longest horizontal throw by this diffuser type. Moreover, in the case with bar grille, the entire sitting zone of the meeting room environment covered by the air age not more than 300s.

For simplicity of the analyses, only the CO_2 exhaled by the occupants is considered in the present research work. In terms of CO_2 concentration for all of the studied cases, a significant impact of the air terminal type is noticed as shown in Figure 7.14. The low CO_2 concentration of about (0.0012 - 0.0019) in terms of mass fraction of air is seen in the case with the bar grille, whereas the highest mass fraction of about (0.0015 - 0.0030) for CO_2 concentration on the entire plane A is observed with the drum louver diffuser case. This is because of the poorer air distribution in the occupied zone by drum louver diffuser.

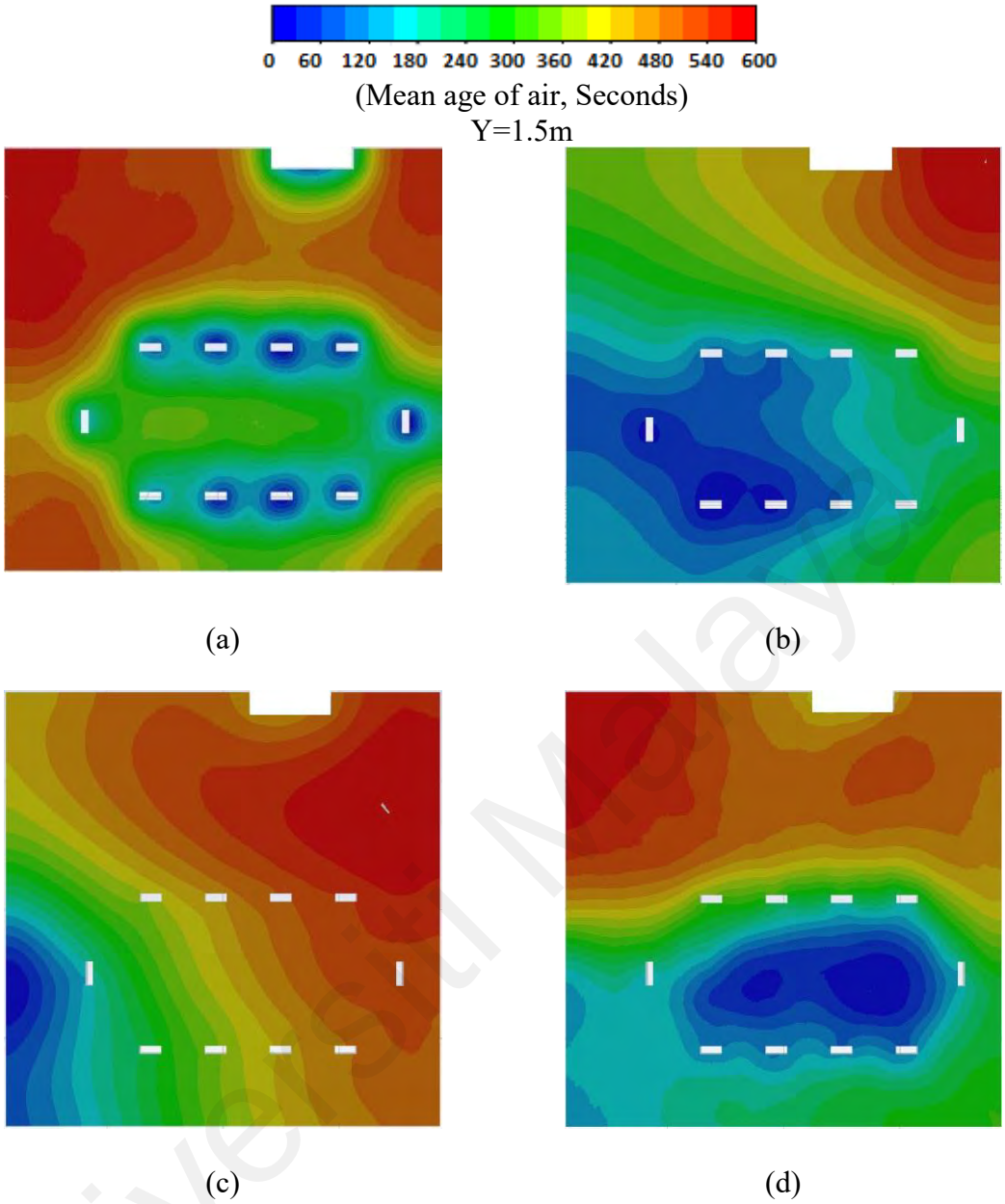

Figure 7.13: Mean age of air in the meeting room in the cases with (a) Bar grille (b) Double deflection grille (c) Drum louver diffuser and (d) Jet slot diffuser

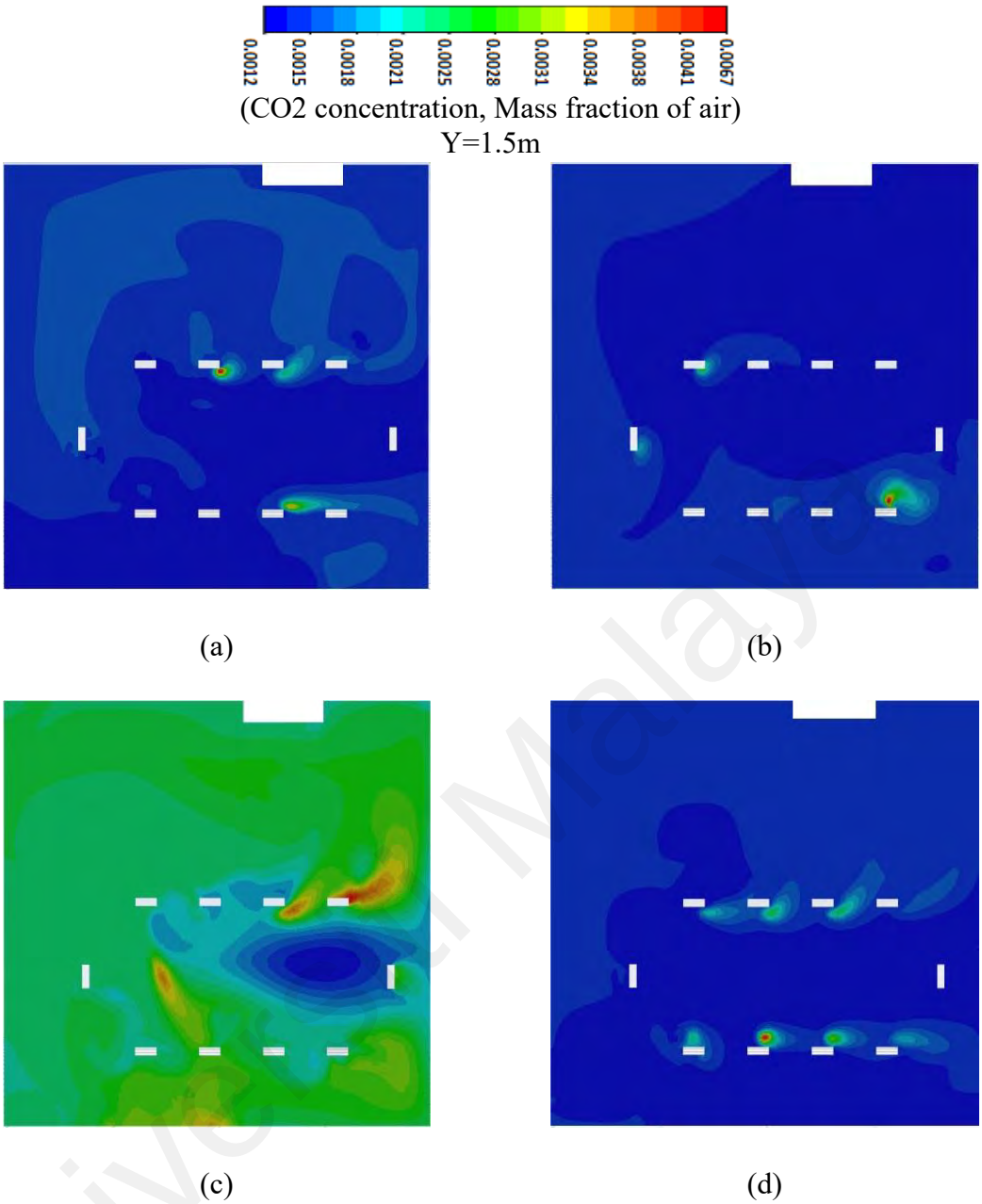

Figure 7.14: CO_2 concentration in the meeting room in the cases with (a) Bar grille (b) Double deflection grille (c) Drum louver diffuser and (d) Jet slot diffuser

7.5 Summary

This study compared the ventilation performance of four different types of supply air terminal devices under laboratory and meeting room environments. The air conditioning system used in this investigation to treat the outdoor air for mechanical ventilation is the novel system designed by combining the VRF system with the stratum ventilation system. The functional performance of the ASTDs was evaluated on three aspects: airflow distribution and pattern, thermal comfort and indoor air quality. It was

concluded that the ASTDs have considerable impact on the performance of mechanical ventilation system regardless of the indoor environment type. Based on all evaluation indices, the air diffusion performance using the bar grille terminal type was entirely within the acceptable range. Among all, the jet slot diffuser performed worst in providing thermal comfort for the occupant and airflow distribution into the space. Whereas, the drum louver diffuser performance was found poorer in terms of IAQ for the entire breathing zone. Under the similar initial and boundary conditions, the air age within the complete occupied zone in double deflection grille case was younger than that of all other diffuser types. However, the lowest CO2concentration in the breathing zone is obtained under the bar grille diffuser case. Above all, the VRF-SV system installed with the bar grille as ASTD can provide better thermal comfort, improved IAQ and uniform temperature and velocity distribution. Thus, the bar grille is recommended to be used in small-to-large size applications installed with VRF-SV system.

CHAPTER 8: NODAL AND ENERGY MODELLING OF THE VRF-SV HYBRID SYSTEM INSTALLED IN A BUILDING IN THE TROPICS

8.1 Introduction

Air-conditioning and mechanical ventilation (ACMV) systems are the major shareholders of the overall energy consumption in tropical buildings (Kwong, Adam, & Sahari, 2014). Several governments in East Asia have taken proactive measures by elevating the indoor temperature setting to cut off the energy needs of the ACMV systems (Z. Lin, Lee, et al., 2011). However, the energy-saving measures must not lead to scarifies in the comfort and health of the buildings' occupants. To cope with the recommended elevated indoor temperatures together with the compliance of the ASHRAE's thermal comfort standards, Yau and Umair (Y. H. Yau & Umair, 2022) proposed a novel ACMV system by integrating the variable refrigerant flow (VRF) system with the stratum ventilation (SV) air distribution system for tropical buildings. The hybrid system was designed using coupled, decoupled, and fully integrated approaches. The hybrid system was proposed as an energy-efficient substitute for the conventional central air conditioning systems in tropical buildings. It was designed with the following characteristics,

- Air at high temperature supplies directly into the breathing zone.
- The positive thermal gradient was set up with a modest airflow velocity (< 0.8 m/s) in the entire breathing zone.

Yau and Umair (Y. H. Yau & Rajput, 2022) numerically investigated the performance of the VRF-SV hybrid system in terms of indoor air quality and thermal comfort in a large retail facility in the tropics. The results revealed that the VRF-SV hybrid system could create a thermally comfortable environment in small to large size tropical buildings following a proper design strategy.

In a room installed with a VRF-SV hybrid system (please refer Figure 3.2 in Chapter 3), the outdoor air conditioned by the dedicated outdoor air system (DOAS) is delivered directly into the breathing zone of the room through air supply terminals located on the sidewalls of the room. Different settings have been configured for exiting the exhaust air in this system, such as exhaust from the ceiling or exhaust from sidewalls. When the supply air jet enters the occupied zone, particularly near the heat sources and occupants, some airflows upward due to buoyancy and the exhaust on the ceiling. It then blends with the updraft caused by convection due to heat transmitted through the building envelope. Finally, some rising airflow exit outside, while the rest is recirculated back and merges into the supply air jet. On the other hand, due to buoyancy and the human blockage, a portion of the cool supply air dips down in the occupied zone, resulting in heat exchange with the surrounding air. When the temperature of the downdraft is the same as the ambient air, it splits into two parts: one is entrained into the boundary layer near the outer wall as a wall-bounded flow, and the other recirculates back to be mixed with the supply airflow stream.

Moreover, the internal temperature distribution influences the performance of an air-conditioning system. Therefore, a good thermal gradient is desirable for indoor thermal comfort and energy efficiency. To provide a simplified temperature prediction model to the engineering practitioners, Huan et al. (Huan et al., 2018) developed a nodal model for stratum ventilation that can predict the vertical temperature profile and calculates the supply parameters and cooling loads quickly and conveniently.

Research on the VRF integrated mechanical ventilation systems focuses mainly on control optimization (Laughman et al., 2018; Lee et al., 2017) and performance evaluation of the combined system (Electric, 2018; Zhao et al., 2017). Very few studies have been reported analyzing the energy consumption of the integrated system in

buildings. Jiang et al. (Jiang et al., 2013) compared desiccant-assisted VRF to HR-based VRF and standalone VRF systems. Simulations demonstrate that, while desiccant-assisted VRF systems consume slightly more energy than standalone VRF systems in certain climates, they can save a significant amount of energy (almost 20% less) than HR-VRF systems. To the best of the author's knowledge, no study has been found analyzing the energy characteristics of the VRF and ventilation combined system when installed with stratum ventilation air distribution.

Therefore, this study was designed following two objectives. The first objective was to develop the simplified nodal model of the VRF integrated stratum ventilation system when installed in a large retail shop in the tropics. The second objective was to develop the TRNSYS simulation model of the VRF-SV hybrid system and compare the annual energy consumption of the fully integrated and decoupled design configurations with multi-split AC systems and standalone VRF system.

8.2 Building Description and ACMV System Types

Partly illustrated in Figure 8.1, a retail shop facility with 345.95m^2 covered area and 2.74m height is considered a case study building in this study. It comprises 30% of the ground floor of a 13-story virtual office building in Petaling Jaya, Kuala Lumpur, Malaysia. Based on the key features of the building, the thermal parameters of the building envelope, heat gains, and internal loads for ACMV systems are shown in Table 8.1. The sensible cooling load calculated is 21.16 kW, and the latent cooling load is 3.28 kW for the retail shop building. The indoor space condition is set to 55% RH and 24°C DBT. The outdoor design conditions were selected as 35 °C DBT and 27.7 °C WBT. The retail shop is operated for 10 hours from 10:00 am until 08:00 pm on weekdays.

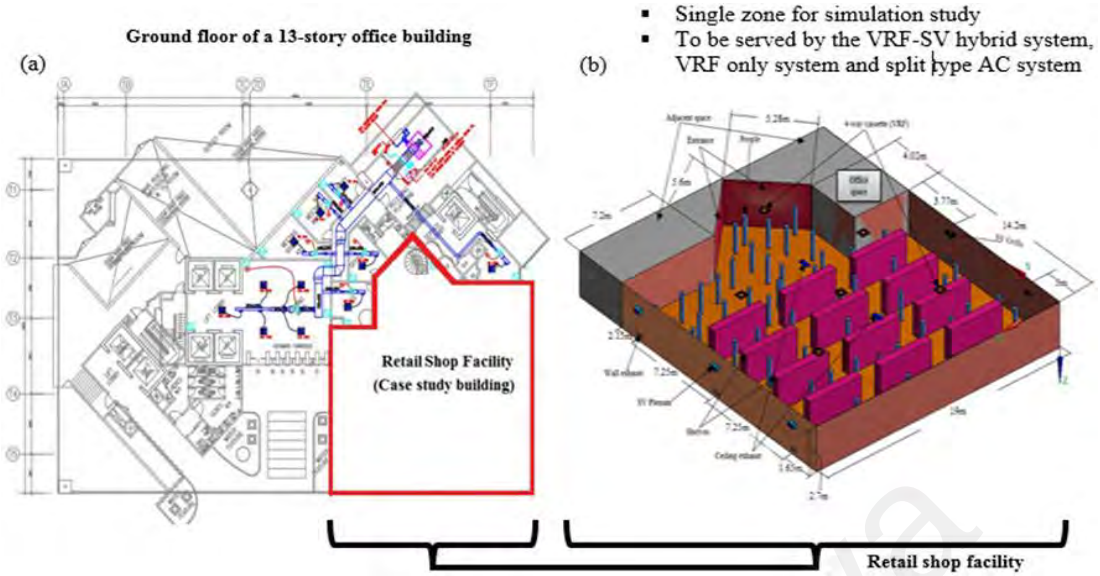

(a) (b)

Figure 8.1: (a) Overview of the ground floor of a virtual office building (b) description of the simulation model geometry (right)

Table 8.1: Heat gains and internal load

Item	Area (m^2)		U-value	
Exterior wall-a	52.06		0.54 W/m^2.K	
Exterior wall-b	38.90		0.54 W/m^2.K	
Exterior wall-c	19.73		0.54 W/m^2.K	
Exterior wall-d	49.86		0.54 W/m^2.K	
Roof	345.97		0.38 W/m^2.K	
Floor	345.97		2.89 W/m^2.K	
Exterior windows	0.099		1.48 W/m^2.K SC = 0.61	
Glass doors	13.2		0.71 W/m^2.K	
Item	Parameter			
Lighting load	34 W/m^2			
	CLF		Ballast multiplier	
	1		1	
Equipment load	17.8W/m^2			
	Desktops	Monitors	Laptops	Refrigerators
	0.13kW	0.14kW	0.165kW	5.74kW
Occupancy (maximum)	56 Persons 73.2 W/person (sensible) and 58.6 W/person (latent)			

It should be noted that different ACMV systems were designed and installed in the retail shop facility for energy consumption analyses. To simplify the energy modeling and to make the studies comparable, all the cooling systems were designed as standalone. The analyses were performed for the following four air conditioning systems.

8.2.1 Multi-split Type AC System (Baseline System)

A split-type AC system serves the entire retail shop space with no aid of outdoor air for ventilation. This system is used to keep the indoor temperature at 24 ^{o}C degrees. The outdoor unit of this system is mounted on the building's roof and is connected to many internal units, each with a 2.5 HP capacity. The retail business was outfitted with 13 indoor units to handle the entire space's thermal load. These indoor units have a ceiling cassette type. In this AC system, no outside air is brought into the targeted room for ventilation. Furthermore, this system is expected to run at full capacity at all times from 10 am until 8 pm on weekdays throughout the year.

8.2.2 VRF System (No Ventilation)

The baseline AC system was then compared to the standalone VRF system. To match the horsepower of the baseline system, a VRF system of 32 HP was chosen. In addition, the VRF system is expected to operate at the same time as that of the multi-split system and to be fully operational at all times of the day throughout the year. The VRF system is expected to be installed the same way as the baseline system, with the outdoor unit located on the rooftop and no outdoor air for ventilation.

8.2.3 VRF-SV Hybrid System (Decoupled Design)

In this design, the VRF and stratum ventilation systems are integrated to achieve their tasks separately (as seen in Figure 3.2 in Chapter 3). The VRF indoor terminal unit caters to the sensible load, whereas the DOAS unit treats the OA. The fully conditioned

air is then supplied into the space through a stratum ventilation air distribution system using grilles or diffusers to attain the latent load. A 24HP VRF system was used in this AC system for attaining the sensible load not met by the SV system. For further details about the design and the working principle of this system please refer to Chapter 3 of this thesis.

8.2.4 VRF-SV Hybrid System (Fully Integrated Design)

A new method of integrating the VRF system with a stratum ventilation system to supply fully conditioned air directly into the space through the SV air distribution strategy. The conditioned air at elevated temperature is provided to cater to the complete load of the room. No separate VRF indoor terminal is required in this design method. This design approach reduces the overall system capacity and overcomes the large installation space requirement by the ACMV systems in tropical countries like Malaysia and Singapore. The complete design details of this system can be found in Chapter 3 of this thesis.

8.3 Research Methodology

The methodology of this study is divided into two parts; the first part discusses the nodal model structure and development. The configuration 5 and configuration 6 of the VRF-SV fully integrated design are considered in this study for nodal model development and validation. For details of both configurations please refer chapter 3 of this thesis. In the second part of the research methodology, the TRNSYS simulation models are developed and modified based on different AC systems used. The bin weather data (bin method) is used in the simulation instead of typical mean year (TMY) data since the former presents a more accurate representation of the weather data.

8.3.1 Simplified Nodal Modelling

The structure and principle of the models and the parameters involved are discussed here in the following subsections for each configuration.

8.3.1.1 Description of the Huan's Model (Reference Study)

A typical characteristic of stratum ventilation is that the vertical temperature profile is sandwiched distributed in the room. The lowest temperature in the breathing zone (0.5m–1.7m) and relatively higher temperatures in the lower and upper zone (W. Zhang, Hiyama, Kato, & Ishida, 2013). Thus, for stratum ventilation, the air temperatures in the breathing and lower and upper zones are critical factors of the vertical temperature profile.

This model is based on the following assumptions: (1) The temperature of the inner surfaces of the room enclosures is uniform;(2) the temperature gradients between the breathing zone and the near-floor zone and between the breathing zone and the near-ceiling zone are linear respectively; (3) the updrafts induced by the temperature difference between the interior partition surfaces and room air are negligible; and (4) the ratio of convective and radiant heat gains from internal heat sources is half to half (i.e., 50%convection and 50% radiation).

(a) ***Initial airflow division***

The distribution of the temperature nodes in a typical office environment with exhaust at the ceiling is shown in Figure 8.2(a). Based on Huan's model, the sketch diagram of the auxiliary temperature nodes and energy balances is shown in Figure 8.2 (b). The initial airflow can be described as the fraction of supply air ($F_{ln} - m_{s)}$ that goes directly to the near-floor zone, and the remaining part $(1 - F_{ln}).m_s$ goes towards the core zone of the room, where the core temperature is T_n. Then the fraction of the inflow that comes to the near-floor zone ($F_{ln} - m_{s)}$ circulates back to the core zone of the

room. Then the combined air moves upward toward the exhaust grill at T_{ex}. With the help of the moderate convective flows from the heated sources (people, equipment, and lighting). In this case, the air in the upper zone moves rather by natural convective sources than by strong momentum flows. As a result, the vertical air temperature gradient is developed from the temperature near the floor that is cooled by the fraction of the supply air (80%).

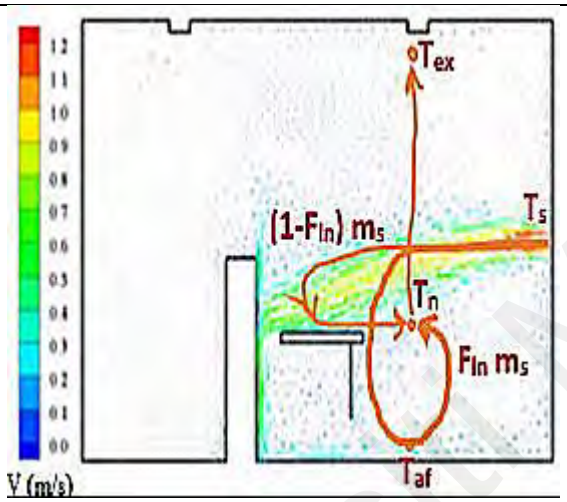

m_s	Supply airflow rate (m^3/s)
m_j	Airflow rate of the recirculating air generated by the entrainment of the supply airflow (m^3/s) $m_j = 0.32\ (x/d_0)m_s$ x = Distance from the air jet to the air terminal (m) d_0 = Hydraulic diameter of the air terminal (m)
F_{ln}	Fraction of the cooling energy from supply air mixes into the near-floor zone. F_{ln} = 0.8

(a)

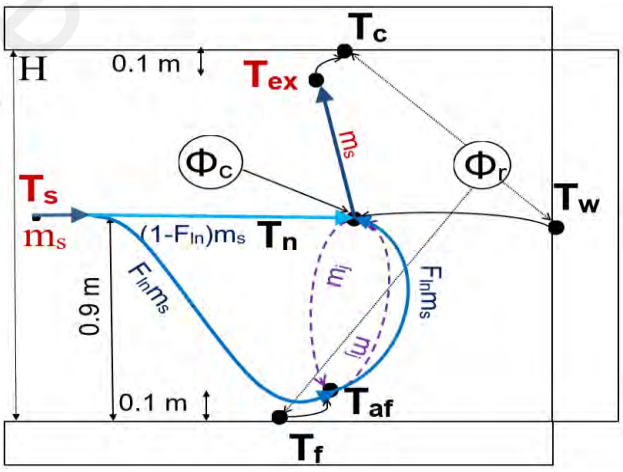

(b)

Figure 8.2: (a) Distribution of the temperature nodes in a typical office environment with exhaust at the ceiling (b) Sketch diagram based on Huan's model

8.3.1.2 Modified Huan's Model for Ceiling Exhaust Configuration

In this modified Huan model, the initial airflow division is the same as in the reference model. As shown in Figure 8.3(a), the fraction ($F_{ln}.m_{s)}$ is going to the near-floor area, and the remaining part $(1 - F_{ln}).m_s$ towards the core zone of the room where the temperature is T_n. Then the fraction of the inflow air comes to the near-floor zone ($F_{ln}.m_{s)}$ is lifted by the strong convective flows from the heat sources up to the ceiling exhaust level T_{ex}. Then this flow circulates to the core zone of the room at T_n.

In this air-distribution case, the temperature near the floor T_{af} is not cooled by the supply air. That's why it is estimated to be the same floor temperature. This case is characterized by high momentum flows (A_r = 4.103, which is 10 times lower than in Huan's measurements) and high internal heat gains. It causes intensive up flowed air towards the ceiling. Since the ceiling height is comparatively low (2.7 m), the flows return down to the core zone of the room. In this case, the temperature near the floor T_{af} is not cooled by the supply air due to the numerous obstacles and strong upward air flows that omit the zone near the floor. That's why the temperature T_{af} is estimated to be the same as the floor temperature T_f. In this case, the temperature gradient is developed from the core zone of the room. Since the room air is well-mixed, the air temperature can be estimated to be the same upper the floor zone (from 0.5m height) to the near-ceiling zone at the height (H-0.1) m.

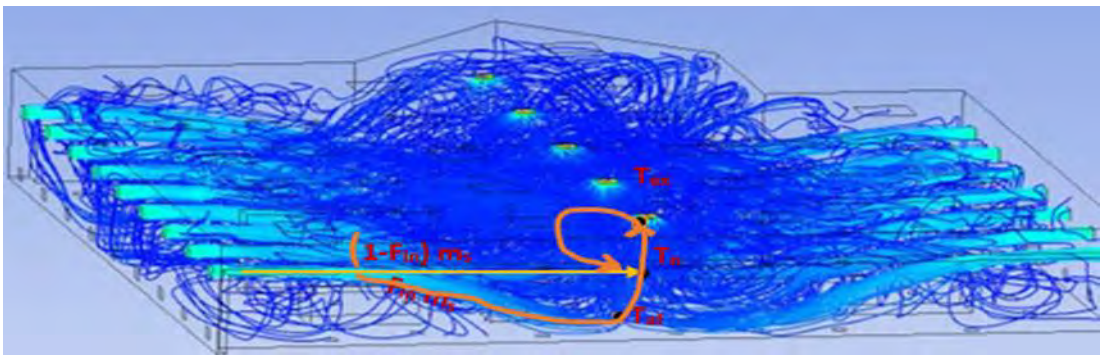

(a)

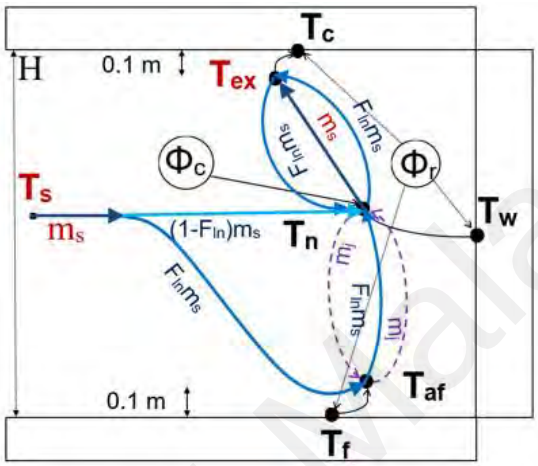

(b)

Figure 8.3: (a) Distribution of the airflow streamlines in the retail shop model in ceiling exhaust configuration (b) Nodal model diagram based on Huan's model

(a) ***Mathematical Description of the Model***

The detailed descriptions of the energy equation established in this model to describe the energy transfer process are presented here as follows,

The general convective heat balance for the room air can be expressed as,

$$\phi_c = m_s C_p (T_{ex} - T_s) \tag{8.1}$$

The energy conservation near-floor zone (at the height of 0.1m from the floor) can be illustrated by Equation (8.2),

$$A_f \alpha_{c,f} (T_f - T_{af}) + m_j C_p (T_n - T_{af}) - F_{ln} m_s C_p (T_n - T_{af}) + F_{ln} m_s C_p (T_s - T_{af}) = 0 \tag{8.2}$$

The energy balance at the core zone of the room (at the height of 0.9m) can be expressed as in Equation (8.3),

$$A_w\alpha_{c,w}(T_w - T_n) + m_j C_p(T_{af} - T_n) - F_{ln}m_s C_p(T_s - T_n) + m_s C_p(T_s - T_n) + F_{ln}m_s C_p(T_{ex} - T_n) + \phi_c = 0 \quad (8.3)$$

The energy conservation equation of the near–ceiling zone (at the height of 2.6m from the floor) can be expressed as,

$$\alpha_{c,c}A_c(T_c - T_{ex}) + m_s C_p(T_n - T_{ex}) + F_{ln}m_s C_p(T_n - T_{ex}) = 0 \quad (8.4)$$

The energy balance at the surfaces can be expressed by the equations (8.5), (8.6), and (8.7),

The energy balance on the floor,

$$\alpha_{c,f}(T_f - T_n) + \alpha_{r,f}(T_f(F_{f-w} + F_{f-c}) - (F_{f-w}T_w + F_{f-c}T_c) = \frac{\phi_r}{A_t} \quad (8.5)$$

The energy balance at the walls,

$$\alpha_{c,w}(T_w - T_n) + \alpha_{r,w}(T_w(F_{w-f} + F_{w-c}) - (F_{w-f}T_f + F_{w-c}T_c) = \frac{\phi_r}{A_t} \quad (8.6)$$

The energy balance at the ceiling,

$$\alpha_{c,c}(T_c - T_{ex}) + \alpha_{r,c}(T_c(F_{c-f} + F_{c-w}) - (F_{c-f}T_f + F_{c-w}T_w) = \frac{\phi_r}{A_t} \quad (8.7)$$

8.3.1.3 Modified Huan's Model for Wall Exhaust Configuration

In this modified Huan model, the initial airflow division is the same as in the reference model. As shown in Figure 8.4(a), the fraction $F_{ln}.m_s$ is going to the near-floor area, and the remaining part $(1 - F_{ln}).m_s$ towards the core zone of the room T_n. Then the fraction of the inflow air after coming to the near-floor zone $m_s.F_{ln}$ circulates to the core zone of the room T_n forming a mixing vortex of the room air. The air near the floor is mix with the air in the core zone of the room, so $T_{af} = T_n$. The exhaust temperature T_{ex} is placed under the supply air terminals in this air-distribution case. The

presented model calculates this temperature, but it does not include T_{ex} in the vertical temperature gradient structure. The air is evenly mixed in the case of low exhaust and relatively high momentum ($A_r = 4.10^3$). Thus, the temperature gradient is not developed in this case, and only one temperature is enough to calculate.

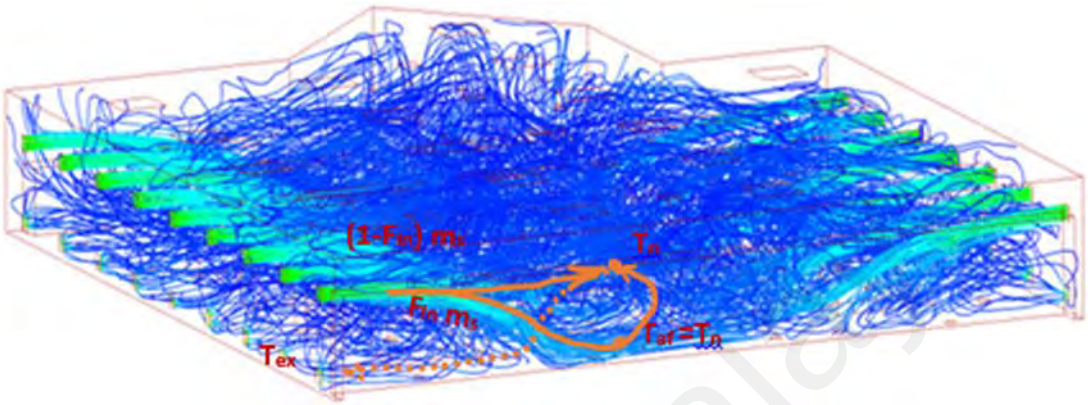

(a)

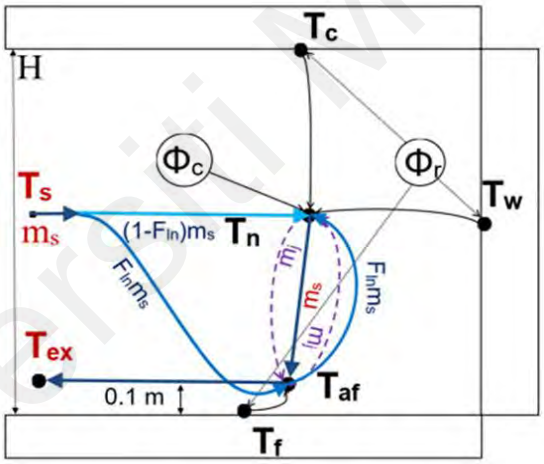

(b)

Figure 8.4: (a) Distribution of the airflow streamlines in the retail shop model in wall exhaust configuration (b) Nodal model diagram based on Huan's model

(a) ***Mathematical Description of the Model***

The detailed descriptions of the energy equation established in this model to describe the energy transfer process are presented here as follows,

The general convective heat balance for the room air can be expressed as,

$$\phi_c = m_s C_p (T_{ex} - T_s) \qquad (8.8)$$

The energy conservation near-floor zone (at the height of 0.1m from the floor) can be illustrated by Equation (8.9),

$$A_f\alpha_{c,f}(T_f - T_{af}) + m_j C_p(T_n - T_{af}) - F_{ln}m_s C_p(T_n - T_{af}) + F_{ln}m_s C_p(T_s - T_{af}) + m_s C_p(T_n - T_{af} = 0 \quad (8.9)$$

The energy balance of the room air (at the heights from 0.1 m to (H-0.1) m) in Eq. (8.10),

$$\alpha_{c,c}A_c(T_c - T_{ex}) + A_w\alpha_{c,w}(T_w - T_n) + m_j C_p(T_{ex} - T_n) - F_{ln}m_s C_p(T_s - T_n) + m_s C_p(T_s - T_n) + \phi_c = 0 \quad (8.10)$$

The energy conservation equation of the exhaust air can be expressed as,

$$A_f\alpha_{c,f}(T_f - T_{af}) + m_j C_p(T_n - T_{ex}) - F_{ln}m_s C_p(T_n - T_{ex}) + F_{ln}m_s C_p(T_s - T_{ex}) + m_s C_p(T_n - T_{ex}) = 0 \quad (8.11)$$

The energy balance at the surfaces can be expressed by the equations (8.12), (8.13), and (8.14),

The energy balance on the floor,

$$\alpha_{c,f}(T_f - T_{ex}) + \alpha_{r,f}(T_f(F_{f-w} + F_{f-c}) - (F_{f-w}T_w + F_{f-c}T_c) = \frac{\phi_r}{A_t} \quad (8.12)$$

The energy balance at the walls,

$$\alpha_{c,w}(T_w - T_n) + \alpha_{r,w}(T_w(F_{w-f} + F_{w-c}) - (F_{w-f}T_f + F_{w-c}T_c) = \frac{\phi_r}{A_t} \quad (8.13)$$

The energy balance at the ceiling,

$$\alpha_{c,c}(T_c - T_n) + \alpha_{r,c}(T_c(F_{c-f} + F_{c-w}) - (F_{c-f}T_f + F_{c-w}T_w) = \frac{\phi_r}{A_t} \quad (8.14)$$

The variables used in the equations mentioned above are expressed as follows,

ϕ_r= Radiative component of total heat gains (W)

ϕ_c= Convective component of total heat gains (W)

A_t= Total area of the room surfaces (m^2)

T_f= Area-weighted mean temperature of the floor surface (°C)

T_w= Area-weighted mean inner surface temperature of the walls (°C)

T_n= Area-weighted mean temperature of the core zone (°C)

T_c= Area-weighted mean temperature of the ceiling surface (°C)

A_f= Floor area (m^2)

$\alpha_{r,f}$= Radiant heat transfer coefficient of the floor (W/ (m^2K))

F_{f-w}= Radiation view factor between the floor and the walls

F_{f-c}= Radiation view factor between the floor and the ceiling

A_w= area of the walls (m^2)

$\alpha_{r,w}$= Radiant heat transfer coefficient of the walls (W/ (m^2K))

F_{w-f}= Radiation view factor between the walls and the floor

F_{w-c}= Radiation view factor between the walls and the ceiling

A_c= Ceiling area (m^2)

$\alpha_{r,c}$= Radiant heat transfer coefficient of the ceiling (W/ (m^2K))

F_{c-f}= Radiation view factor between the ceiling and the floor

F_{c-w}= Radiation view factor between the ceiling and the walls

8.3.2 TRNSYS Simulation Modelling

In this research part, the TRNSYS simulation tool was used for hour-by-hour system performance simulation. This tool is well known for analyzing hourly energy use by the ACMV systems installed in buildings. To simulate the above presented ACMV systems in a case study building, i.e., Retail shop, operating performance data for each ACMV system (obtained from the manufacturer) was used in the TRNSYS simulation program. The discussion on the performance data is presented in subsequent sections.

8.3.2.1 Bin Weather Data

Since the bin method provides more accurate forecasting of the weather data, this study utilized this method instead of typical mean year (TMY) weather data. This data is intended to be employed in the developed TRNSYS models for simplified energy calculations. For the sake of this study, the bin weather data (dry bulb temperature and relative humidity) for Petaling Jaya, Malaysia, from 2007 to 2016 was obtained from Yau et al., (2020). The bin basket data for the dry bulb temperature is shown in Figure 8.5. For readers' understanding, the detailed hourly bin dry bulb temperature and relative humidity values for the Petaling Jaya are presented in Table C.1 and C.2 in Appendix C of this thesis.

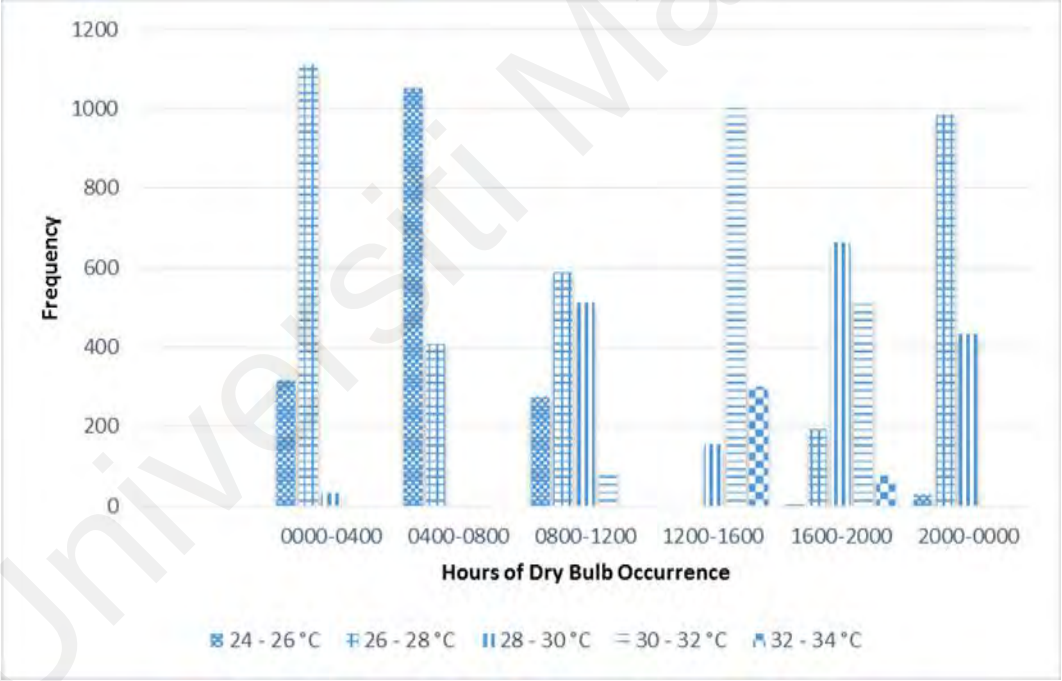

Figure 8.5: Bin basket data of Petaling Jaya, Kuala Lumpur for the dry bulb temperature

8.3.2.2 Description of the Developed TRNSYS Models

Based on the ACMV systems mentioned above, different simulation models were developed in the TRNSYS simulation studio to compare their annual energy consumption when installed in the case study building. Details of the developed models are presented in Table 8.2.

Table 8.2: Details of the developed models

Model Type	**ACMV System Type**	**System Task**
Baseline model	Multi-split type AC system	Multi-split system (sensible cooling) AHU (OA ventilation)
Modified model-1	VRF system	VRF system (sensible cooling) AHU (OA ventilation)
Modified model-2	VRF-SV hybrid system (Decoupled design)	SV system (OA ventilation + sensible) VRF system (Remaining sensible)
Modified model-3	VRF-SV hybrid system (Fully-integrated design)	Total cooling load catered by the combined system

(a) ***Baseline Simulation Model***

To simulate the split type AC system (baseline system) in case study building using TRNSYS simulation studio, all the components and types must be defined in the studio. The modular type flexible nature of the TRNSYS software allows the creation of non-standard components to be added to the TRNSYS Library and represented in the simulation model.

Thirteen units of split type AC system with 2.5HP each serve the entire retail shop facility with no outdoor air for ventilation. This system is assumed to be operated at full capacity. The configuration of the indoor units of this system is ceiling cassette type. This system works on the direct expansion principle, maintaining the indoor temperature at 24ºC.

If the power input and cooling capacity of the AC system installed in the building is known, the COP of that system at various outdoor temperatures can be calculated. In this study, the bin temperature acts as the outdoor temperature. The linear equations for cooling capacity and power input are developed considering the bin temperature as a function of both. The developed equations based on the performance data (as shown in

Table E.1 in appendix E) obtained from the manufacturer of this system are shown in Table 8.3. Based on the operating performance data, the performance curve for the multi-split type AC system is shown in Figure 8.6.

Table 8.3: Linear functional equations of split type unit system

Operating Performance	Linear Function (kW)
Cooling Capacity	$13[9.435 - 0.061(T_{bin})]$
Power Input	$13[1.21 + 0.038(T_{bin})]$

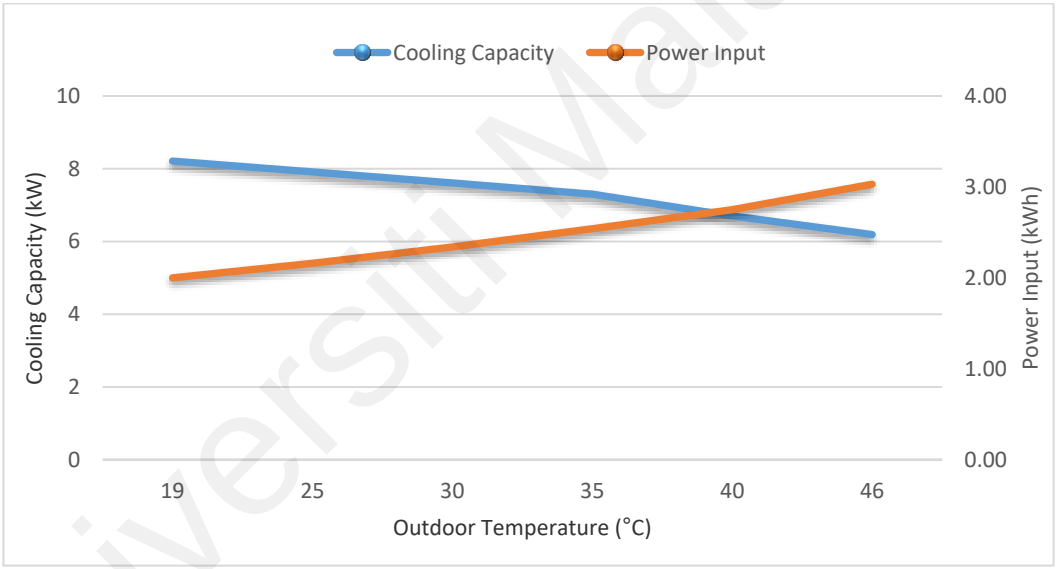

Figure 8.6: Performance curve of multi-split type unit system

The TRNSYS model of the baseline simulation when using a multi-split type AC system in the retail shop facility is shown in Figure 8.7. The process and function of each component used in the model are collectively summarized in Table D.1 in appendix D. It should be noted that the green-lined box in Figure 8.7 represents the simulation of the target building in occupied operating hours, whereas the red-lined box represents the simulation in unoccupied operating hours.

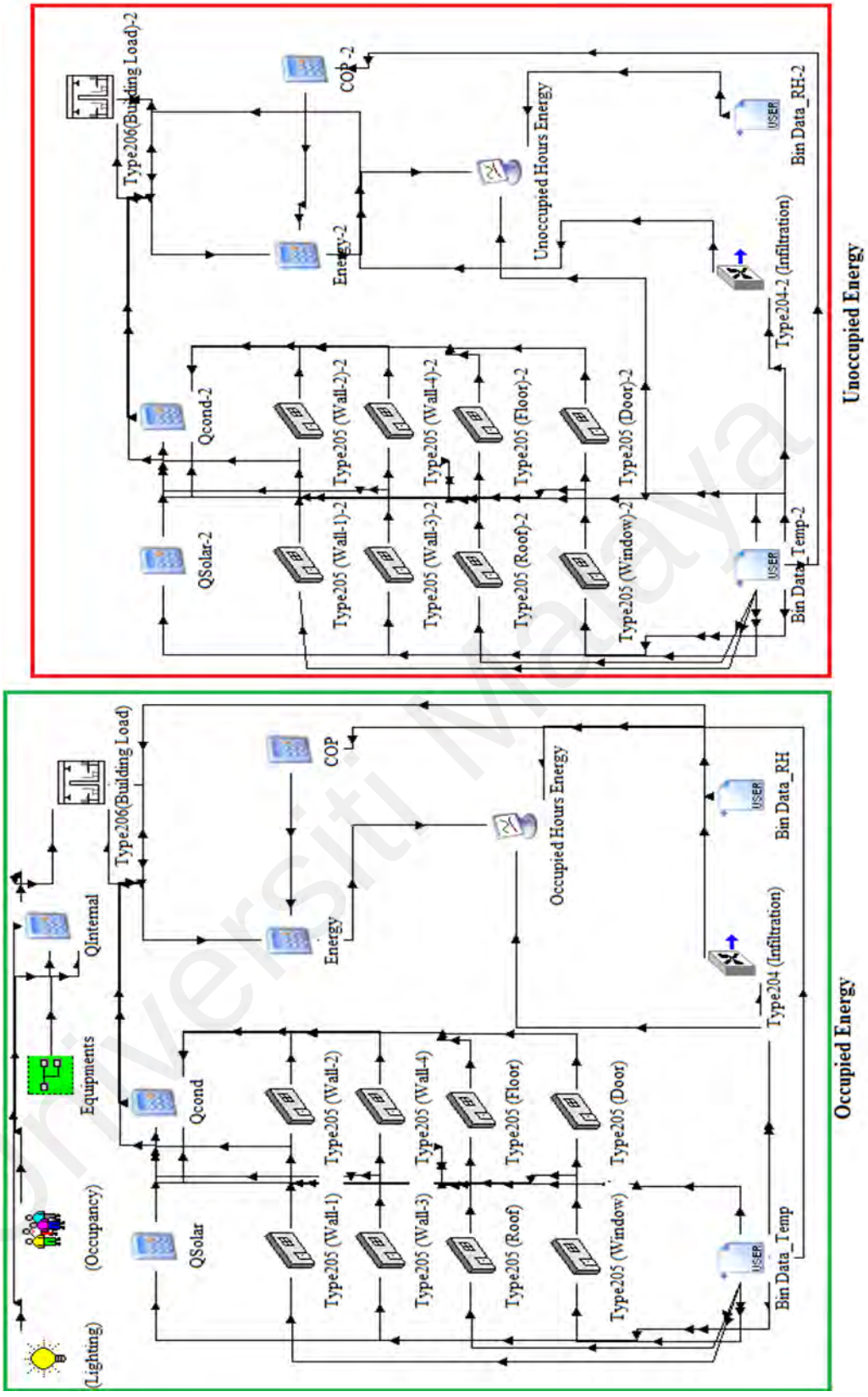

Figure 8.7: TRNSYS model of the baseline simulation

(b) ***Modified Model-1***

In this simulation model, a VRF system of 32HP is chosen to be compared with the baseline simulation, where this system's horsepower can match up with the split type AC system's horsepower. The configuration of the indoor units of this VRF system is ceiling cassette type. The installation of this system in this building is assumed to be the same as the split type AC system, where this system operates on the direct expansion principle, maintaining the indoor temperature at 24ºC. Furthermore, this system is expected to be fully operated at all times of the day throughout the entire year.

The procedure to obtain the linear functions of cooling capacity and power input of this system are the same as the split type AC system. The developed linear functional equations are shown in Table 8.4. The operating performance detail for this VRF system is shown in Table E.3 in appendix E. The operating performance curve based on the operating performance data of this system is shown in Figure 8.8.

Table 8.4: Linear functional equations of 32HP VRF system

Operating Performance	Linear Function (kW)
Cooling Capacity	[107.09 - 0.7388(T_{bin})]
Power Input	[19.727 + 0.4975(T_{bin})]

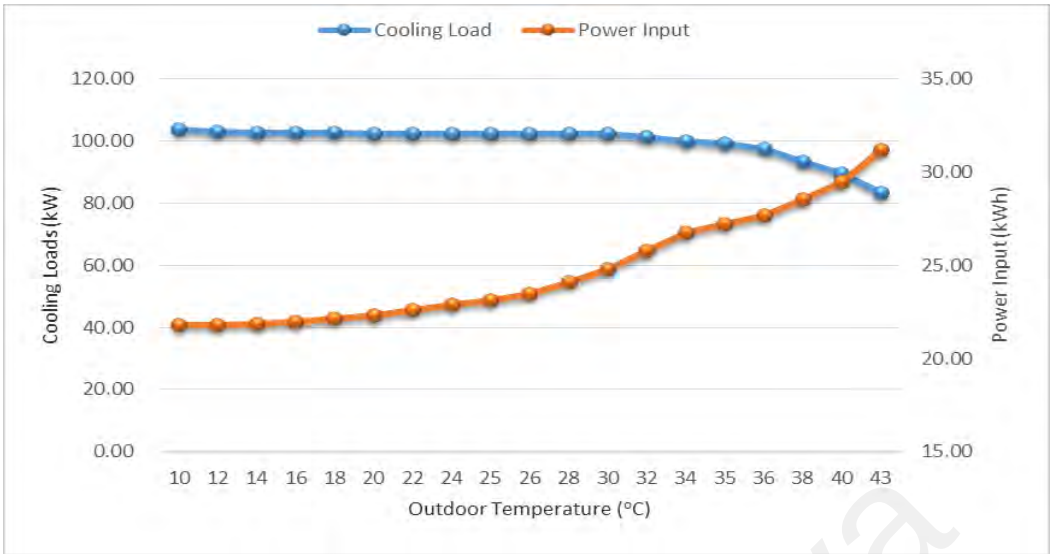

Figure 8.8: Performance curve of 32HP VRF system

The TRNSYS simulation layout of the modified model-1 when using the VRF system in the retail shop facility is shown in Figure 8.9. The process and function of each component used in this model are collectively summarized in modified model-3 section. Like the baseline simulation model, the green-lined box in Figure 8.9 represents the simulation in occupied operating hours and the red-lined box in unoccupied operating hours.

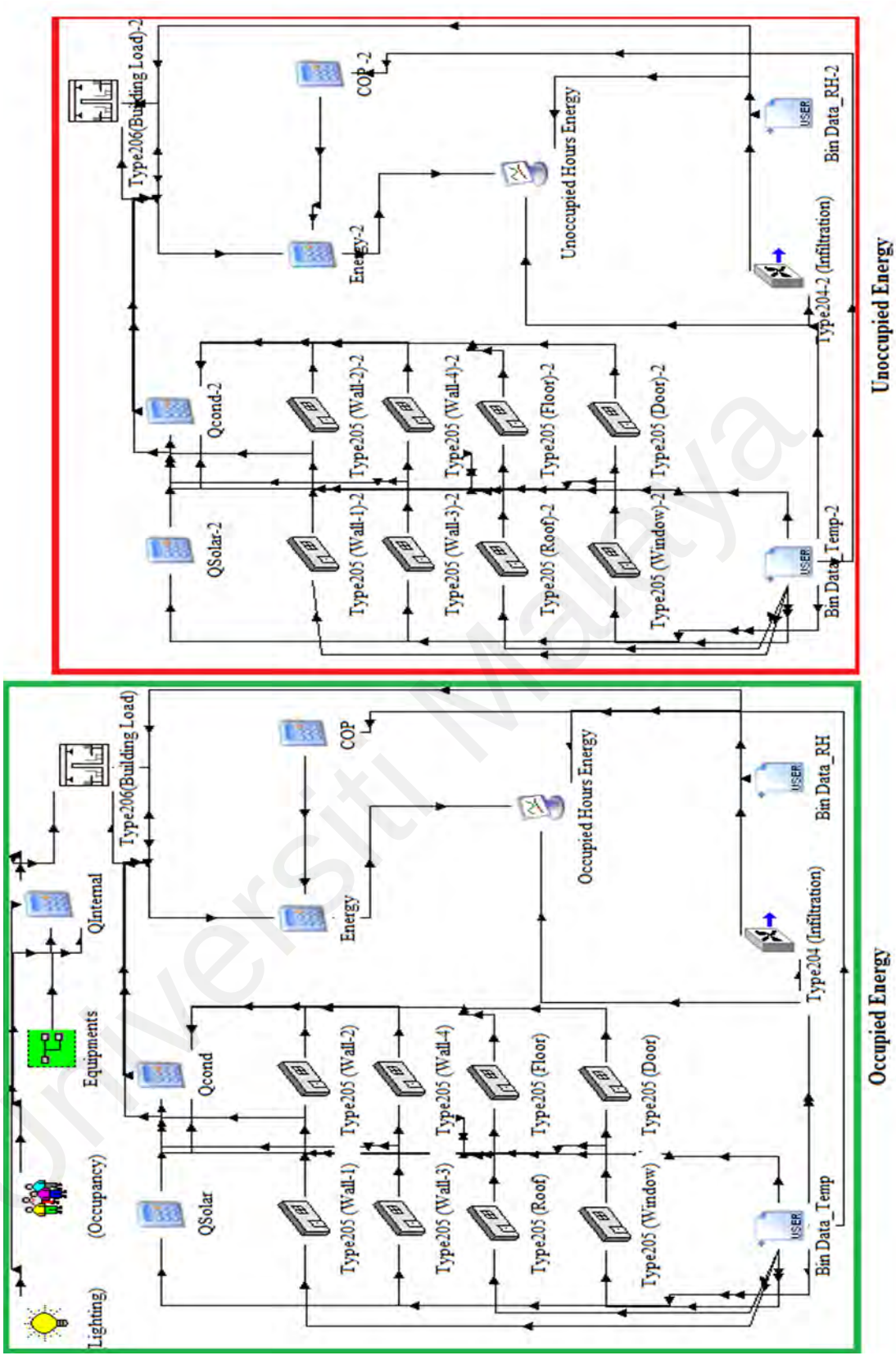

Figure 8.9: TRNSYS simulation layout of the modified model-1

(c) ***Modified Model-2***

This simulation model used a decoupled design of the VRF-SV hybrid system to compare the energy consumption with the baseline simulation model. A 24HP VRF system was used in this model to cater to the rest of the cooling load not met by the VRF DX coil operated DOAS system, in which OA is supplied to the target building through the SV air distribution system. The sufficient amount of air to be supplied through SV air distribution is initially approximated. The approximation is made by calculating the total airflow rate required to be supplied through diffusers for the uniform distribution of air into the target building. In this design, 5 bar grille diffusers were used, each requiring 297.2 cfm (0.14 m^3/s) of air to supply at a distance of 9.5 m with 2.5 m/s face velocity and 0.25 m/s terminal velocity. The total amount of supply air required was 1486 cfm (0.70 m^3/s). To fulfill this requirement, an extra amount of 867cfm (0.41m^3/s) of OA was added to the minimum ventilation load needed for the target building.

For the separate VRF system, the configuration of the indoor units used is the same as used in previous models. The installation of this hybrid system in this building is assumed to be the same as in the previous models, where the system operates to maintain the indoor temperature at 24ºC. Furthermore, this hybrid system is expected to be fully operated throughout the entire year at all times of the day.

The energy consumption of this hybrid system in the target building is calculated using the COPs of both of the systems separately.

The COP of the DOAS system is calculated using the following equations (Jani, Mishra, & Sahoo, 2018),

$$\mathrm{COP} = \frac{\mathrm{Q_{cc}}}{\mathrm{E_t}} \tag{8.15}$$

where Q_{cc} is the cooling capacity of the DX coil and E_t is the total energy consumption of the DOAS system.

The cooling capacity of the VRF DX coil is expressed by the equation,

$$Q_{cc} = \rho \times \dot{V}_{sa,t} (h_i - h_o) \quad (8.16)$$

where,

Q_{cc} = cooling coil capacity, kW

ρ = supply air density, kg/m^3

$\dot{V}_{sa,t}$ = supply air flowrate (total), m^3/s

h_i & h_o = supply air enthalpies across VRF DX coil, kJ/kg

The total energy consumption of the DOAS is calculated using the equation,

$$E_t = E_{comp} + E_{supply\ fan} + E_{return\ fan} + E_{other} \quad (8.17)$$

where,

E_t= total energy consumption, kW

E_{comp}= compressor energy consumption, kW

$E_{supply\ fan}$= supply fan energy consumption, kW

$E_{return\ fan}$= return fan energy consumption, kW

E_{other} = energy consumption by other equipment, such as driving motors of enthalpy and sensible wheels, kW

The procedure to obtain the linear functions of cooling capacity and power input of the decoupled VRF system to measure the system COP is the same as obtained earlier. The developed linear functional equations are shown in Table 8.5. The operating performance details for this VRF system is shown in Table E.3 in Appendix E. The

operating performance curve based on the operating performance data of this system is shown in Figure 8.10.

Table 8.5: Linear functional equations of 24HP VRF system

Operating Performance	Linear Function (kW)
Cooling Capacity	[79.723 - 0.55 (T_{bin})]
Power Input	[13.111 + 0.3306 (T_{bin})]

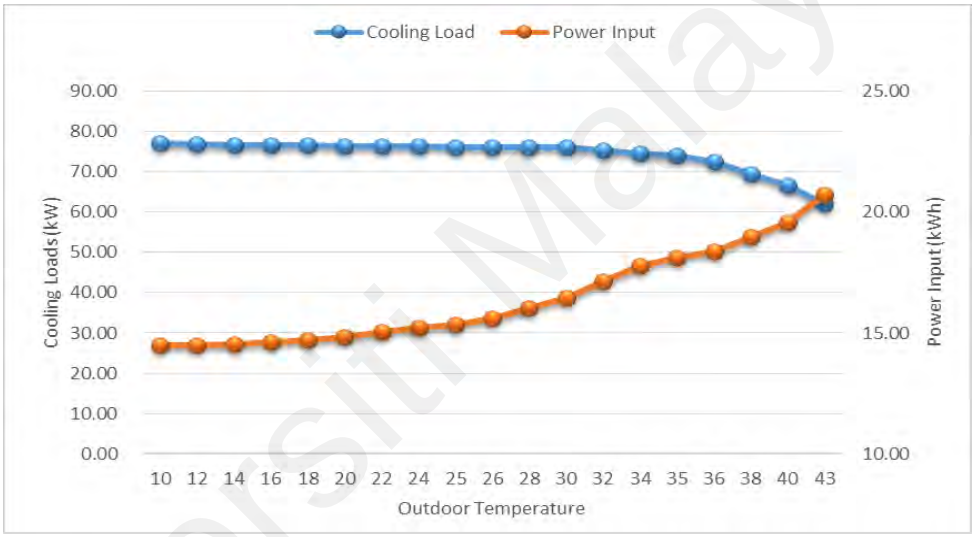

Figure 8.10: Performance curve of 24HP VRF system

The TRNSYS simulation layout of the modified model-2 when using decoupled design of the VRF-SV hybrid system in the retail shop facility is shown in Figure 8.11. The model represents only the occupied hours of energy consumption. The process and function of each component used in this model are collectively summarized in modified model-3 section.

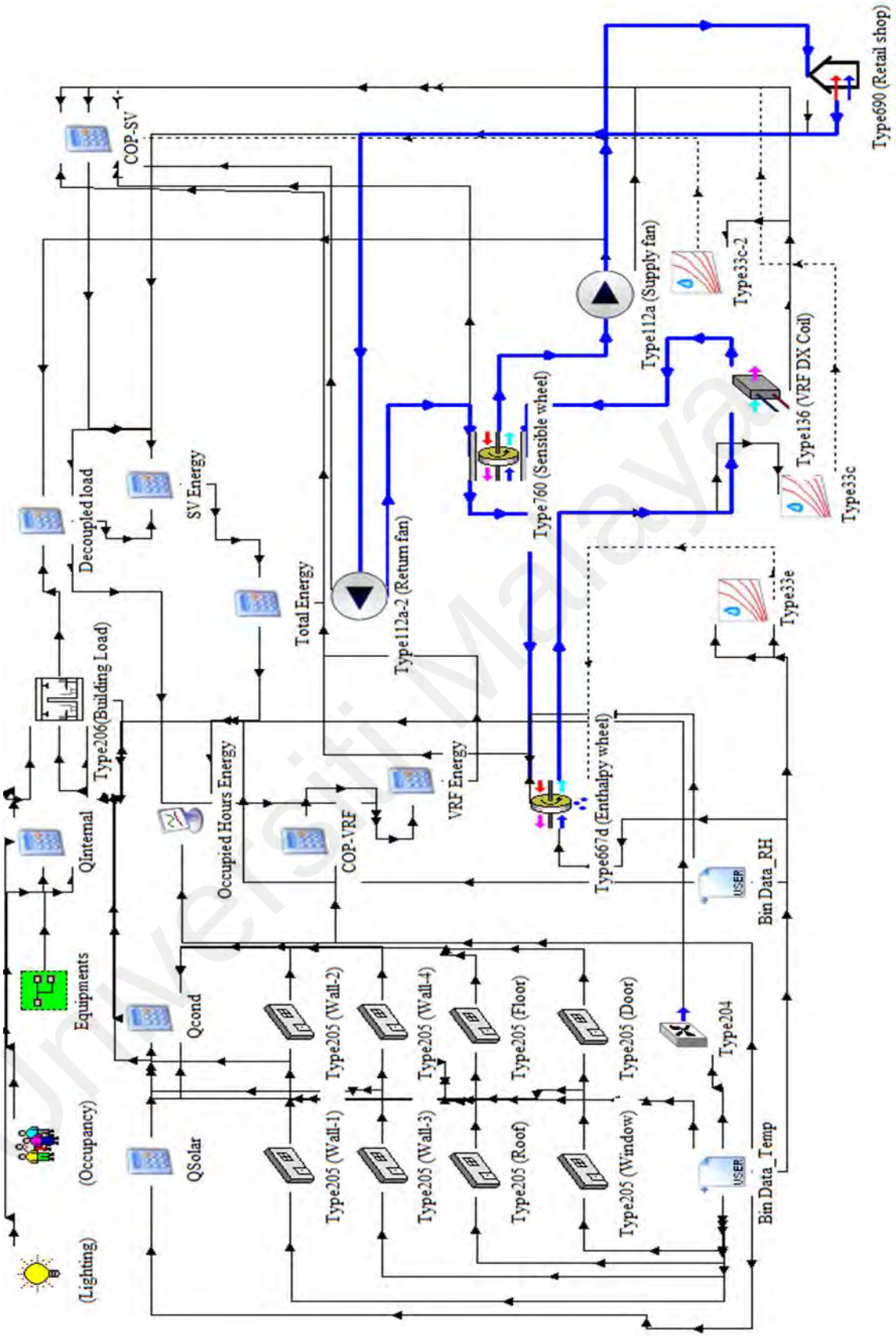

Figure 8.11: TRNSYS simulation layout of the modified model-2

(d) ***Modified Model-3***

In this simulation model, a fully integrated design of the VRF-SV hybrid system was used to compare the energy consumption with the baseline simulation model. In this approach, the VRF and DOAS systems are integrated so that no separate VRF indoor units are required for sensible cooling. Unlike the decoupled method discussed earlier, this method entirely relies on the VRF DX coil installed inside the DOAS system to treat the required supply air (OA+RA) fully.

The required supply air quantity for the target building is estimated first by considering the supply air temperature and total sensible cooling load of the building. The initially calculated minimum OA for ventilation based on the ASHRAE standard(ANSI/ASHRAE-62.1, 2019) is supplied into the mixing chamber in the DOAS system after passing through the enthalpy wheel. To fulfill the total supply air requirement of the target building, the remaining amount of air is obtained from the return air duct and directed into the mixing chamber. The mixture of both air streams is then cooled (at saturation point) by the VRF DX coil and reheated by the sensible wheel before supplying to the target building through the SV diffusers. Please see chapter 3 and chapter 4 for the detailed design guidelines and working principle of this system

The energy consumption of this hybrid system in the target building is calculated using the COP of the integrated system using the same equations as in section (1) for the decoupled VRF-SV system

The TRNSYS simulation layout of the modified model-3 when using a fully integrated design of the VRF-SV hybrid system in the retail shop facility is shown in Figure 8.12. The model represents only the occupied hours of energy consumption. Restricted by the length of this chapter, the process and functional representation of

each component used in the simulated models are collectively summarized in Table D.1 in appendix D.

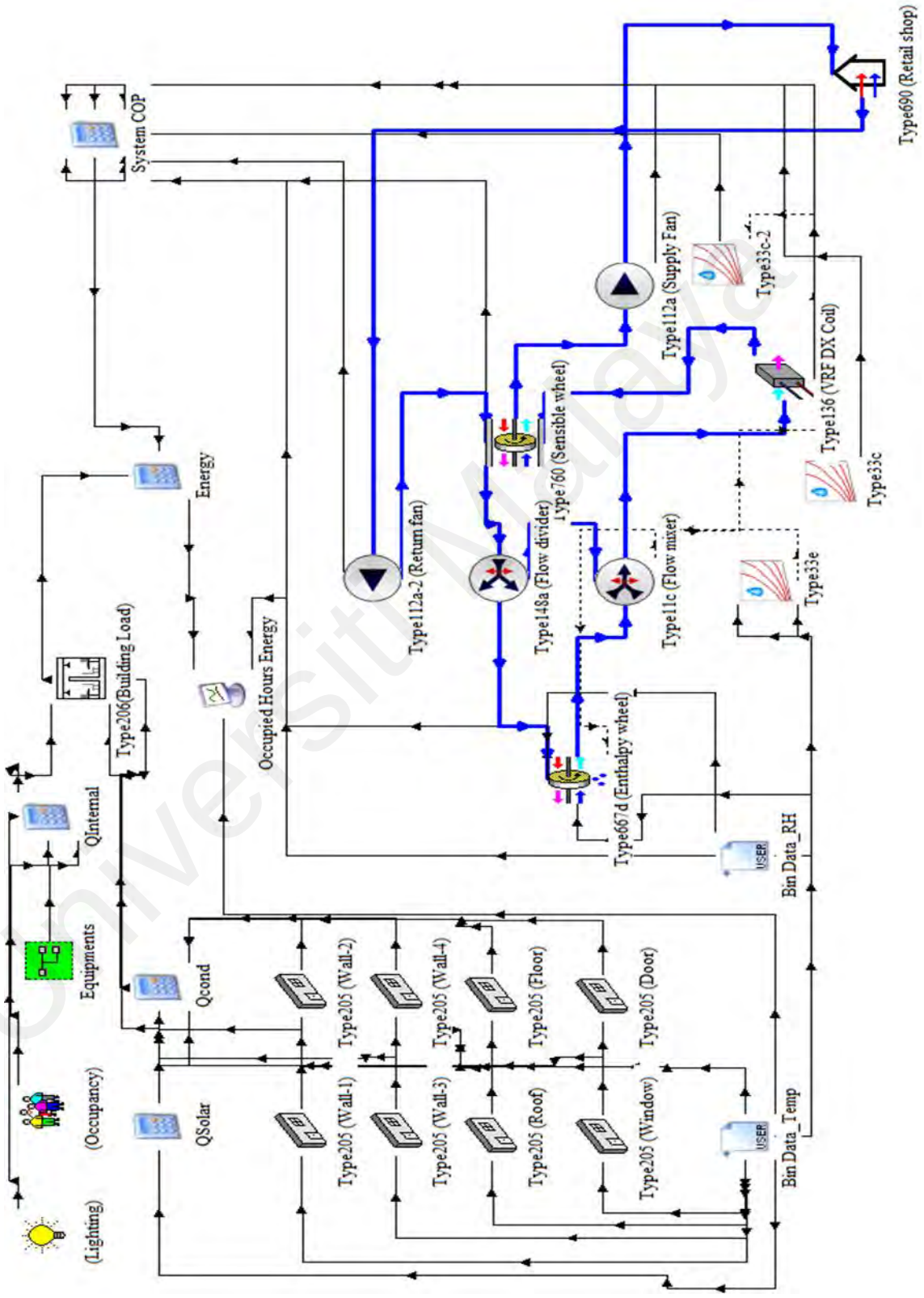

Figure 8.12: TRNSYS simulation layout of the modified model-3

8.4 Results and Discussion

8.4.1 Validation of the Developed Nodal Model

The simulations and model calculation results were compared and analyzed in this section. The model predicted results are compared with the simulation results obtained at the locations as marked in Figure 8.13(a).

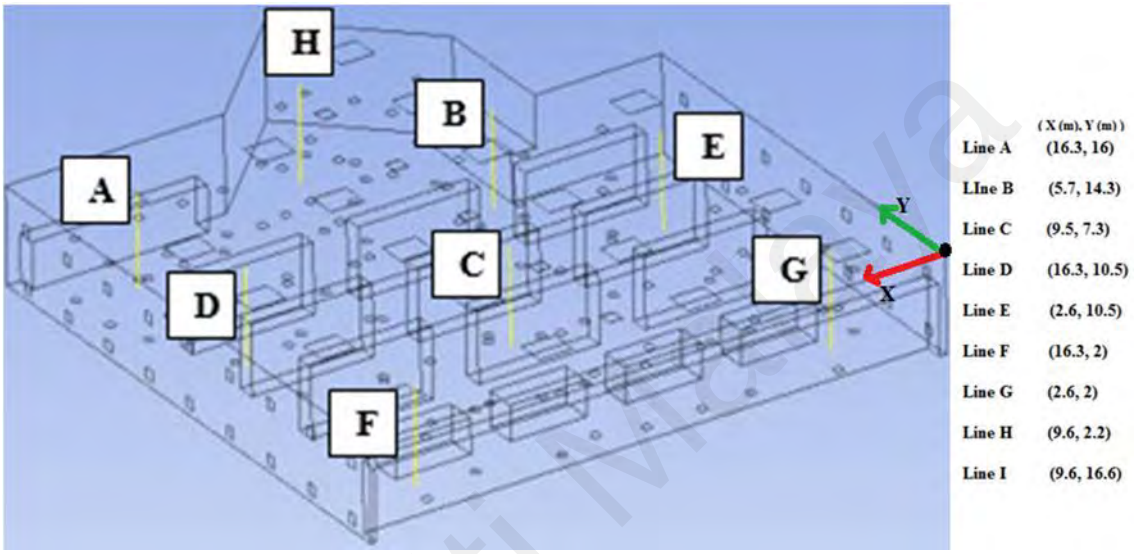

(a)

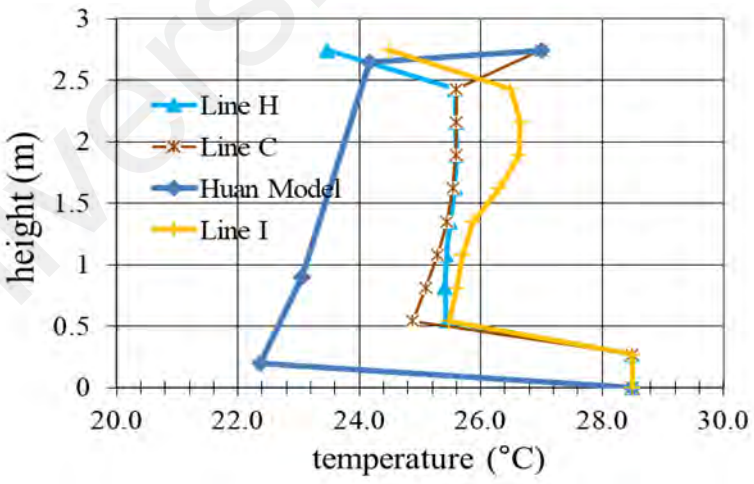

(a)

Figure 8.13: (a) Simulations with measuring locations (b) nodal modelling predicted vertical temperature profile

8.4.1.1 Ceiling Exhaust Configuration

One of the main applications of the developed model is to be coupled with an energy simulation tool to improve the accuracy of the energy calculation for buildings with stratum ventilation. Therefore, the mean temperature crossing a plane (horizontal section), which is relevant to energy consumption, was examined in this study. Figure 8.14 (a) compares the calculations and simulation predictions of the reference model (Huan's model). A significant difference can be observed, which indicates the model's inaccuracy in temperature profile prediction for large SV applications. Contrastively, a good match in the simulated and modified nodal model calculations is shown in Figures 8.14 (b) and (c).

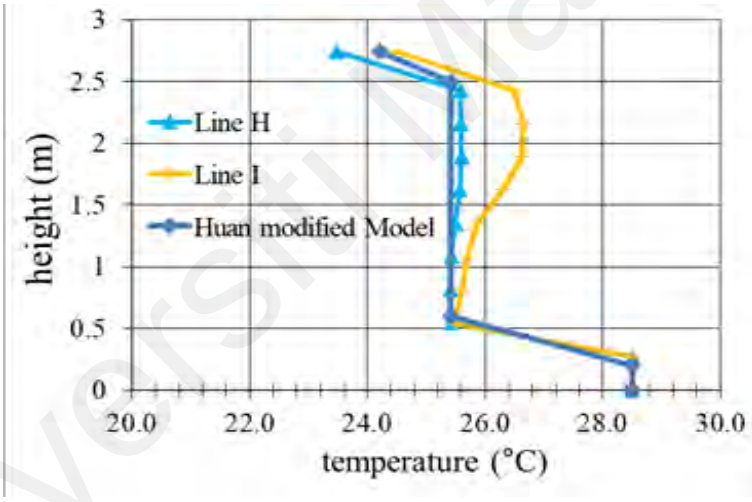

(a)

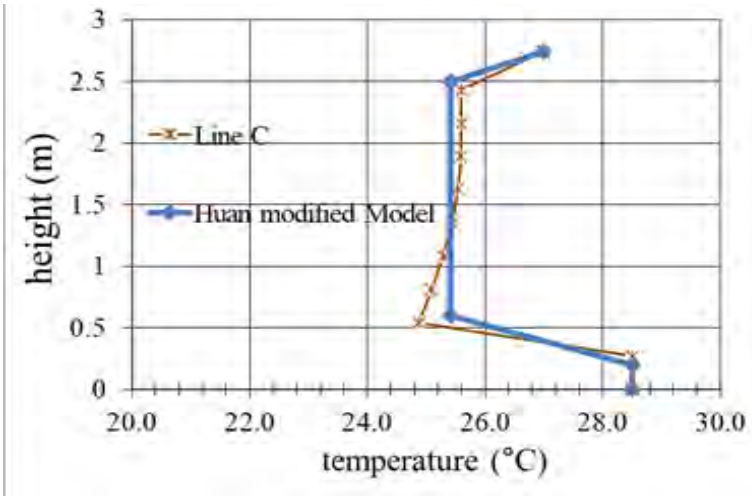

(b)

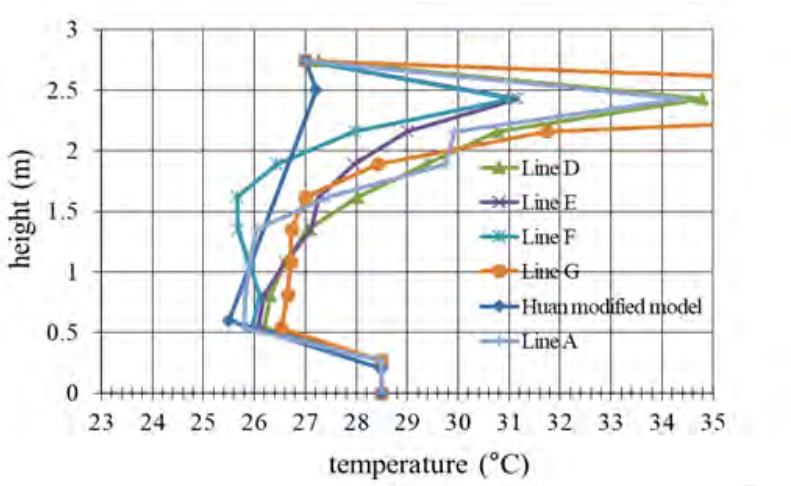

(c)

Figure 8.14: Comparison between simulated and nodal model predicted results (a) reference model and (b) & (c) modified model

8.4.1.2 Wall Exhaust Configuration

Similar to the previous sub-section, the results obtained with the current simulations are compared and presented in Figure 8.15. The simulated results are compared with both the reference and modified models. In both configurations of air terminals, significant temperature gradients are observed near the ceiling zone (Fig. 8.15b), which was mainly caused by the heat gains from lighting units.

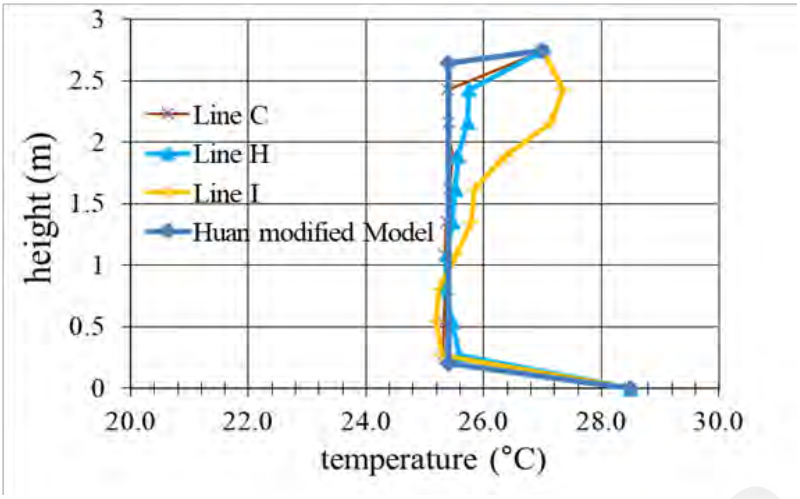

(a)

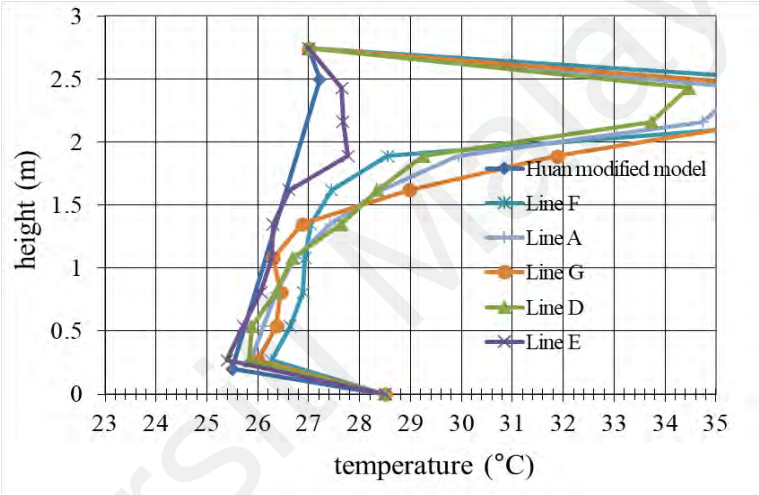

(b)

Figure 8.15: Comparison between simulated and nodal model predicted results

8.4.1.3 Discussions on the Nodal Modelling Results

The simplified nodal models do not contain the heat transfer calculation caused by near local heat gain sources. In addition, nodal models are not universal in predicting the temperature gradient since they cannot count all the factors affecting the indoor airflows. When internal heat gains split into several highly asymmetric plumes, it may generate a stratification profile with several neutral levels. The simplified nodal model does not cover this complicated indoor temperature distribution. However, the temperature gradient in this zone is out of the occupied zone. In addition, in many cases, these local heat gains do not significantly affect the occupied zone temperature.

The model is also inapplicable when internal heat gains are predominately radiative or located out of the occupied zone. In that case, convective heat transfer in the room surfaces heated by the radiative gains can compete with the convective heat gains in the occupied zone, creating a close to linear temperature gradient without an identifiable neutral level.

In practical applications, the room air temperatures are affected by the variation of heat gains in operation time and thermal mass effect, which are not considered in the steady-state models. Besides, most dynamic calculation methods assume either complete mixing of zone air or linearized temperature gradient. Therefore, the dynamic analysis of temperature gradient development would benefit future studies in this direction.

8.4.2 TRNSYS Energy Modelling

8.4.2.1 Simulation Results

In this research, the bin weather data is used to simulate different ACMV systems in a tropical retail shop building. The simulation with a multi-split type AC system was considered the baseline simulation. That AC system was then replaced with the VRF, VRF-SV decoupled and VRF-SV fully integrated systems in the successive simulation models. The simulated results of all models are based on the energy consumption at many outdoor temperatures (bin temperatures) distributions for every 4 hours shifts in Petaling Jaya, Malaysia, from the years 2007 to 2016 (refer to Figure 8.5).

As shown in Figures 8.16 - 8.19, the simulation results for all ACMV systems are divided into occupied and unoccupied periods, where the occupied period is 3650 hours and the unoccupied period is 5110 hours. It is pertinent to mention that the number of hours for occupied and unoccupied periods in this simulation are selected based on the relation between the bin weather data used in the present research with the target

building operating hours. The red and blue lines represent the midpoint of the bin temperature and bin relative humidity intervals based on the bin weather data, while the pink line represents the amount of energy consumption of the simulated ACMV systems.

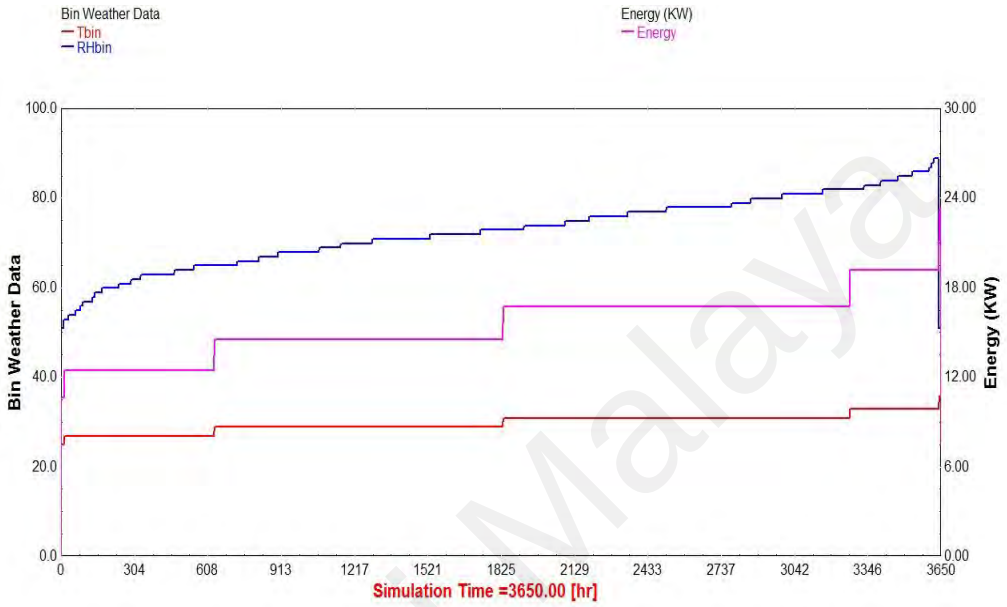

)a(

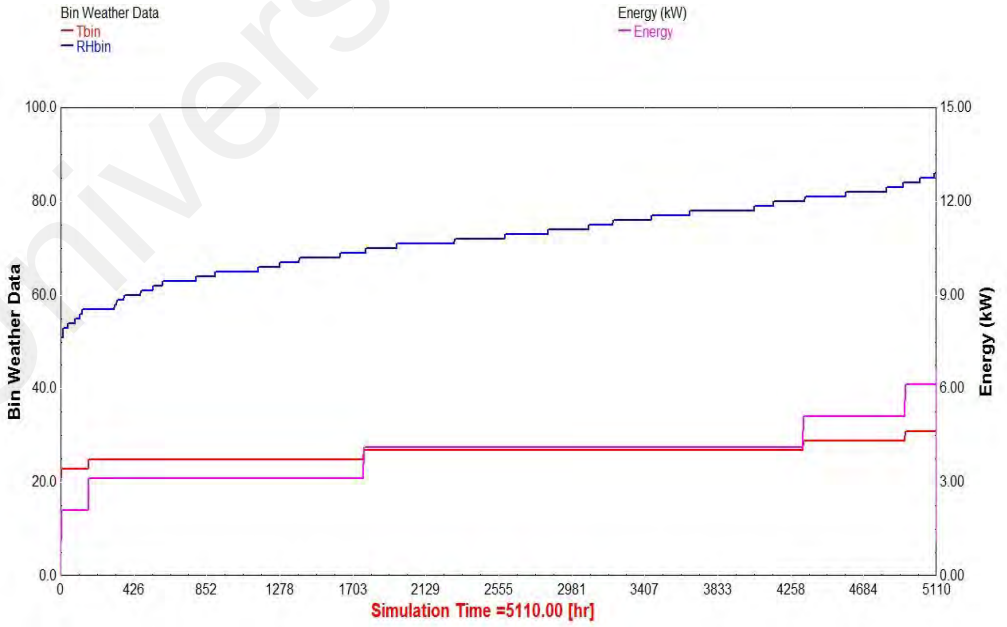

)b(

Figure 8.16: Simulated result for split type AC system (no ventilation) (a) occupied period (b) unoccupied period

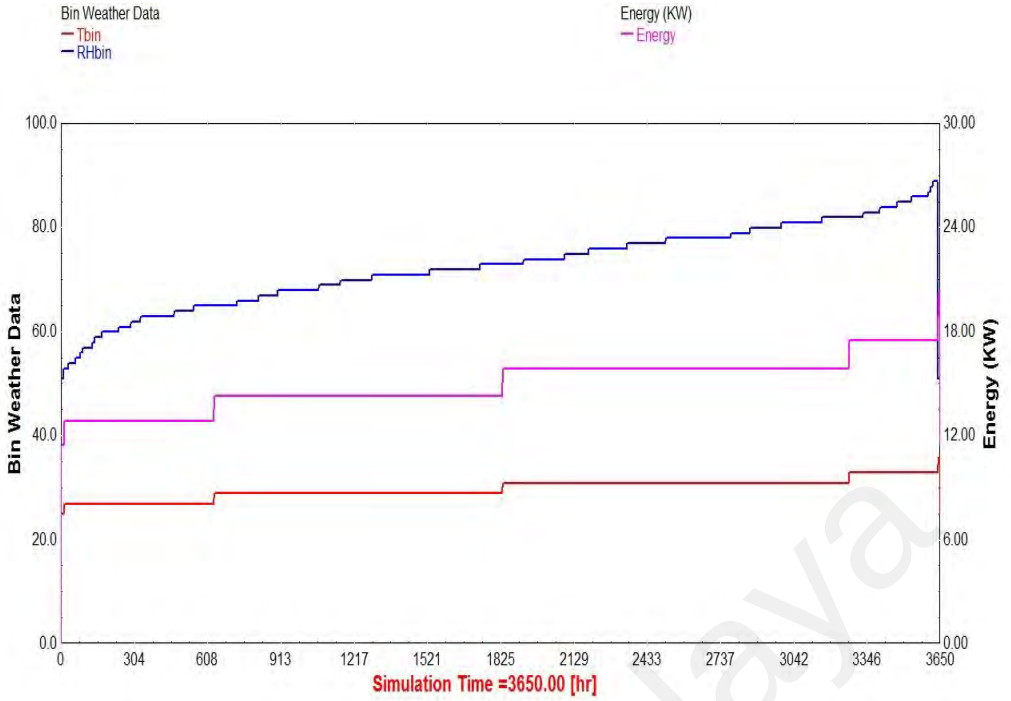

(a)

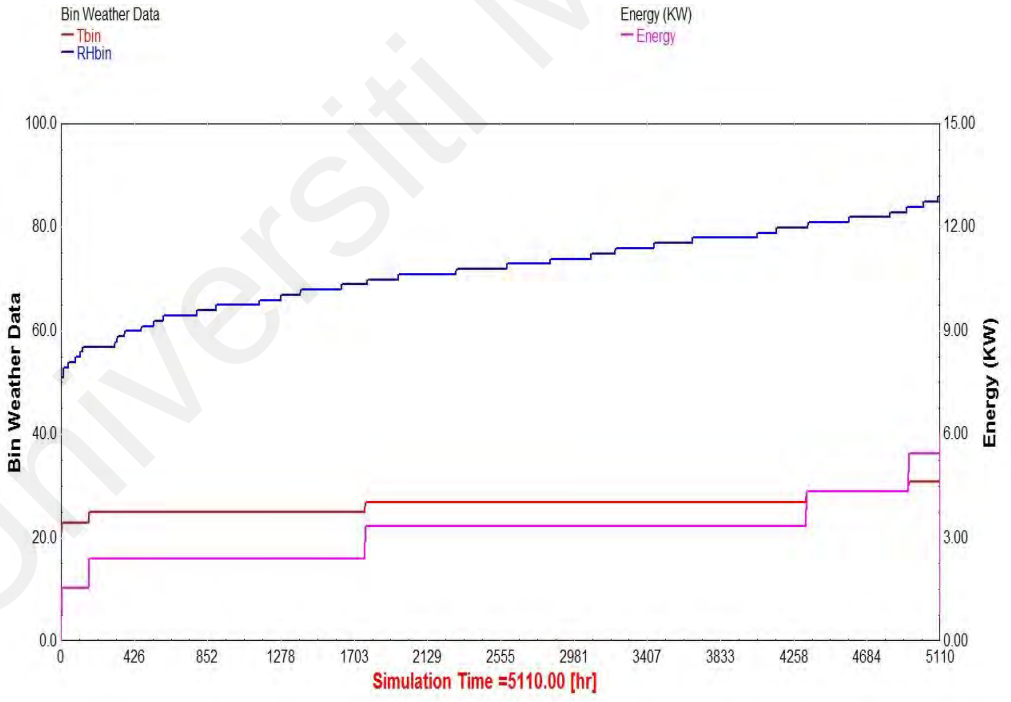

(b)

Figure 8.17: Simulated result for VRF system (no ventilation) (a) occupied period (b) unoccupied period

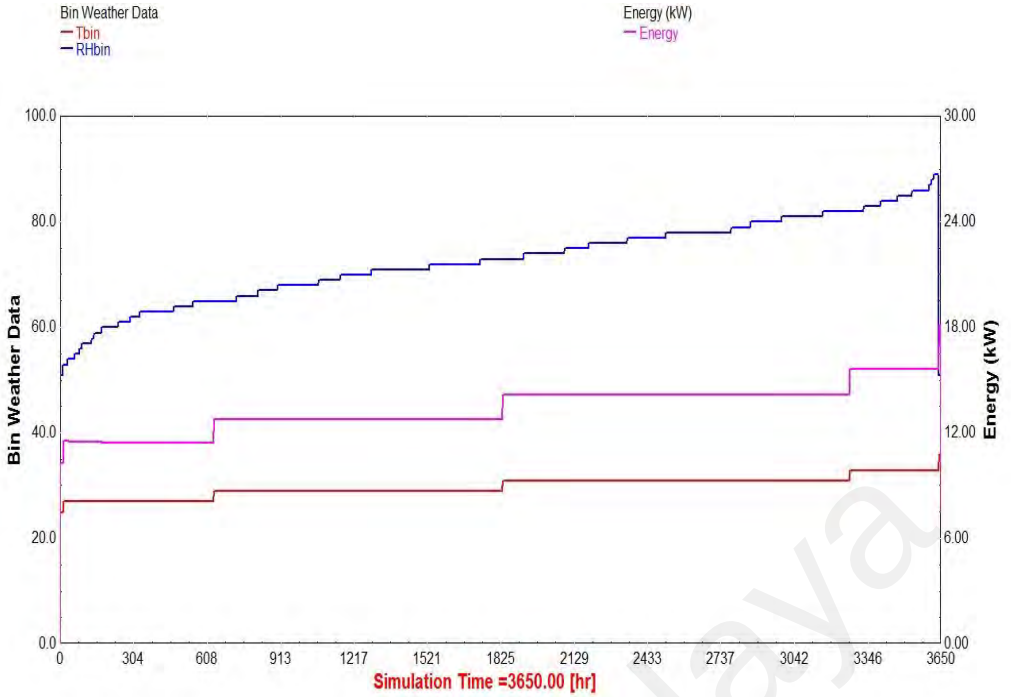

)a(

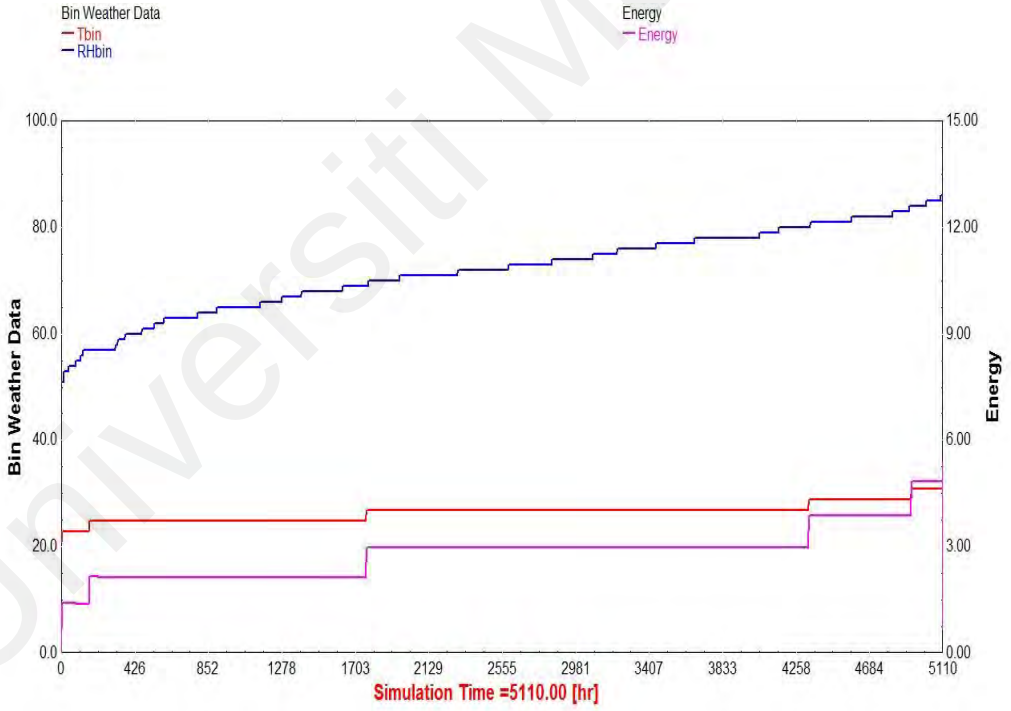

(b)

Figure 8.18: Simulated result for the VRF-SV decoupled system (a) occupied period (b) unoccupied period

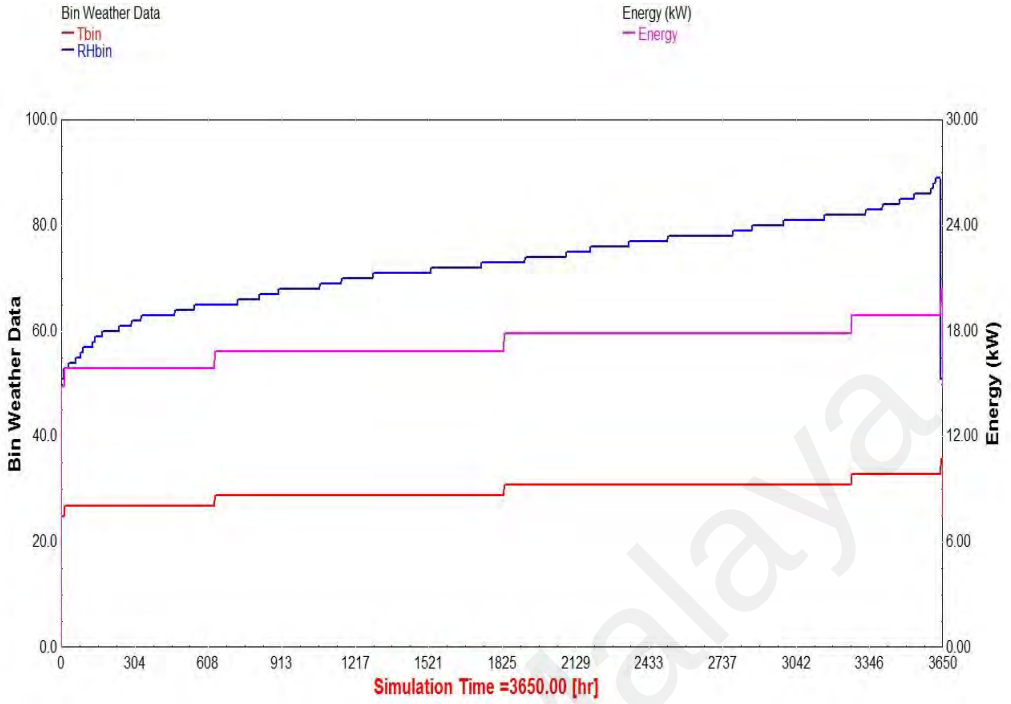

)a(

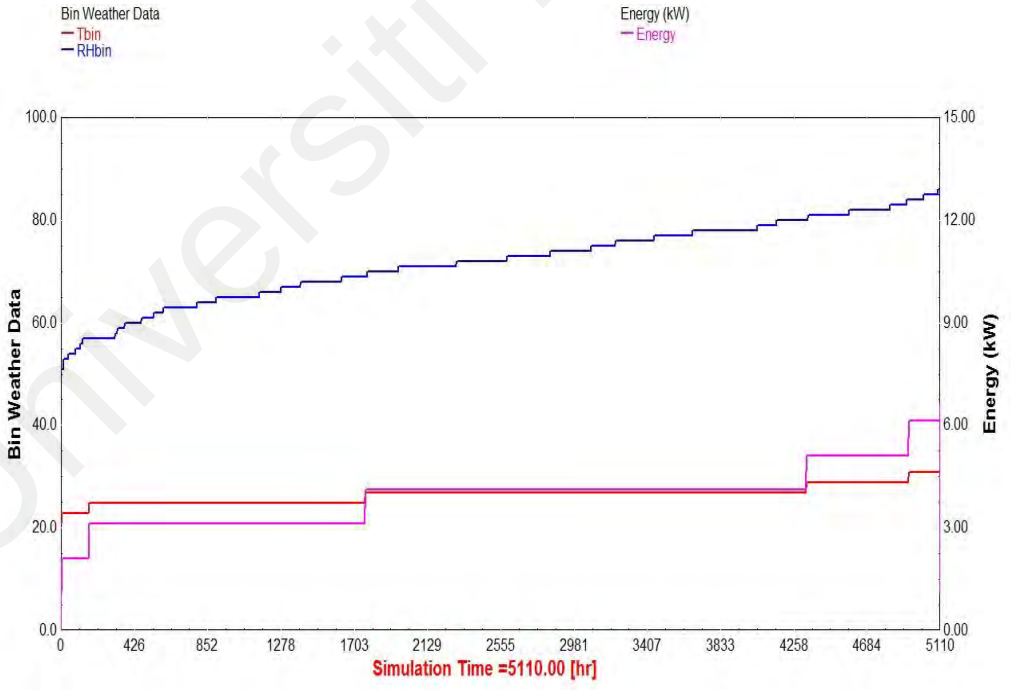

(b)

Figure 8.19: Simulated result for the VRF-SV fully integrated system (a) occupied period (b) unoccupied period

8.4.2.2 Annual Energy Consumption Analysis

The simulated results of the ACMV systems are quantitatively calculated, as shown in Figure 8.20. By multiplying the frequencies for every midpoint of the bin temperature interval with the energy consumption at each of the midpoint of the bin temperature interval, the result of occupied and unoccupied periods is totalized for each system.

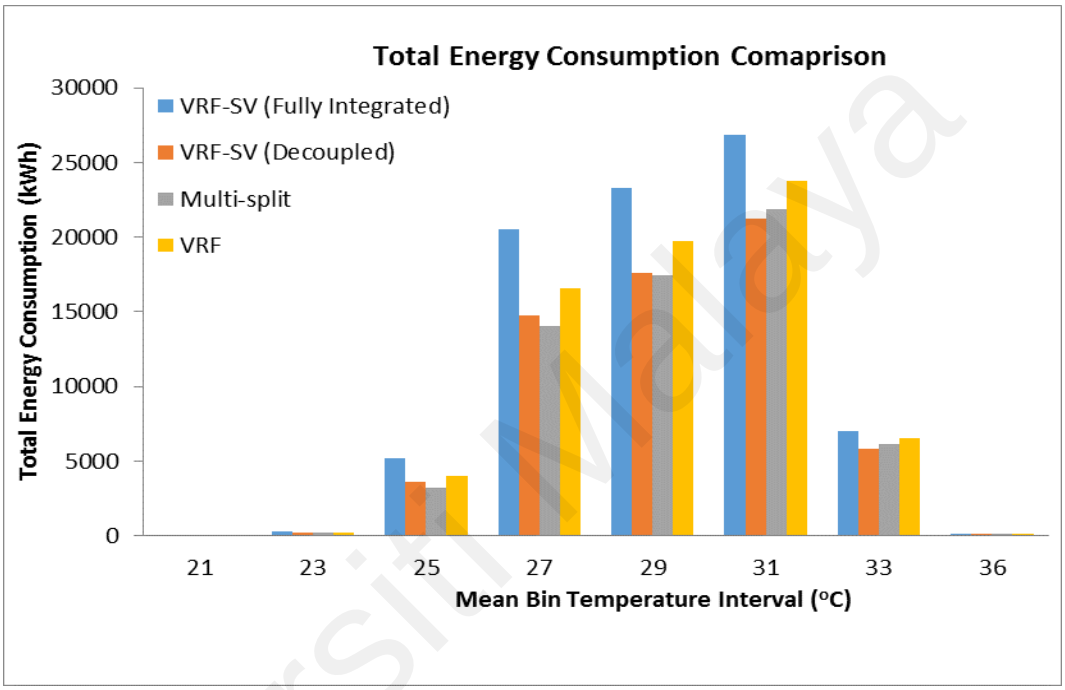

Figure 8.20: Comparison of the total annual energy consumption (kWh)

Figure 8.20 shows that the highest energy consumption occurred in all simulated cases when the bin temperature interval was 31°C. This is because of the inverse impact of the outdoor temperature on the COP of the ACMV system. The total energy consumption by any of the ACMV systems at higher temperatures such as 33ºC and 36ºC is comparatively low due to the low frequencies of these bin temperature intervals. The result suggests that sometimes the temperature in Malaysia can reach its highest peak at about 33°C, which is extremely warm, and it rarely goes below 25°C. Thus, it can be concluded that Malaysia has high daytime temperatures, which are between 25°C to 33°C. It should be noted that the lowest values at 21ºC and 23º C in Figure 8.20 are observed because of the low energy consumption in that temperature intervals. The

reason is that Malaysia's temperature never reaches below 23ºC, as shown in the bin weather data in Petaling Jaya, Malaysia in years 2007 to 2016 (please refer to Figure 8.5).

Figure 8.20 shows that the annual energy consumption when the building is installed with VRF system or VRF-SV decoupled system is the lowest compared to the other two ACMV systems in almost every midpoint of the bin temperature interval. However, the later was found most suitable and efficient with fresh air ventilation. The overall total the annual energy consumption for the VRF-SV decoupled system and only VRF system is 63,401.6 kWh and 71,010.6 kWh, respectively, where the difference is 7,609 kWh (i.e., around 10.7%) which is due to the use of heat recovery devices (enthalpy and sensible wheels) in the VRF-SV decoupled system. The fully integrated design of the VRF-SV hybrid system performed worst in energy consumption due to the conditioning of an excessive amount of supplied air (a mixture of OA and RA streams). This clearly shows that the VRF-SV hybrid system can save more energy when compared with the VRF or multi-split type air conditioning systems.

8.5 Summary

This study carried out a series of simulations to study the nodal and energy modeling of the VRF-SV hybrid system in a tropical building. Firstly, the nodal model was developed based on Huan's model (Huan et al., 2018) for the target building under ceiling exhaust configurations. Then the developed model was modified based on the CFD results of the ceiling and wall exhaust configurations. The nodal modeling results showed that more accurate predictions of the vertical temperature profiles were obtained through modified models compared to the reference model for both configurations. Secondly, the TRNSYS simulation results of the energy use analyses of the ACMV system in the target building revealed that the VRF-SV hybrid system's decoupled

design could save a significant amount of building energy compared to the other AC systems. A required amount of outdoor air is also provided in this system for better IAQ. Thus, recommended for large tropical applications.

CHAPTER 9: PERFORMANCE EVALUATION OF AN ARCHITECTURALLY DESIGNED VERTICAL HIGH CAPACITY LINEAR SLOT DIFFUSER IN A TROPICAL ATRIUM

9.1 Introduction

The atrium building represents a large space building, often having a story height of more than 5m and a total volume above 10,000 m^3 (Jiying, 2015). The atrium comprises several stories that allow the other building levels link together. In most countries, an atrium is a crucial feature in the architectural design of the shopping malls, lobbies of large commercial buildings (Acosta, Varela, Molina, Navarro, & Sendra, 2018; Al-Waked, Nasif, Groenhout, & Partridge, 2021; Jiying, 2015; Liu, Chen, Jun, & Haoru, 2017; O'Donohoe, Gálvez-Huerta, Gil-Lopez, Dieguez-Elizondo, & Castejon-Navas, 2019; Wu, Zhou, & Li, 2021; Yong, Wong, Du, Qing, & Tu, 2014). Since the atriums are glazed structures, the impact of the external temperature conditions on internal thermal stratification and human comfort is significant (Huang et al., 2007; Lin & Tsai, 2014). In summer, the excessive solar heat gain causes higher energy consumption by the air distribution systems in such buildings. Besides, the air stratification affects thermal comfort and performance of the atrium.

The suitable design and performance of the air distribution system influence the overall building energy consumption and improves the local thermal comfort and indoor air quality (IAQ) (Lopez, Galvez Huerta, Castejon Navas, & Gerard O'Donhoe, 2018; Posner et al., 2003). During the ventilation design of the high ceiling applications, the common issues faced by the design engineers are the temporal variability of the cooling loads, which varies from 30W/m^2 to 140W/m^2 (Loveday, Kenneth C. Parsons, Ahmed H. Taki, Simon G. Hodder, & Jeal, 1998), and their non-linear spatial distribution (S. Wang & Ma, 2008). However, an adaptive control system can adjust the supply airflow rate and temperature with a varying thermal load. Still, the preservation of acceptable

thermal comfort levels depends mainly on the performance of air distribution systems (Lopez, Galvez-Huerta, Castejon-Navas, & Gomez-Garcia, 2013). Nada et al. (2016) found the underfloor air distribution (UFAD) as a more effective ventilation strategy for large spaces under the increased ceiling height. Keeping in mind the objective of a low-cost ventilation solution for tropical atrium buildings, F. Wang and Abdullah (2011) investigated the pressurized ventilation strategy. Under this numerical study, a parametric analysis was carried out to see how the internal thermal conditions (i.e., air movement and temperature distribution) change with the variation in supply and return terminals' opening ratio or arrangements. The simulation results revealed the significant impact of the inlet/outlet opening area ratio and their arrangements on the performance of internal thermal conditions. Some other studies also reported the investigations on the different designs for the air distribution systems and their inlet/outlet terminals arrangements in large space buildings (Hussain & Oosthuizen, 2012a; Liu et al., 2017; H. Wang et al., 2019). Based on the literature reviewed and because of the high energy-related demands of the air conditioning systems in such buildings, a proper design of the air distribution system that can provide a better thermal environment in an energy-efficient manner is inevitable.

Compared to conventional well-mixed air-distribution systems in atriums, a bottom level cool air supply system targeting only the lower zone can save up to 40% of the total energy (Yong et al., 2014). However, little attention has been paid to this strategy. Still, the traditional overhead air distribution systems are being used in the air conditioning of the atrium buildings (Hussain & Oosthuizen, 2012b), and the benefits of supplying ventilation at a low level are thoroughly overlooked. Besides, one of the typical low-level air distribution system attributes is to provide a relatively cool and conditioned air jet directly into the breathing zone (Zheng et al., 2018). The air rises after getting heated by the internal heat sources (occupants and objects). The

characteristic of the low-level air distribution strategy is to maintain a thermal stratification within the breathing zone and to create a lower thermal gradient between the head and foot levels. On the other hand, effectively supplying air to the breathing zone is still a problem to be solved with this strategy type.

Nowadays, computational fluid dynamics (CFD) techniques have been widely adopted in research to predict indoor air distribution and thermal comfort in large atrium-type buildings (Rundle, Lightstone, Oosthuizen, Karava, & Mouriki, 2011; H. Wang et al., 2019). Hussain and Oosthuizen (Hussain & Oosthuizen, 2012a) numerically studied the buoyancy-driven low-level ventilation strategy in an atrium building. The results of that study were compared with the small-scaled experimental work (Hussain & Oosthuizen, 2012b). The research concluded that the temperature distribution, airflow patterns, and ventilation flow rate obtained through CFD simulations perfectly matched the analytical and experimental results. The literature reviewed shows that the Reynolds-Averaged Navier–Stokes (RANS) k-ε (2-equations) turbulence models have been widely used to predict the airflow and temperature distribution in atrium geometries. On the other hand, some studies performed with the k-ω (2-equations) turbulence models have shown their potential in predicting indoor airflow with better accuracy and numerical stability than k-ε models. However, it is often considered as unresolved for which turbulence model to be used due to the complex behavior of the flow in the atrium. Based on the above challenges, this research was designed to evaluate the performance of an architecturally designed, vertical oriented, high-capacity linear slot diffuser (HCLSD) when installed at a low level on the sidewall of the atrium building. A simplified model of the atrium building was initially developed to avoid the computational complexities of using the actual atrium model. The verification and validation of the most common turbulence models were performed against experimental data. The verified and validated turbulence model

was then employed in the full-scale simulation to predict the temperature and velocity distribution within the atrium.

9.2 Overview of Simulated Atrium

The air distribution performance of the vertically oriented HCLSD is extensively studied in a three-story atrium building using numerical and experimental approaches. The studied atrium is the part (4th to 6th levels) of an anonymous super tall building located in Kuala Lumpur, Malaysia. As this atrium was built at the lower part of the skyscraper, surrounded by a cluster of high-rise buildings from all sides, the heat gain through solar radiation was negligible due to the shading effect. Therefore, solar radiation is not considered to simplify the thermal comfort assessment in this atrium building. The atrium has a hexagonal shape surrounding the main lobby area connected to the retail facilities and offices. The plan view of the atrium with its surroundings and its cross-sectional view are shown in Figures 9.1(a) and 1(b), respectively. The key dimensional elements of the atrium and the supply and exhaust diffuser details are listed in Table 9.1. The supply and exhaust diffusers were installed adjacently on the four sidewalls of the atrium. The inlet and outlet slots were sized based on the airflow rate calculated using building's thermal load following ASHRAE standards (ANSI/ASHRAE-62.1, 2019).

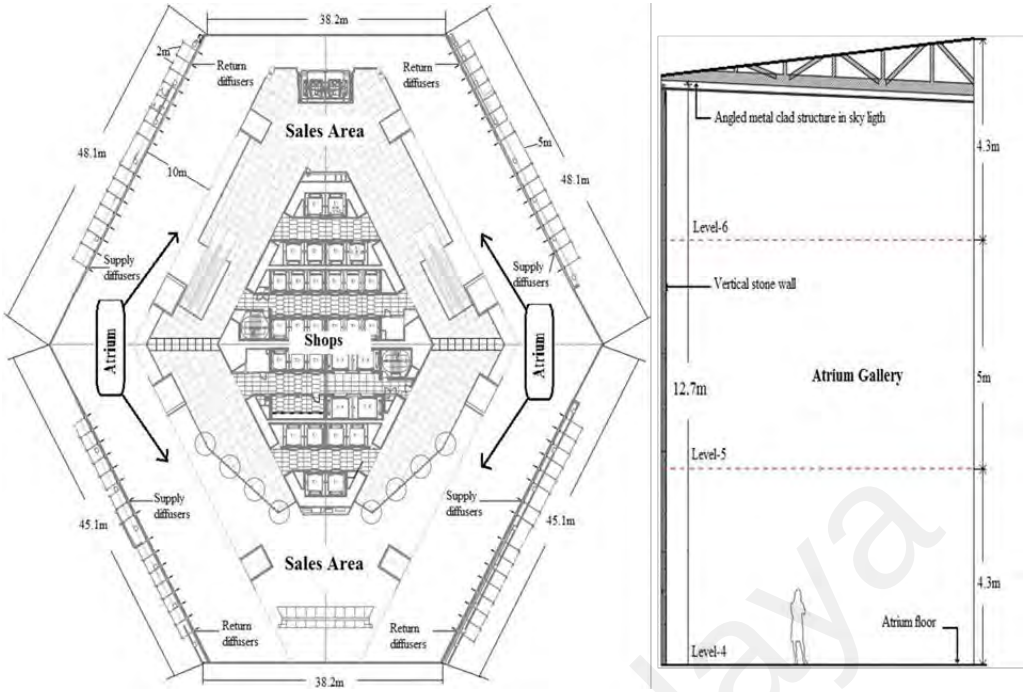

(a) (b)

Figure 9.1: (a) The Plan view of the atrium location (b) Cross-sectional side-view of the atrium building

Table 9.1: Specifications of diffusers of the atrium building

Item	Dimensions /Details
Height of the atrium	12.7 m (3 floors)
Width of the atrium	10.0 m
Area of the atrium	2.5×10^3 m^2
Volume of the atrium	3.2×10^4 m^3
Supply terminals	2000mmx40mm slot area, 32 Nos, 525 L/s airflow rate (8 on each side wall, 2 m apart)
Return/Exhaust terminals	2000mmx40mm slot area, 32 Nos, 525 L/s airflow, 0 Pa gauge Pressure (8 on each side wall, 2 m apart)

9.3 Research Methodology

9.3.1 Experimentation

The experiments were performed in an air diffuser testing laboratory at Prudentaire Engineering Private Ltd. The laboratory was located at the core of a building with no boundary wall exposed to solar radiation. A small-scale simplified model of the atrium was set up in the laboratory with the dimensions 6 m (L) x 5.4 m (W) x 2.74 m (H). An experimental setup was established with the installation of vertically oriented, architecturally designed HCLSD in the simplified atrium model. In addition, a rectangular outlet was set up on the same wall for exhaust airflow. The schematic diagram of the experimental chamber is illustrated in Figure 9.2. The experiments were conducted to validate the CFD model used to simulate simplified atrium geometry. The HCLSD of dimensions 2000mm x 40mm was initially fabricated and installed vertically on the sidewall of the experimental facility. The flexible duct of diameter 200mm was attached to the oval-shaped neck of the plenum box of the diffuser. The plenum box was sized as per the geometry of the slot diffuser. A centrifugal fan powered by a 3-phase asynchronous motor was used to supply the air to the chamber through HCLSD. A variable air volume (VAV) damper was installed in the supply air duct to regulate the airflow rate as per the testing requirement. A smoke generator was also employed to visualize the flow behavior from the slot diffuser. The smoke was supplied into the flexible duct after controlling the flow rate through the VAV damper.

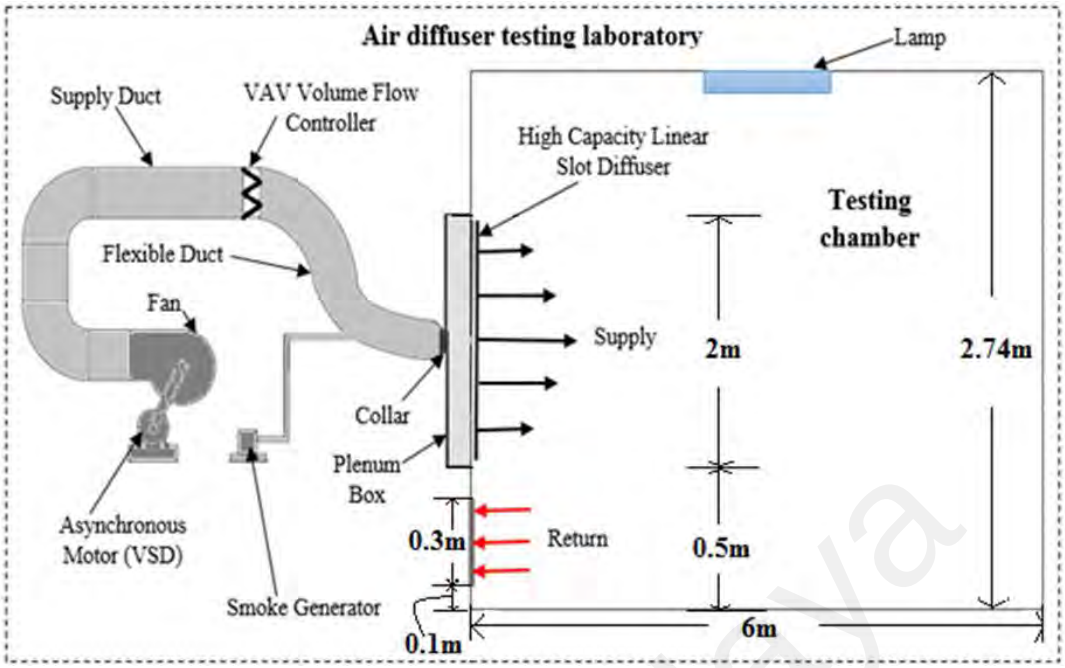

Figure 9.2: Schematic diagram of the testing chamber with experimental facilities

9.3.1.1 Measurement Methods and Equipment

Detailed environmental conditions of the laboratory were measured before the actual testing started. The temperature of all the internal surfaces was checked by using the ZTH-VAV belimo temperature adjustment tool. The Alnor 440-A hot wire anemometer (seen in Figure 9.3(a)) was used to measure the indoor temperature at different locations for the determination of the room average. The accuracy of the measuring equipment was ± 0.3°C for temperature, 0.015 m/s for velocity, and ± 13% for relative humidity. The actual measurements were taken every 1 hour after the fan was started delivering air at 525 l/s with a fluctuation of less than 5%. At the 4th hour of the fan operation, the room achieved the steady-state condition when the mean air temperatures at supply inlet, return outlet, and at the center of the room did not exceed more than 1°C variation (Y. H. Yau, K. S. Poh, & A. Badarudin, 2018b). The difference in the room's internal surface temperatures also dropped below 0.1°C during that period. That is all done to make the environment closest to isothermal. The measured values of the temperature at different time segments are presented in Table 9.2.

There was no proper space for installing the return slot diffuser in the experimental chamber, as it is positioned in the actual atrium model. Hence, the assumption was made by positioning the return outlet on the bottom left of the supply diffuser in the experiment and the simplified simulation model by considering the insignificant effect on the flow pattern with the said arrangement. Figure 9.3(b) depicts the locations where measurements were taken to verify and validate the numerical models.

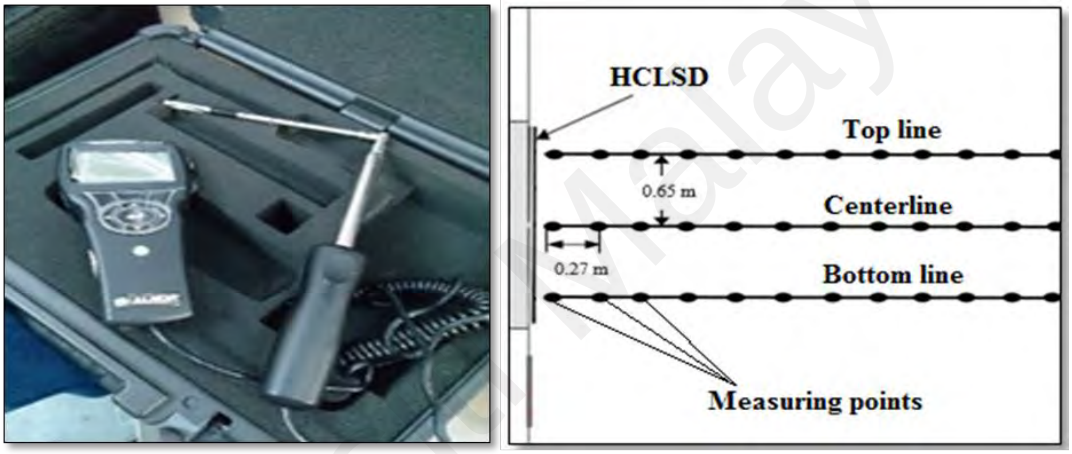

(a) (b)

Figure 9.3: (a) Alnor 440-A anemometer (b) Layout of the measurement locations

Table 9.2: Laboratory air and internal surface temperature measurement

Hour	1st	2nd	3rd	4th
Supply air temperature (°C)	28.8	29.6	30.1	30.7
Return air temperature (°C)	28.6	29.4	29.9	30.2
Room air temperature (°C)	28.0	29.6	29.8	30.3
Wall 1 surface temperature (°C)	29.2	29.3	30.0	30.1
Wall 2 surface temperature (°C)	29.0	29.3	30.1	30.1
Wall 3 surface temperature (°C)	28.6	28.9	29.5	29.6
Wall 4 surface temperature (°C)	28.2	28.4	30.1	30.2
Ceiling surface temperature (°C)	29.5	29.9	30.7	30.8
Floor surface temperature (°C)	28.6	28.8	29.6	29.5

9.3.2 Computational Fluid Dynamics (CFD) Study

Although the experimental analyses provide the most accurate results (H. Chen, 2014; Hussain & Oosthuizen, 2012b; Haiguo Yin, Li, Liu, Sun, & Chen, 2016), it sometimes feels difficult to achieve the ideal steady conditions in a realistic environment. For this reason, the simulation-based research method is now commonly used to study the indoor environment with desired boundary conditions. The results obtained from the experiments can be used to check the reliability of the numerical models and methods. Therefore, a simplified model of the atrium with a single HCLSD was initially simulated for the verification and validation studies. The validated numerical model was then employed for the performance evaluation of the vertically-oriented HCLSD in the full-scale atrium simulation.

The ANSYS software was used in this research work to solve the basic governing equations (Y. H. Yau et al., 2018b) for the flow field inside the model room. The simulation study adopted the buoyancy model, the mass continuity equation, energy equation, and momentum equation (Z. Lin, Tian, et al., 2011; Y. H. Yau et al., 2018b) by adopting the buoyancy model. The basic transport equations given in the following subsection were solved by using the finite volume method and discretized into simple algebraic form by the SIMPLE second-order upwind scheme. A standard wall function was employed in the present study to obtain the flow properties near-wall region. The Boussinesq model was used in studying the buoyancy effect. The convergence criteria for the residuals of continuity, velocity, ω, ε, and k were less than $10^{-4,}$ and the energy was less than 10^{-6} (Hussain et al., 2012; Yong CHENG et al., 2014). All simulations were run on two Workstations, each with an Intel Xeon (R) CPU E3-1240 v5 3.5GHz processor, 32GB RAM, and Windows 7 Professional 64-bit operating system, and took between 4 and 8 hours for the simplified model and 72 to 96 hours for the actual atrium model to complete for their respective grid sizes.

9.3.2.1 Background Theory

The thermal field distribution and airflow motion in the studied domain are completely governed by the laws of conservation of mass, momentum, and energy. The following mathematical models for these three laws are solved in the present study using a commercially available CFD code, ANSYS fluent (FLUENT, 2013).

Conservation of mass:

$$\partial\rho/\partial t + \partial(\rho u)/\partial x + \partial(\rho v)/\partial y + \partial(\rho w)/\partial z = 0 \quad (9.1)$$

Conservation of momentum:

X-momentum,

$$\rho \frac{Du}{Dt} = \partial\sigma xx/\partial x + \partial\tau xy/\partial y + \partial\tau zx/\partial z + \sum \text{Fxbody forces} \quad (9.2)$$

Y-momentum,

$$\rho \frac{Du}{Dt} = \partial\tau xy/\partial x + \partial\sigma yy/\partial y + \partial\tau zy/\partial z + \sum \text{Fybody forces} \quad (9.3)$$

Z-momentum.

$$\rho \frac{Du}{Dt} = \partial\tau xz/\partial x + \partial\tau yz/\partial y + \partial\sigma zz/\partial z + \sum \text{Fzbody forces} \quad (9.4)$$

where, σ_{xx}, σ_{yy} and σ_{zz} are the stresses due to normal viscous components acting perpendicular to the dimensions.

Conservation of energy:

$$\rho \frac{DE}{Dt} = \partial/\partial x \left[\lambda \frac{DE}{Dt}\right] + \partial/\partial y \left[\lambda \frac{DE}{Dt}\right] + \partial/\partial z \left[\lambda \frac{DE}{Dt}\right] - \partial (up)/\partial x - \partial (vp)/\partial y$$

$$- \partial (wp)/\partial z + \varphi \quad (9.5)$$

where, φ is the function that shows energy dissipation work done on the fluid, later converted into thermal energy.

9.3.2.2 Simplified CFD Model

Because of the high computational power requirement for a full-scale atrium simulation, a simplified CFD model was developed for the verification and validation studies. The model was designed based on the size and setup of the experimental chamber. Figure 9.4 shows the isometric view of the simplified small-scale atrium model. The boundary conditions set up for this simplified study are summarized in

Table 9.3. To obtain more accurate results, the domain was discretized using high quality unstructured tetrahedral mesh elements, as shown in Figure 9.5.

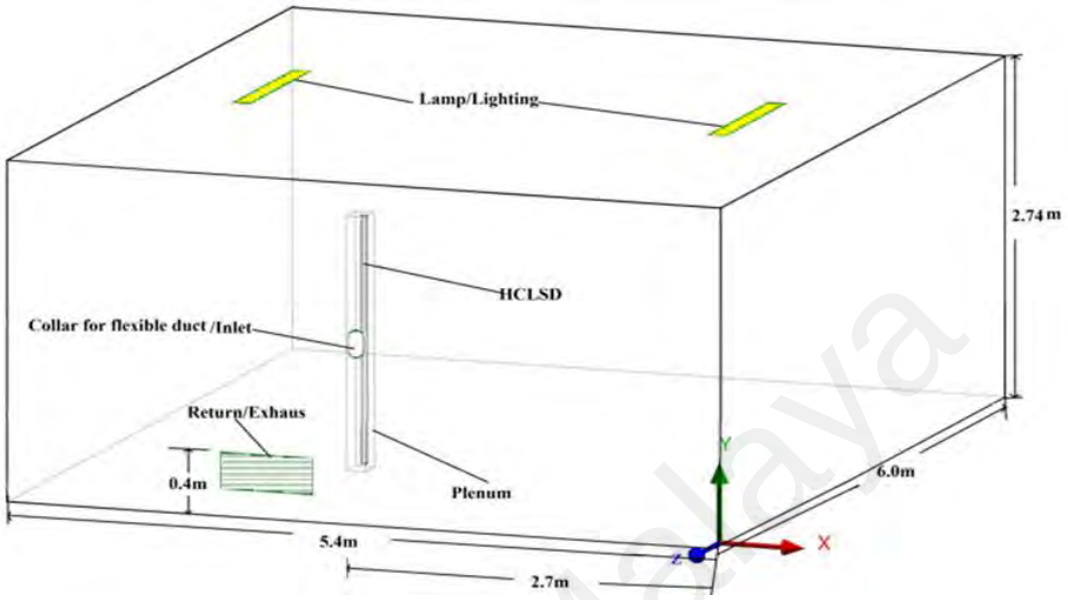

Figure 9.4: Isometric view of the simplified small scale atrium model

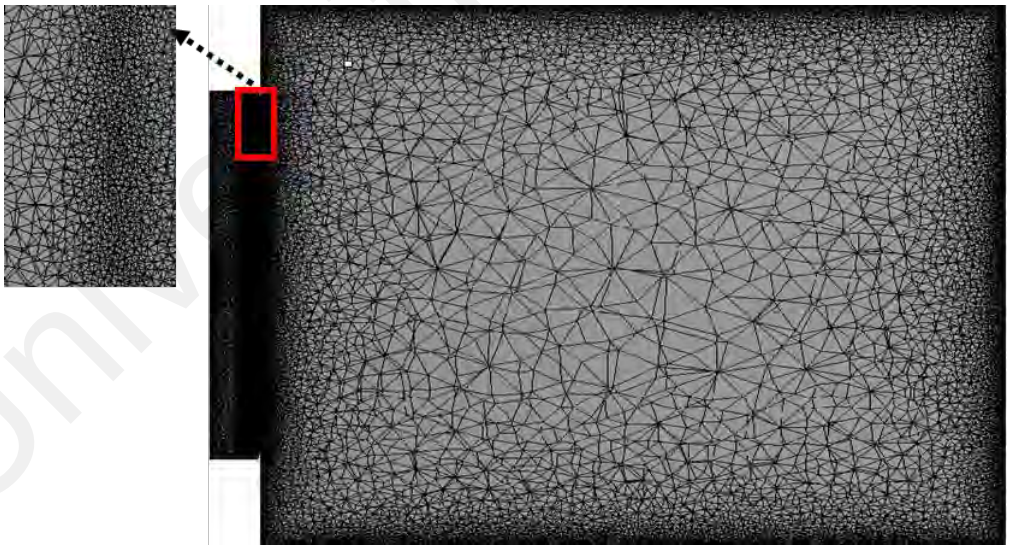

Figure 9.5: High quality unstructured tetrahedral mesh for a simplified model

(a) Verification and Validation Studies

A reliable numerical investigation of the indoor airflow requires the proper boundary conditions and quality of the mesh and depends on the applied turbulence model (H.

Chen, 2014; Stamou & Katsiris, 2006). Many turbulence models have been developed based on RANS, such as RNG k-ε, Standard k-ε, k-ω SST, etc. That is why the turbulence model's verification and validation study is crucial to ensure the best numerical representation of the physical model. The five most important turbulence models were employed in the verification study. Figure 9.6 compares the plane air velocity profile generated through a smoke test with the simulation results obtained using chosen turbulence models. They all showed a similar pattern as observed in the smoke test photograph, except for the SST k-ω model. However, the closest match to the smoke flow pattern came out with the RNG k-ε turbulence model. It can easily be realized that the upper edge of the flow plume in the smoke test is moving upward; the same is also noticed in the RNG k-ε model.

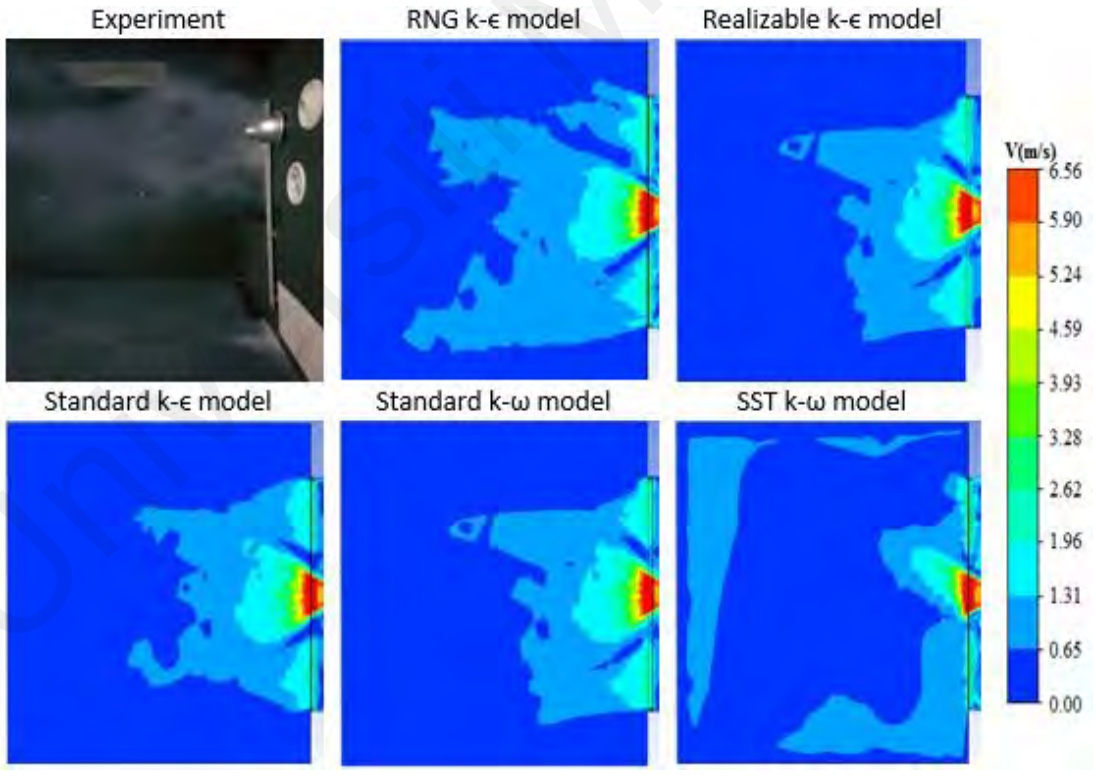

Figure 9.6: Plane air velocity profile through an experimental test and numerical simulations

The verification of the numerical model was further endorsed by comparing the centerline air velocity values extracted from the simulations using different numerical models with the experimentally measured values. Figure 9.7 shows the horizontal

centerline velocity profile of an actual model with various predicted turbulence models. No exact match was found between the experimental and simulated values. Despite that, the k-ε turbulence models somehow show a similarity in profile with the experimental results. The nearest prediction to the measured data was observed with the RNG k-ε model. A spike in the measured velocity values was seen at a distance of 1.08m and 1.35m from the diffuser. This variation is perceived may be due to the difficulties faced in manual measurements using a hand-held tool (i.e. Hot-wire anemometer).

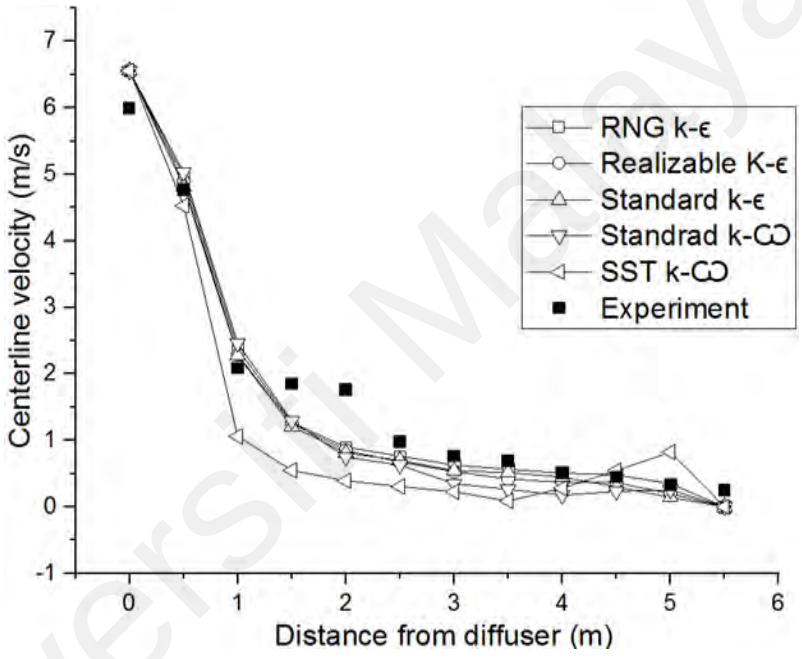

Figure 9.7: A horizontal centerline velocity profile of an actual and various predicted turbulence models

In addition, a lower velocity value was obtained from the measurement at the initial point (diffuser face). It is due to the frictional loss of the airflow within the plenum box. Thus, considering the captured and quantitative results, the RNG k-ε model was thought to be used to validate the experimental data with the actual atrium building simulations. Due to the inconsistency in temperature in the actual environment, the air velocity was compared to validate the numerical model with the measured data. The airflow velocity at different locations (as seen in Figure 9.3(b)) was extracted from the simulation study and compared with the actual measured values.

Figure 9.8 depicts a slight discrepancy in air velocity between modelling and experimental data. Although, a similar trend was seen in the velocity drop between the results. Compared with the top-line data, a large difference in the measure and simulated values along the bottom line was recorded at a 1 m distance from the diffuser. Along the top and bottom measuring lines, the maximum difference obtained between the simulation and experimental data was 17.5% and 30%, respectively. This may be due to the up moving direction of the flow as observed in the simulation and experimental airflow patterns. According to a study conducted by Zhang et al., (2007), if the error between the turbulence model and experimental result for predicting airflow in an enclosed environment is less than 20%-30% at most measured points, the model accuracy is considered acceptable. Therefore, this verification and validation study demonstrated that the RNG k-ε model could be regarded as accurate enough for further studies.

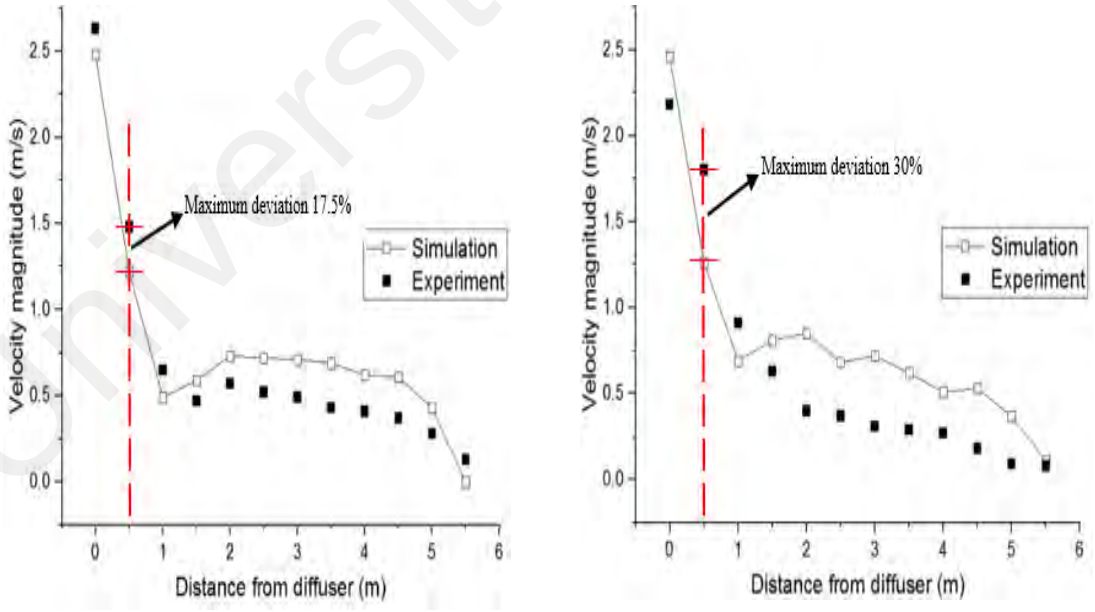

(a) (b)

Figure 9.8; Comparison of simulated results with experimental data (a) Top-line (please refer to Figure 3b) (b) Bottom line

9.3.2.3 CFD simulation of the Actual Atrium Model

The actual model of the atrium (as seen in Figures 9.9 (a) & (b)) was simulated using a validated turbulence model. The airflow pattern and temperature profile inside the domain were studied to evaluate HCLSD performance at different deflector angles. The boundary conditions used for the actual simulation domain are summarized in Table 9.3. The primary purpose of this detailed study was to investigate the flow performance of the HCLSD; therefore, no heat sources were considered in the domain for ease of simulation.

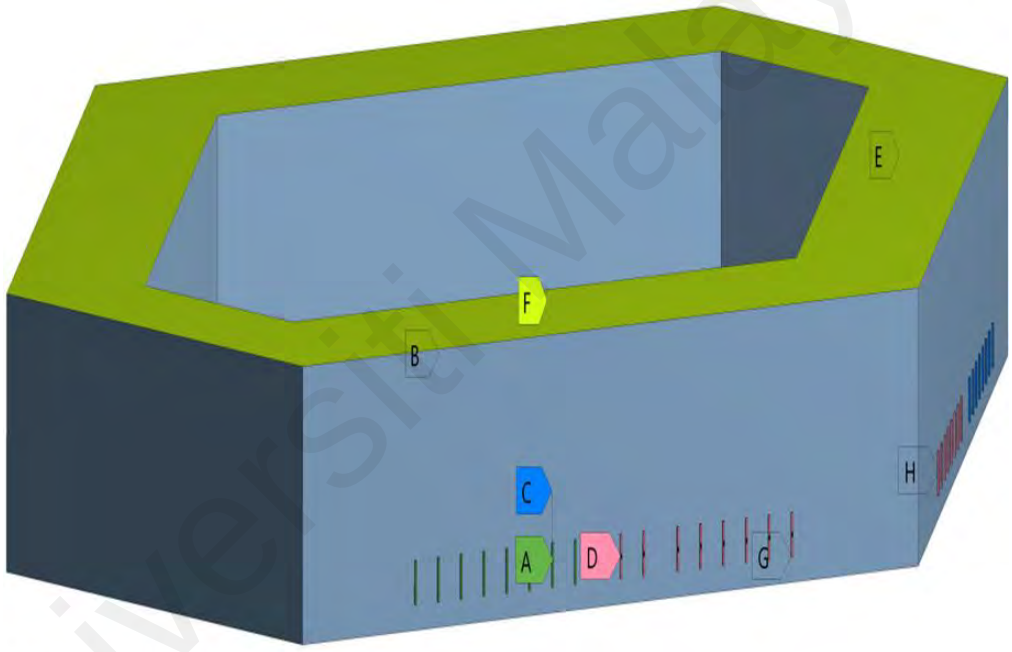

A=Return outlet, B=Floor, C=Plenum box
D=Supply inlet, E=Glass ceiling, F=Back wall
G=Diffuser grille, H=Front wall

(a)

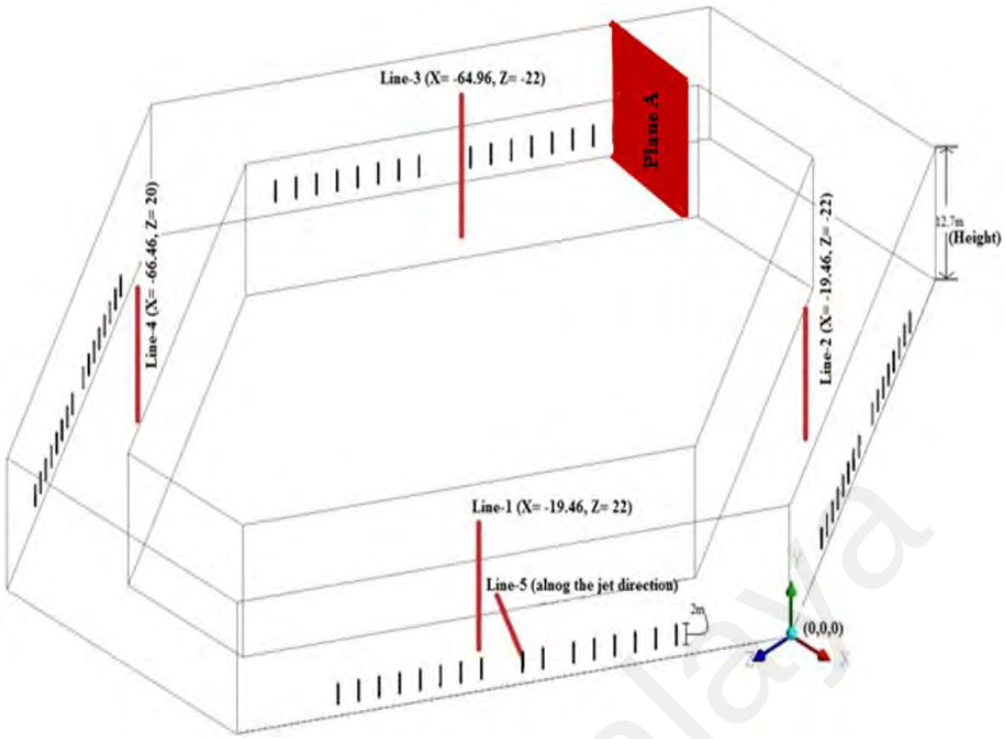

(b)

Figure 9.9: (a) The actual model of the atrium building (b) model with vertical/horizontal measuring lines and plane

Sixty-four (64) numbers of HCLSD were installed in the atrium building, sixteen on each long sidewall. Each side of the atrium building was installed with eight supply diffusers and eight return diffusers for a uniform air supply throughout the building. This arrangement satisfies the designing needs for an air supply system that can maintain optimum room air conditioning whilst becoming an integral part of the architectural concept of the project.

Table 9.3: Boundary conditions for the simulation

Boundary	Conditions
Supply air inlet (32 Nos. HCLSD)	Airflow rate = 890 CMH Air temperature = 19°C Air velocity = 6.56 m/s
Exhaust air outlet (32 Nos. HCLSD)	Pressure outlet
Walls	Surface temp. = 28.5°C
Ceiling	Surface temp. = 27°C
Floor	Surface temp. = 27°C
Grille	Adiabatic
Plenum box	Adiabatic

(a) ***Mesh Sensitivity Analyses***

To ensure the mesh independency of the actual atrium model, the whole domain was discretized with unstructured tetrahedral mesh elements by varying the minimum/max elements and wall surface sizes. The higher cell density was used near the atrium walls, diffuser blades, and locations where higher temperature and velocity gradients were expected (as seen in Fig 9.10). Table 9.4 shows the details of the grid independence test analyses. The average volumetric temperature of the domain was considered as the verifying parameter for this test. Due to the computational limitations, a low incremental step is used in this study to generate the refined mesh. The mesh refining was continued until the volumetric average indoor temperature for consecutive mesh sizes dropped below 0.01°C. Thus, the results obtained with mesh-III were decided to be good enough for further analyses.

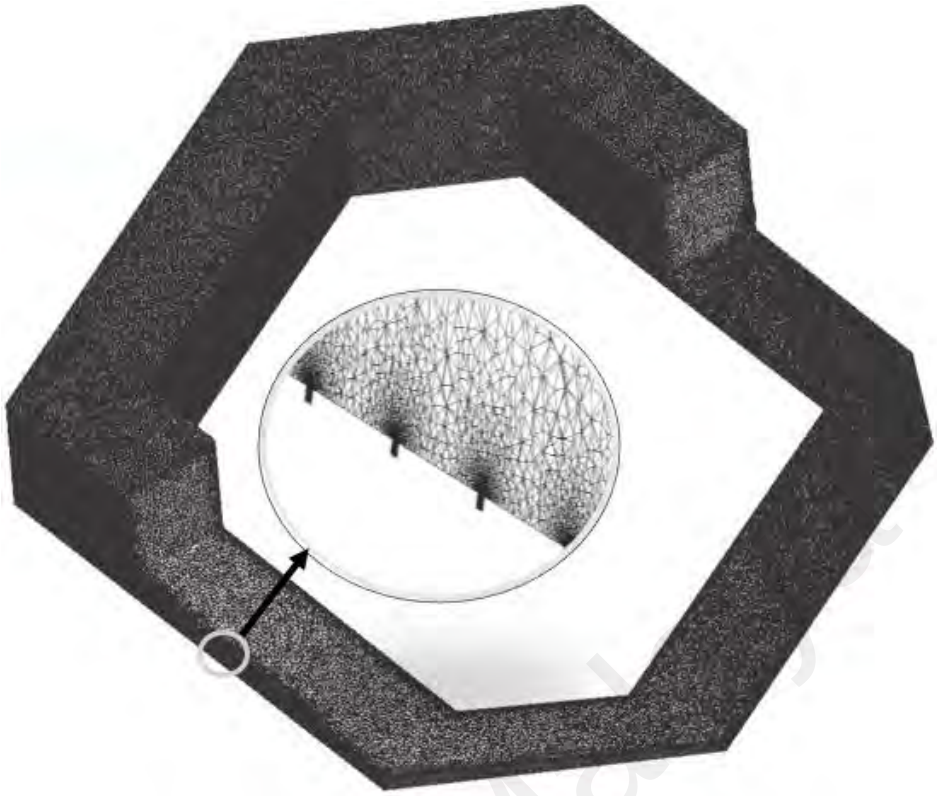

Figure 9.10: Mesh cross-section of the atrium building

Table 9.4: Grid independent test

Mesh	Element Size (Max./Min./ Diffuser) (Meters)	Total Number of Elements	Volumetric Average of the Atrium Temperature	Relative Difference
Coarse Mesh (I)	1.5/0.8/0.006	30.3 millions	25.08 °C	0.23 °C
Medium Mesh (II)	0.8/0.3/0.006	32.7 millions	25.31 °C	0.03 °C
Fine Mesh (III)	0.5/0.2/0.006	36.7 millions	25.34 °C	0.01 °C
Finer Mesh (IV)	0.5/0.1/0.006	58.2 millions	25.33 °C	

(b) ***Studied Cases***

Since the deflector angles greatly affect the airflow pattern and cause changes in the air velocity and temperature distributions (Aziz, Gad, Mohammed, & Mohammed, 2012), the performance of the HCLSD in the atrium building is investigated at different deflector angles from 0º to 25º. The deflector angles are actually the angle of inclination of the diffuser blades on the vertical plane. Different cases with HCLSD in atrium buildings using these deflector angles have been designed; Table 9.5 shows the parametric details of those cases. For a detailed understanding of the readers, the geometries of the diffuser with various deflector angles are also presented in Figure 9.11. The CFD simulation for each case is modelled and computed sequentially during the investigations.

Table 9.5: Parameters of six cases

Cases	Effective opening width of the HCLSD (mm)	Deflector (Blade) angle (ϕ)
Case-1	40.0	0
Case-2	34.8	5
Case-3	29.8	10
Case-4	25.0	15
Case-5	19.6	20
Case-6	14.8	25

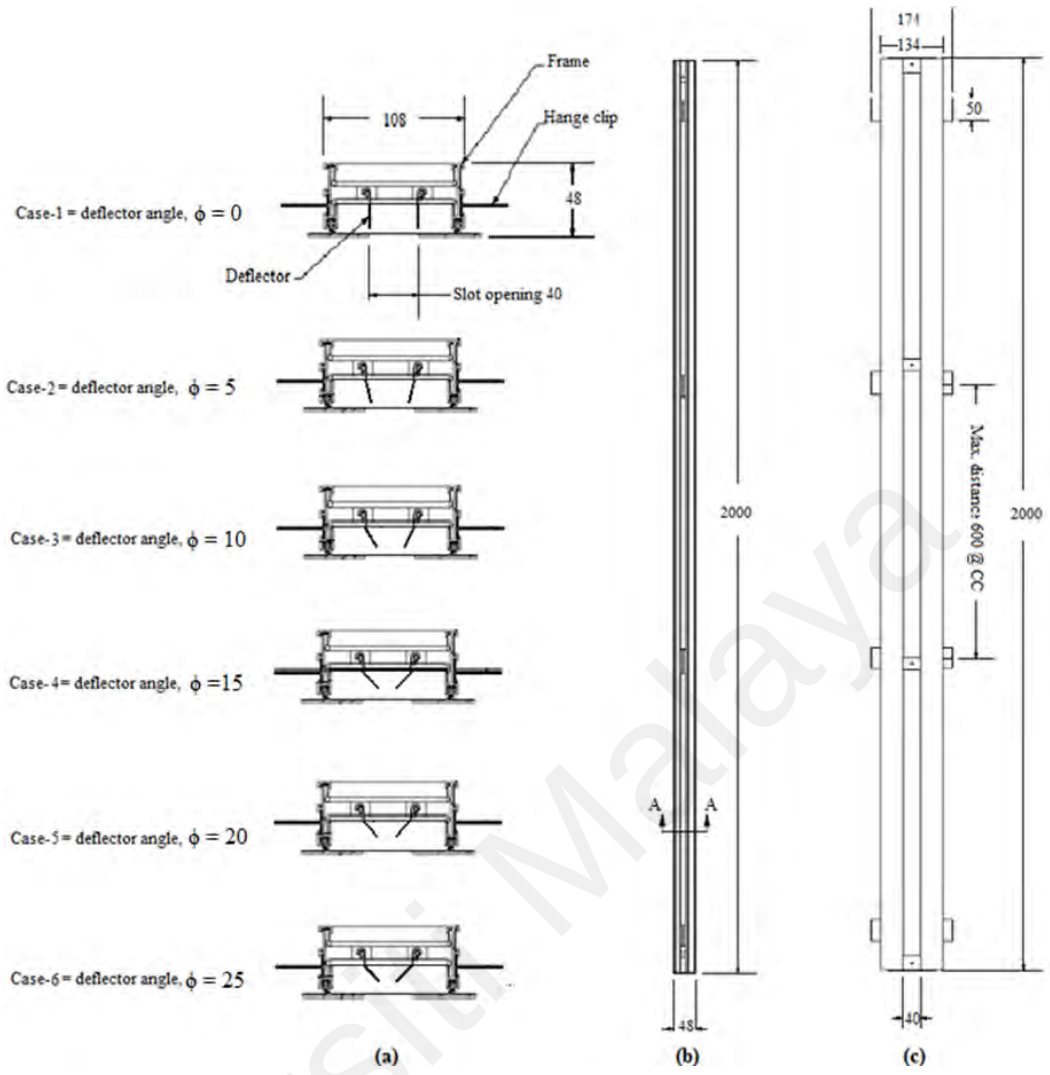

Figure 9.11: Geometrical model of the HCLSD (a) section A-A with different deflector angles, (b) side view and (c) front view (all measurements are in mm)

9.4 Results and Discussion

With the verified and validated CFD model, the effect of the deflector angles, the temperature field distribution, and the airflow pattern inside the actual atrium building were numerically investigated. The performance of the HCLSD in the atrium building was evaluated using different deflector angles along the measuring lines and on the sectional planes.

9.4.1 Effect of Deflector Angle on HCLSD Performance

The effect of six values of the deflector angles, such as 0º, 5º, 10º, 15º, 20º, and 25º, is investigated at constant airflow supply where the inlet velocity is 6.56 m/s; inlet

temperature is 19ºC, isothermal ceiling at 27ºC and isothermal walls at 28.5ºC. Their effect on the HCLSD performance was measured and compared in terms of vertical temperature and velocity distributions from floor to ceiling height of the atrium.

Figure 9.12 represents the measured values for studied cases. It can be seen that the temperature distributions in the studied cases (0º - 25º angles) have almost similar profile establishment at all measuring locations. However, the case with 0º deflector angle has induced a slightly higher airflow velocity of about ≤0.22 m/s at the lower level of the measuring locations (L1-L4). Overall, a uniform temperature stratification is generated with the low-level air supply in the studied atrium, as shown in Figure 9.13(a)-(d).

As shown in Figure 9.13, the primary airflow in the case of 0º–deflector developed higher velocity entrainment of more than 33% than the other cases at the diffuser face. The airflow velocity in the 0º case remained slightly higher along with the throw distance and coincided with the other cases after an 8m distance from the diffuser. This case is thus considered for further investigations.

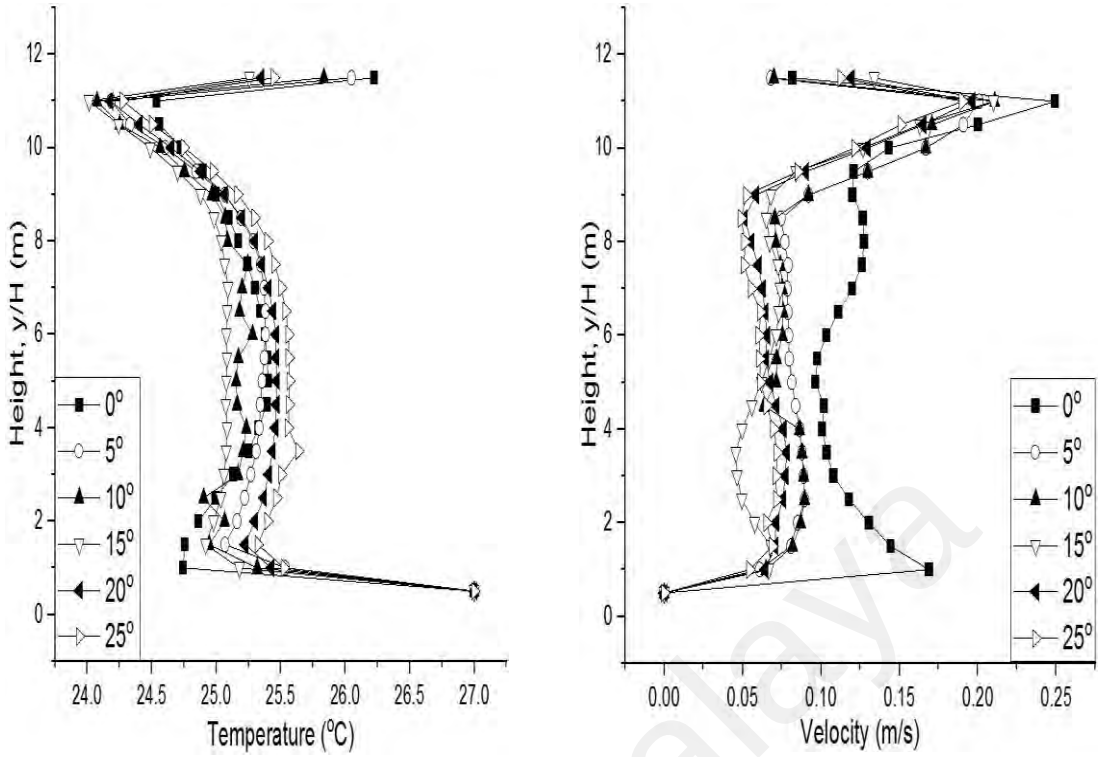

(a)

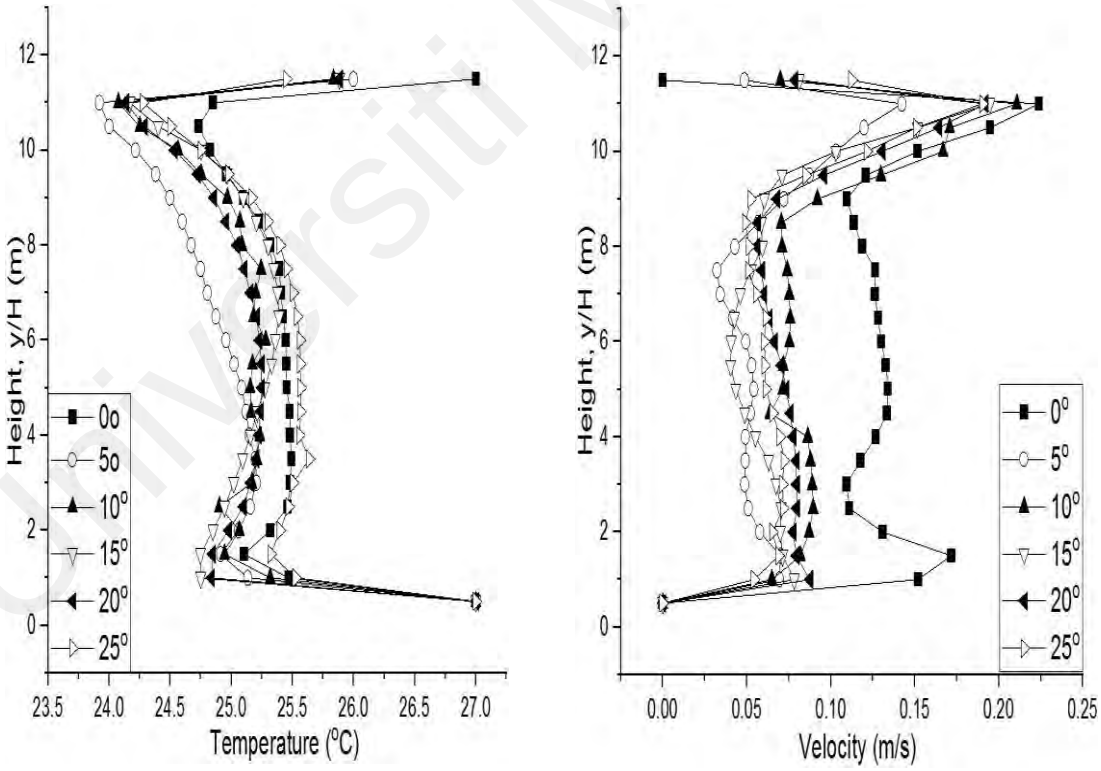

(b)

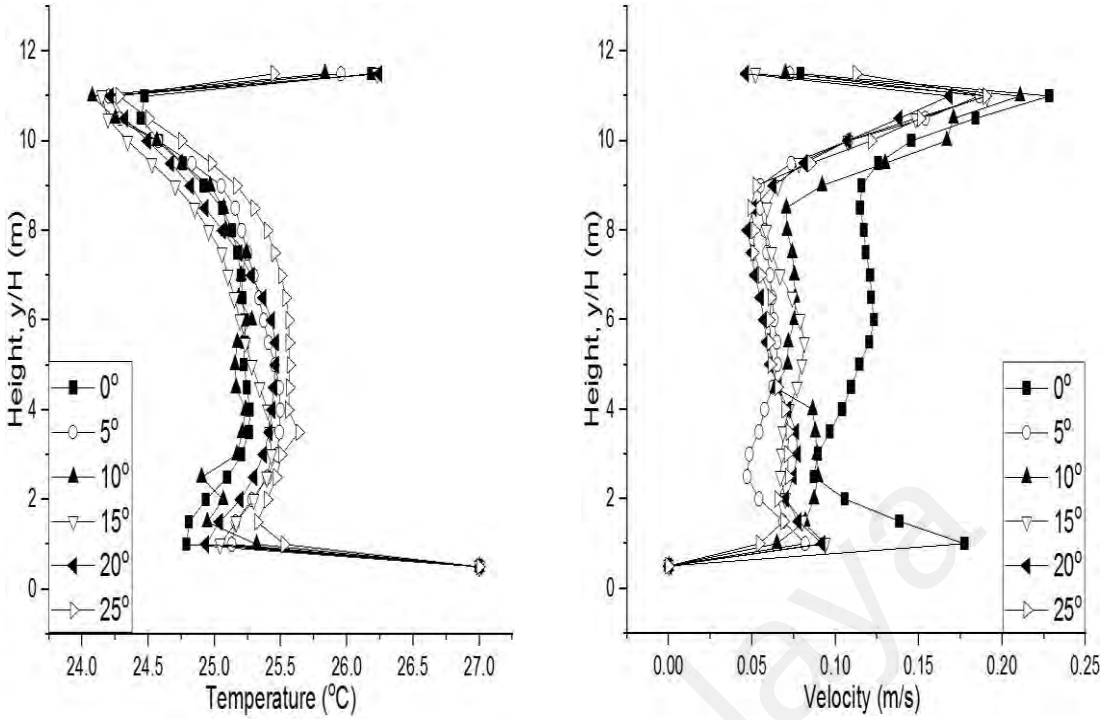

(c)

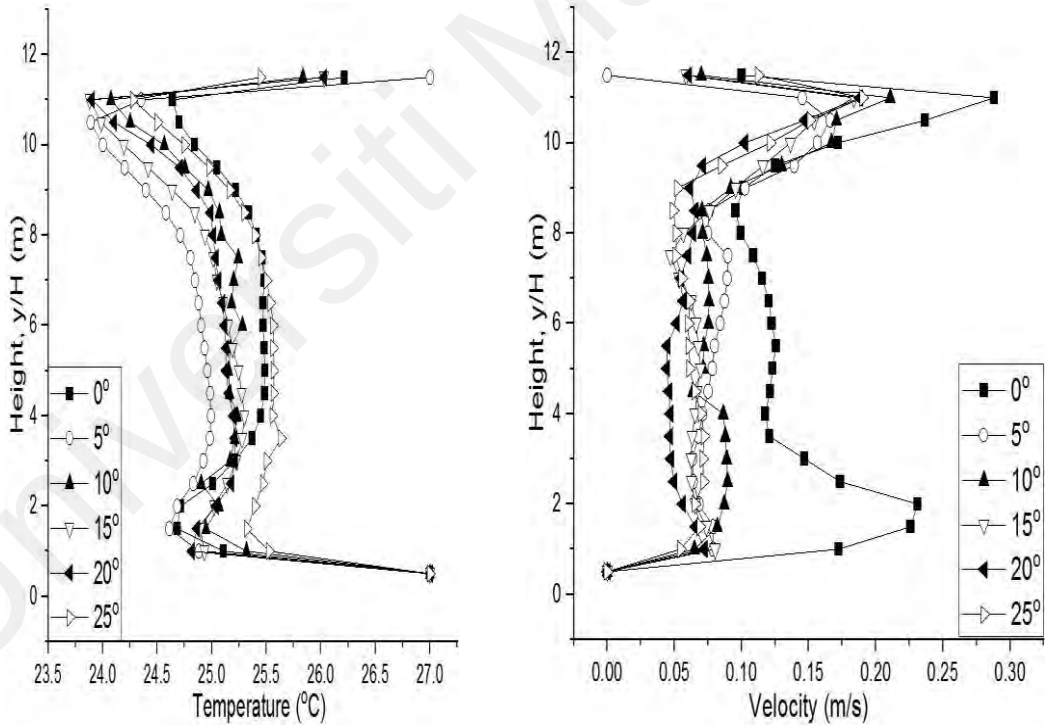

(d)

Figure 9.12: Effect of deflector angles (ϕ = 0° to 25°) on the performance of HCLSD in studied atrium (a)Line 1, (b)Line 2, (c)Line 3 and (d)Line 4

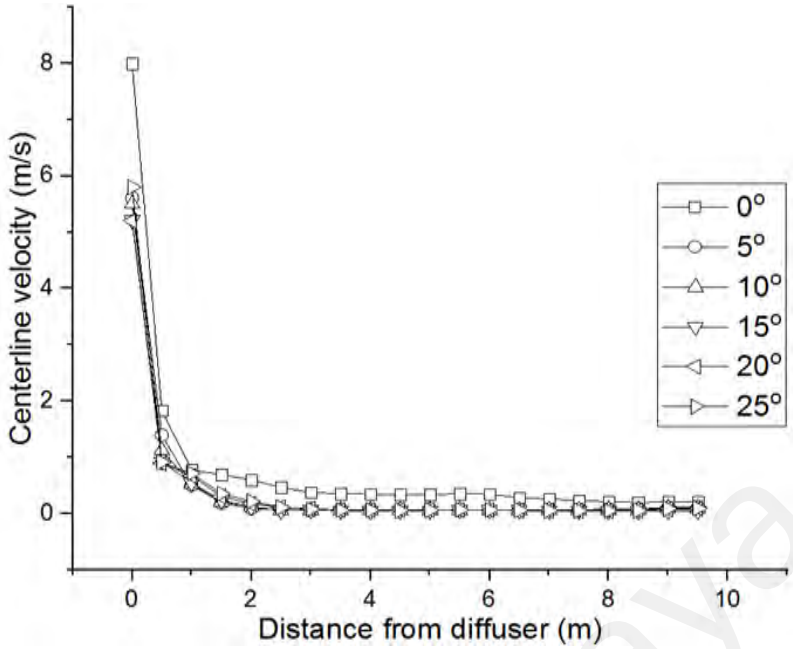

Figure 9.13: Effect of deflector angles (ϕ = 0º to 25º) on the throw performance

9.4.2 Effect on Temperature Field Distribution (Case-1, ϕ = 0º)

The results obtained in case-1 for temperature field distribution on different sectional planes inside the actual domain were numerically illustrated in Figure 9.14. Plane A (marked in Figure 9.9(b)) was along the direction of the airflow from the diffuser. Plane B (ZX Plane, Y= 2.16m at the mid-height of the diffuser) and Plane C ((ZX Plane, Y= 7.96m) were perpendicular to the height of the atrium model.

As shown in Plane A in Figure 9.14, a stratified thermal plume was developed in the lower zone of the atrium building. After making contact with the opposite wall, the flow plume moves upward alongside the wall and returns to the supply. The temperature distribution of airflow through all the supply diffusers is shown in Figure 9.14(b). A lower temperature zone was created in front of the supply diffuser, whereas an effective thermal diffusion was also observed on the entire plane.

A slightly higher temperature was recorded in the zones far away from the supply inlets. To provide a comfortable thermal environment to the occupants, the air supply inlets are required to be installed in those areas as well.

(a)

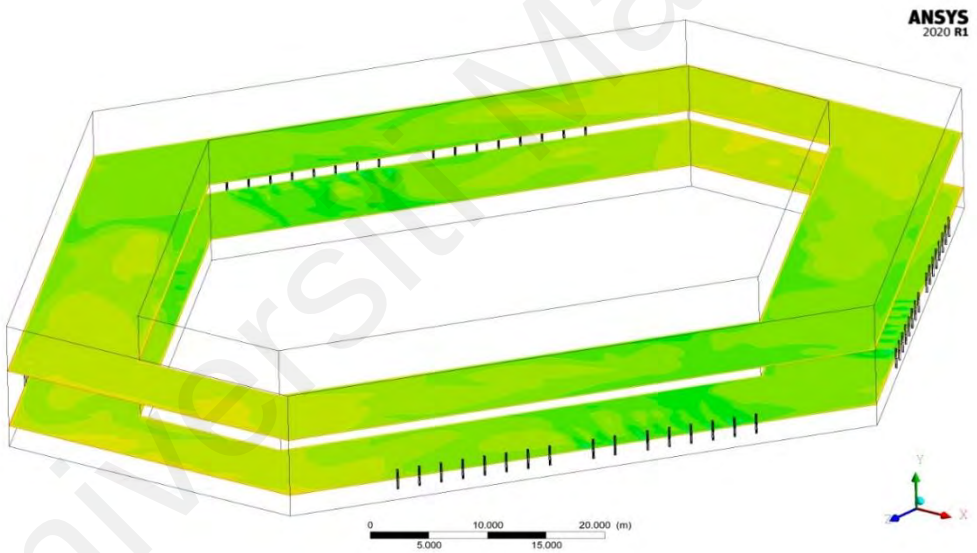

(b)

Figure 9.14: Temperature contours in the atrium space (Case-1) (a) Plane A and (b) Plane B&C

9.4.3 Effect on Airflow Distribution (Case-1, $\phi = 0^{o}$)

The airflow distribution for case-1 in the atrium building was presented through velocity fields on the aforementioned planes, streamlined directions and velocity vectors. Figure 9.15(a) shows the flow jet from the HCLSD. The flow profile similarity with the smoke test further validated the applied numerical model for the atrium study.

The airflow throw from all the HCLSDs can be visualized in Figure 9.15(b). A strong throw was noticed in the middle of the diffuser. After covering some horizontal distance, the flow plumes from each diffuser got combined and created a joint flow towards the opposite wall. After coming out from the diffuser, it was noticed that the air covered some horizontal distance and then fell down due to the gravitational force.

The velocity streamlines and field vectors inside the studied domain were presented in Figure 9.15(c) & (d), respectively. A proper mixing ability of the supply air in the entire atrium space was found. The strong regions were located near the diffusers, and a weak flow was detected in the other spaces of the atrium. No hot spots were found in any of the atrium regions due to the proper design of the air distribution system.

Figure 9.15(b) shows the velocity vector field on Plane B. A more uniform field was established throughout Plane B, except for the frontier region of the supply diffusers. The velocity vectors showed lower values of wind speed near the occupied zone. The area average value of the air velocity on Plane B was 0.16m/s. This value is found within the human thermal comfort range in the occupied zone.

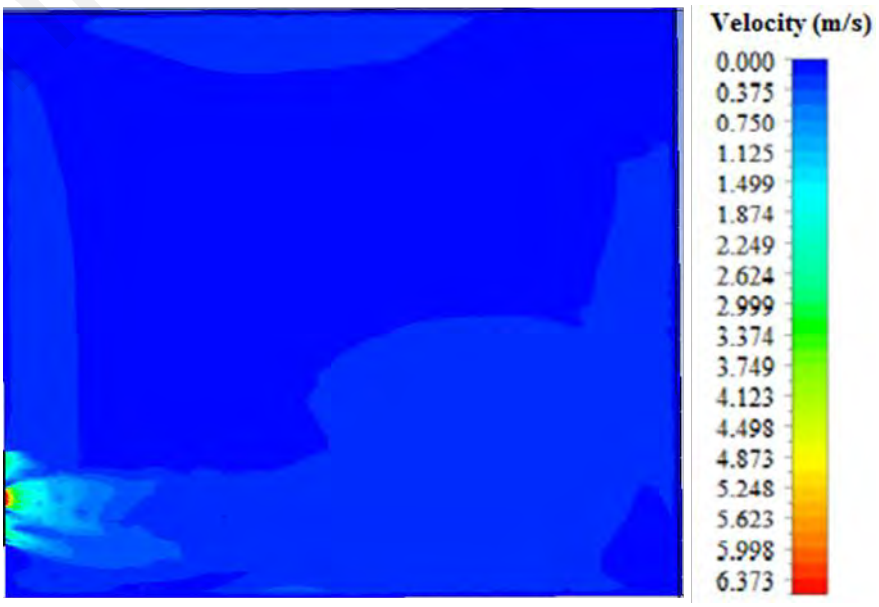

(a)

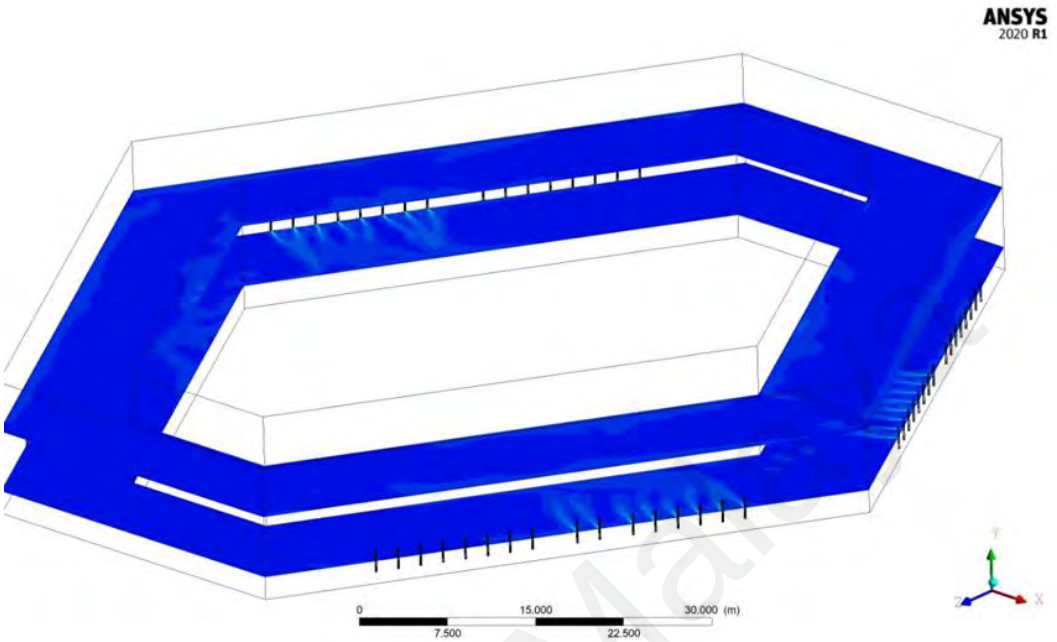

(b)

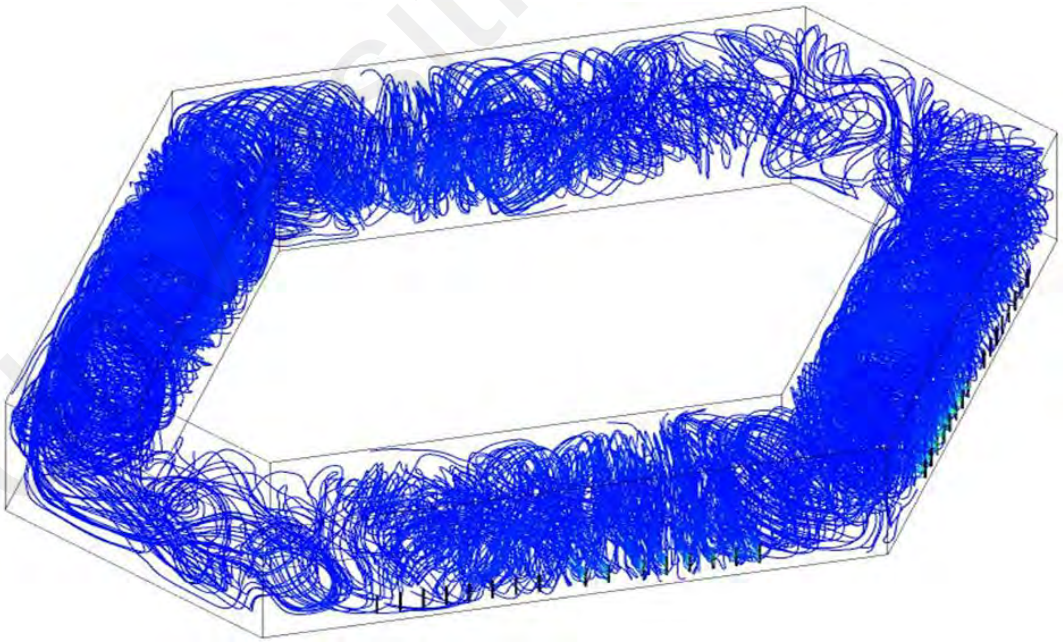

(c)

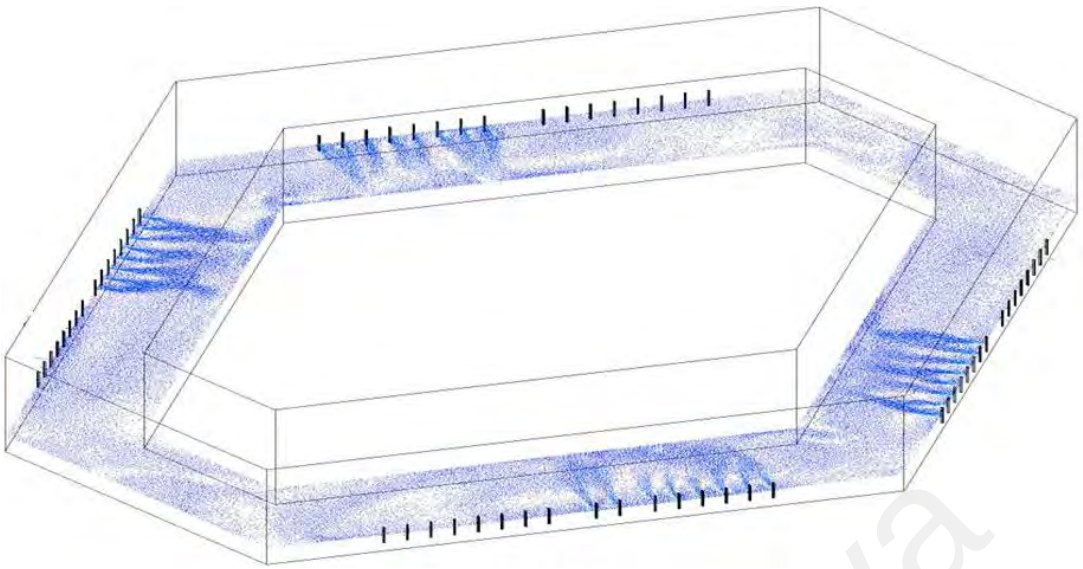

(d)

Figure 9.15: Velocity field of Plane A (b) Velocity field of Plane B&C, (c) Velocity streamlines of the model, and (d) Velocity vector of Plane B

9.4.4 Perception of Thermal Comfort (Case-1, $\phi = 0^o$)

P.O. Fanger developed the PMV/PPD model (Fanger, 1970), which uses heat-balance equations and empirical skin temperature studies to quantify thermal comfort. It is the most recognized and accepted model applied for thermal comfort studies. The PMV index range between [-0.5, +0.5] for an indoor air-conditioned environment is considered very comfortable by ISO 7730, and for just a comfortable level, the PMV index must be lied between [-1, +1]. The corresponding values for PPD against the above PMV ranges are 20% and 10%, respectively. In other words, PMV index values between [-1, +1] and [-0.5, +0.5] equate to 80% and 90% satisfaction of the indoor population, respectively. In this study, both indices were calculated in the simulation software by using UDF codes.

In Figure 9.16(a), under case-1 (when $\phi=0^o$), the PMV distribution at four locations along lines 1 to 4 are presented. The PMV values at all locations were found between +0.1 and +0.9, except for some higher points where the value exceeded a bit. A little warm sensation was noticed in the entire occupied zone of the atrium building, but it

was still within the allowable range. The higher thermal sensation (PMV=≥+0.4) was observed at locations in front of the exhaust diffusers, as seen in Figure 9.16(b).

Figure 9.17(a) shows the PPD distribution along the selected line locations. All the PPD values were found within the 20% range except for some higher points near the ceiling, where the values exceeded a bit to the comfort range. However, in the entire occupied zone of the atrium building, the PPD index was found under the required comfort range, i.e., between 4% to 20%. Figure 9.17(b) shows that some regions reached more than 20%, but that is still within the grade II comfort range, i.e., ≤27%.

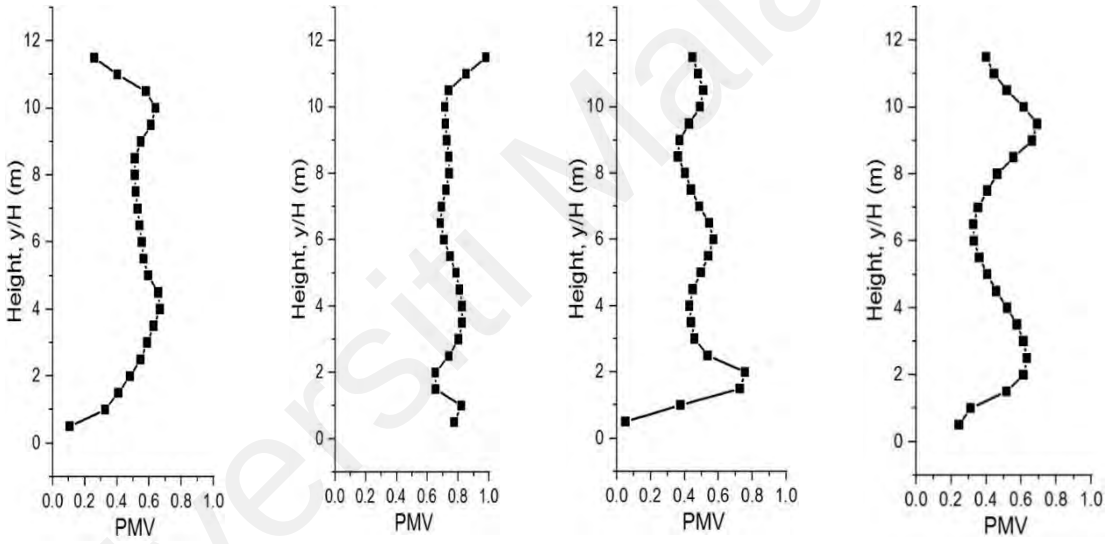

Line 1 Line 2 Line 3 Line 4

(a)

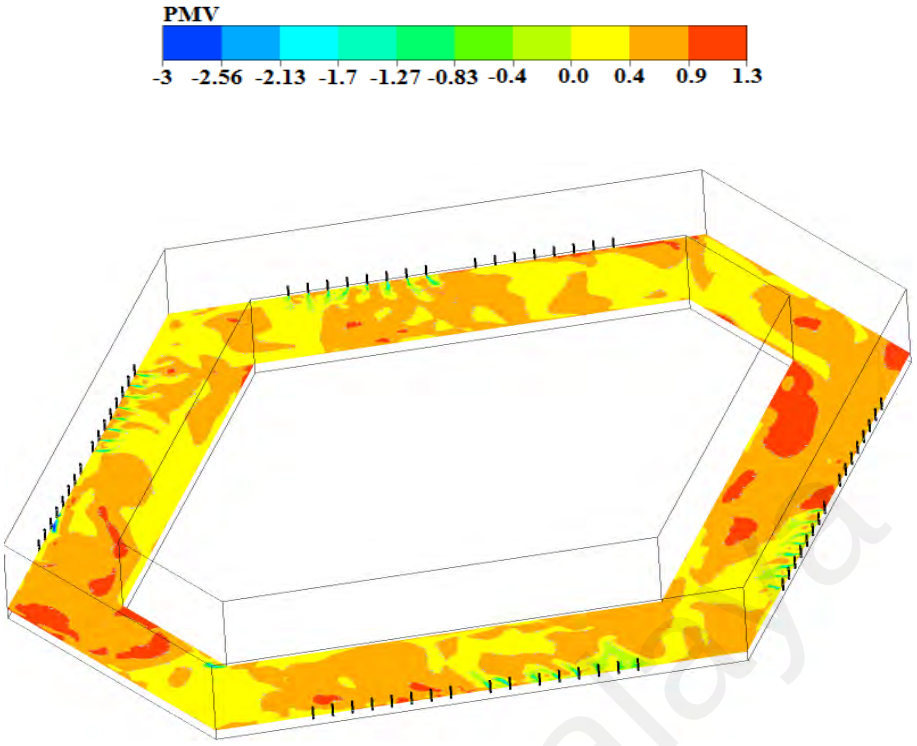

(b)

Figure 9.16: PMV distribution (a) along vertical lines (b) at plane B (Y=2.16m)

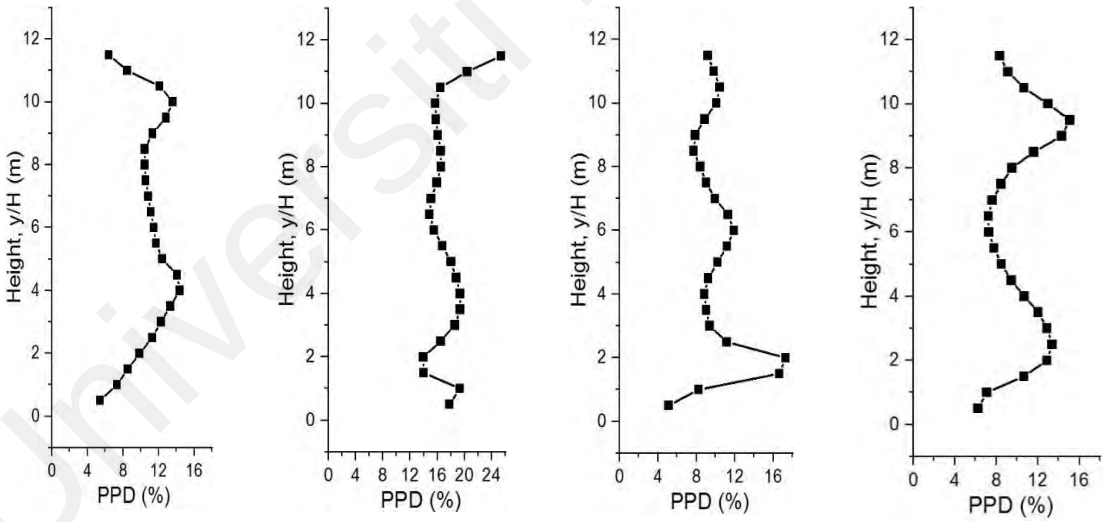

Line 1 Line 2 Line 3 Line 4

(a)

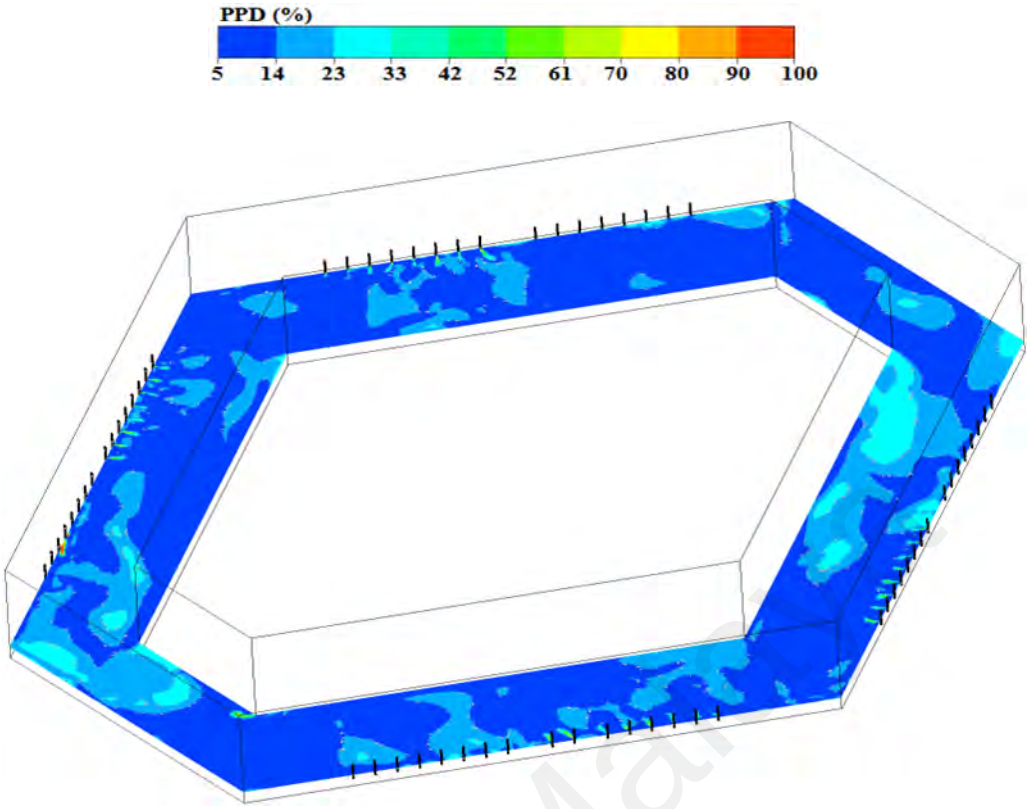

(b)

Figure 9.17: PPD distribution (a) along vertical lines (b) at plane B (Y=2.16m)

9.5 Summary

The performance of the architecturally designed, vertically-oriented high capacity linear slot diffuser (HCLSD) in a large atrium was studied with numerical simulations and physical experimentation. The experimental work was carried out in the laboratory environment with a single HCLSD installed vertically at the centre of the sidewall. The numerical results were then compared with the experimentally performed smoke test results. The RNG k-ε model best represents the numerical model of the physical environment. In the next step, the actual atrium model was developed and simulated by employing the verified and validated numerical model to investigate the HCLSD performance in the atrium. The outcome can be concluded as follows:

- No significant difference in predicted vertical temperature profiles was found among all the deflector angles. However, the case with $\phi = 0^{o}$ deflector angle was observed

with a higher airflow velocity of about ≤ 0.22 m/s at the lower level of the measuring locations (L1-L4). More than a 33% increase in the air velocity due to the 0^o deflector angle is noticed at the diffuser face.

- A good thermal distribution in the atrium space was seen due to the properly designed air supply system (at $\phi = 0^o$) with values between 24ºC - 27ºC in the entire breathing zone. The temperature of the atrium increased with the increase in the height of the domain. The average temperature within the occupied zone was found under the acceptable human thermal comfort range, with the supply air at 19ºC.
- The airflow velocity at 0^o deflector angle was also found within the acceptable range (<0.8m/s) for the entire occupied zone, except for some zones near the supply inlets. The airflow field in front of the diffusers was stronger, which decayed gradually along the throw path and reached about 0.2m/s at an 8 m distance from the diffuser.
- The PMV-PPD thermal comfort models were also evaluated using UDF codes in Ansys simulations. For both indices, the values were found within the acceptable range of thermal comfort at all measuring locations. Thus, it can be concluded that HCLSD provided better thermal comfort when installed vertically along the sidewalls of the atrium space.

CHAPTER 10: CONCLUSIONS AND FUTURE WORK

10.1 Introduction

The previous chapters have presented the design guidelines, performance evaluation and optimization, energy and nodal modelling of the VRF integrated stratum ventilation system in the tropical building. The research work can be divided into five main categories, namely, Design integration of the VRF and the stratum ventilation system, Performance evaluation of different configurations of the designed system, performance optimization of the selected design configuration, air distribution study for large tropical atrium (as case study) and the energy consumption analyses of the designed system i.e., VRF-SV hybrid system.

The findings of this complete thesis are summarized below based on the above-mentioned categories.

10.2 Performance Evaluation: Different Configurations

- Two ventilation integration design strategies (i.e. coupled (fully-integrated) and decoupled) were adopted for an in-depth understanding of the combined system performance.
- The decoupled design with configurations 1 to 4 (as discussed in Chapter 3) provided a non-uniform temperature and velocity distribution in the occupied zone, whereas the last two configurations served by the VRF-SV fully integrated design showed that the thermal comfort can be uniformly realized in the entire occupied zone.
- The results revealed from configurations 5 and 6 confirmed a good potential of the VRF-SV integrated design to be employed in large ACMV applications in the tropics.

- The indoor air velocity was modest in the work zone of the retail facility and has not exceeded 0.8 m/s throughout the zone, and thus, it complies with the standard ASHRAE 55-2020 (ASHRAE, 2020).
- The thermal gradient was found positive and under an acceptable range between the head and foot level for standing occupants.
- Both the simulation results and experimental assessment suggest that the thermal environment created in the occupied zone by the VRF-SV fully integrated design can be treated as uniform with energy saving potentials.

10.3 Performance Optimization: Selected Configuration

10.3.1 Experimental Study

- In this part of study, the air distribution and thermal comfort performance of the VRF-SV hybrid system with five types of air supply terminal devices (ASTDs) i.e., bar grille, double deflection grille, perforated diffuser, drum louvre and linear slot diffusers were successfully investigated through laboratory based experiments.
- The higher outflow of about 30% was observed when the supply air entry was in line with the flow direction with collar attachment on the front face of the plenum box (Front collar orientation) compared to the other orientations.

Based on the detailed experimental results, the author of this thesis concluded that:

- Uniform temperature distribution at all locations was created with bar grille diffuser, while the temperature value fluctuated at about 22.5 °C.
- Influential or distinct performance in terms of velocity distribution was not observed with any of the studied diffuser types.
- The ADPI for the bar grille was calculated as 92.8%. The ADPI values for all other ASTD types fell below the minimum required range.

- The thermal sensation and comfort survey suggested that the bar grille provided a better thermal environment than all other diffuser types. For the bar grille case, 70% of the subjects graded the thermal sensation as slightly cool, whereas 60% rated the thermal comfort as comfortable.
- The airflow visualization using smoke tests showed a longer airflow throw in the case with double deflection grille, while the flow in the perforated diffuser case was shorter and highly diffusive. The jet entrainment with the bar grille case was uniform and moderate.

10.3.2 Numerical Study

- In this part of study, the ventilation performance of all the ASTDs explained in section 10.4.1 except the perforated diffuser was investigated under the actual laboratory and meeting room environments.
- The functional performance of the ASTDs was evaluated on three aspects: airflow distribution and pattern, thermal comfort and indoor air quality and it was concluded that the ASTDs have considerable impact on the performance of mechanical ventilation system regardless of the indoor environment type.
- Based on all evaluation indices, the air diffusion performance using the bar grille terminal type was found entirely within the acceptable range.
- Among all, the jet slot diffuser performed worst in providing thermal comfort for the occupant and airflow distribution into the space. Whereas, the drum louver diffuser performance was found poorer in terms of IAQ for the entire breathing zone.
- Under the similar initial and boundary conditions, the air age within the complete occupied zone in double deflection grille case was found younger than that of all other diffuser types.
- However, the lowest CO_2 concentration in the breathing zone is obtained under the bar grille diffuser case.

- Above all, the VRF-SV system installed with the bar grille as ASTD can provide better thermal comfort, improved IAQ and uniform temperature and velocity distribution. Thus, the bar grille is recommended to be used in small-to-large size applications if installed with VRF-SV hybrid system.

10.4 Nodal and Energy Modelling: VRF-SV Hybrid System

The outcome of this study can be concluded as follows:

10.4.1 Simplified Nodal Modelling

- The huan's model (Huan et al., 2018) was developed as a reference model based on the airflow direction for the wall and ceiling exhaust configuration of the VRF-SV hybrid system in a large retail shop facility.
- The reference model provided inaccurate prediction of the vertical temperature profiles for both of the studied cases.
- Then, the model was modified following the airflow streamlines directions for both cases and found that the modified models provided accurate predictions of the vertical temperature profile. Thus, recommended to be used in prediction of vertical temperature profile for energy and load calculation in large SV applications.

10.4.2 Energy Modelling: TRNSYS Simulation

- The simulation with split type AC system was considered as the baseline simulation. That AC system was then replaced with VRF, VRF-SV decoupled and VRF-SV fully integrated systems in the successive simulation models.
- The simulated results of all of the models are based on the energy consumption at many outdoor temperatures (bin temperatures) distributions for every 4 hours shifts in Petaling Jaya, Malaysia for the years 2007 to 2016 (refer Figure 9.1).

- The simulation results for all of the ACMV systems are divided into occupied and unoccupied periods, where the occupied period is 3650 hours and the unoccupied period is 5110 hours.
- The simulated results for the ACMV systems are quantitatively calculated by multiplying the frequencies for every midpoint of the bin temperature interval with the energy consumption at each of the midpoint of the bin temperature interval and then, the results of the occupied and unoccupied periods are totalized for each system.
- It was found that the highest energy consumption occurred in all of the simulated cases when the bin temperature interval was 31°C. This is because of the inverse impact of the outdoor temperature on the performance of the ACMV systems.
- The total energy consumption by any of the ACMV system at higher temperature such as 33ºC and 36ºC is comparatively low due to the low frequencies of these bin temperature intervals.
- The results of this study revealed that the annual energy consumption when the building is installed with VRF system or VRF-SV decoupled system are lowest compared to the other two ACMV systems in almost every midpoint of the bin temperature interval. However, the VRF-SV decoupled system found most suitable and efficient as it comes with fresh outdoor air for ventilation.
- The overall annual energy consumption for the VRF-SV decoupled system and the VRF only system is 63401.6 kWh and 71010.6 kWh, respectively, where the difference is 7609 kWh (i.e. around 10.7%) which is due to the use of heat recovery devices (enthalpy and sensible wheels) in the former system.
- The fully integrated design of the VRF-SV hybrid system performed worst in energy consumption due to the conditioning of excessive amount of supplied air (mixture of OA and RA streams).

10.5 Air Distribution Performance Study: Large Atrium Building as Case Study

The performance of the architecturally designed, vertically-oriented high capacity linear slot diffuser (HCLSD) in a large atrium was also studied as a part of this thesis using numerical simulations and physical experimentation. The actual atrium model was developed and simulated by employing the verified and validated numerical model for the in-depth investigation of the HCLSD performance at different deflector angles (0^o to 25^o) in the atrium building. The outcome can be concluded as follows:

- No significant difference in predicted vertical temperature profiles was found among all the deflector angles. However, the case with $\phi = 0o$ deflector angle was observed with higher airflow velocity of about ≤ 0.22 m/s at the lower level of the measuring locations.
- More than 33% increase in the air velocity due to the 0^o deflector angle is noticed at the diffuser face.
- A good thermal distribution in the atrium space was seen due to the properly designed air supply system (at $\phi = 0^o$) with values between 24^oC - 27^oC in the entire breathing zone. The temperature of the atrium increased with the increase in the height of the domain. The average temperature within the occupied zone was found under the acceptable human thermal comfort range with the supply air at 19^oC.
- The airflow field in front of the diffusers was stronger, which decayed gradually along the throw path and reaches about 0.2m/s at 8 m distance from diffuser.

10.6 Future Work and Recommendations

The present research work has investigated the performance of VRF-SV hybrid system in terms of airflow distribution, thermal comfort assessment and energy consumption. This research was conducted considering a large building in the tropical

climate of Kuala Lumpur, Malaysia. Therefore, it is an effective step towards assessing the potential of VRF integrated mechanical ventilation systems in tropical buildings. However, this research can further be improved by considering following recommendations,

- In terms of design, as already described in this thesis, coupled (integrated) and decoupled strategies were used in integration of VRF and SV systems. Therefore, further study in this direction could be performed by using different design strategies for getting more energy efficient solutions of the combined system for tropical buildings.
- The performance of the designed VRF-SV hybrid system in a retail shop building in the tropical climate was investigated. The hybrid system was modelled and simulated in the case study building. The performance of the hybrid system was evaluated based on the desired indoor and idealistic outdoor conditions. According to the results, this study justifies the performance of the designed system in terms of improved IAQ, enhanced thermal comfort and increased energy savings. However, the author recommends the actual testing of the integrated design in variety of the climatic conditions to more understand the suitability of this design to be adopted in non-tropical buildings as well. To study the effects of climate change on this novel VRF-SV hybrid system can also be a future research direction.
- In air distribution side, further research is needed to be carried out in optimization of the discharge airflow rate, supply air temperature, inlet air velocity and fresh outdoor air ratio.
- In the future, the impact of varying the SA temperature for SV and refrigerant evaporating temperature for VRF FCUs on overall energy efficiency of the VRF-SV hybrid system could also be evaluated.

- Apart from that, the design modification in the air supply diffusers can also be an insight to be explored in order to obtain a better outcome in terms of the airflow throw and thermal distribution for relatively large applications.
- Finally, the use of renewable energy resources with the advanced and smart control techniques to enhance the performance of VRF-SV hybrid system in tropical buildings can also be explored.

REFERENCES

ASHRAE 55-2004, A. A. S. (2004). Thermal environmental conditions for human occupancy. ASHRAE.

Abe, O. O., Simonson, C. J., Besant, R. W., & Shang, W. (2006). Effectiveness of energy wheels from transient measurements. Part I: Prediction of effectiveness and uncertainty. *International Journal of Heat and Mass Transfer, 49*(1), 52-62. doi:https://doi.org/10.1016/j.ijheatmasstransfer.2005.08.002

Acosta, I., Varela, C., Molina, J. F., Navarro, J., & Sendra, J. J. (2018). Energy efficiency and lighting design in courtyards and atriums: A predictive method for daylight factors. *Applied Energy, 211*, 1216-1228. doi:https://doi.org/10.1016/j.apenergy.2017.11.104

Afify, R. (2008). Designing VRF Systems. *ASHRAE Journal, June 2008.*

Ahmadzadehtalatapeh, M. (2011). *Measurements And Modeling Of The Horizontal Heat Pipe Heat Exchangers For Saving Energy And Improving Thermal Comfort In Air-Conditioning Systems In The Tropics.* (Ph.D), University of Malaya, Malayisa.

Al-Waked, R., Nasif, M., Groenhout, N., & Partridge, L. (2021). Natural ventilation of residential building Atrium under fire scenario. *Case Studies in Thermal Engineering, 26*, 101041. doi:https://doi.org/10.1016/j.csite.2021.101041

Alahmer, A., & Alsaqoor, S. (2018). Simulation and optimization of multi-split variable refrigerant flow systems. *Ain Shams Engineering Journal, 9*(4), 1705-1715. doi:10.1016/j.asej.2017.01.002

Ameen, A., Choonya, G., & Cehlin, M. (2019). Experimental Evaluation of the Ventilation Effectiveness of Corner Stratum Ventilation in an Office Environment. *Buildings, 9*(7). doi:10.3390/buildings9070169

Ammi Amarnath, & Morton Blatt. (2008). Variable Refrigerant Flow: An Emerging Air Conditioner and Heat Pump Technology. *ACEEE Summer Study on Energy Efficiency in Buildings*.

ANSI/ASHRAE-62.1. (2019). Ventilation for Acceptable Indoor Air Quality. *ASHRAE*.

ANSI/ASHRAE. (2017). Thermal Environmental Conditions for Human Occupancy (Standard 55-2017).

Ansys. (2015). *ANSYS Fluent Theory Guide*

ASHRAE. (2010). ASHRAE-55-2010, Thermal Environmental Conditions for Human Occupancy. *American Society of Heating, Refrigerating and Air-Conditioning Engineers, Inc. Atlanta, U.S.A-2010*.

ASHRAE. (2013). Ventilation for Acceptable Indoor Air Quality.

ASHRAE. (2015). ASHRAE Design Guide for Dedicated Outdoor-Air Systems.

ASHRAE. (2019). Ventilation for Acceptable Indoor Air Quality. In *ANSI/ASHRAE Standard 62.1-2019*.

ASHRAE. (2020). ASHRAE 55-2020. In *Thermal Environmental Conditions for Human Occupancy*

ASHRAE Handbook-Fundamentals. (2017). *ASHRAE*.

Awbi, H. B. (2015). Ventilation and Air Distribution Systems in Buildings. *Frontiers in Mechanical Engineering, 1*. doi:10.3389/fmech.2015.00004

Aynur, T. N., Hwang, Y., & Radermacher, R. (2008a). Experimental Evaluation of the Ventilation Effect on the Performance of a VRV System in Cooling Mode—Part I: Experimental Evaluation. *HVAC&R Research, 14*(4), 615-630. doi:10.1080/10789669.2008.10391029

Aynur, T. N., Hwang, Y., & Radermacher, R. (2008b). Simulation Evaluation of the Ventilation Effect on the Performance of a VRV System in Cooling Mode—Part II, Simulation Evaluation. *HVAC&R Research, 14*(5), 783-795. doi:10.1080/10789669.2008.10391039

Aynur, T. N., Hwang, Y., & Radermacher, R. (2010a). Integration of variable refrigerant flow and heat pump desiccant systems for the cooling season. *Applied Thermal Engineering, 30*(8), 917-927. doi:https://doi.org/10.1016/j.applthermaleng.2010.01.002

Aynur, T. N., Hwang, Y., & Radermacher, R. (2010b). Integration of variable refrigerant flow and heat pump desiccant systems for the cooling season. *Applied Thermal Engineering, 30*(8-9), 917-927. doi:10.1016/j.applthermaleng.2010.01.002

Azad, A. S., Rakshit, D., Wan, M. P., Babu, S., Sarvaiya, J. N., Kumar, D. E. V. S. K., . . . Seoh, A. (2018). Evaluation of thermal comfort criteria of an active chilled beam system in tropical climate: A comparative study. *Building and Environment, 145*, 196-212. doi:10.1016/j.buildenv.2018.09.025

Aziz, M. A., Gad, I. A. M., Mohammed, E. S. F. A., & Mohammed, R. H. (2012). Experimental and numerical study of influence of air ceiling diffusers on room air flow characteristics. *Energy and Buildings, 55*, 738-746. doi:10.1016/j.enbuild.2012.09.027

Baglivo, C. (2021). Dynamic Evaluation of the Effects of Climate Change on the Energy Renovation of a School in a Mediterranean Climate. *Sustainability, 13*(11). doi:10.3390/su13116375

Bakker, P. (2013). *Energy Efficiency in Buildings*. Retrieved from

Beggs, C. B., Kerr, K. G., Noakes, C. J., Hathway, E. A., & Sleigh, P. A. (2008). The ventilation of multiple-bed hospital wards: review and analysis. *Am J Infect Control, 36*(4), 250-259. doi:10.1016/j.ajic.2007.07.012

Berlanga, F. A., de Adana, M. R., Olmedo, I., Villafruela, J. M., San José, J. F., & Castro, F. (2018). Experimental evaluation of thermal comfort, ventilation performance indices and exposure to airborne contaminant in an airborne infection isolation room equipped with a displacement air distribution system. *Energy and Buildings, 158*, 209-221. doi:10.1016/j.enbuild.2017.09.100

Bhatia, A. *Cooling Load Calculations and Principles*. Retrieved from

Brager, G. S., & de Dear, R. J. (1998). Thermal adaptation in the built environment: a literature review. *Energy and Buildings, 27*(1), 83-96. doi:https://doi.org/10.1016/S0378-7788(97)00053-4

Brauer, H. (1973). Mathematical Models of Turbulence. Von B. E. Launder u. D. B. Spalding. Academic Press, London–New York 1972. 1. Aufl., V, 169 S., zahlr. Abb., geb., £ 2.50. *Chemie Ingenieur Technik, 45*(3), 143-143. doi:https://doi.org/10.1002/cite.330450309

Chen, A., & Chang, V. W. C. (2012). Human health and thermal comfort of office workers in Singapore. *Building and Environment, 58*, 172-178. doi:https://doi.org/10.1016/j.buildenv.2012.07.004

Chen, H. (2014). Experimental and numerical investigations of a ventilation strategy – impinging jet ventilation for an office environmen. *Linköping Studies in Science and Technology Dissertation No. 1606*.

Chiang, W.-H., Wang, C.-Y., & Huang, J.-S. (2012). Evaluation of cooling ceiling and mechanical ventilation systems on thermal comfort using CFD study in an office for subtropical region. *Building and Environment, 48*, 113-127. doi:10.1016/j.buildenv.2011.09.002

Choi, J.-H., Loftness, V., & Aziz, A. (2012). *Post-occupancy evaluation of 20 office buildings as basis for future IEQ standards and guidelines*.

Chow, T. T., Fong, K. F., Givoni, B., Lin, Z., & Chan, A. L. S. (2010). Thermal sensation of Hong Kong people with increased air speed, temperature and humidity in air-conditioned environment. *Building and Environment, 45*(10), 2177-2183. doi:10.1016/j.buildenv.2010.03.016

Chung, M. H., Yang, Y. K., Lee, K. H., Lee, J. H., & Moon, J. W. (2017). Application of artificial neural networks for determining energy-efficient operating set-points of the VRF cooling system. *Building and Environment, 125*, 77-87. doi:https://doi.org/10.1016/j.buildenv.2017.08.044

Conceicao, E., Rosa, S., Custodio, A., Andrade, R., Meira, M., Manuela, M., & Lucio, J. R. (2010). Study of Airflow around Occupants Seated in Desks Equipped with Upper and Lower Air Terminal Devices for Slightly Warm Environments. *HVAC&R Research, 16*(4), 401-412. doi:10.1080/10789669.2010.10390912

Control., E. C. f. D. P. a. (2020). Heating, ventilation and air-conditioning systems in the context of COVID-19: first update. *European Centre for Disease Prevention and Control*.

Coussirat, M., Guardo, A., Jou, E., Egusquiza, E., Cuerva, E., & Alavedra, P. (2008). Performance and influence of numerical sub-models on the CFD simulation of free and forced convection in double-glazed ventilated façades. *Energy and Buildings, 40*(10), 1781-1789. doi:https://doi.org/10.1016/j.enbuild.2008.03.009

CR-1752. (1999). Ventilation for buildings - Design criteria for the indoor environment. *CEN, Brussels*.

Daghigh, R. (2015). Assessing the thermal comfort and ventilation in Malaysia and the surrounding regions. *Renewable and Sustainable Energy Reviews, 48*, 681-691. doi:10.1016/j.rser.2015.04.017

DAIKIN. (2019). VRF product catalog. *DAIKIN North America LLC, USA*.

de Dear, R. J., Leow, K. G., & Foo, S. C. (1991). Thermal comfort in the humid tropics: Field experiments in air conditioned and naturally ventilated buildings in Singapore. *International Journal of Biometeorology, 34*(4), 259-265. doi:10.1007/bf01041840

Dennis, A. (2017). Global trends in thermal comfort in air conditioned and naturally ventilated offices in six climates. *MS thesis, Indoor Environmental Quality (IEQ), UC Berkeley*.

Department of Energy, U. (2015). An assessment of energy technologies and research oppertunities. *Quadrennial Technology Review*.

Devecioğlu, A. G., & Oruç, V. (2020). Energetic performance analysis of R466A as an alternative to R410A in VRF systems. *Engineering Science and Technology, an International Journal, 23*(6), 1425-1433. doi:https://doi.org/10.1016/j.jestch.2020.04.003

Ejaz, A., Jamil, F., & Ali, H. M. (2022). A novel thermal regulation of photovoltaic panels through phase change materials with metallic foam-based system and a concise comparison: An experimental study. *Sustainable Energy Technologies and Assessments, 49*, 101726. doi:10.1016/j.seta.2021.101726

Electric, M. (2018). DOAS and VRF: Applying Systems for High-Performance Buildings.

Elliott, M. S., & Rasmussen, B. P. (2013). Decentralized model predictive control of a multi-evaporator air conditioning system. *Control Engineering Practice, 21*(12), 1665-1677. doi:10.1016/j.conengprac.2013.08.010

Ellis, F. P. Thermal comfort in warm and humid atmospheres; observations on groups and individuals in Singapore. (0022-1724 (Print)). doi:D - CLML: 5425:17714:112:226 OTO - NLM

EN-15251. (2006). Indoor environmental input parameters for design and assessment of energy performance of buildings addressing indoor air quality, thermal environment lighting and acoustics. *CEN, Brussels*.

Enteria, N., Cuartero-Enteria, O., & Sawachi, T. (2020). Review of the advances and applications of variable refrigerant flow heating, ventilating, and air-conditioning systems for improving indoor thermal comfort and air quality. *International Journal of Energy and Environmental Engineering*. doi:10.1007/s40095-020-00346-0

Fanger, P. O. (1970). *Thermal comfort. Analysis and applications in environmental engineering*: Copenhagen: Danish Technical Press.

Feit, J. (2019). The Emergence of VRF as a Viable HVAC Option. *BUILDINGS Podcast*.

Felix, M., & Elsamahy, E. (2017). The Efficiency of Using Different Outer Wall Construction Materials to Achieve Thermal Comfort in Various Climatic Zones. *Energy Procedia, 115*, 321-331. doi:10.1016/j.egypro.2017.05.029

Fergus Nicol, Michael Humphreys, & Susan Roaf. (2012). Adaptive Thermal Comfort: Principles andPractice, Routledge, Abingdon,.

FLUENT. (2013). ANSYS Fluent Users Guide. Canonsburg, PA.

Fong, M. L., Hanby, V., Greenough, R., Lin, Z., & Cheng, Y. (2015). Acceptance of thermal conditions and energy use of three ventilation strategies with six exhaust configurations for the classroom. *Building and Environment, 94*, 606-619. doi:10.1016/j.buildenv.2015.10.024

Fong, M. L., Lin, Z., Fong, K. F., Hanby, V., & Greenough, R. (2017). Life cycle assessment for three ventilation methods. *Building and Environment, 116*, 73-88. doi:10.1016/j.buildenv.2017.02.006

Ga, G. (1995). Evaluation of room air distribution systems using computational fluid dynamics. *Energy and Buildings*(23), 83-93.

Gebremedhin, K. G., & Wu, B. X. (2003). Characterization of flow field in a ventilated space and simulation of heat exchange between cows and their environment. *Journal of Thermal Biology, 28*(4), 301-319. doi:https://doi.org/10.1016/S0306-4565(03)00007-X

Giama, E. (2022). Review on Ventilation Systems for Building Applications in Terms of Energy Efficiency and Environmental Impact Assessment. *Energies, 15*(1). doi:10.3390/en15010098

Goetzler, W. (2017). Variable Refrigerant Flow Systems. *ASHRAE Journal*.

Guangming Chu, Yanghong Sun, Tong Jing, Yan Sun, & Sun, Y. (2017). *A Study on Air Distribution and Comfort of Atrium with Radiant Floor Heating.* Paper presented at the 10th International Symposium on Heating, Ventilation and Air Conditioning.

H. M. Hashemian, M. Hashemian, & Riggsbee, E. T. (1995). *New Sensor for Measurement of Low Air Flow Velocity*. Retrieved from Knoxville, USA:

Halibart, J., Zwolińska, K., Borowski, M., & Jaszczur, M. (2021). Analysis of the Velocity Distribution in the Plenum Box with Various Entries. *Energies, 14*(12), 3630. doi:10.3390/en14123630

Han, X., Zhang, X., Wang, L., & Niu, R. (2013). A novel system of the isothermal dehumidification in a room air-conditioner. *Energy and Buildings, 57*, 14-19. doi:https://doi.org/10.1016/j.enbuild.2012.10.039

Hirashima, S. Q. d. S., Katzschner, A., Ferreira, D. G., Assis, E. S. d., & Katzschner, L. (2018). Thermal comfort comparison and evaluation in different climates. *Urban Climate, 23*, 219-230. doi:https://doi.org/10.1016/j.uclim.2016.08.007

Hout, D. I. (1998). Air distribution for comfort and IAQ. *KRUEGER, Excellence in Air Distribution*.

Hu, S. C. (2003). Airflow characteristics in the outlet region of a vortex room air diffuser. *Building and Environment, 38*(4), 553-561. doi:https://doi.org/10.1016/S0360-1323(02)00187-7

Huan, C., Wang, F., Wu, X., Lin, Z., Ma, Z., & Wang, Z. (2018). Development of a nodal model for predicting the vertical temperature profile in a stratum-ventilated room. *Energy and Buildings, 159*, 99-108. doi:10.1016/j.enbuild.2017.10.084

Huang, C., Zou, Z., Li, M., Wang, X., Li, W., Huang, W., . . . Xiao, X. (2007). Measurements of indoor thermal environment and energy analysis in a large space building in typical seasons. *Building and Environment, 42*(5), 1869-1877. doi:https://doi.org/10.1016/j.buildenv.2006.02.016

Humphreys, M., & Hancock, M. (2007). Do people like to feel 'neutral'? Exploring the variation of the desired sensation on the ASHRAE scale. *Energy and Buildings, 39*, 867-874. doi:10.1016/j.enbuild.2007.02.014

Hussain, S., & Oosthuizen, P. H. (2012a). Numerical study of buoyancy-driven natural ventilation in a simple three-storey atrium building. *International Journal of Sustainable Built Environment, 1*(2), 141-157. doi:10.1016/j.ijsbe.2013.07.001

Hussain, S., & Oosthuizen, P. H. (2012b). Validation of numerical modeling of conditions in an atrium space with a hybrid ventilation system. *Building and Environment, 52*, 152-161. doi:https://doi.org/10.1016/j.buildenv.2011.12.016

Hussain, S., Oosthuizen, P. H., & Kalendar, A. (2012). Evaluation of various turbulence models for the prediction of the airflow and temperature distributions in atria. *Energy and Buildings, 48*, 18-28. doi:10.1016/j.enbuild.2012.01.004

III, H. B. K. (2017). Flow/Variable Refrigerant Volume (VRF/VRV) Systems an alternative to central plants. *25th National Conference on Building Commissioning, utah USA*.

International Standard Organization (ISO-7730) -Ergonomics of the thermal environment. (2005).

Ismail, M. R., & Barber, J. M. (2001). A Field Study to Determine Inside Design Conditions for Malaysian Air Conditioning Systems. *Architectural Science Review, 44*(1), 83-99. doi:10.1080/00038628.2001.9697456

Jae-Weon Jeong, & Stan Mumma. (2006). Designing a Dedicated Outdoor Air System with Ceiling Radiant Cooling Panels. *ASHRAE Journal*(October,2006).

Jamaludin, N., Mohammed, N. I., Khamidi, M. F., & Wahab, S. N. A. (2015). Thermal Comfort of Residential Building in Malaysia at Different Micro-climates. *Procedia - Social and Behavioral Sciences, 170*, 613-623. doi:10.1016/j.sbspro.2015.01.063

Jani, D. B., Mishra, M., & Sahoo, P. K. (2018). Performance analysis of a solid desiccant assisted hybrid space cooling system using TRNSYS. *Journal of Building Engineering, 19*, 26-35. doi:https://doi.org/10.1016/j.jobe.2018.04.016

Jeong, J.-W., & Mumma, S. A. (2005). Practical thermal performance correlations for molecular sieve and silica gel loaded enthalpy wheels. *Applied Thermal Engineering, 25*(5), 719-740. doi:https://doi.org/10.1016/j.applthermaleng.2004.07.018

Jiang, Y., Ge, T., & Wang, R. (2013). Performance simulation of a joint solid desiccant heat pump and variable refrigerant flow air conditioning system in EnergyPlus. *Energy and Buildings, 65*, 220-230. doi:10.1016/j.enbuild.2013.06.005

Jin Zhou, Hing-wah Chau, Ye Kang, Dominique Hes, Masa Noguchi, & Aye, L. (2018). Comparing Mixing Ventilation and Displacement Ventilation in University Classrooms. *ZEMCH 2018 International Conference, Melbourne, Australia*.

Jiying, L. (2015). A Numerical Study of the Indoor Thermal Environment in an Air-Conditioned Large Space Building. 69-72. doi:10.1109/icicta.2015.26

Kalmár, F. (2015). Innovative method and equipment for personalized ventilation. *Indoor Air, 25*(3), 297-306. doi:https://doi.org/10.1111/ina.12138

Kam, I. M. S. (2006). 25.5 Deg C and Human Thermal Comfort. *Energy Efficiency Office, Electrical & Mechanical Services Department, The Government of Hong Kong Special Administrative Region*.

Karunakaran, R., Iniyan, S., & Goic, R. (2010). Energy efficient fuzzy based combined variable refrigerant volume and variable air volume air conditioning system for buildings. *Applied Energy, 87*(4), 1158-1175. doi:10.1016/j.apenergy.2009.08.013

Katili, A., Boukhanouf, R., & Wilson, R. (2015). *Space Cooling in Buildings in Hot and Humid Climates – a Review of the Effect of Humidity on the Applicability of Existing Cooling Techniques*.

Khan, M. Z. U., Younis, M. Y., Akram, N., Akbar, B., Rajput, U. A., Bhutta, R. A., . . . Zahid, F. B. (2021). Investigation of heat transfer in wavy and dual wavy micro-channel heat sink using alumina nanoparticles. *Case Studies in Thermal Engineering, 28*, 101515. doi:https://doi.org/10.1016/j.csite.2021.101515

Khedari, J., Yamtraipat, N., Pratintong, N., & Hirunlabh, J. (2000). Thailand ventilation comfort chart. *Energy and Buildings, 32*, 245-249. doi:10.1016/S0378-7788(00)00050-5

Kim, D., Cox, S. J., Cho, H., & Im, P. (2018). Model calibration of a variable refrigerant flow system with a dedicated outdoor air system: A case study. *Energy and Buildings, 158*, 884-896. doi:10.1016/j.enbuild.2017.10.049

Kim, J., Song, D., Kim, S., Park, S., Choi, Y., & Lim, H. (2020). Energy-Saving Potential of Extending Temperature Set-Points in a VRF Air-Conditioned Building. *Energies, 13*(9), 2160.

Kim, W., Jeon, S. W., & Kim, Y. (2016). Model-based multi-objective optimal control of a VRF (variable refrigerant flow) combined system with DOAS (dedicated outdoor air system) using genetic algorithm under heating conditions. *Energy, 107*, 196-204. doi:10.1016/j.energy.2016.03.139

Köppen, W. (2012). Weather and climate. *Met Office*.

Kubicek, B., Hribernik, W., Brauner, G., Faltin, C., Musai, F., Semlitsch, B., & Popovac, M. (2009). *CFD analysis of the turbulent flow field and thermal behavior of high-current electric switchgear*.

Kwong, Q. J., Adam, N. M., & Sahari, B. B. (2014). Thermal comfort assessment and potential for energy efficiency enhancement in modern tropical buildings: A review. *Energy and Buildings, 68*, 547-557. doi:10.1016/j.enbuild.2013.09.034

Laughman, C. R., Bortoff, S. A., & Qiao, H. (2018). Integrated Control of Multi-Zone Buildings with Ventilation and VRF systems in Cooling Mode. *Mitsubishi Electric Research Laboratories*.

Lee, J., Yoon, H., Im, P., & Song, Y.-h. (2017). Verification of Energy Reduction Effect through Control Optimization of Supply Air Temperature in VRF-OAP System. *Energies, 11*(1), 49. doi:10.3390/en11010049

Li, R., Sekhar, S. C., & Melikov, A. K. (2010). Thermal comfort and IAQ assessment of under-floor air distribution system integrated with personalized ventilation in hot and humid climate. *Building and Environment, 45*(9), 1906-1913. doi:10.1016/j.buildenv.2010.03.003

Li, R., Sekhar, S. C., & Melikov, A. K. (2011). Thermal comfort and indoor air quality in rooms with integrated personalized ventilation and under-floor air distribution systems. *HVAC and R Research,Scopus, 17*, 829-846.

Li, Z., Wang, B., Li, X., Shi, W., Zhang, S., & Liu, Y. (2017). Simulation of recombined household multi-split variable refrigerant flow system with split-type air conditioners. *Applied Thermal Engineering, 117*, 343-354. doi:10.1016/j.applthermaleng.2017.02.003

Lin, & Tsai. (2014). An experimental study on a full-scale indoor thermal environment using an Under-Floor Air Distribution system. *Energy & Buildings, 80*(Complete), 321-330. doi:10.1016/j.enbuild.2014.05.028

Lin, X., Lee, H., Hwang, Y., & Radermacher, R. (2015). A review of recent development in variable refrigerant flow systems. *Science and Technology for the Built Environment, 21*(7), 917-933. doi:10.1080/23744731.2015.1071987

Lin, Z. (2011). Effective draft temperature for evaluating the performance of stratum ventilation. *Building and Environment, 46*(9), 1843-1850. doi:https://doi.org/10.1016/j.buildenv.2011.03.005

LIN, Z. (2014). Stratum Ventilation – A Solution to Meet Challenges to Contemporary Air Distribution. *REHVA Journal*.

Lin, Z., Chow, T. T., Tsang, C. F., Fong, K. F., & Chan, L. S. (2005). CFD study on effect of the air supply location on the performance of the displacement ventilation system. *Building and Environment, 40*(8), 1051-1067. doi:10.1016/j.buildenv.2004.09.003

Lin, Z., Chow, T. T., Tsang, C. F., Fong, K. F., & Chan, L. S. (2009). Stratum ventilation – A potential solution to elevated indoor temperatures. *Building and Environment, 44*(11), 2256-2269. doi:10.1016/j.buildenv.2009.03.007

Lin, Z., Lee, C. K., Fong, S., Chow, T. T., Yao, T., & Chan, A. L. S. (2011). Comparison of annual energy performances with different ventilation methods for cooling. *Energy and Buildings, 43*(1), 130-136. doi:10.1016/j.enbuild.2010.08.033

Lin, Z., Tian, L., Yao, T., Wang, Q., & Chow, T. T. (2011). Experimental and numerical study of room airflow under stratum ventilation. *Building and Environment, 46*(1), 235-244. doi:10.1016/j.buildenv.2010.07.018

Lin, Z., Yao, T., Chow, T. T., Fong, K. F., & Chan, L. S. (2011). Performance evaluation and design guidelines for stratum ventilation. *Building and Environment, 46*(11), 2267-2279. doi:10.1016/j.buildenv.2011.05.006

Liu, Chen, H., Jun, L., & Haoru, L. (2017). Study on the Distribution of Vertical Temperature in a Large Space Building using Low-Sidewall Air Supply System based on Block-Gebhart Model. *Procedia Engineering, 205*, 2631-2638. doi:https://doi.org/10.1016/j.proeng.2017.10.205

Liu, S., & Novoselac, A. (2015). Air Diffusion Performance Index (ADPI) of diffusers for heating mode. *Building and Environment, 87*, 215-223. doi:10.1016/j.buildenv.2015.01.021

Liu, T., Liu, Z., Li, G., & Zuo, Z. (2015). Comparative Study of Numerical Simulation of Indoor Thermal Environment in the Pattern of Personalized Ventilation and Stratum Ventilation. *Procedia Engineering, 121*, 785-791. doi:10.1016/j.proeng.2015.09.031

Liu, W., Lian, Z., & Yao, Y. (2008). Optimization on indoor air diffusion of floor-standing type room air-conditioners. *Energy and Buildings, 40*(2), 59-70. doi:https://doi.org/10.1016/j.enbuild.2007.01.010

Lojuntin, S. A. (2017). IMPLEMENTATION OF MS1525 & LOW CARBON BUILDINGS.

Lopez, Galvez-Huerta, M. A., Castejon-Navas, J., & Gomez-Garcia, V. (2013). Experimental analysis of energy savings and hygrothermal conditions improvement by means of air curtains in stores with intensive pedestrian traffic. *Energy and Buildings, 67*, 608-615. doi:https://doi.org/10.1016/j.enbuild.2013.08.058

Lopez, Galvez Huerta, M. A., Castejon Navas, J., & Gerard O'Donhoe, P. (2018). Compliance with Energy Savings and Labour Legislation Requirements in Wide-Open Industrial Buildings Refurbishment. *Dyna, 93*(1), 155-159. doi:10.6036/8297

Loveday, Kenneth C. Parsons, Ahmed H. Taki, Simon G. Hodder, & Jeal, L. D. (1998). Designing for Thermal Comfort in Combined Chilled Ceiling/Displacement Ventilation Environments. *ASHRAE TRANSACTIONS*.

Macpherson, R. K. (1973). Thermal stress and thermal comfort. *Ergonomics, 16*(5), 611-622. doi:10.1080/00140137308924552

Mallick, F. H. (1996). Thermal comfort and building design in the tropical climates *Energy and Buildings, 23*, 161-167.

MATLAB. (2005). MATLAB The Language of Technical Computing, Version 7. *The Mathworks, Natick, MA*.

Melikov, A., Ivanova, T., & Stefanova, G. (2012). Seat headrest-incorporated personalized ventilation: Thermal comfort and inhaled air quality. *Building and Environment, 47*, 100-108. doi:10.1016/j.buildenv.2011.07.013

Melikov, A. K., Popiolek, Z., Silva, M. C. G., Care, I., & Sefker, T. (2007). Accuracy Limitations for Low-Velocity Measurements and Draft Assessment in Rooms. *HVAC&R Research, 13*(6), 971-986. doi:10.1080/10789669.2007.10391465

Milind Vishwanath Rane, Deepa M Vedartham, & Niranjan Bastakoti. (2016). Design Integration of Dedicated Outdoor Air System with Variable Refrigerant Flow System. *International Refrigeration and Air Conditioning Conference Paper · August 2015, The University of Nottingham, University Park Nottingham NG7 2RD*.

Morovat, N., & Maerefat, M. (2013). Analysis of Thermal Comfort in Space Equipped with Stratum Ventilation and Radiant Cooling Ceiling.

N.Aynur, T. (2010). Variable Refrigerant Flow Systems, A Review. *Energy & Buildings, 42*(42), 1106-1112.

Nada, S. A., El-Batsh, H. M., Elattar, H. F., & Ali, N. M. (2016). CFD investigation of airflow pattern, temperature distribution and thermal comfort of UFAD system for theater buildings applications. *Journal of Building Engineering, 6*, 274-300. doi:10.1016/j.jobe.2016.04.008

Nastase, I., Meslem, A., Vlad, I., & Colda, I. (2011). Lobed grilles for high mixing ventilation – An experimental analysis in a full scale model room. *Building and Environment, 46*(3), 547-555. doi:https://doi.org/10.1016/j.buildenv.2010.08.008

National Development and Reform Commission (NDRC). Low Carbon Green Growth Roadmap for Asia and the Pacific. *China's National Development and Reform Commission*.

Navid, & Maerefat, M. (2015). Ventilation and Thermal Performance in A Hybrid System of Hydronic Radiant Cooling and Stratum Ventilation in Residential Room. *Sharif Mechanical Engineering, 2*, 113-124.

Neeraj Ahirwar, Prof. Ankesh Kumar Pataskar, & Nagpure, D. S. k. (2017). CFD Analysis of Temperature Stratification and the Effect of Diffuser Inlet Position inside the System. *International Journal for Scientific Research & Development, 5*(1).

Nicol, J. F., Raja, I. A., Allaudin, A., & Jamy, G. N. (1999). Climatic variations in comfortable temperatures: the Pakistan projects. *Energy and Buildings, 30*, 261–279.

Nicol, J. F., & Roaf, S. (2017). Rethinking thermal comfort. *Building Research & Information, 45*(7), 711-716. doi:10.1080/09613218.2017.1301698

Nielsen, P. V. (2000). Velocity distribution in a room ventilated by displacement ventilation and wall-mounted air terminal devices. *Energy and Buildings, 31*(3), 179-187. doi:https://doi.org/10.1016/S0378-7788(99)00012-2

O'Donohoe, P. G., Gálvez-Huerta, M. A., Gil-Lopez, T., Dieguez-Elizondo, P. M., & Castejon-Navas, J. (2019). Air diffusion system design in large assembly halls. Case study of the Congress of Deputies parliament building, Madrid, Spain. *Building and Environment, 164*, 106311. doi:10.1016/j.buildenv.2019.106311

Olanrewaju, A. I., Adedeji, K. A., Sulaiman, M. A., Giwa, S. O., Nwaokocha, C. N., & Layeni, A. T. (2019). Design and Engineering Economic Analysis of a Variable Refrigerant Flow (VRF) and Mini-Split Air Conditioning System. *Current Journal of Applied Science and Technology*, 1-25. doi:10.9734/cjast/2019/v34i130111

Park, D. Y., Yun, G., & Kim, K. S. (2017). Experimental evaluation and simulation of a variable refrigerant- flow (VRF) air-conditioning system with outdoor air processing unit. *Energy and Buildings, 146*, 122-140. doi:10.1016/j.enbuild.2017.04.026

Piljae Im, Malhotra Mini, Jeffrey D Munk, & Lee, J. (2016). Cooling season full and part load performance evaluation of Variable Refrigerant Flow (VRF) system using an occupancy simulated research building. *International Refrigeration and Air Conditioning Conference, Purdue University*.

Posner, J. D., Buchanan, C. R., & Dunn-Rankin, D. (2003). Measurement and prediction of indoor air flow in a model room. *Energy and Buildings, 35*(5), 515-526. doi:https://doi.org/10.1016/S0378-7788(02)00163-9

Rahmati, B., Heidarian, A., & Jadidi, A. M. (2018). Investigation in performance of a hybrid under-floor air distribution with improved desk displacement ventilation system in a small office. *Applied Thermal Engineering, 138*, 861-872. doi:10.1016/j.applthermaleng.2018.03.015

Raish, J. Thermal Comfort, design for people.pdf.

Ricciardi, P., & Buratti, C. (2012). Thermal comfort in open plan offices in northern Italy: An adaptive approach. *Building and Environment, 56*, 314-320. doi:https://doi.org/10.1016/j.buildenv.2012.03.019

RJ, d. D., & GS, B. (2002). Thermal comfort in naturally ventilated buildings: revisions to ASHRAE Standard 55. Energ Build;34(6): 549–561,.

Rohdin, P., & Moshfegh, B. (2007). Numerical predictions of indoor climate in large industrial premises. A comparison between different k–ε models supported by field measurements. *Building and Environment, 42*(11), 3872-3882. doi:https://doi.org/10.1016/j.buildenv.2006.11.005

Rundle, C. A., Lightstone, M. F., Oosthuizen, P., Karava, P., & Mouriki, E. (2011). Validation of computational fluid dynamics simulations for atria geometries. *Building and Environment, 46*(7), 1343-1353. doi:10.1016/j.buildenv.2010.12.019

Rupp, R. F., Vásquez, N. G., & Lamberts, R. (2015). A review of human thermal comfort in the built environment. *Energy and Buildings, 105*, 178-205. doi:10.1016/j.enbuild.2015.07.047

Saab, R., Al Quabeh, H., & Hassan Ali, M. I. (2018). Variable refrigerant flow cooling assessment in humid environment using different refrigerants. *J Environ Manage, 224*, 243-251. doi:10.1016/j.jenvman.2018.07.031

Saber, E. M., Tham, K. W., & Leibundgut, H. (2016). A review of high temperature cooling systems in tropical buildings. *Building and Environment, 96*, 237-249. doi:10.1016/j.buildenv.2015.11.029

Said, Z., Ghodbane, M., Tiwari, A. K., Ali, H. M., Boumeddane, B., & Ali, Z. M. (2021). 4E (Energy, Exergy, Economic, and Environment) examination of a small LFR solar water heater: An experimental and numerical study. *Case Studies in Thermal Engineering, 27*, 101277. doi:10.1016/j.csite.2021.101277

Sajadi, B., Saidi, M. H., & Mohebbian, A. (2011). Numerical investigation of the swirling air diffuser: Parametric study and optimization. *Energy and Buildings, 43*(6), 1329-1333. doi:https://doi.org/10.1016/j.enbuild.2011.01.018

Seppänen, O. (2008). Ventilation strategies for good indoor air quality and energy efficiency. *International Journal of Ventilation, 6*(4), 297-306.

Shaik Gulam Abul Hasan, Syeda Saniya Fatima, & Kumar, G. S. (2015). DESIGN OF A VRF AIR CONDITIONING SYSTEM WITH ENERGY CONSERVATION ON COMMERCIAL BUILDING. *INTERNATIONAL JOURNAL OF ENGINEERING SCIENCES & RESEARCH TECHNOLOGY*.

Shang, C., Huang, X., Zhang, Y., & Chen, M. (2019). Outdoor thermal comfort in a tropical coastal tourist resort in Haikou, China. *Indoor and Built Environment*, 1420326X1986233. doi:10.1177/1420326x19862337

Shen, C., Gao, N., & Wang, T. (2013). CFD study on the transmission of indoor pollutants under personalized ventilation. *Building and Environment, 63*, 69-78. doi:10.1016/j.buildenv.2013.02.003

Smoljan, D., Balen, I., & Hr, D. (2010). Influence of a plenum box design on uniformity of the radial air jet issuing from a vortex diffuser. *Strojarstvo, 52*, 379-386.

Sookchaiya, T., Monyakul, V., & Thepa, S. (2010). Assessment of the thermal environment effects on human comfort and health for the development of novel air conditioning system in tropical regions. *Energy and Buildings, 42*(10), 1692-1702. doi:10.1016/j.enbuild.2010.04.012

Sorrell, S. (2015). Reducing energy demand: A review of issues, challenges and approaches. *Renewable and Sustainable Energy Reviews, 47*, 74-82. doi:https://doi.org/10.1016/j.rser.2015.03.002

Stamou, A., & Katsiris, I. (2006). Verification of a CFD model for indoor airflow and heat transfer. *Building and Environment, 41*(9), 1171-1181. doi:10.1016/j.buildenv.2005.06.029

Stavrakakis, G. M., Koukou, M. K., Vrachopoulos, M. G., & Markatos, N. C. (2008). Natural cross-ventilation in buildings: Building-scale experiments, numerical simulation and thermal comfort evaluation. *Energy and Buildings, 40*(9), 1666-1681. doi:10.1016/j.enbuild.2008.02.022

Suhafizudin Bin Zainal Anuar, Mohamad Suhaimi Bin Yahaya, Jusnan Bin Hasim, Suhilah Binti Mohd Ali, & Shamsuddin, M. K. B. (2016). STUDYING THE VARIABLE REFRIGERANT VOLUME (VRV) SYSTEM AND DETERMINING THE ROOT CAUSE OF ITS PROBLEM IN BUILDING 37, AGENSI NUKLEAR MALAYSIA.

Sui, X., & Zhang, X. (2012a). Effects of radiant terminal and air supply terminal devices on energy consumption of cooling load sharing rate in residential buildings. *Energy and Buildings, 49*, 499–508. doi:10.1016/j.enbuild.2012.02.052

Sui, X., & Zhang, X. (2012b). Effects of radiant terminal and air supply terminal devices on energy consumption of cooling load sharing rate in residential buildings. *Energy and Buildings, 49*, 499-508. doi:10.1016/j.enbuild.2012.02.052

Sun, Y., & Smith, T. F. (2005). Air flow characteristics of a room with square cone diffusers. *Building and Environment, 40*(5), 589-600. doi:10.1016/j.buildenv.2004.07.018

Szczepanik-Scislo, N., & Schnotale, J. (2020). An Air Terminal Device with a Changing Geometry to Improve Indoor Air Quality for VAV Ventilation Systems. *Energies, 13*(18). doi:10.3390/en13184947

Technologies, C. U. (2014). Integrating VRF Systems for Improved Efficiency and Comfort. *Carrier Engineering Newsletter, 2*(2).

Tian, L., Lin, Z., & Wang, Q. (2011). Experimental investigation of thermal and ventilation performances of stratum ventilation. *Building and Environment, 46*(6), 1309-1320. doi:10.1016/j.buildenv.2011.01.002

Ting Yao, & Lin, Z. (2014). Numerical Study Of The Effect Of Air Terminal Layouts On The Performance Of Stratum Ventilation System. *International High Performance Buildings Conference, Purdue University Purdue e-Pubs*.

Tu, Q., Mao, S., Feng, Y., & Guo, D. (2011). Heating control strategy in fresh air processor matched with variable refrigerant flow air conditioning system. *Energy Conversion and Management, 52*(7), 2542-2554. doi:https://doi.org/10.1016/j.enconman.2011.02.007

Villafruela, J. M., Sierra-Pallares, J. B., Castro, F., Álvaro, A., & Santiago-Casado, P. (2018). Experimental and numerical study of the influence of the plenum box on the airflow pattern generated by a swirl air diffuser. *Experimental Thermal and Fluid Science, 99*, 547-557. doi:https://doi.org/10.1016/j.expthermflusci.2018.08.021

Wan, H., Cao, T., Hwang, Y., & Oh, S. (2020). A review of recent advancements of variable refrigerant flow air-conditioning systems. *Applied Thermal Engineering, 169*, 114893. doi:https://doi.org/10.1016/j.applthermaleng.2019.114893

Wang, F., & Abdullah, A. H. (2011). Investigating thermal conditions in a tropic atrium employing CFD and DTM techniques. *International Journal of Low-Carbon Technologies, 6*(3), 171-186. doi:10.1093/ijlct/ctr005

Wang, H., Zhou, P., Guo, C., Tang, X., Xue, Y., & Huang, C. (2019). On the calculation of heat migration in thermally stratified environment of large space building with sidewall nozzle air-supply. *Building and Environment, 147*, 221-230. doi:10.1016/j.buildenv.2018.10.003

Wang, S., & Ma, Z. (2008). Supervisory and Optimal Control of Building HVAC Systems: A Review. *HVAC&R Research, 14*(1), 3-32. doi:10.1080/10789669.2008.10390991

WEC. (2013). *Composing Energy Futures to 2050*. Retrieved from

Wu, P., Zhou, J., & Li, N. (2021). Influences of atrium geometry on the lighting and thermal environments in summer: CFD simulation based on-site measurements

for validation. *Building and Environment*, 107853. doi:10.1016/J.BUILDENV.2021.107853

Y.H. Yau, K.S. Poh, & Badarudin, A. (2018). A numerical airflow pattern study of a floor swirl diffuser for UFAD system. *Energy and Buildings, 158*, 525-535. doi:10.1016/j.enbuild.2017.10.037

Yamtraipat, N., Khedari, J., & Hirunlabh, J. (2005). Thermal comfort standards for air conditioned buildings in hot and humid Thailand considering additional factors of acclimatization and education level. *Solar Energy, 78*(4), 504-517. doi:10.1016/j.solener.2004.07.006

Yao, & Lin. (2014a). An experimental and numerical study on the effect of air terminal layout on the performance of stratum ventilation. *Building and Environment, 82*, 75-86. doi:10.1016/j.buildenv.2014.08.016

Yao, & Lin. (2014b). An experimental and numerical study on the effect of air terminal types on the performance of stratum ventilation. *Building and Environment, 82*, 431-441. doi:10.1016/j.buildenv.2014.09.021

Yao, & Lin. (2014c). An investigation into the performance of fabric diffusers used in stratum ventilation. *Building and Environment, 81*, 103-111. doi:10.1016/j.buildenv.2014.06.016

Yao, T., & Lin, Z. (2014a). An experimental and numerical study on the effect of air terminal types on the performance of stratum ventilation. *Building and Environment, 82*, 431-441. doi:10.1016/j.buildenv.2014.09.021

Yao, T., & Lin, Z. (2014b). An investigation into the performance of fabric diffusers used in stratum ventilation. *Building and Environment, 81*, 103-111. doi:10.1016/j.buildenv.2014.06.016

Yau, Poh, K. S., & Badarudin, A. (2018). A numerical airflow pattern study of a floor swirl diffuser for UFAD system. *Energy and Buildings, 158*, 525-535. doi:https://doi.org/10.1016/j.enbuild.2017.10.037

Yau, Wong, C. M., Ong, H. C., & Chin, W. M. (2020). Application of the bin weather data for building energy analysis in the tropics. *Energy Efficiency, 13*(5), 935-953. doi:10.1007/s12053-020-09862-8

Yau, Y. H., Poh, K. S., & Badarudin, A. (2018a). An investigation of thermal environment of an existing UFAD system in a high-rise office building in the tropics. *J Environ Health Sci Eng, 16*(2), 313-322. doi:10.1007/s40201-018-0319-1

Yau, Y. H., Poh, K. S., & Badarudin, A. (2018b). A numerical airflow pattern study of a floor swirl diffuser for UFAD system. *Energy and Buildings, 158*, 525-535. doi:10.1016/j.enbuild.2017.10.037

Yau, Y. H., & Rajput, U. A. (2022). Thermal Comfort Assessment and Design Guidelines of a VRF-Integrated Stratum Ventilation System for a Large Tropical

Building. *Arabian Journal for Science and Engineering*. doi:10.1007/s13369-022-06823-4

Yau, Y. H., Rajput, U. A., Rajpar, A. H., & Lastovets, N. (2022). Effects of Air Supply Terminal Devices on the Performance of Variable Refrigerant Flow Integrated Stratum Ventilation System: An Experimental Study. *Energies, 15*(4), 1265. doi:10.3390/en15041265

Yau, Y. H., & Umair, A. R. (2022). Numerical simulation of a novel VRF-SV hybrid system performance in a large retail facility in the tropics. *Journal of Building Performance Simulation, 15*(3), 323-344. doi:10.1080/19401493.2022.2047225

Yin, H., Li, A., Liu, Z., Sun, Y., & Chen, T. (2016). Experimental study on airflow characteristics of a square column attached ventilation mode. *Building and Environment, 109*, 112-120. doi:10.1016/j.buildenv.2016.09.006

Yin, H., Yang, C., Yi, L., Yu, J., Wu, Y., Deng, Y., & Tang, Z. (2020). Ventilation and air conditioning system of deep-buried subway station in sub-tropical climates: Energy-saving strategies. *Applied Thermal Engineering, 178*, 115555. doi:https://doi.org/10.1016/j.applthermaleng.2020.115555

Yong, Wong, K. K. L., Du, H., Qing, J., & Tu, J. (2014). Design configuration for a higher efficiency air conditioning system in large space building. *Energy and Buildings, 72*, 167-176. doi:10.1016/j.enbuild.2013.12.041

Yong CHENG, Zhang LIN, Weiqin WU, & YAO, T. (2014). Performance evaluation of stratum ventilation with slot diffuser using CFD. *Indoor environment*.

Yonghua Zhu, Xinqiao Jin, Zhimin Du, Xing Fang, & Fan, B. (2014). An energy-saving control strategy for VRF and VAV combined air conditioning system in heating mode. *International Refrigeration and Air Conditioning Conference, Purdue University*.

Yu, K., Cao, Z., & Liu, Y. (2017). Research on the optimization control of the central air-conditioning system in university classroom buildings based on TRNSYS software. *Procedia Engineering, 205*, 1564-1569. doi:10.1016/j.proeng.2017.10.261

Yu, X., Yan, D., Sun, K., Hong, T., & Zhu, D. (2016). Comparative study of the cooling energy performance of variable refrigerant flow systems and variable air volume systems in office buildings. *Applied Energy, 183*, 725-736. doi:10.1016/j.apenergy.2016.09.033

Zhai, Z., & Rivas, J. (2018). Promoting variable refrigerant flow system with a simple design and analysis tool. *Journal of Building Engineering, 15*, 218-228. doi:10.1016/j.jobe.2017.11.011

Zhang, R., Sun, K., Hong, T., Yura, Y., & Hinokuma, R. (2018). A novel Variable Refrigerant Flow (VRF) heat recovery system model: Development and validation. *Energy and Buildings, 168*, 399-412. doi:10.1016/j.enbuild.2018.03.028

Zhang, S., Lin, Z., Ai, Z., Huan, C., Cheng, Y., & Wang, F. (2019). Multi-criteria performance optimization for operation of stratum ventilation under heating mode. *Applied Energy, 239*, 969-980. doi:10.1016/j.apenergy.2019.01.248

Zhang, W., Hiyama, K., Kato, S., & Ishida, Y. (2013). Building energy simulation considering spatial temperature distribution for nonuniform indoor environment. *Building and Environment, 63*, 89-96. doi:https://doi.org/10.1016/j.buildenv.2013.02.007

Zhang, Z., Zhang, W., Zhai, Z. J., & Chen, Q. Y. (2007). Evaluation of Various Turbulence Models in Predicting Airflow and Turbulence in Enclosed Environments by CFD: Part 2—Comparison with Experimental Data from Literature. *HVAC&R Research, 13*(6), 871-886. doi:10.1080/10789669.2007.10391460

Zhao, Jianbo, C., Haizhao, Y., & Lingchuang, C. (2017). The development and experimental performance evaluation on a novel household variable refrigerant flow based temperature humidity independently controlled radiant air conditioning system. *Applied Thermal Engineering, 122*, 245-252. doi:https://doi.org/10.1016/j.applthermaleng.2017.04.056

Zhao, H., Liu, Z., & Zuo, Z. (2015). Numerical Simulation of Indoor Thermal Environment Effected by Air Supply Temperature and Grille Angle on Stratum Ventilation in a Typical Office. *Procedia Engineering, 121*, 779-784. doi:10.1016/j.proeng.2015.09.030

Zheng, C., You, S., Zhang, H., Zheng, W., Zheng, X., Ye, T., & Liu, Z. (2018). Comparison of air-conditioning systems with bottom-supply and side-supply modes in a typical office room. *Applied Energy, 227*, 304-311. doi:10.1016/j.apenergy.2017.07.078

Zhivov, A., Skistad, H., Mundt, E., Posokhin, V., Ratcliff, M., Shilkrot, E., & Strongin, A. (2001). 7. Principles of air and contaminant movement inside and around buildings. In.

Zhivov, A., Skistad, H., Mundt, E., Posokhin, V., Ratcliff, M., Shilkrot, E., . . . Yang, Y. (2020). Chapter 7 - Principles of air and contaminant movement inside and around buildings. In H. D. Goodfellow & R. Kosonen (Eds.), *Industrial Ventilation Design Guidebook (Second Edition)* (pp. 245-370): Academic Press.

Zhou, Y. P., Wu, J. Y., Wang, R. Z., & Shiochi, S. (2007). Energy simulation in the variable refrigerant flow air-conditioning system under cooling conditions. *Energy and Buildings, 39*(2), 212-220. doi:10.1016/j.enbuild.2006.06.005

Zhu, Y., Jin, X., Du, Z., Fan, B., & Fang, X. (2014). Simulation of variable refrigerant flow air conditioning system in heating mode combined with outdoor air processing unit. *Energy and Buildings, 68*, 571-579. doi:10.1016/j.enbuild.2013.09.042

Zhu, Y., Jin, X., Du, Z., Fan, B., & Fu, S. (2013). Generic simulation model of multi-evaporator variable refrigerant flow air conditioning system for control analysis.

International Journal of Refrigeration, 36(6), 1602-1615. doi:10.1016/j.ijrefrig.2013.04.019

Zhu, Y., Jin, X., Du, Z., & Fang, X. (2015). Online optimal control of variable refrigerant flow and variable air volume combined air conditioning system for energy saving. *Applied Thermal Engineering, 80*, 87-96. doi:10.1016/j.applthermaleng.2015.01.030

Zhu, Y., Jin, X., Du, Z., Fang, X., & Fan, B. (2014). Control and energy simulation of variable refrigerant flow air conditioning system combined with outdoor air processing unit. *Applied Thermal Engineering, 64*(1-2), 385-395. doi:10.1016/j.applthermaleng.2013.12.076

Zhu, Y., Jin, X., Fang, X., & Du, Z. (2014). Optimal control of combined air conditioning system with variable refrigerant flow and variable air volume for energy saving. *International Journal of Refrigeration, 42*, 14-25. doi:10.1016/j.ijrefrig.2014.02.006